MEASUREMENT OF DELIGNIFICATION DIVERSITY WITHIN KRAFT PULPING PROCESSES

A Thesis Submitted by

Brian S. Boyer

B.S., 1991, Western Michigan University

M.S., 1993, Institute of Paper Science and Technology

in partial fulfillment of the requirements
for the degree of Doctor of Philosophy
from the Institute of Paper Science and Technology

May 1998

ABSTRACT

The objective of this research was to measure delignification diversity within kraft pulping processes. Pulps were prepared from loblolly pine using 2.5-mm-thick chips and 10.0-mm-thick chips to produce controlled pulps with narrow and broad lignin content distributions. In addition, pulps were obtained from a conventional single vessel continuous digester before and after conversion to Lo-solids™ pulping and Lo-level™ feed. Interfiber variability in density was measured and inferred to lignin content in each mill process condition and related to laboratory pulp interfiber uniformity. In addition, the application of infrared microspectroscpy in quantitative single fiber analyses was investigated.

The new density gradient column designed for this project provided improved structural integrity and a near linear optical path for imaging. Cross-polarization techniques provided high contrast images of the cellulose fibers through digital image averaging. Experimental techniques were modified to increase measurement accuracy and precision. The standard error of prediction was 6.5 kappa number for single fiber kappa number analyses, and measurement error was insignificant. Density gradient column Valonia cellulose density measurements were not statistically different than X-ray diffraction and electron diffraction estimates of Valonia cellulose density. The average kraft holocellulose density was 1.5458 ±0.0015 g/ml, and the calculated lignin density was 1.2719 ±0.0090 g/ml.

Lignin content distributions were modeled using a composite of two normal distributions termed distribution A and distribution B. Distribution A was limited to a delignification minimum of approximately 20 kappa number, whereas distribution B was limited to a

delignification minimum of approximately 35 kappa number. The quantity of distribution B contributed a maximum of 35-40%, regardless of chip thickness or process condition. The overall standard deviation in kappa number ranged from 11.5 to 17.7 in 10.0-mm-thick chip pulps and from 2.2 to 9.0 in 2.5-mm-thick chip pulps. Standard deviations for the component distributions were statistically different for each pulp sample, and distribution B disappeared with extended delignification in 2.5-mm-thick chip pulps.

Efforts to use infrared microspectroscopy were unsuccessful in determining interfiber lignin content diversity. However, difference spectra taken at each stage of delignification suggest that lignin becomes highly substituted when pulping continues beyond 30 kappa number.

TABLE OF CONTENTS

LIST OF FIGURES AND TABLES

Main Figures

Appendix Figures:

Main Tables:

Appendix Tables:

CHAPTER ONE: INTRODUCTION

The purpose of this thesis work has been to measure kraft pulping uniformity on a fiber-to-fiber basis. Using interfiber measurements to relate the physical and chemical characteristics of kraft pulp has provided the pulp and paper industry with fundamental information on the effects of nonuniform pulping. This microscale measurement was developed to advance the industry's understanding of macroscale pulp quality differences.

Delignification uniformity in this thesis refers to the ability of a process to subject a given wood furnish to uniform reaction conditions in all parts of the digester. The ultimate goal of pulping is to produce a uniform product on a fiber-to-fiber basis with maximum strength and yield at a given kappa number. Minimizing interfiber lignin content diversity will result in an increase in pulp quality[1].

CAUSE OF NONUNIFORMITY IN PULP

Nonuniform pulp can result from interdigester and intradigester nonuniformity[2]. Interdigester nonuniformity can be the result of a fluctuation in chemical charge application, H-factor calculation, furnish swings, etc. Intradigester nonuniformity may result from heterogeneous chip size, inhomogeneous or insufficient liquor flux, and unequal temperature and/or chemical distribution inside and outside of the chips[2,3-5]. Improvements in uniformity generally imply that there are fewer overcooked and undercooked chips[1].

PURPOSE OF THE STUDY

The objective of chemical pulping is to delignify wood and produce individual wood fibers. Uniform delignification results in pulps of higher strength and yield than nonuniform delignification[1-3]. Nonuniform delignification can lower the quality of pulp by increasing bleaching chemical demand[2,4,6,7]. Recently, development in pulping has focused on extended delignification processes[8-14]. Increasing interfiber uniformity may allow for extended delignification without unacceptable cellulose degradation. In turn, less bleaching chemical may be required to reach the desired level of delignification, thus providing a positive environmental impact[6]. Development of fiber-to-fiber uniformity measurement methods will help isolate conditions that are promoting an inhomogeneous product and provide a step forward towards optimized pulping processes.

PAST RESEARCH

Process optimization relates directly to the achievement of a high quality product and higher profits, thus, it is the goal of any industrial operation. The quality of the final product is dependent on the raw materials and process conditions in which the raw materials are subjected. For example, the pulp and paper industry uses unbleached laboratory pulps as the realistic quality potential of a given fiber source[4,15-17]. Results from quality comparisons of mill pulps to laboratory or pilot-plant pulps are readily available in the literature[1,3,4,15-39].

Pulping uniformity is reliant on homogeneous conditions within the digester vessel. Wood species, chip size distribution, and the temperature and chemical profile within the

digester are major considerations in process optimization. Figure 1 is descriptive of pulping process uniformity considerations.

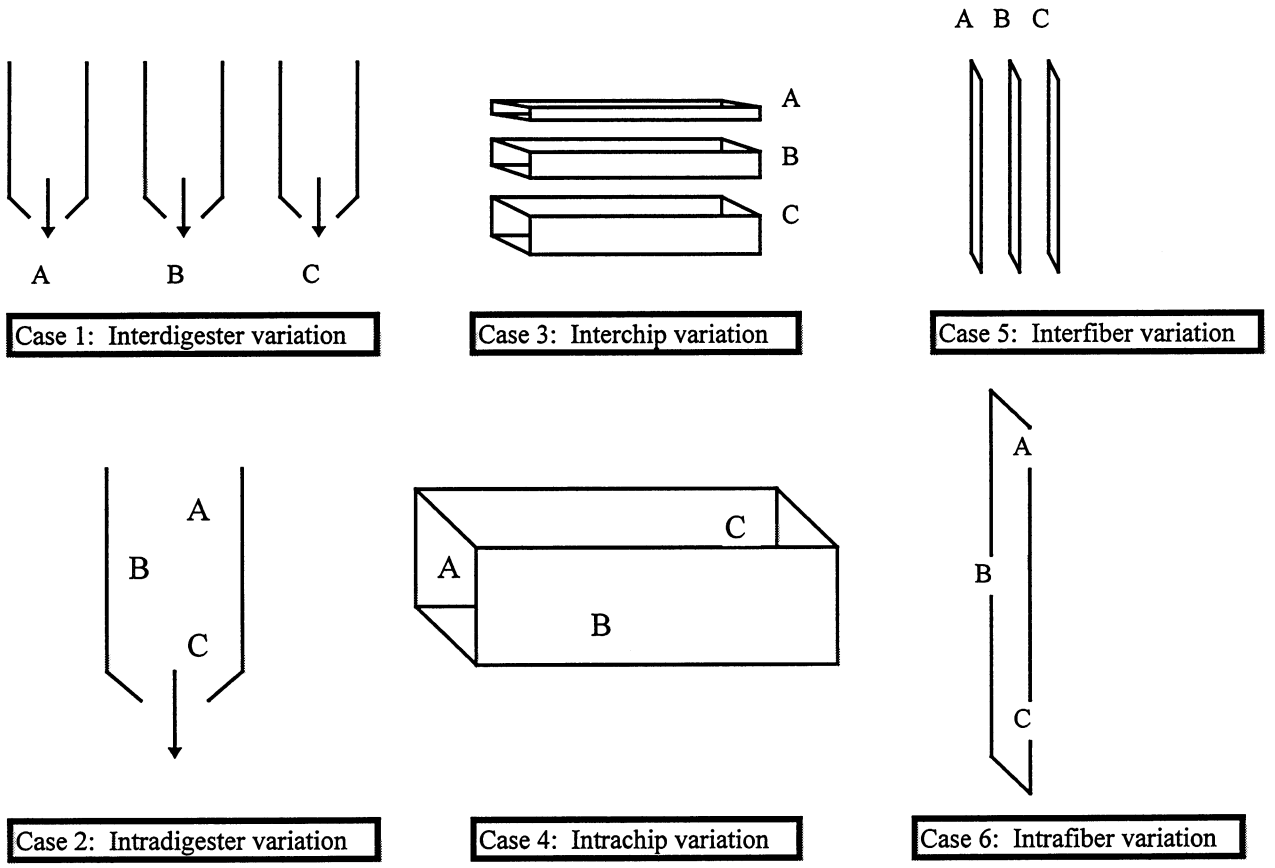

Figure 1. Pulping uniformity considerations.

There are six general considerations relevant to kraft pulping uniformity: interdigester, intradigester, interchip, intrachip, interfiber, and intrafiber. The points A, B, and C in the diagrams represent positions that may vary in uniformity. Variabilities in cases 1-4 are assumed to produce the interfiber diversity concept of case 5 and may also result in the intrafiber diversity of case 6.

It is difficult to provide a process that delignifies each region of the heterogeneous chip equally. Chip structure and process conditions are the source of all nonuniformities in the pulping process. One possible source of delignification diversity may be inherent in the wood

structure--differences between earlywood and latewood. Small differences have been found to exist between earlywood and latewood delignification, but have not been proven to be a major source of interfiber diversity[40-45]. Variation exists in wood morphology with regard to earlywood, latewood, juvenile wood, mature wood, sapwood, heartwood, ring age, and height above ground. Geographic location also plays a large part in the variability of wood[46-49]. In fact, variability within a specific tree and among a stand of the same species can be as pronounced as the differences found among the various species of southern pine[50]. Table 1 lists average morphological characteristics of loblolly pine *(Pinus taeda).*

Table 1. Loblolly pine earlywood and latewood morphological characteristics.

	earlywood	latewood	reference
cell wall, μm	5.02	12.30	51
cell lumen, μm	43.47	17.58	51
cell diameter, μm	53.50	42.17	51
tracheid length, μm	4.23	4.37	51
relative # of tracheids in a 1/6" annual ring (50%EW/50%LW)	57	87	52
# of pits per tracheid	100-200	25	40,53
lignin distribution, %			
2° wall	72	81	54
middle lamella	28	19	54

(It should be noted that the percentages listed are on the basis of the wood present in that particular increment. The earlywood:latewood ratio has a direct correlation with the amount of latewood 2° wall lignin relative to earlywood 2° wall lignin present within an annual ring.)

If the wood fibers were homogeneous in chemistry and physical structure, it may be expected that delignification would be relatively uniform within small diffusion limitations. From Table 1, it is apparent that wood fibers do exhibit differences.

Paulson[55] was the first to measure interfiber diversity within pulps using a density gradient column. Tichy and Procter[6] used this technique to define, mix, and measure the quality of nonuniform pulps. Horng, Mackie, and Tichy[15,16] later used the technique to define and

explain these nonuniformities in mill-produced pulps. These studies will be discussed further in Chapter Three. Other investigations have included UV microspectroscopy[56] and fluorescence microphotometry[57]. Pulp quality inferences have been made by mixing pulps with assumed levels of uniformity[58,59], and a patent[60] was granted for a UV fluorescence application.

THESIS OBJECTIVES

The thesis proposal addressed the physical and chemical limitations in kraft pulping and proposed a technique to quantify delignification diversity on a microscale using fiber density relationships. It has been shown that pulp quality is inversely proportional to delignification diversity. However, there have been few observations of this diversity at the interfiber level. The most likely source of nonuniformities in kraft pulping was assumed to be chip thickness, and sufficiently thick chips have been shown to be diffusion-limited. Chips that are thin enough to provide reaction rates independent of diffusion limitations are considered chemical reaction-limited. Chapter Two provides a discussion of these controlling factors. The original objectives were stated as follows:

1. Provide comprehensive data on interfiber uniformity using the density gradient column and the fully developed thermal density column.

2. Determine the cause of standard deviations present in density measurements of fully bleached pulps.

3. Compare nonuniform pulps from diffusion-limited cooks to uniform pulps from chemical-reaction-limited cooks.

4. Measure pulp quality as a function of interfiber diversity.

5. Utilize the developed interfiber measurement procedure to analyze and predict pulp quality from mill-produced pulp.

The original list of objectives was modified as a result of changes in the proposed experimental approach. Objective 1 was changed due to failure of the thermal density column approach. Multiple difficulties inherent in the technique development led to elimination of objective 4 and modification of objective 5. The overall objective of quantifying kraft pulping diversity on a microscale using fiber density relationships remains the same. However, the thesis objectives were changed as follows:

1. Provide comprehensive data on interfiber uniformity using the density gradient column and FTIR microspectroscopy.

2. Determine the cause of standard deviations present in density measurements of fully bleached pulps.

3. Compare nonuniform pulps from diffusion-limited cooks to uniform pulps from chemical reaction-limited cooks.

4. Utilize the developed interfiber measurement procedure to analyze delignification diversity in mill-produced pulps.

CHAPTER TWO: KRAFT PULPING

PRINCIPLES

Pulping Chemistry

Kraft delignification is an alkaline process that utilizes NaOH and Na_2S as active chemicals in the liquor to remove lignin from wood, and is based on approximately five steps: 1) movement of pulping chemicals to the chip surface; 2) diffusion of the pulping chemicals to the reaction site; 3) reaction between the pulping chemicals and the lignin; 4) diffusion of the degraded lignin to the chip surface; and 5) movement of degraded lignin into the bulk liquor. Steps 1 and 5 do not normally impede delignification , whereas one of steps 2 through 4 may be rate limiting[61].

There are three distinct phases of delignification during kraft pulping: initial, bulk, and residual. The initial phase consists primarily of the cleavage of linkages of the α-aryl ether type in free phenolic lignins. Approximately 15-25% of the lignin is removed during the initial phase, with the amount removed dependent on the wood species and cooking conditions[62]. The bulk phase consists of the cleavage of the β-aryl ether type lignins, and comprises 75-85% of the delignification. The residual phase removes lignin types that are more resistant to kraft pulping. About 2-3% of the lignin content in pulp is considered resistant[61]. At least part of the lignin present in the residual phase is condensed lignin produced during the delignification process. Bleaching chemicals are required to remove this type of lignin from the pulp[61].

The relative amounts of lignin in earlywood and latewood suggest that the lignin available for reaction would be higher in earlywood, resulting in preferential earlywood lignin dissolution. However, some lignin types are more reactive than others.

Lignin Reactivity

Kraft delignification has been seen to dissolve lignin almost exclusively from the secondary wall during the initial and early bulk phases of delignification[63,64]. The concentration of phenolic hydroxy and methoxy groups is directly related to the ease of pulping and both groups are found more frequently in secondary wall lignin. In fact, about 88% of spruce secondary wall lignin has been observed to follow first-order kinetics, as compared to only about one-third of the middle lamella lignin[63]. Middle lamella lignin is low in methoxy and phenolic hydroxy groups as compared to secondary wall lignin[63,64]. Removal of middle lamella lignin is not physically limited by the secondary wall of the fiber[64]. Rather, a lower percentage of methoxy groups would indicate that fewer syringyl units are present in the middle lamella. Syringyl lignin units inhibit condensation reactions that lead to the more resistant condensed lignin structures.

Pulping of wood occurs by exposing the lignin to pulping chemicals that enter the wood structure by means of penetration and diffusion. Penetration is the movement of liquid into the capillaries of wood under the influence of a pressure gradient, whereas diffusion refers to the movement of ions through water and is a comparatively slow process[65]. Complete impregnation of the wood with cooking liquor is the first step in achieving uniform delignification[66].

Cooking chemicals may enter the wood structure in various ways: diffusion through the outer boundary of the chip, penetration into the fiber lumens followed by diffusion through the cell wall, or progression between the fibers, starting at a pit membrane. Relationships between chip dimensions and mass transfer are prevalent in the literature[18,65,67-102]. Excellent review articles are available on this topic[72,87-90,93].

Pulping Limitations and Ways to Minimize Them

The literature contains many studies of penetration and diffusion of fluids into wood[91,95]. Studies have also been performed to show the effects of pH on mass transfer[96-98]. Earlier research utilized gravimetrics[53,99] and radioactive tracers[65,100-102] to monitor penetration and diffusion. More recent studies have impregnated, frozen in liquid nitrogen, and photographed chips to try to establish the role of penetration and diffusion in pulping[2,103].

Penetration

The penetration of wood with cooking chemicals is directly related to wood permeability. The number, size, and degree of obstructions within the wood structure dictate the permeability[52]. Due to the structural differences within wood, it can be expected that the permeability would be different with respect to the longitudinal, radial, and tangential directions. Indeed, the ratio of permeability for waterflow in saturated southern pine sapwood in the longitudinal:radial:tangential directions is approximately 100:4:1 [52].

The tracheids of loblolly pine average 3-5-mm in length. Since wood chips are over 5-mm long, the cooking chemical must pass through a series of adjacent cell wall openings to

travel through the chip by means of the penetration mechanism. The majority of the fluid flow exists between the longitudinal tracheids and will now be discussed.

It has been shown that the pit pairs allow for passage of chemicals between tracheids[104]. The pit contains a membranous valve-like structure with a center torus and a peripheral margo. Penetration occurs through the margo, unless the pit is aspirated. The aspiration (i.e., closed pit structure) is representative of what can occur from the deposition of extractives, or simply from the surface tension forces of water[52].

Increasing the moisture content of wood may increase the permeability of pulping chemicals by reducing pit aspirations, thereby releasing the torus from the pit aperture. Although the margo is more easily penetrated in earlywood, its flexibility may lead to increased pit aspiration due to the surface tension forces of water[52,53,104]. With regard to latewood, a smaller number of pits, lower permeability of the margo, and higher occurrence of resin encrustation may hinder fluid flow regardless of a moisture increase[52]. Therefore, chip moisture affects the penetration that occurs at early stages of the kraft pulping process. Presteaming is considered a way of exceeding penetration limitations and will be discussed in a later section.

Diffusion

At some point in the cook, penetration is essentially complete and the transport of alkali into the chip is controlled by diffusion. Stone[95,96] believed that fibers have virtually no passages for direct liquid movement into the middle lamella, and must delignify strictly by a diffusion mechanism. Hartler and Onisko[90,94] stated that most chemicals transported into the chip have arrived by the time bulk phase delignification begins. It was also emphasized that most of the

chemicals brought in by penetration are used up through the neutralization of extractives and carbohydrate degradation products. According to Luner[105], this immediate reaction of the alkaline cooking chemical increases the concentration gradient and accelerates diffusion.

Diffusion will occur wherever water is present. This includes the water within the cell wall, pit membranes, and fiber lumens. It has also been shown that diffusion is not dependent on the pits alone, but is dependent on the total cross-sectional area of the diffusion paths and the distance to be traveled by the ions[96]. The cell wall capillaries that allow ionic diffusion are not seen microscopically, but can be assumed to exist from the nearly equal three directional diffusion brought about by swelling under alkaline conditions[96]. Alkaline swelling is considered a way of minimizing diffusion limitations and will be discussed in a later section.

Diffusion through a porous surface is modeled by Fick's Second Law, and describes the dependence of pulping chemical flux through the chip on the concentration gradient across the chip[106]. The equation is stated as

$$\frac{dC}{dt} = D\frac{d^2C}{dx^2} \tag{1}$$

where D is the diffusion coefficient; C is the concentration of cooking chemical at time t, and x is the position of the cooking chemical as it progresses in the chip.

The temperature dependence of the diffusion coefficient has been expressed by the following equation[62,98,107]:

$$D = KT^{1/2}e^{-Ea/RT} \tag{2}$$

where, D is the diffusion coefficient; K is a proportionality constant; T is the temperature; Ea is the activation energy of diffusion, and R is the gas constant. Knowing the diffusion coefficient at different temperatures allows for calculation of the activation energy of diffusion.

Each phase of delignification has an associated energy of activation. Comparing activation energy values is a method of determining whether chemical transport into the chip or chemical reaction is the controlling factor. The activation energy for diffusion through wood according to Equation (2) has been found to be approximately 50 kJ/mol[62]. Initial phase delignification has an activation energy of 40-50 kJ/mol[62,107]. When comparing the activation energies, it is apparent that initial phase delignification is diffusion-limited. This has been further reinforced by showing that the initial phase of delignification is zero order in EA, meaning there is no observed dependence on chemical concentration. Bulk phase delignification has an activation energy of 130-150 kJ/mol[93,98,108,109]. Relying on the formation of quinone methide compounds and S_N2 reactions, the bulk phase has the highest activation energy of all three delignification phases. A comparison of the activation energies would imply that under ideal conditions, bulk phase delignification is chemical reaction-limited. Ideal conditions are those where the wood structure does not impede mass transfer. Residual phase delignification has an activation energy of 90-120 kJ/mol[61,98,109] and is also chemical reaction-limited under ideal conditions.

Penetration and diffusion are also affected by pH and various pretreatments. Effects of pH and steaming pretreatments on the mass transfer of pulping chemical will now be discussed as a means of exceeding pulping limitations.

pH-Alkaline Swelling of Fibers

Pulping under alkaline conditions has advantages. The most notable advantage is the equalization of diffusion rates brought about by the swelling induced formation of transient cell wall capillaries. The capillaries exist in proportion to the amount of alkaline induced fiber swelling, and this swelling is somewhat dependent on the extent of the cook[110]. For instance, the flow through the transient cell wall capillaries is only about 0.01-0.02% of the flow through the pits, with water alone as the swelling agent[53].

The impact of pH on the effective capillary cross-sectional area (ECCSA) was measured by Stone[96], relating rates of chemical diffusion directly to the porosity of the solid medium. The ECCSA is a conductivity resistance ratio. It is obtained by saturating wood with cooking chemical and measuring the resistance to conductivity between platinum electrodes. Likewise, the resistance to conductivity is measured in kraft cooking liquor in the absence of wood. In alkaline processes over pH 12.9, it was concluded that diffusion in the transverse directions was approximately equal to the diffusion in the longitudinal direction. This method of minimizing pulping limitations is unique to the alkaline pulping process[71,72,96,111]. Kraft delignification typically has a starting pH of 13.5-14.0[112].

Diffusion of pulping chemical across the 7 μm fiber wall is clearly much more difficult without alkaline swelling, and would otherwise occur mainly through intertracheid pit membranes. Much research has been performed with regard to alkaline pulping chemical and its mass transfer into wood chips[40,53,101,102, 104]. A comprehensive report of the findings is beyond the scope of this thesis, but it should be noted that alkaline conditions provide superior mass transfer within wood chips at pH values of 12.9 or higher. Therefore, ensuring that the alkali charge is

sufficient throughout the cook should help to exceed diffusion limitations that may otherwise exist under alkali limited conditions.

Steam Pretreatment

Presteaming reduces digester heat-up time, improves chip impregnation, increases chip moisture content, and displaces entrapped air within the chips[52,99,112,113]. Both atmospheric and pressurized conditions can be used to enhance penetration by dissolving some of the pitch that may cause pit aspirations. Theoretical and practical applications of chip presteaming have been investigated by many researchers[40,92,99,111,113,114].

Chip Thickness

Chip thickness and pulping temperature have the greatest effect on pulp heterogeneity, and are directly related to diffusion in wood[3,72,84,87-90,93,94,101,115]. Kulkarni and Nolan[93], and others[72,87], provide data showing that 3-mm is the optimal chip thickness. In other words, chips over 3-mm-thick become nonuniformly pulped. Others have stated that observable nonuniformities occur with chip thicknesses over 2-mm[3,76,88,90,94].

The chip surface area is larger on the top and bottom than on the side, and the distance traveled across the thickness is the shortest for diffusion[112]. Figure 2 is a diagram of a wood chip, illustrating the direction in which chemicals enter the chip.

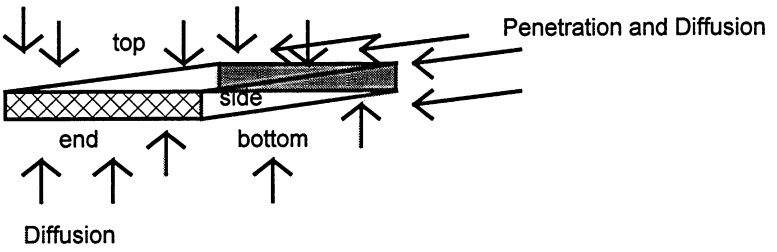

Figure 2. Diagram illustrating chemical entry into a wood chip.

Akhtaruzzaman[72,77] stated that approximately 80% of all kraft pulp mills operate with a majority of chip thicknesses in the range of 3-7-mm. However, oversize chips have been found in varying degrees within pulp mills, ultimately adding to the nonuniformity of the product[15,16].

Chip thickness is fundamental to the process of chip screening and chip quality assessment. Hatton[83] discussed the importance of chip screening while stressing the advantages of lignin content uniformity. Techniques for thorough sampling of chip quality before the chips are unloaded from the delivery trucks are practiced[78], as well as chip quality improvement efforts[79,81]. The disturbing fact is that poor chip quality and uniformity is detrimental to all downline operations, not just pulping[72]. Low quality chips produce a low quality pulp, which may then produce a low quality product. Therefore, assessment of nonuniformity in pulping should really begin at the chipper.

Kraft delignification is an old process. Kleppe[20,21] produced excellent review articles explaining the history and goals of the process. Since that time, much work has been done to improve the quality of kraft pulp, and much is left to do[3,4,116-118]. Manufacturers of commercial digesters recognized the benefits of extending delignification and began to implement the following four basic principles[119-121]: 1) hydroxide concentrations should be kept as low as possible beginning in the early stages; 2) hydrosulfide concentrations should be kept as high as

possible beginning in the early pulping stages; 3) dissolved lignin and sodium concentrations should be kept as low as possible, especially in later pulping stages; 4) temperature should be kept as low as possible, especially at the beginning and end of bulk delignification. Innovations based on these principles exist in the Beloit RDH™ process[122-125], the Ahlstrom-Kamyr MCC/EMCC™ and Kamyr A/B ITC™ processes[126-131], the Sunds Superbatch™ process[132], and the IMPCO Enerbatch™ process[133], now owned by Beloit. The following discussion describes some of the recent work done to improve pulp quality as a function of pulping uniformity in conventional and modified pulping processes.

BATCH DIGESTER STUDIES

A technique that has been used in recent years to assess digester performance is the hanging-basket technique. Blume[27] brought forth the first paper describing specific uses for this technique, and credits the Charleston mill of West Virginia Pulp and Paper Company for introducing the technique in 1950.

MacLeod[4,17,22-26,28,32,35-38] has measured quality in both batch and continuous digesters, where the hanging-basket technique was used to more fully assess uniformity in batch digesters. The major discovery of these studies was that pulp inside a batch digester prior to blowing is capable of having strength values near those of laboratory pulps. After blowing, pulp strength can be 20-30% lower[28,36,37]. Through reapplication of the hanging-basket technique, MacLeod[22,23] was able to identify that strength is primarily lost in the discharge system of batch processes. This observation was unique to softwood operations, whereas hardwoods were considered to be thin-walled and flexible enough to withstand the discharge[1,25,28,32].

Tikka et al.[1,18,29,67] used a three basket array to measure delignification uniformity and strength distribution within batch digesters. Data on both conventional and displacement heating processes were obtained[1,29], along with data on chip thickness effects[18,67]. Conventional cooks displayed kappa number deviations of about 10 units between baskets, whereas Sunds Superbatch™ displacement heating cooks displayed kappa number deviations of 2-4 units between baskets. These results were shown for average kappa values of 19 and 30[1,29]. Chip thickness screening systems were found to reduce rejects considerably. These results led to subsequent batch and continuous digester mill scale studies, where complete fiber lines were switched to modern chip thickness and fines screening[134]. Rejects and knots were reduced by 60 and 70%, respectively. Pulping yield increased by 0.5%, tear strength increased 1 unit at constant tensile, viscosity increased 5%, and 10% less alkali was required in the O_2 bleaching stage for a given kappa reduction[134].

Anderson and Rea[30] used the triple basket technique to measure interdigester and intradigester variability within batch digesters. Both directly and indirectly heated digesters were found to produce a highly nonuniform product, where each exhibited a range of at least 10 kappa units between baskets. Process conditions were improved as a result of the study, where a minimum variability of 2.5 units in the indirectly heated digesters was achieved.

More recently, work has been done by Gullichsen et al.[3], regarding pulping uniformity within a batch digester using a three-tier hanging basket technique. Although past research has shown that chip thickness is critical to pulp uniformity[69-77,90], this work differs from previous studies[1,29,30] in that it relates within chip delignification uniformity to intradigester region using the familiar hanging-basket technique[2,5,103,107,135]. It was found that chips over 2-mm-thick were

nonuniformly pulped. Chips over 5-mm-thick were poorly delignified, resulting in steep kappa gradients across the chips that produced a loss of overall yield and pulp strength.

A method has yet to be developed that has the advantages of the hanging basket technique for continuous digesters. In fact, the only published intradigester studies that have been performed to improve pulp quality in continuous digesters were done over 30 years ago by Knutsson and Stockman[33] and Annergren, Ohrn, and Rydholm[34].

CONTINUOUS DIGESTER STUDIES

Early Kamyr continuous digester systems were inferior to the batch digester systems with regard to strength and ease of beating. Jansson[33,136] of Kamyr AB developed a technique to sample pulp "through-the-wall" of a continuous digester vessel with the hope of obtaining information to improve pulp quality. The discovery was that pulp of very high quality was present prior to discharge from the digester. Jansson's[33,136] sampling technique aided in improving continuous digester pulp quality, ultimately leading to the elimination of the hot blow[33,34].

Since the earlier studies[33,34,136], mills have not been receptive to the idea of drilling a hole through the side of an operating Kamyr continuous digester. Until intradigester sampling is possible, process optimization will need to occur as a result of analyses outside of the continuous digester vessel.

Pulp strength delivery problems still exist among the Kamyr digester systems installed throughout the world in the last 40 years[4]. Virtually all of the softwood cases that have been measured show strength delivery problems, ranging from 60-80% strength delivery based on

laboratory-produced standards[4]. Older vessels show strength deliveries of 70-75%, whereas newer designs can reach the low-to mid-80% range. Modern digester designs continue to have pulp quality problems. In fact, modern digester designs have pulp strengths equal to the older vessels[4]. Many factors need to be evaluated to determine what is causing a reduction in pulp quality, such as mechanical damage, temperature variation in the cook zone, and nonuniform chip movement.

Becker[19] performed pilot plant simulations of conventional continuous cooking and extended modified continuous cooking (EMCC) with various chip thicknesses. A continuous cook with no presteaming gave appreciable rejects with the thicker chips, whereas the EMCC process with presteaming gave negligible rejects, even with the thickest chips. The EMCC pulps were stronger in all cases at kappa numbers comparable to the conventional cooks. It should be noted, however, that continuous digester simulations are similar to batch cooks; plug flow is not simulated under laboratory conditions.

Horng, Mackie, and Tichy[15,16] have published the only data relating interfiber uniformity to continuous digester process conditions. The performances of six Kamyr continuous digesters were evaluated and will be discussed further in the density gradient column section of this paper.

Tikka[137] investigated the results of switching to modern chip thickness and screening systems in continuous digester pulping operations. Based on earlier research[67,134], significant improvements throughout the fiber line were expected. Results were most dramatic in this study: rejects were reduced by 85%, tear strength increased 1 unit at constant tensile, oxygen delignification required less alkali, and brown stock strength delivery increased from 83-89%.

Simulation models have been developed to predict the behavior of kraft pulping processes. Christensen, Albright, and Williams[138], Burazin and McDonough[139], and Gustafson et al. at the University of Washington[2,5,103,107,135,140-142] have developed computer simulation models. Although the simulations provide useful information, they could be further validated with actual uniformity data[3,4].

ON-LINE ANALYSES

On-line analysis systems such as the STFI OPTI-Kappa™ [143] have been implemented to control process conditions and maintain pulp quality. The inability to access pulp from the inside of digesters forces operators to rely on these sensors. At the present time, there are no on-line measurement systems available to measure interfiber uniformity.

Process control in the pulp and paper industry has been improved with the implementation of on-line analysis instruments that monitor the lignin content of pulp exiting the digester and at various points in the bleaching process[142-146]. In addition, conductivity sensors have been made available to monitor the ionic strength of pulping liquor[147-150]. Titrimetric procedures have been used to monitor residual alkali[151], but involve a much longer delay time. The major aim of on-line analysis is to alert operators to variability in process conditions[142,152]. Steps can then be taken to reduce process variability and produce pulps of higher quality[142].

Interestingly, heterogeneity in continuous digester delignification has been observed with the advent of on-line kappa number analyzers[143,152]. A constant fluctuation of at least ± 5-10% in a time scale of tens of minutes has been observed[152], but did not coincide with kappa number

profiles in the pulp obtained at fixed 2-hour intervals. This suggests that mixed stock may mask significant interfiber lignin content diversity.

TASK OBJECTIVES

Process optimization in kraft pulping is a continuous effort with the goal of higher profits and lower environmental impact. It has been shown by some of the most prominent scientists in the industry that measurements of interfiber pulping uniformity can aid in understanding the benefits of cost intensive process modifications. Interfiber uniformity measurements will improve upon the current knowledge of kraft pulping fundamentals, ultimately leading to a better understanding of macroscale pulp quality.

Continuous digesters have the greatest need for pulp uniformity measurements[4,15,16]. Neither intradigester nor intrachip studies are practical for continuous digesters at this time. A method to diagnose interfiber uniformity at the digester discharge will provide useful information and lead to further process optimization in these systems. Furthermore, an investigation of Lo-solids™ pulping[153,154] and Lo-level™ feed[155] process conversions will provide information on state-of-the-art advancements. Lo-solids™ pulping is a process modification that maintains the third principle of minimizing dissolved lignin and sodium content during the residual phase. Multiple "cheater flows" are added to points of circulation to aid in the reduction of dissolved lignin and sodium[154]. Lo-level™ feed is an alternative chip feed system that provides plug flow of wood chips through a presteaming vessel. This modification allows sufficient presteaming of chips under atmospheric pressure, thus eliminating the need for a pressurized presteaming vessel. The result is a system that requires less space, is more flexible, and allows the impregnation stage to operate at lower temperatures.

The following were the objectives of this portion of the thesis work: 1) produce 2.5-mm-thick chip pulps to serve as uniform pulp standards, 2) produce 10.0-mm-thick chip pulps to serve as diffusion-limited nonuniform pulps, and 3) acquire mill-produced pulps from a single vessel continuous digester that has been subject to Lo-solids™ and Lo-level™ feed modifications.

EXPERIMENTAL

Materials

Chemicals

Table 2 lists the necessary chemicals. For common analyses, such as kappa number, viscosity, and ABC titrations, chemicals from the common laboratory supply were used.

Table 2. Chemical listing.

Chemical	Vendor
sodium sulfide, analytical grade	VWR
sodium hydroxide, analytical grade	VWR
sodium chlorite, analytical grade	Aldrich
sodium acetate, analytical grade	Aldrich
sodium thiosulfate, technical grade	Aldrich

Wood Source

The wood used in all laboratory experiments was provided by Georgia Pacific of Madison, Georgia. Rotary cut 0.100 inch-thick (2.5-mm) veneer in 4 ft x 8 ft sheets was produced from the bottom 8 ft section of a 22-year-old loblolly pine for uniform pulping experiments. The inner 4-inch core of the log was excluded in veneer cutting. The middle 8 ft section was used to produce 10.0-mm-thick chips for nonuniform pulping experiments. All chips

were hand-cut to 25-mm in the longitudinal direction, 25-mm in the tangential direction, and well mixed prior to pulping. Chip thickness was based on the radial direction in both the 2.5 and 10.0-mm-thick chips.

Equipment

In addition to a standard MK digester™ arrangement, a presteaming vessel and large dessicator jar were used to presteam and impregnate chips. Figure 3 illustrates the presteaming vessel that was built from 1-inch-thick acrylic and used to displace entrained air within chips with steam.

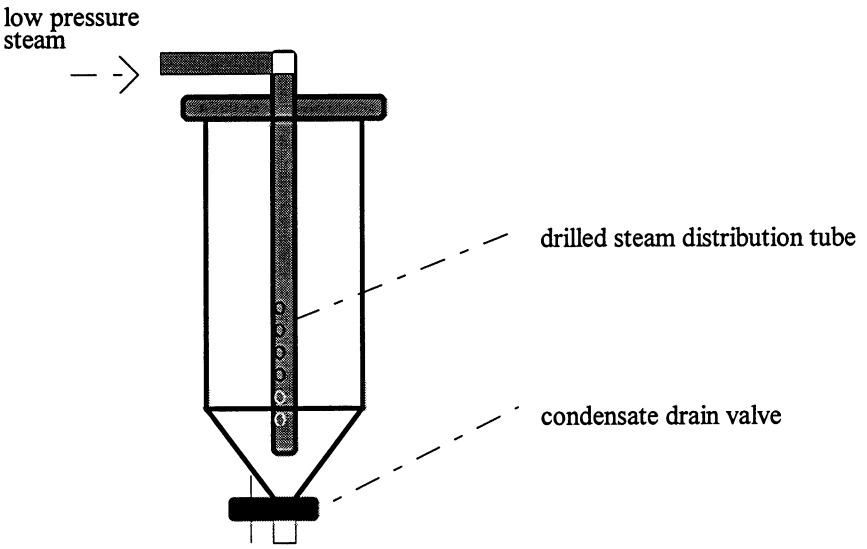

Figure 3. Presteaming vessel.

Presteaming provided a pressure gradient for impregnation when chips were quickly covered by the cooler ambient cooking liquor[40,92,99,111,113,114]. In addition, condensed steam provided a pathway for chemical diffusion while reducing the time required to reach cook temperature and displacing entrapped air[99,52,112,113]. A stainless steel distribution tube was designed to create an equal distribution of steam throughout the chip mass, and a condensate

drain valve was installed to minimize fluctuations in alkali charge from condensed steam. The condensate drain valve was closed immediately after presteaming, and ambient cooking liquor was quickly added to produce the pressure gradient. The chip/liquor slurry was then transferred to the large dessicator jar. If any floating chips were observed, a water aspirator vacuum was repeatedly applied until all chips sank.

Methods

A range of laboratory kraft pulps were produced from 2.5-mm-thick chips and 10.0-mm-thick chips to assess the dependence of interfiber uniformity on diffusion limitations. Pulp lignin contents varied from a maximum of approximately 60 kappa number to the minimum achievable kappa number for each chip furnish. Effective alkali, sulfidity, and liquor-to-wood ratio were held constant at 40 gpl, 30%, and 6:1, respectively.

All pulp samples were produced from 500 g O.D. chips according to the following procedure: 1) presteam chips for 2 hours under atmospheric pressure; 2) implement water aspirator vacuum to assist in chip impregnation when necessary; 3) use a constant EA of 40 gpl for all pulps with L:W ratio of 6:1, corresponding to a 24% charge on wood; 4) use a constant sulfidity of 30% based on AA for all pulps; and 5) vary pulping temperature from 150-170°C to achieve desired H-factors.

Mill-produced pulps were obtained from Gulf States Paper Corporation, Demopolis, Alabama. The pulps originated from the following continuous digester process conditions: 1) conventional feed and conventional cooking; 2) conventional feed and Lo-solids™ cooking[153,154]; and 3) Lo-level™ feed and Lo-solids™ cooking[155].

RESULTS

Laboratory Pulps

Table 3 summarizes information on the laboratory-produced kraft pulps used in this study. A liquor to wood ratio of 6:1 was chosen to enhance mass transfer of cooking chemicals into the hand-cut chips, and percent sulfidity was based on active alkali. All pulps were subject to chlorite holopulping and serve as lignin-free pulp standards for the sample set[156].

Table 3. Description of laboratory pulps.

Parameter	1	2	3	4	7	9
chip thickness, mm	10.0	2.5	10.0	2.5	10.0	2.5
temperature, C	150	150	170	165	160	154
H-factor	548	548	2803	1892	1274	786
kappa number	63.7	54.6	23.4	15.9	33.4	33.9
viscosity, cP	46.07	44.97	16.88	17.19	37.58	
yield, unscreened	0.520	0.442	0.423	0.394	0.482	0.455
yield, screened	0.515	0.442	0.413	0.394	0.474	0.455
time to temperature, min.	60	60	60	60	60	60
time at temperature, min.	240	240	240	240	240	240
L:W=6:1, EA=24% on wood 30% sulfidity (based on AA)						

Mill Pulps

Mill-produced pulps were obtained from Ahlstrom-Kamyr. The pulps originated from the following continuous digester process modifications: 1) conventional feed and conventional cooking; 2) conventional feed and Lo-solids™ cooking[153,154]; and 3) Lo-level™ feed and Lo-solids™ cooking[155]. The pulps were obtained during a series of modifications to a conventional single vessel continuous digester. All pulps were subject to chlorite holopulping to serve as lignin-free pulp standards[156].

Table 4. Description of mill pulps.

Sample	Description	Kappa Number	Viscosity, cP
Kamyr 1964	**conventional feed/conventional cook**	31.4	34.7
Kamyr 832	**Lo-level feed/Lo-solids cook**	24.6	27.3
Kamyr 4170	**conventional feed/Lo-solids cook**	24.1	22.2

DISCUSSION

The pulps in Table 3 came from a set of 15 pulps whose characteristics are further described in Figure 4, Figure 5, and Appendix A. Figure 4 shows that a larger amount of lignin removal occurred at a given H-factor with 2.5-mm-thick chips. The alkali had a shorter diffusion distance to the reaction site, and dissolved lignin was required to leach through a shorter diffusion distance from inside the chip into the cooking medium. Moreover, it is proposed that a wider alkali concentration gradient existed between the outer chip boundary and center for 10.0-mm-thick chips than for 2.5-mm-thick chips[87,72].

Figure 5 shows that pulps from 2.5-mm-thick chips were of substantially higher viscosity than pulps from 10.0-mm-thick chips at a given kappa number. This viscosity difference was assumed to result from overcooking of the chip perimeter relative to the chip center in the thick chips[72,76,90,94,115]. Early research by Hartler et al.[90,94] did not show viscosity differences in the range of 3-7 mm chip thickness, whereas that of Akhtaruzzaman et al.[72,76] and Gullichsen[115] did show that viscosity decreases markedly with an increase in chip thickness at a given kappa number.

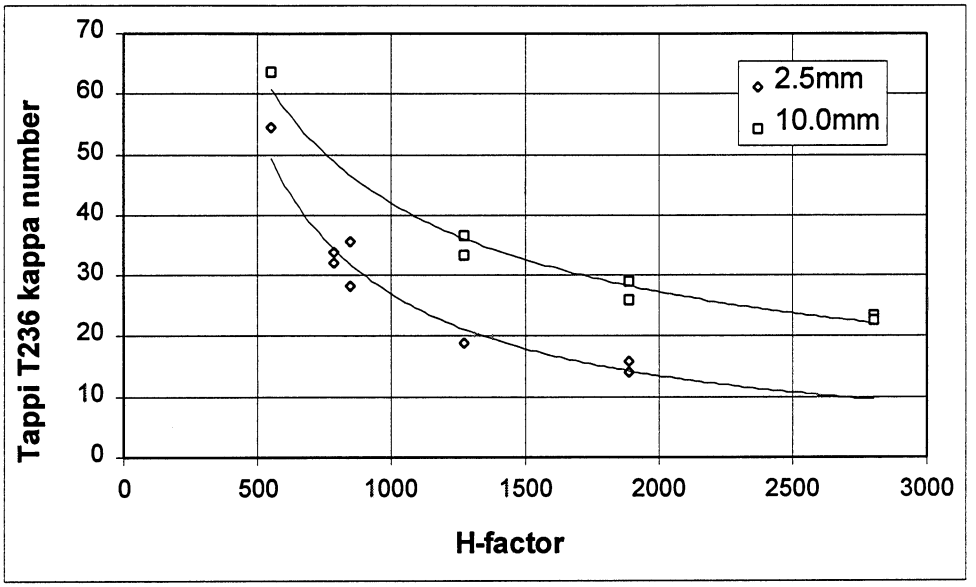

Figure 4. Tappi T236 kappa number vs. H-factor for laboratory pulps.

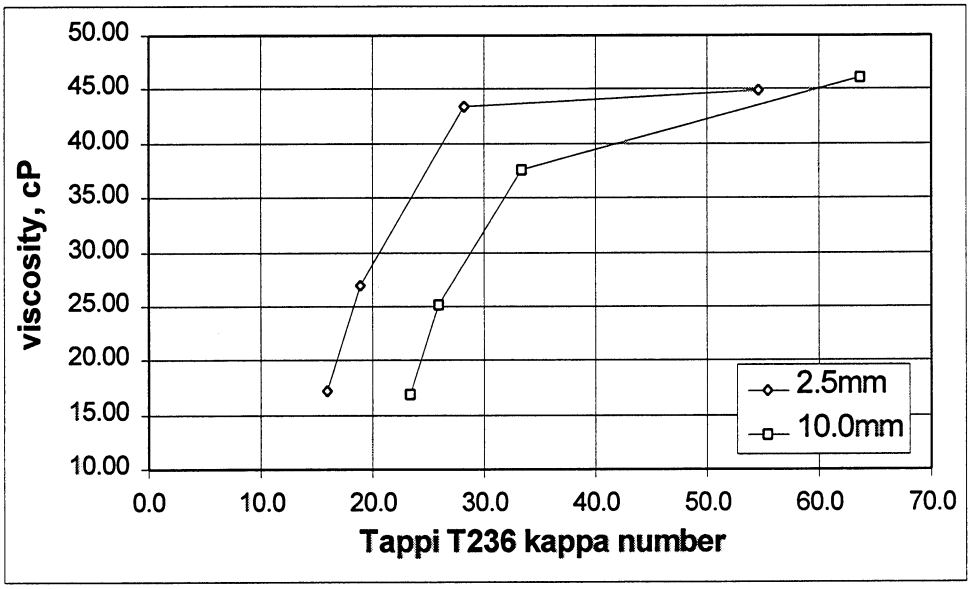

Figure 5. Viscosity vs. Tappi T236 kappa number.

Differences in viscosity and kappa number obtained from extreme differences in chip thickness have shown early evidence of delignification diversity. Density gradient column distributions were successful in providing further insight into kraft pulping limitations.

CHAPTER THREE: DENSITY GRADIENT COLUMN

PRINCIPLES

General Applications

The concept of the density gradient column was first documented by Galileo in 1630 by submerging a ball of wax in a fresh water/saltwater gradient[157]. In 1855, Fick demonstrated the principle of the interdiffusion of miscible liquids. In 1936, Lindstrom and Lange began monitoring chemical reactions in density gradient columns. In the early 1960's, ultracentrifuge techniques were being utilized to disperse macromolecules in density gradients. Oster and Yamamoto[157] provide an excellent review of density gradient techniques and their history.

Density gradient columns are very sensitive instruments used to measure density distributions, and can provide measurements accurate to 10^{-7} g/ml. This resolution is more than sufficient, because the most accurate densities are typically reported to only 10^{-5} g/ml. Essentially, the column is a mixture of completely miscible solvents whose composition varies with column height. Density gradients can be produced by diffusion[157], mixing[157-159], or ultracentrifugation[157].

The density gradient column has many applications. For example, it can monitor the extent of a chemical reaction. Changes in bond type, quantity of isomer, degree of crystallinity, etc. can be measured and related to density changes[157]. The application of most interest in this study is the ability to separate samples as a result of differing component densities.

The textile industry has utilized the density gradient column to assess what type of fibers a textile sample contains. For instance, cellulose acetate, wool, and viscose rayon have densities of 1.27,1.30, and 1.54 g/ml, respectively. A density spectrum of this type can be obtained in 10-15 minutes, allowing for a quantitative analysis of fiber type and distribution[160].

Another technique of interest to the development of the density gradient column involves measurement of the degree of fiber crystallinity. Nickerson[161-163] hydrolyzed amorphous regions of cellulose, and Tessler[160] used this technique and observed an increase in sample density with a decrease in amorphous material. The method was verified by Conrad and Scroggie[164] using x-ray analysis.

Development in the Pulp and Paper Industry

The choice of solvents to use in determining the density of wood cell wall substance has been troublesome for well over a century[165]. From 1862-1914, specific gravity values ranging from 1.45-1.56 g/ml were obtained using aqueous salt solutions[166]. Selective adsorption of salt or water was suspected to occur in the complex porous fibers[165,167].

From 1927-1943, the effect of solvent polarity on measurements of wood cell wall density was investigated. Stamm[165] confirmed variations that arise due to solvent polarity. Polar solvents were found to give higher fiber specific gravity values than nonpolar solvents. The specific gravity of soda boiled cotton fiber was found to be 1.62, 1.55, and 1.57 g/ml for displacement values using water, toluene, and helium gas, respectively. The difference was explained on the basis that water was so strongly absorbed that it became packed on the internal structure and occupies a smaller volume than free water. Nonpolar solvents like toluene were not

adsorbed, and due to their small attraction for wood and comparatively large molecular size, they did not completely penetrate the wood structure[165]. Helium and nonpolar solvents were assumed to enter the wood substance to an equal extent and provided similar displacement density measurements.

In 1946, Hermans[168] developed a method for measuring wood fiber specific gravity in carbon tetrachloride. After taking numerous specific gravity measurements of both dry and water containing cellulose, dry cellulose was assumed to provide the most accurate measurements. Water containing fibers provided higher cell wall density values believed to result from greater solvent penetration. It was previously stated that water molecules could reorient to a density ranging from 1.13-1.25 g/ml within fiber cell walls and result in the increased cell wall densities so often observed[165,167].

In 1964, Yiannos[169] studied the microporosity of wood cell walls. This study indicated a range of cell wall void volumes by comparing calculated apparent cell wall densities. It was estimated that cell wall void volumes ranged from 9.5-51.5%[165]. Differences in cell wall porosity were assumed to exist as a result of pulping and bleaching processes.

In 1966, Wilfong[170], a student of Stamm at N.C. State University, believed that molecular packing due to increased solvent accessibility created differences in displacement density values. He showed that very fine subdivision of wood is necessary to obtain complete removal of air and subsequent penetration by toluene. Toluene displacement density values were found to be equal to helium values. Nonpolar solvents were then considered capable of providing true cell wall densities. Hermans[168] initiated the use of chloroform and carbon tetrachloride in wood fiber

density measurements. Based on the cotton cellulose work of Davidson[171] in 1927, chloroform and carbon tetrachloride can also be considered nonpolar and nonpenetrating solvents.

In concurrence with Wilfong[170], Stone, Scallan, and Aberson[172] used mercury intrusion to obtain cell wall density values that were in excellent agreement with helium displacement values. Of most interest in this study was the effect that freeze-drying had on the cell wall structure. Freeze-dried bleached sulphite pulp from black spruce was compared to solvent exchange dried pulp from the same source. Mercury intrusion pressures of up to 15000 psi were used to determine porosities down to 70 angstroms in diameter. Pore size distributions were very different between the two samples. The freeze-dried sample showed very little presence of micropores, indicating that the freeze-drying process does collapse micropores. In contrast, the solvent exchange dried sample confirmed the presence of micropores with diameters gradually reducing to about 100 angstroms. In fact, mercury intrusion density values for solvent exchange dried fibers were unable to exceed ~1.34 g/ml at 15000 psi, whereas freeze-dried fibers asymptotically approached the helium values of ~1.56 g/ml with only about 200 psi mercury intrusion pressure.

Later in 1966, Stamm and Sanders[173] used the technique of Wilfong[170] to establish a means of determining the holocellulose-lignin content of wood specimens. This was the first effort at estimating wood fiber chemical composition using specific gravity measurements. The main components of wood fiber are cellulose, hemicellulose, and lignin. This investigation proved that specific volumes of cell wall components are additive[173]. Individual measurements of lignin, holocellulose, and alpha-cellulose density with the suspension technique provided densities of 1.335, 1.521, and 1.528 g/ml, respectively. The same values were measured using

fibers with known compositions. From this, Paulson[55] proposed that the density of an unbleached fiber is inversely related to its content of noncellulosic material, especially lignin.

In 1971, Paulson[55] was the first to qualitatively measure interfiber lignin content uniformity. A density gradient column technique based on the flotation method of Hermans[168,174] and the specific volume additivity method of Stamm and Sanders[173] was able to show that chip thickness and reaction wood do contribute to nonuniformity. Compression wood has a high concentration of lignin in the S2 layer, along with interfiber spaces that allow preferential dissolution of middle lamella lignin. Therefore, the extent of S2 layer delignification may vary. Mass transfer limitations were assumed to have produced a chemical gradient in the 6-mm-thick chips, causing a broad fiber density range.

In 1981, Tichy and Procter[6] used Paulson's[55] method to quantitatively measure the effect of lignin content diversity on pulp quality. Lignin content uniformity was found to be wood species dependent, and a relationship did appear to exist between interfiber uniformity and pulp quality[6]. Bleaching chemical demand for a given kappa number reduction increased by as much as 22% in the CE portion of a CEHDED bleaching sequence for nonuniform pulps. Decreases in lignin content uniformity resulted in strength decreases of 6% in brownstock and 16% in fully bleached pulps.

In 1984, Ehrnrooth[175] used carbon tetrachloride and toluene as the nonpenetrating solvent combination in density gradient column measurements of acid-chlorite delignified fibers. Densities of lignin, hemicellulose, and α-cellulose were found to be 1.397, 1.520, and 1.559 g/ml, respectively. The lignin and cellulose values were significantly higher than those reported by Stamm and Sanders[173].

In 1992, Wandelt and Mroz[176] used a thermal density separation technique to estimate pulp yield from NSSC pulps. Pellets of fiber were produced, vacuum impregnated, and allowed to equilibrate with the solvent medium. Temperature ramping was used to vary solvent density, and the density of the pellet was considered equal to the density of the solvent when the pellet began to sink. Yield was then determined as a function of density, where crystalline pulp component densities were assumed to average 1.588 g/ml and amorphous pulp component densities were assumed to average 1.330 g/ml[174,176]. Carbon tetrachloride and chloroform were used as the suspension medium, and results accurate to ±2% were obtained within 1-3 hrs.

In 1985, Horng, Mackie, and Tichy[15,16] provided the most recent utilization of the density gradient column as it pertains to this thesis. The premise of this study was that performance efficiencies have rarely been found to exceed 85%, and interfiber nonuniformities were postulated as a cause for decreased performance efficiencies[15,28]. The ratio of the tear strength of mill-produced pulp to the tear strength of laboratory-produced pulp, at constant tensile, defined the digester performance efficiency. It was shown that a definite relationship existed among pulp strength, liquor flux, and interfiber uniformity in continuous digesters.

Density Gradient Column Limitations

Density gradient columns are known for high accuracy and versatility[157]. Although degree of chemical reaction, extent of crystallinity, etc., can be observed using density gradient columns, the technique has proven to be tedious and provides information only on small samples[6,15,16,55]. Therefore, advancements in this area will now require either improved density gradient column techniques or some alternative method of assessing lignin content on an interfiber basis. This chapter will describe how the density gradient column has been modified to

provide up to four density diversity analyses per week. In addition, the following chapter will describe an attempt at measuring individual fiber lignin content with FTIR microspectroscopy.

TASK OBJECTIVES

Most agree that a negative relationship should exist between pulp quality and lignin content diversity in bleachable grade pulps. An increase in interfiber diversity may result in decreased pulp strength, yield, viscosity, and bleachability. Likewise, an increase in interfiber uniformity would be expected to produce higher strength, yield, viscosity, and bleachability. Improvements in uniformity should assist in producing acceptable pulps of lower lignin content prior to bleaching. The relationship between lignin content and fiber density will allow interfiber kappa number diversity to be quantified in both laboratory- and mill-produced pulps. Ultimately, the goal of this thesis is to provide the pulp and paper industry with a reliable delignification diversity measurement procedure.

Delignification diversity measurements were made using improved density gradient column techniques on thin chip laboratory pulps, thick chip laboratory pulps, and mill pulps. The following were the objectives of the bulk of the density gradient column section of this thesis: 1) establish a sensitive and reproducible procedure while isolating sources of measurement variability; 2) identify measurement variability inherent in kraft holopulps of various process origins to establish variability unrelated to lignin; 3) measure delignification diversity in diffusion-limited nonuniform pulps from 10.0-mm-thick chips; 4) measure delignification diversity in chemical reaction-limited uniform pulps from 2.5-mm-thick chips; 5) measure delignification diversity in mill-produced pulps from various continuous digester kraft

processes; and 6) model delignification diversity distributions to further dilineate distinct differences between process conditions.

EXPERIMENTAL

Materials

Chemicals

Table 5 lists the necessary chemicals for density gradient column analyses. See the following section for special preparation of chemicals.

Table 5. Chemical listing.

Chemical	Vendor
tetrachloroethylene, technical grade	VWR, Fischer
chloroform, technical grade	VWR, Fischer
nitrogen gas, UHP	Air Products
3A, 4A, and 13x molecular sieves	VWR, Fischer
calcium chloride	
calcium sulfate with indicator, Drierite™	Fischer
qualitative filter paper, grade 415	VWR
coulometric single solution	VWR
liquid nitrogen, low pressure	Air Products

Special Treatment of Chemicals

Ultra-high purity $N_{2(g)}$ contains <3.5 ppm water. The gas was further dried by first passing it through a 3 ft x 1/2 inch $CaSO_4$ drying tube and then through a 1ft x 3/4 inch u-tube filled with 13x molecular sieves. Typically, 13x molecular sieves alone provide $N_{2(g)}$ conditions of less than 1 ppb[177]. The $CaSO_4$ was included as an initial drying stage and indicator. The ultra-dry $N_{2(g)}$ was used exclusively and provided an extremely dry environment for transfer and storage of the anhydrous solvents.

Anhydrous C_2Cl_4 and $CHCl_3$ were prepared by storing technical grade solvents over 3A and 4A aluminosilicate molecular sieves for a minimum of two days. The solvents were then filtered through a coarse fritted filter during transfer into a 3 L distillation flask, distilled, transferred, and stored under $N_{2(g)}$. These solvents were initially purified using standard solvent purification procedures[178,179] and regenerated by distillation under $N_{2(g)}$. The distillation column was packed with 6-mm glass beads to a height of 6 inch in the path of the distillate to maximize separation efficiency. The final stage in solvent drying used 1.8 g of grade 415 qualitative filter paper dried under a vacuum better than $5x10^{-3}$ torr for at least 24 hours. Solvents were injected into 2 L side-arm flasks containing the vacuum-dried filter paper and mixed with a magnetic stir bar for an additional 12 hours. These solvents were used for vacuum impregnation and gradient production in the density gradient column.

The solvents were recovered using aspirator vacuum with 8-mm capillary tubing. Calibration beads were also removed using this technique with 2-mm capillary tubing. The solvents were filtered through a 350 ml fritted glass filter to remove fiber and other impurities and then used to flush out any remaining fibers from the columns. Filtered solvents were stored over the molecular sieves in preparation for regeneration through distillation.

Solvent regeneration involved separation through distillation. The distillation apparatus provided excellent separation of the chloroform/tetrachloroethylene mixture. The distillation flask temperature was heated slowly to 60°C to control distillate collection at about 2 drops per second. The final fraction of distillate began separation at approximately 100°C and continued to approximately 120°C. This was indicative of a maximum boiling azeotrope, so the small fraction remaining in the distillation flask was discarded. A chloroform/amylene mixture constituted the

initial low density fraction, whereas a chloroform/tetrachloroethylene mixture constituted the final high density fraction.

All solvent transfers were done through teflon lined tygon tubing, stainless steel needles and cannula, and gum rubber septa to maintain solvent dryness. New septa were always used and secured with copper wire. Drying tubes filled with $CaSO_4$ were used to prevent entrainment of atmospheric moisture during solvent transfers and gradient production, and $N_{2(g)}$ was used for all solvent transfer and storage. Side-arm flasks were equipped with high vacuum teflon/viton stopcocks to avoid use of silicon grease. Molecular sieves were regenerated periodically at 110°C in a drying oven. The filter paper used in the final stage of solvent drying was regenerated using 12 hours of vacuum better than $5x10^{-3}$ torr.

Equipment

Density Gradient Column and Ancillary Equipment

The density gradient column apparatus was of custom design. Although commercial designs and standard technique documentation are available[181], the custom apparatus was designed according to the requirements of this research. A dual column apparatus was designed to expedite analyses, and chloroform and tetrachloroethylene were chosen to form the high density dispersion medium for kraft pulp fibers. Figure 6 and Figure 7 describe components that were combined to provide good optical characteristics for imaging.

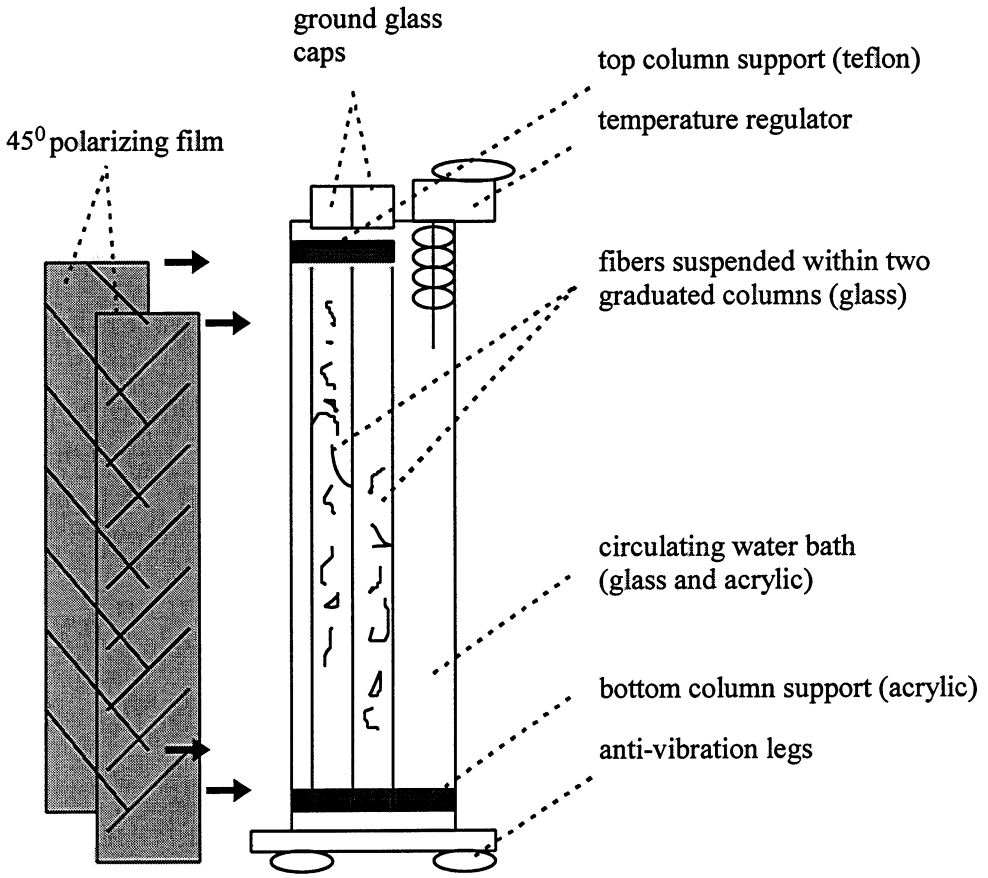

Note:

- Acrylic components that may contact solvents are covered with matching polypropylene sheets.
- Column necks are constricted and held in place with adjustable teflon guides.
- Top and bottom column supports contain stainless steel adjustment screws.
- Anti-vibration legs are attached to an aluminum base.
- Polarizing film is sandwiched between glass panes.
- Two fully adjustable 36 inch fluorescent bulbs are housed in a molded stainless steel shroud and connected to the back of the column for imaging (not visible).
- The drawing is not to scale.

Figure 6. Density gradient column design.

Additional equipment required to form the density gradient is shown in Figure 7. A screw-jack was added to support the filling apparatus, as the high density solvents and apparatus make the combined leverage of this fixture approximately 10 ft*lb at its center.

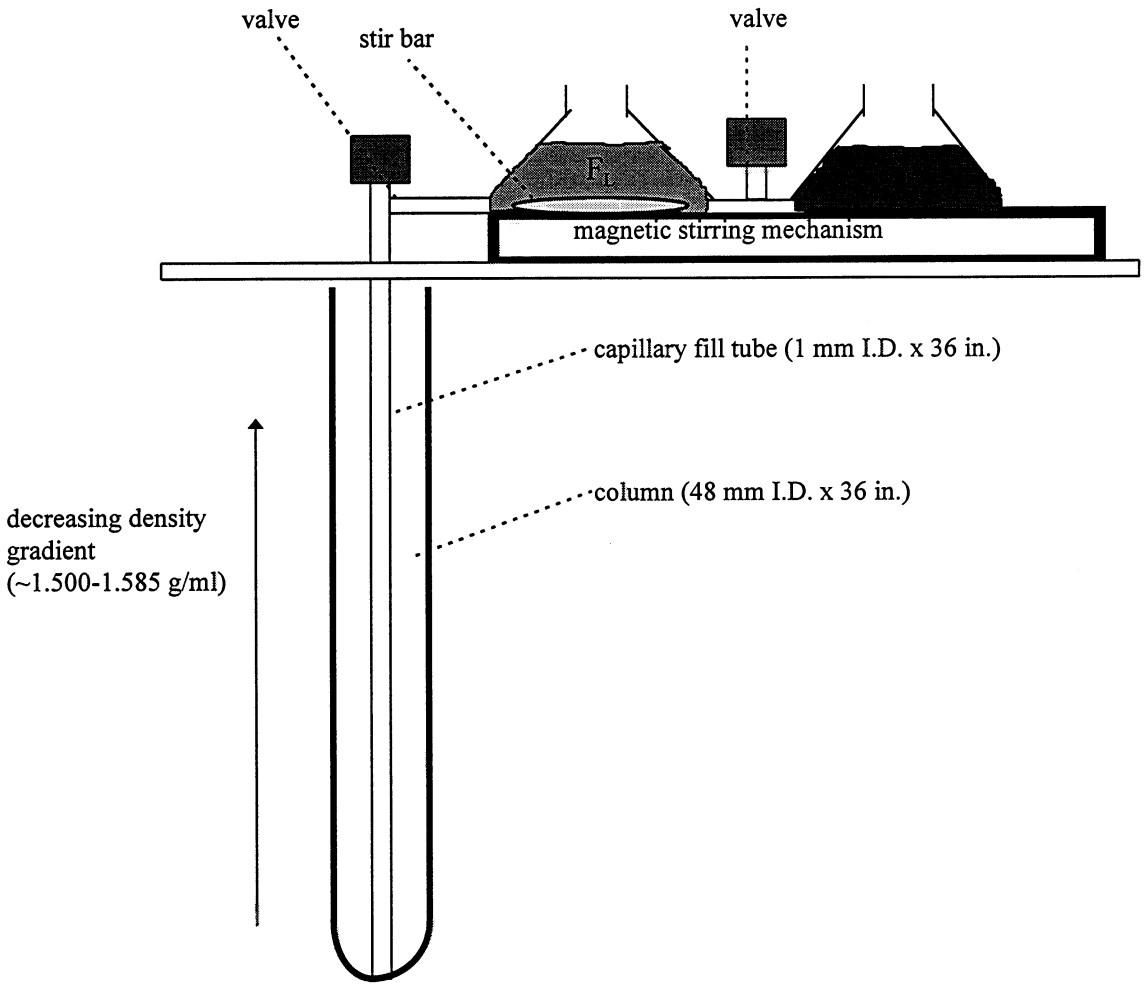

Note:

- Acrylic components that may contact solvents are covered with matching polypropylene sheets.
- The magnetic stirrer platform contains stainless steel adjustment screws for leveling.
- 12 -mm x 5 -mm viton o-ring ball and socket joints are used in connections.
- Teflon/viton o-ring high vacuum valves are used.
- The drawing is not to scale.

Figure 7. Density gradient column filling apparatus.

Additional items necessary for the density gradient column procedure are listed in Table 6.

Development of the density gradient column apparatus and technique was in concurrence with development of an imaging technique. Low quality images of poor reproducibility result in excess propagated error, ultimately affecting the precision of data. The apparatus shown in Figure 8 provided high quality reproducible images.

Table 6. Additional density gradient column components.

Item	Vendor
pycnometer bottles, 10 ml (+/-0.0003 g/ml)	Ace Glass
drying tubes	VWR, Kontes
36 inch x 8 mm glass tubing+3 inch x 0.5 mm I.D. tubing	(in-house)
gum rubber septa	Aldrich
copper wire	Ace Hardware
12, 16, and 18 g luer-lok needles/cannula	Aldrich
teflon sleeved tygon tubing	Aldrich
1 ft x 3/4 inch glass u-tube	Lilly Glass
graduated drop funnel	Kontes
200 ml filter funnel with 24/40 joints	Kontes

Digital images were obtained using an Electrim EDC1000U monochrome computer camera linked to a personal computer. The camera used a 12.5-75.0-mm focal length zoom lens and produced high resolution images in an 1134 x 972 interlaced mode or 1134 x 486 noninterlaced mode. Moreover, the camera software could perform a multitude of image enhancements to assist in obtaining high quality images for image analysis. Vashaw Scientific, Inc.[180] provided state-of-the-art video equipment and expertise for preliminary testing of this particular application. Optimas™ image analysis software was used to determine projected fiber area.

Methods

The density gradient column apparatus consists of a water bath containing two 2 inch x 36 inch columns graduated in centimeter intervals to indicate sample position. The columns were maintained at 23.0 ±0.2°C and calibrated with glass beads accurate to ±0.0002 g/ml by certification[181]. Column production was a strict anhydrous procedure to control experimental error. Solvent water concentrations were monitored through Karl Fischer titrations using an

Aquastar Model C3000 Karl Fischer Titrator[182]. APPENDIX B contains an explanation of the Karl Fischer titration in water analyses[178].

Density Gradient Column Imaging Apparatus and Data Analysis Software

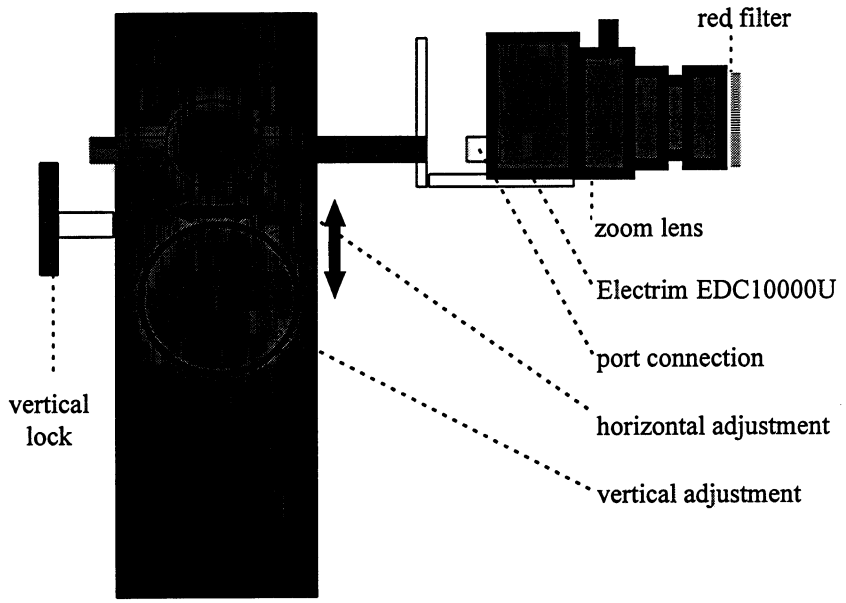

Imaging arrangement:

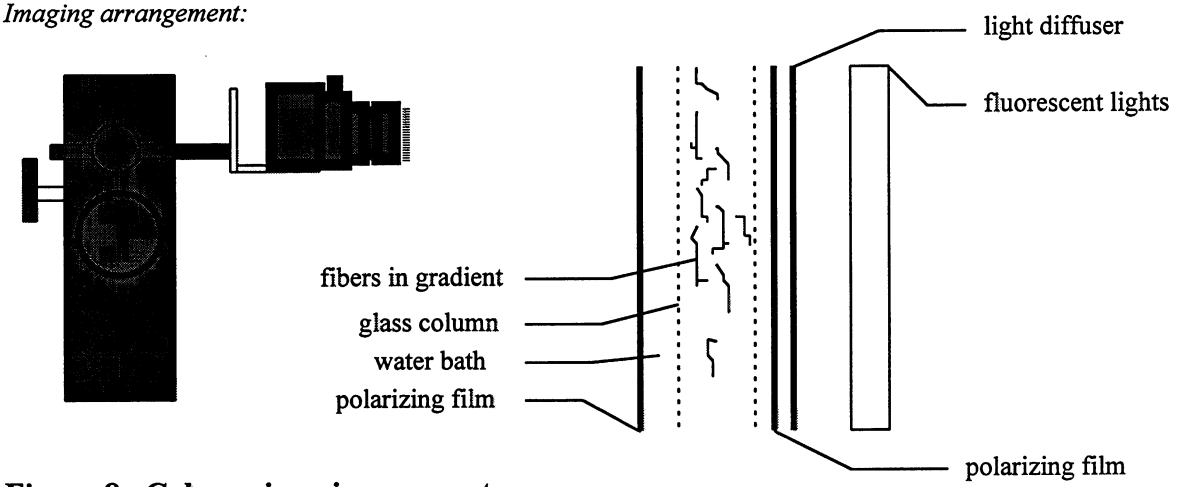

Figure 8. Column imaging apparatus.

Fiber Preparation

Approximately 5 g O.D. pulp was taken from well-mixed brownstock, freeze-dried from water for 48 hours and stored in a dessicator filled with $CaSO_4$. A 1-2 mg fiber sample was then removed and vacuum-dried for 24 hours at vacuums better than $5x10^{-3}$ torr in 250 ml side-arm

flasks. Concurrently, two 1.8 g O.D. sheets of filter paper were vacuum-dried from the same source for a minimum of 12 hours in separate 2 L side-arm flasks for use in the final solvent drying stage. An aliquot of 40 ml anhydrous chloroform was filtered through a teflon syringe filter and injected into the 1-2 mg of vacuum-dried fiber under vacuum. Freshly prepared anhydrous chloroform was used to impregnate the vacuum-dried pulp fiber. The 100 ml glass syringe, 18 g needle, and teflon syringe filter were initially dried by repeated flushing with impregnation solvent. All fiber samples were allowed to remain under vacuum until the moment of impregnation to avoid vacuum fluctuations.

At the moment of impregnation, the glass manifold stopcock was closed to avoid transfer of chloroform vapor into the vacuum system. Being especially careful to not transfer an entrained air bolus, the syringe filter was removed and the septa was pierced to introduce impregnation solvent. If the impregnation solvent and fibers were extremely dry, complete dispersion of the fibers could be achieved using a standard 1inch magnetic mixing bar with minimal shear for approximately 30 minutes. Flocculated samples could take up to12 hours to disperse. Care was taken to avoid "hammering" of the magnetic stir bar on the side-arm flask walls to reduce the risk of fiber breakage.

Column Production and Imaging

The density gradient columns were initially dried with a high flow rate of $N_{2(g)}$ through 36 inch x 8-mm glass tubing prior to gradient production. A low flow rate of $N_{2(g)}$ was applied for at least two hours to desorb water molecules from the glass column walls. The glass tubing was fitted to the empty density gradient columns with rubber stoppers, and $N_{2(g)}$ flow was regulated by a 3 inch x 0.5-mm capillary tube fixed into the rubber stopper. Likewise, the column filling

apparatus was flushed for at least 15 minutes. Viton o-ring ball joints were designed for all filling apparatus connections to avoid use of silicon grease.

Column production required preparation of two solvents, F_L and F_D, to establish the density range appropriate for the samples under investigation according to standard column formation procedure[181]. The F_L solvent was of low density, and the F_D solvent was of high density. After establishing the desired density range, the anhydrous solvents were transferred through a fritted filter into a graduated 1 L 24/40 dropping funnel. Both erlenmeyer flasks were capped with $CaSO_4$ drying tubes to prevent entrainment of moisture during gradient production.

The impregnated fiber samples were poured into pre-dried density gradient columns through 36 inch x 9-mm glass tubes fitted with 24/40 joints. The ground glass joints fastened to the side-arm flasks and facilitated transfer of slurried fiber into the columns without atmospheric moisture adsorption. The high and low density gradient solvents were volumetrically transferred with a graduated dropping funnel into the gradient production flasks. The density gradient was then formed under the 40 ml fiber slurry through 36 inch x 1.0-mm glass capillary tubing using the "slip-under-method"[55,157]. Production of the gradient took approximately 1 hr 10 minutes following introduction of the impregnated fiber slurry.

Data aquisition and analysis was accomplished using high resolution digital images obtained using an Electrim EDC1000U monochrome camera in the noninterlaced mode with digital averaging through a personal computer. Images were obtained using cross-polarization techniques, and a red lens filter was used to reduce transmission of unpolarized light. Image averaging and enhancement capabilities of the digital camera reduced dark current artifacts. The columns were photographed in 9 cm x 9 cm frames and image analyzed for projected particle

area in 1 cm vertical increments to maximize frame usage and resolution of data. Optimas™ image analysis software provided measurements of projected area to correlate with column position in 1 cm column increments. Manual threshold settings were used to separate real images from artifacts. Local adaptive background filtering was occasionally used, however, the optical techniques developed in this thesis resulted in excellent original image quality.

The plots of incremental fiber area vs. column position were normalized through trapezoidal approximations to a total integrated area of unity. These histograms were modeled using two normal distributions through minimization of the χ^2 goodness-of-fit parameter[253]. Distribution A was first modeled to a minimum χ^2 value while neglecting the lower density tail. The lower density tail was then modeled by distribution B. The six parameters that controlled the composite normal distribution were manually iterated to minimize the overall χ^2 parameter and model density diversity within the overall distribution. Individual fiber densities were converted to density gradient column kappa numbers through the secondary analysis.

To calculate measurement error inherent in image acquisition and analysis, a mill-produced kraft brownstock and its respective kraft holopulp was photographed three times by initially centering directly in front of the image for the first set. The second and third image sets were taken by rotating the camera to the left and right approximately 5 degrees. Each set was image analyzed, where the means and standard deviations were compared in Table 13. In order to distinguish sampling error from overall random error, kraft holopulps were produced from 2.5-mm-thick chip pulps, 10.0-mm-thick chip pulps, and mill pulps. Table 10 and Table 11 compare random error inherent in both brownstock and holopulp analyses.

RESULTS

The following discussion provides pulp fiber density measurements using a suspension technique[166] with various solvents. Solvent selection is discussed while further elaborating on experimental techniques of water concentration measurements, anhydrous solvent preparations, fiber preparations, production of density gradient columns, data and error analyses, and the image acquisition and data analysis technique. Measurements of delignification diversity are then provided for the laboratory pulps and mill pulps.

Solvent Selection

An early examination of solvent combinations led to the use of nonpolar solvents. Table 7 provides the densities of 30 kappa number brownstock softwood fibers and bleached softwood fibers obtained using a suspension method[166] with a variety of polar and nonpolar solvent combinations. Fibers were dispersed in solvent mixtures of predetermined densities and allowed to equilibrate overnight. Solvent mixture densities were varied until floating fibers sank or until fibers that have sunk begin to rise. Average fiber densities were then estimated.

Table 7. Fiber densities as determined by various solvents using the suspension method.

sample	solvent combination	density (g/ml)
30 kappa number softwood brownstock	solvent exch. Acet. to Cl_3EtOH to $CHCl_3/C_2Cl_4$	1.522
	Cl_3EtOH, CCl_4	1.599
	Cl_3EtOH, Br_3CH	1.610
	EtOH, CCl_4, Cl_3EtOH, Br_3CH, H_2O	1.618
	$Zn(NO_3)_2$	1.616
	CsCl	1.670
bleached softwood fiber	solvent exch. Acet. to Cl_3EtOH to $CHCl_3/C_2Cl_4$	1.532
	$Zn(NO_3)_2$	1.630
	CsCl	1.672

When varying the solvent composition, or solvent polarity in the case of Table 7, cell wall density measurements also vary. In fact, a comparison of the density obtained using the EtOH, CCl_4, Cl_3EtOH, Br_3CH, H_2O suspension medium to the density obtained using the aqueous inorganic $Zn(NO_3)_2$ suspension medium shows little difference. The reliance of fiber density on solvent polarity has been verified in Table 7, and strict adherence to nonpolar solvents is necessary. Any attempts at altering solvent densities with the use of polar solvents will be detrimental to experimental reproducibility. Chloroform and tetrachloroethylene were chosen for all subsequent experiments.

Water is a very polar molecule and its concentration in the atmosphere varies. The abundance of water in typical laboratory conditions has created the need to monitor the presence of water in the solvents used for density gradient column work. Anhydrous conditions can be difficult to achieve and maintain, and fiber density appears to vary considerably in the presence of small quantities of water.

Karl Fischer Analysis

Most of the water present in the organic solvents was removed using standard solvent purification procedures[178,179]. However, solvent regeneration through distillations, storage, and handling of solvents can result in gradual accumulation of water. The anhydrous solvents used in this study were guaranteed to contain less than 50 ppm water. This implies that a 3:1 ratio of water to fiber would still remain in a 40 ml dispersion slurry. The hygroscopic nature of wood fibers suggests that water may adsorb to kraft pulp fibers even at these low water concentrations[174]. Data to support this assumption was necessary.

Table 8 provides data used to estimate the miscibility of chloroform and tetrachloroethylene with water. Water concentrations ranging from commercially available anhydrous grade solvents to water saturated solvents were measured to determine solvent/water miscibility, the efficiency of solvent drying and precision of the Aquastar Model C3000 Karl Fischer Titrator[182].

Table 8. Karl Fischer titration data for a wide range of solvents.

Sample	1 (ppm)	2 (ppm)	Average (ppm)	Deviation (ppm)	Description
A	20.6	19.4	20.0	0.8	molec.sieved C2Cl4 from ambient distillation
B	65.1	66.9	66.0	1.3	molec.sieved CHCl3 from ambient distillation
C	14.9	14.2	14.6	0.5	molec.sieved C2Cl4/CHCl3, pre-distillation
D	38.7	40.7	39.7	1.4	Stock tech-grade CHCl3
E	193.5	193.6	193.6	0.1	CHCl3 from top of DGC column (3weeks)
F	4.9	4.6	4.8	0.2	"anhyd."CHCl3
G	13.5	13.9	13.7	0.3	"anhyd."C2Cl4
A'	8.8	8.8	8.8	0.0	'A' into vac.dried paper
B'	15.4	13.9	14.7	1.1	'B' into vac.dried paper
C'	1.9	4.6	3.3	1.9	'C' into vac.dried paper
I	24.1	25.6	24.9	1.1	"anhyd."CHCl3
II	78.8	69.2	74.0	6.8	"anhyd."CH3OH
III	688.5	698	693.3	6.7	water saturated CHCl3
IV	203.6	200.2	201.9	2.4	water saturated 50%CHCl3+50%C2Cl4
V	78.9	70.1	74.5	6.2	water saturated C2Cl4

Samples A through C represent pre-distillation and post-distillation water contents from solvents that were stored over molecular sieves. The 66 ppm water concentration in freshly distilled chloroform has the potential of creating large variations in average fiber density and demonstrates the need for dry $N_{2(g)}$ conditions during the distillation process. Samples D and E represent a chloroform source used for fiber impregnation, and the water content of the same solvent after three weeks residence time in the density gradient column. This demonstrates the potential of chloroform to collect water from ambient air, or possibly from the column walls during filling. Samples F-V represent purchased anhydrous grade solvents, anhydrous solvents prepared by drying with vacuum-dried filter paper, and water saturated solvents.

Vacuum-dried-cellulose was capable of drying solvents to a lower average water content than commercially available solvents. Furthermore, while chloroform has been shown to have a much higher water saturation point than tetrachloroethylene, the saturation point was not additive. The presence of tetrachloroethylene reduced the relative saturation point of the chloroform/tetrachloroethylene mixture. Therefore, it was useful to always keep some tetrachloroethylene mixed with the chloroform to reduce water adsorption.

The sensitivity of the density gradient column technique required a high precision in the water analyses. Aquastar Model C3000 titrations were of high precision, as shown in Figure 9. The standard deviation in water concentrations averaged ≤ 1 ppm in the range of interest for this thesis work. It was suspected that the efficiency of anhydrous solvent preparation was related to the ratio of solvent to vacuum-dried fiber. Figure 10 illustrates how the efficiency of water removal is doubled when decreasing the solvent to paper ratio by a factor of five.

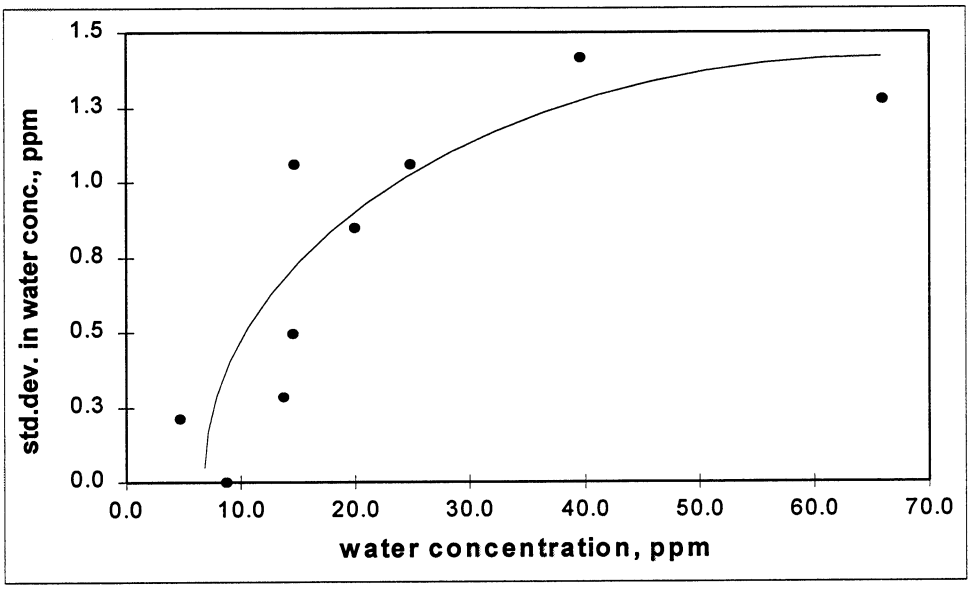

Figure 9. Precision of Karl Fischer titrations.

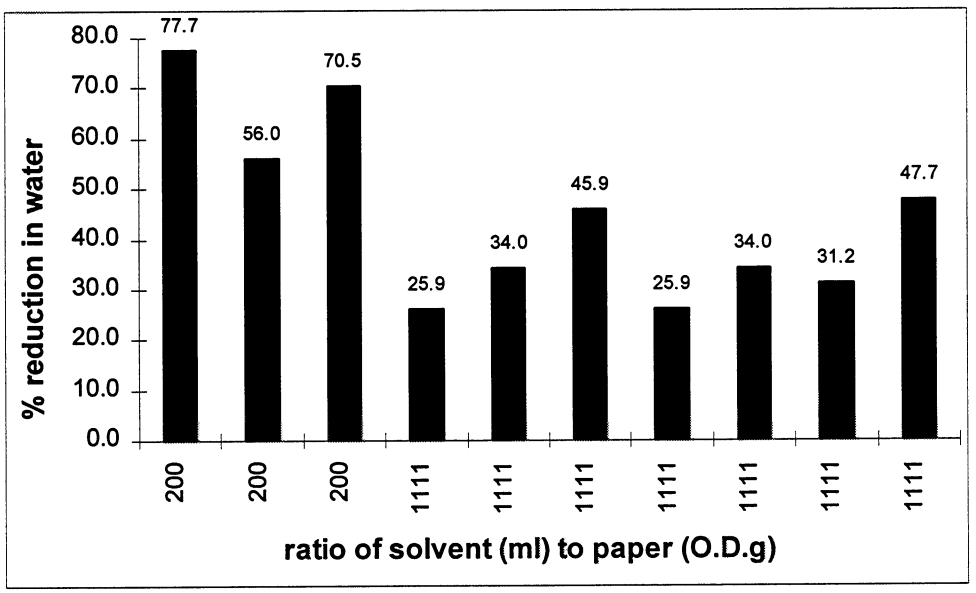

Figure 10. Solvent drying efficiency as related to the solvent/vacuum-dried paper ratio.

Table 9 contains data for Figure 10 and also includes calculations of the water adsorption capacity of cellulose fibers. It was possible to reduce solvent water concentrations by 26-78%. The extent of water removal appears linearly related to the initial solvent water concentration and

the ratio of solvent to vacuum-dried fiber. This finding suggests that multiple stages would be more effective in drying solvents; however, a single stage was used to minimize procedural time requirements. A solvent to vacuum-dried fiber ratio of 1111:1 was used in this thesis for drying of all solvents.

Table 9. Water adsorption capacity of vacuum-dried filter paper in $CHCl_3$ and C_2Cl_4.

sample	solvent (ml)	vac-dried paper (g O.D.)	solv/paper ratio	initial water (ppm)	final water (ppm)	ppm water adsorbed (ppm)	water uptake 150ml solvent (µg)	reduction in water (%)	fiber uptake % water (water/fiber)	correlation coefficient init.wat. vs. %uptake (R^2)
CHCl3	150.0	0.75	200	**65.8**	14.7	51.2	11508.8	77.7	**1.53**	
CHCl3	2000	1.8	1111	**28.3**	15.3	13.0	26000.0	45.9	**1.44**	
CHCl3	2000	1.8	1111	**18.5**	13.7	4.8	9600.0	25.9	**0.53**	
CHCl3	2000	1.8	1111	**18.5**	13.7	4.8	9600.0	25.9	**0.53**	
CHCl3	2000	1.8	1111	**9.7**	6.4	3.3	6600.0	34.0	**0.37**	
CHCl3	2000	1.8	1111	**9.7**	6.4	3.3	6600.0	34.0	**0.37**	**0.727**
C2Cl4	150.0	0.75	200	**20.0**	8.8	11.2	2520.0	56.0	**0.70**	
C2Cl4	2000	1.8	1111	**13.2**	6.9	6.3	12600.0	47.7	**0.34**	
C2Cl4	150.0	0.75	200	**11.0**	3.3	7.8	1743.8	70.5	**0.23**	
C2Cl4	2000	1.8	1111	**9.3**	6.4	2.9	5800.0	31.2	**0.32**	**0.868**

Although some applications of the density gradient column may not be water sensitive, wood fiber density measurements have proven to be extremely sensitive to water[168], especially when discerning between such small differences in interfiber density. Because of this fact, implementation of Karl Fischer analyses to monitor solvent drying efficiency and solvent handling techniques was necessary to density gradient column production.

The relationship between residence time and water removal for a single drying stage is given in Figure 11. All solvents were allowed at least 12 hours residence time following injection of distilled solvents into vacuum-dried filter paper. Chloroform lost about 36% of its water in the first 5 hours, whereas the tetrachloroethylene lost approximately 23%. After 30 hours, both solvents had lost about 46% of the total water present.

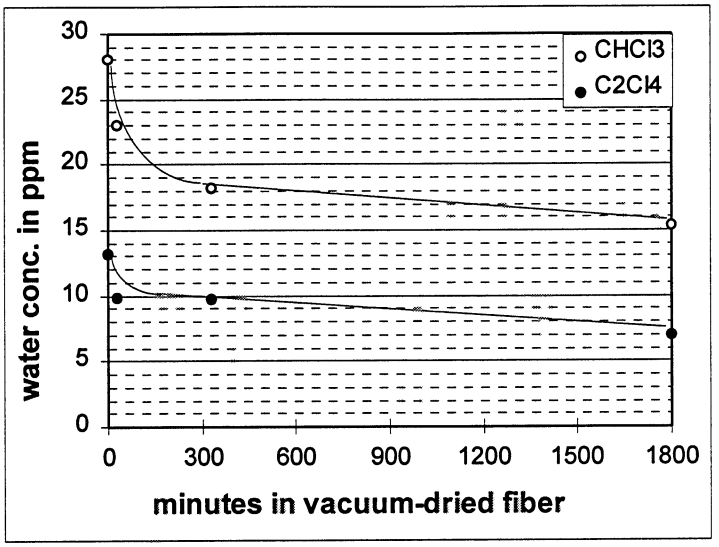

Figure 11. Solvent drying efficiency as related to residence time.

It was no less important to transfer the dry solvents into a dry apparatus. The presence of a water concentration profile in the density gradient column prompted development of the column drying procedure. It was postulated that the low density solvent collected water from the column walls during gradient production. Therefore, a high flow rate of $N_{2(g)}$ was used to evaporate residual water from the column walls following removal of existing solvent and fiber. Figure 12 illustrates the success of the column flush technique.

Production of Anhydrous Solvents

Strict anhydrous handling of purified chloroform and tetrachloroethylene was found to be of paramount importance to density gradient column reproducibility. The chloroform of choice was stabilized with amylenes. Amylenes represent a class of butenes that are nonpolar in character, whereas the more typical use of ethanol as a chloroform stabilizer introduces an uncontrollable level of polar material that can adsorb to the kraft pulp fibers. Tetrachloroethylene does not require a stabilizer.

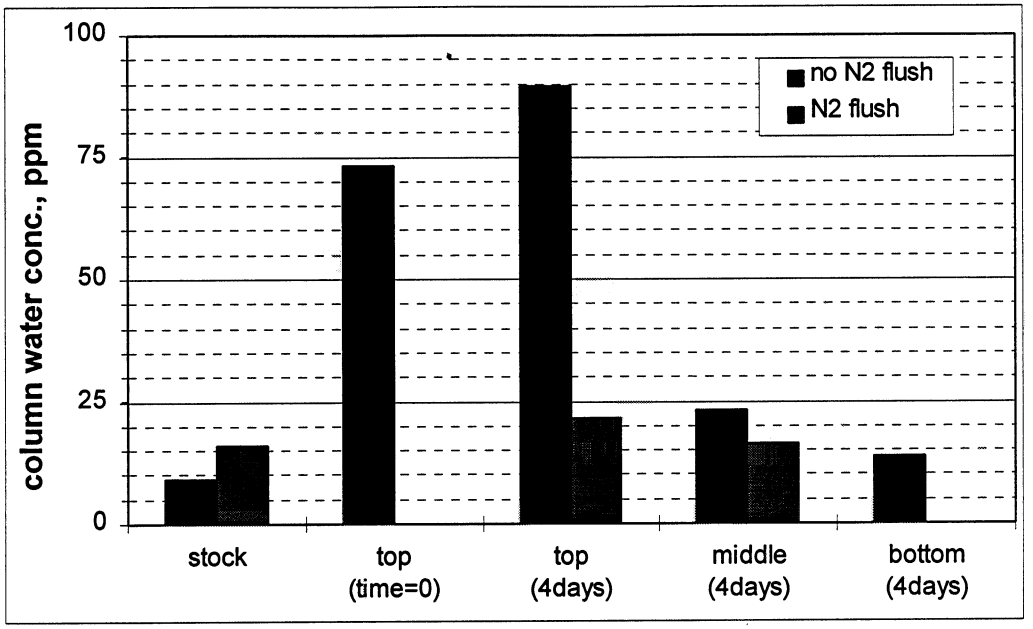

Figure 12. Elimination of the water profile in columns using an ultra-dry $N_{2(g)}$ flush.

Water contents of technical grade solvents have been found to vary from 40-80 ppm in stock chloroform, and from 20-30 ppm in tetrachloroethylene. Anhydrous solvents can be purchased and have been observed to vary in water content from 5-25 ppm for chloroform. Careful anhydrous handling of solvents resulted in controllable water contents of 10-25 ppm in chloroform and 6-15 ppm in tetrachloroethylene.

It is important to assess the accuracy and precision of experimental data. As a result, early error assessments resulted in successful efforts directed towards reducing experimental error through anhydrous distillation, anhydrous handling of solvents and fiber, and impregnation of fibers at vacuums better than $5x10^{-3}$ torr. However, it becomes equally important to interpret the data correctly. Early attempts at modeling fiber density vs. Tappi T236 kappa number histograms resulted in the development of a composite normal distribution. It was postulated that two distinct density distributions may exist within kraft pulps as a result of mass transfer

limitations. The following discussion provides the data analysis that led to verification of the model.

Data Analysis

A simple test can be used to verify a normal distribution fit, as well as any other type of model fit. The Chi-square (χ^2) goodness-of-fit test compares observed values to values from a model fit and is defined as follows:

$$\chi^2 = \sum \left[\frac{(o_i - e_i)^2}{e_i} \right] \tag{3}$$

where the summation is carried through $i = k$ cells with $\nu = k-1$ degrees of freedom; o_i is the observed response from actual data, and e_i is the expected response from the simulated normal distribution model data.

Most fiber frequency vs. density histograms did not fit a single standard normal distribution at the $\alpha = 0.05$ confidence level, according to the χ^2 parameter. However, a linear regression between the observed incremental area data and the corresponding values obtained from normal distributions did suggest a high correlation in many cases. It was not uncommon to see distributions with observed vs. expected correlation coefficients of 0.99 and greater fail the χ^2 goodness-of-fit test. For example, Figure 13 relates observed data to predictions based on a normal distribution. The normal distribution shown has a mean density and standard deviation in mean density equal to that of the observed distribution. A perfect fit between observed and expected data would provide a slope of 1, intercept of 0, and correlation coefficient of 1. Even though the fit appears excellent, the χ^2 value rejected the single normal distribution model. This

is due to the fact that the χ^2 goodness-of-fit test normalizes the difference between observed and expected values. Furthermore, probability tabulations are sensitive to degrees of freedom. Therefore, the differences between observed and expected values are scaled according to relative importance within a given distribution.

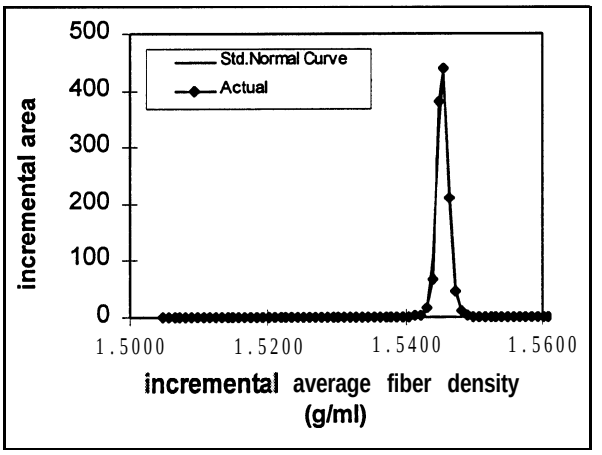

actual data vs. normal data

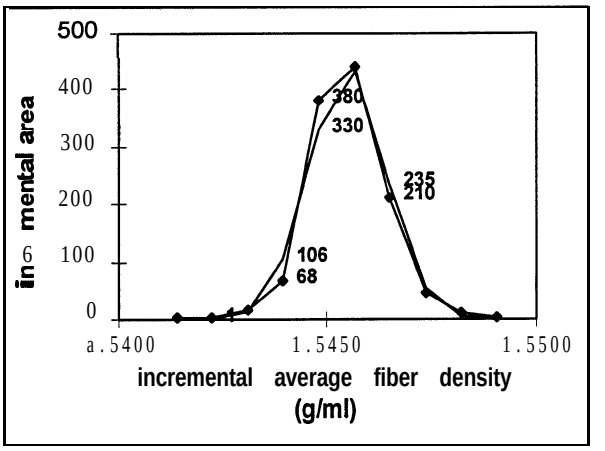

actual data vs. normal data-enlarged

Parameter	actual data
Total χ^2	24.84
Max χ^2 value	13.69
d f	6
acceptable*& α=0.05	12.59
acceptable χ^2, α=0.01	16.81
slope, intercept, R^2	**0.941,-0.0016, 0.990**

"Max χ^2 value" refers to the maximum χ^2 point difference.

Figure 13. Chi-square analysis of kraft holopulp fitted to a normal distribution.

In Figure 13, the sensitivity of the χ^2 goodness-of-fit test became evident when the seemingly good fit did not meet generally accepted χ^2 parameters. Thus, data modeling should be very well controlled through minimization of the χ^2 parameter.

It was postulated that brownstock density distributions may be comprised of two distributions: one distribution may arise from chemical-reaction-limited conditions and the other may arise from diffusion-limited conditions. In light of past research, a mass transfer limitation

must exist where delignification rates decrease and delignification diversity can be expected to increase[1,2,3]. It is at this point that a second normal distribution may begin to develop. The hypothesis appears supported; however, it is not clear that distribution A is purely controlled by chemical reaction limitations and that distribution B is purely controlled by diffusion limitations.

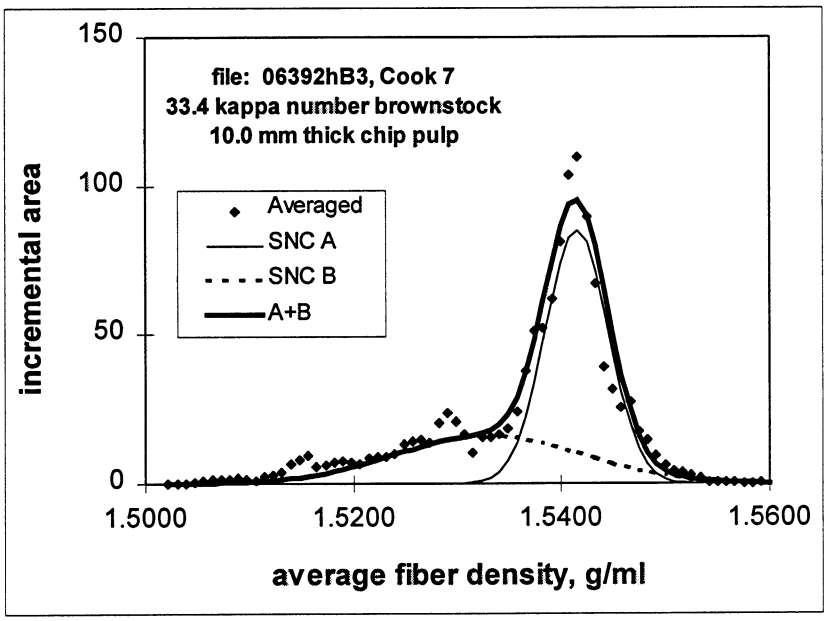

normal curve	A	B
average fiber density	1.5415	1.5330
standard deviation	0.0027	0.0090
fraction of SNC	0.63	0.37
Total χ^2	46.9	
Max χ^2 value	11.0	
d.f.	37	
acceptable χ^2, α=0.05	52.19	
acceptable χ^2, α=0.01	59.89	
kappa number	33.4	
chip thickness, -mm	10.0	

"expected" and "A+B" refers to the normal distribution modeling.
"SNC" refers to the standard normal curve component.
"Max χ^2 value" refers to the maximum χ^2 point difference.

Figure 14. Identification of the composite normal distribution fit.

Figure 14 illustrates how data from a centered-three-point-moving average helped to identify that brownstock distributions are modeled well using two normal distributions. The sum of the two curve fractions equals a total arbitrary area of one for the normalized composite

distribution. This method allowed for an easy estimate of the percent contribution of component distributions. APPENDIX B provides proof that the model can be fit to smoothed data to achieve a fit within χ^2 parameters at the α=0.01 level for nearly all distributions. Those distributions that did not fit according to stated probability parameters were very close and certainly were good fits qualitatively.

Data smoothing removed "noise" that may have been due to occasional flocculations of variable size. The smoothing procedure was used only to identify the trend and fit χ^2 parameters to the normalized composite distribution. The centered three-point moving average was chosen because it had a minimal effect on parameter estimation, whereas use of more data points in the moving average may tend to artificially mask otherwise apparent trends. It should be noted, however, that data smoothing does not meet with universal approval, and for a rigorous estimation of parameters it is neither desirable nor permissible.[183] Therefore, only actual data will be used to illustrate and report average fiber densities, standard deviation in average fiber densities, and secondary analyses of individual fiber kappa number. Figure 15 compares a trend of actual data to the smoothed data obtained using a centered-three-point-moving average.

The independently derived values of Figure 15 are identical with respect to average fiber density and standard deviation for distributions A and B for both averaged and actual data. A negligible difference exists between component contributions for actual and averaged data. This suggests that two normal distributions may model the distributions well, and that noise may be responsible for the large χ^2 parameter calculated from unaveraged data. Values of overall average fiber density and overall standard deviation in average fiber density have been calculated using the second moment about the mean of the "A+B" modeled distributions.

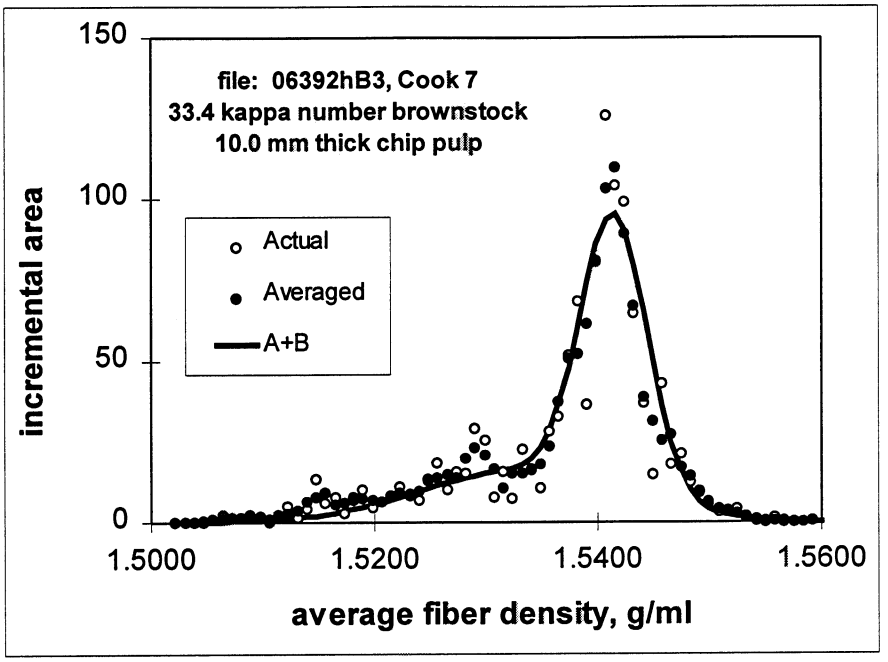

	Averaged Data		Actual Data	
Total χ^2	**46.9**		**126.4**	
Max χ^2 value	11.0		23.0	
d.f.	37		33	
acceptable χ^2, α=0.05	52.19		47.40	
acceptable χ^2, α=0.01	59.89		54.78	
	distribution A	distribution B	distribution A	distribution B
average fiber density	1.5415	1.5330	1.5415	1.5330
standard deviation	0.0027	0.0090	0.0027	0.0090
fraction of total	0.64	0.36	0.63	0.37

"Actual Data" refers to unaveraged data and "A+B" refers to the model estimation.
"Max χ^2 value" refers to the maximum χ^2 point difference.

Figure 15. Relation between actual data and data from three-point moving average.

Application of the Composite Normal Model

The function for a model containing two normal distributions is as follows:

$$F(x) = \frac{1}{\sqrt{2\pi}}\left[\frac{f_A}{S_A}\exp\left\{-\frac{1}{2}\left(\frac{x-\overline{x_A}}{s_A}\right)^2\right\} + \frac{f_B}{S_B}\exp\left\{-\frac{1}{2}\left(\frac{x-\overline{x_B}}{s_B}\right)^2\right\}\right]. \qquad (4)$$

The model divides the overall normalized distribution into two components, distribution A and distribution B, where $f_A + f_B = 1$. These fractional contributions for distribution A and

distribution B provide a novel method of analyzing the physical nature of the kraft pulping process. The mean and standard deviations for the component distributions were given by $\overline{x}$ and s, respectively.

Fitting data to the model involved manual iteration of f_A, $\overline{x_A}$, and s_A until the Chi-square parameter was minimized for one normal distribution. The "tail" of the distribution was ignored initially, and curve B was then applied to the tail to further reduce the χ^2 parameter. All six variables were iterated until the overall χ^2 parameter was minimized. Although averaged data fit the composite normal model well under the $\chi 2$ goodness-of-fit test, noise from actual data often prohibited achieving χ^2 values within probability limits of α=0.05. See APPENDIX B for a compilation of χ^2 values for actual data from the 21 histograms used in this thesis.

Equilibration Time Requirements

Early experimental techniques required a minimum equilibration time of approximately 48 hours for all pulp fibers to solvent exchange and equilibrate within the density gradient. Equilibration time is a mass transfer limitation, and significant experimental error may accrue if this variable is not controlled within reasonable limits. Column preparation procedures based on higher impregnation vacuum and dry solvents required less equilibration time. Figure 16 depicts the extended equilibration time that was required when not using anhydrous solvent preparation and fiber impregnation procedures. Figure 17 and Figure 18 illustrate current equilibration time data for overall average fiber density and overall standard deviation in average fiber density.

The greater equilibration time requirements were assumed to result from a higher degree of adsorption and desorption of entrained air and polar material. Density gradient columns are

known to be extremely stable under conditions of constant temperature[157], and this study has observed no change in gradient quality for up to three weeks. Unfortunately, the behavior of impurities in the system was not constant and resulted in poor reproducibility and the need for improvements in experimental technique.

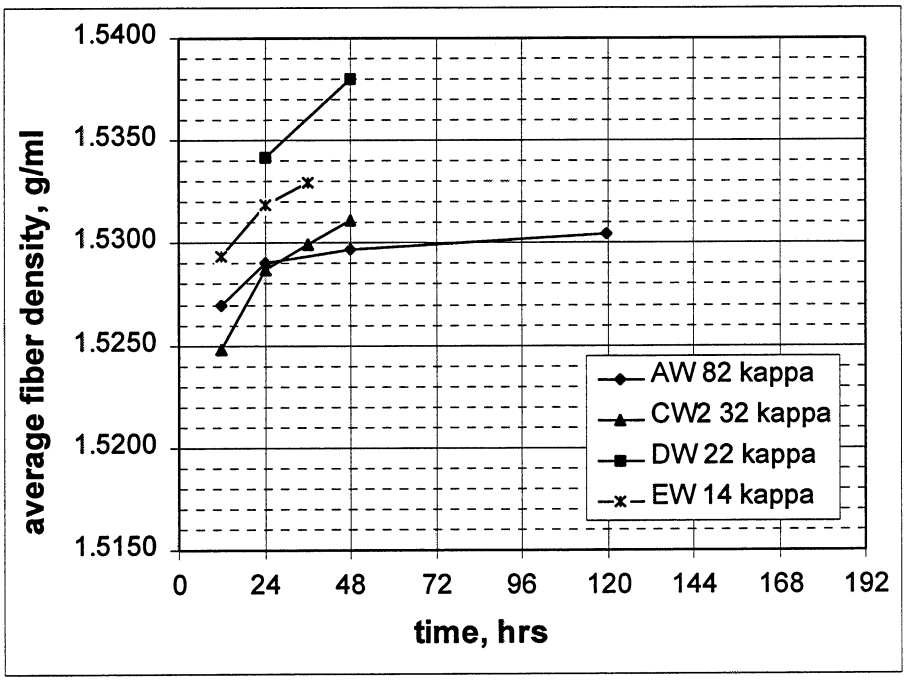

Figure 16. Previous equilibration results based on limited fiber preparation technique.

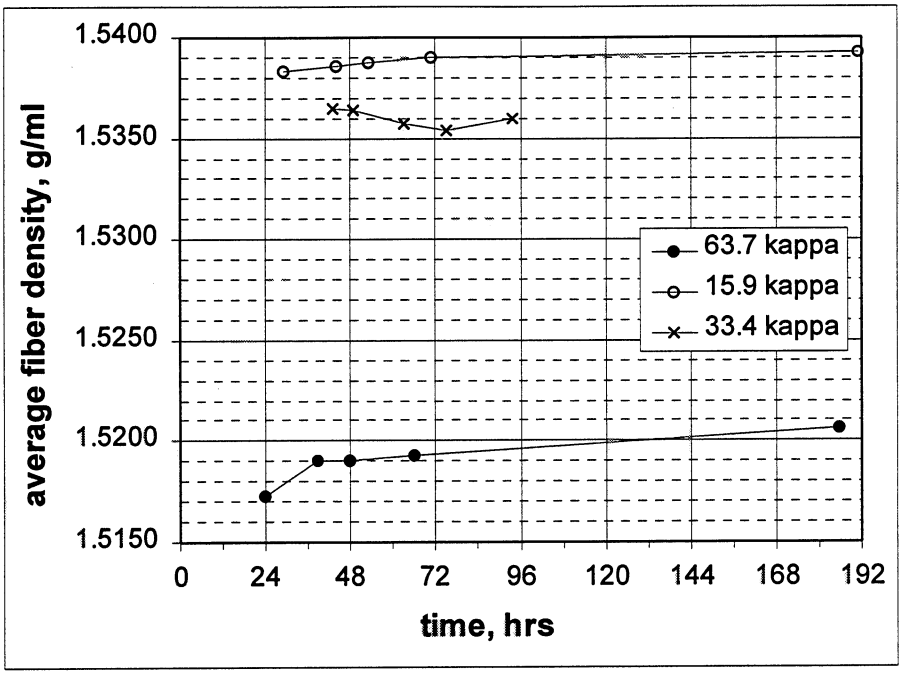

Figure 17. Equilibration time assessment for average densities of 15.9, 33.4, and 63.7 kappa number pulps.

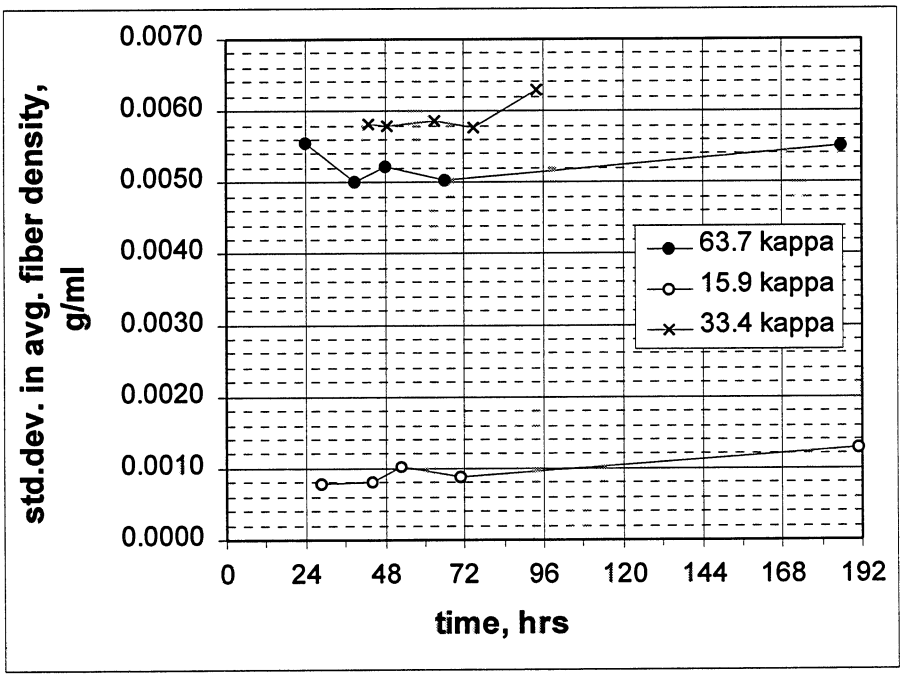

Figure 18. Equilibration time assessment for standard deviation in average fiber density of 15.9, 33.4, and 63.7 kappa number pulps.

The minimum required equilibration time for most pulps was reduced to approximately 36 hours, regardless of kappa number. This was assumed to be due to a reduction in adsorption and desorption of impurities such as water and any entrained gases during equilibration. Minor flocculation may occur between 72 and 96 hours and has resulted in slightly increased standard deviations in average fiber density. Flocculation creates a limitation in image analysis by exceeding the ability of Optimas™ threshold setting to differentiate between fibers and void spaces. Artificially large measures of projected fiber area result for a given increment and can alter the apparent standard deviation in lignin content. Therefore, data acquisition should occur within 40-72 hours to ensure that equilibration error does not exceed the current level of random error. An error analysis follows to describe the precision of data.

Error Analysis

Random Error

The high sensitivity of the density gradient allows for extremely accurate measures of particle density. Unfortunately, the high specific surface area and small particle size of pulp fibers made adsorption of entrained gases and other impurities a formidable problem. Variations in fiber preparation and sampling have been identified as major sources of error. After reducing fiber preparation error through technique modification, there appeared to be a high likelihood that sampling error was the major source of random error.

It was assumed that alkaline hydrolysis and hemicellulose loss could create a correlation between extent of cook and kraft holopulp density. Therefore, correlation coefficients were calculated to determine if kraft holopulp density could be considered constant, regardless of

original brownstock kappa number and kraft pulping conditions. The kraft holopulp data exhibited poor correlations between extent of cook and average fiber density, as well as extent of cook and standard deviation in average fiber density. The lack of correlation between kraft holopulp densities and their respective brownstock kappa number implies that kraft holopulp density can be considered constant in this data set. Table 10 gives an approximation of the random error that would be present without sampling error, along with correlation coefficients for relationships between extent of cook and average fiber density for kraft holopulps. Kraft holopulps appear relatively unaffected by sampling variation. Therefore, it can be assumed that the error inherent in kraft holopulp density is the current level of reproducibility for the density gradient column technique. Hemicellulose content was insignificant at the 95% confidence level of 1.5458 ±0.0030 g/ml.

Table 10. Calculation of random error in density gradient column samples of kraft holopulps.

Description	initial kappa number	mean density (g/ml)	density st.dev. (g/ml)
Kamyr 4170 - Holo	24.1	1.54660	0.00100
Cook 1 - Holo	63.7	1.54550	0.00086
Kamyr 1964 - Holo	31.4	1.54510	0.00122
Kamyr 4170 - Holo	24.1	1.54510	0.00097
Kamyr 832 - Holo	24.6	1.54330	0.00157
Cook 3 - Holo	23.4	1.54729	0.00134
Cook 2 - Holo	54.6	1.54770	0.00090
Averages:		**1.5458**	**0.0011**
Standard Deviation in Averages: (Random Error Assessment)		**0.0015**	**0.0003**
R^2 for mean density vs. kappa number		**0.064**	
R^2 for st.dev. in density vs. kappa number			**0.383**

Table 11. Calculation of random error in density gradient column analyses of 33.4 kappa number, 10.0-mm-thick chip laboratory kraft pulp.

Description	kappa number	mean density (g/ml)	density st.dev. (g/ml)
Cook 7 - BS	33.4	1.53693	0.00511
Cook 7 - BS	33.4	1.53042	0.00565
Cook 7 - BS	33.4	1.53569	0.00587
Cook 7 - BS	33.4	1.53835	0.00714
Averages:		**1.5353**	**0.0059**
Standard Deviation in Averages: (Random Error Assessment)		**0.0035**	**0.0009**

Table 11 shows random error from a brownstock sample that includes sampling error, as evidenced by comparison to Table 10. The brownstock sample varied 0.0035/0.0015 times more than the entire kraft holopulp data set. This suggests that the mean square error can be reduced by a factor of 2.3 through improvements in the sampling method. The level of random error that existed in kraft holopulps, approximately 0.0015 g/ml, indicates the currently achievable reproducibility. While accepting that sampling problems may exist within the kraft holopulp measurements, it was further hypothesized that this level of random error may also be due to one or more of the following variations: 1) the level of fiber impregnation, assumed to be related to vacuum control; 2) variations in the residual water content of fiber samples following impregnation; 3) solvent contamination by polar materials, such as water, ethanol, silicon grease, and molecular sieve material; and 4) deviations in the physical structure of fibers upon impregnation, as a result of variations in the fiber preparation procedure. Variations 1 and 2 were controlled by using a vacuum pump rated at a maximum vacuum of $1x10^{-4}$ torr. The pump was used to dry the fibers and create a driving force for impregnation. Vacuum was monitored with a MacLeod vacuum gauge at better than $5x10^{-3}$ torr. Variation 3 was reduced by eliminating ethanol as a chloroform stabilizer, purifying solvents with a H_2SO_4/water wash, drying all

solvents over $CaCl_2$, and subsequently storing the solvents over molecular sieves. Solvents were further purified by distillation. Average solvent compositions for the 21 columns used in this thesis are tabulated in Table 12.

Three additional sources of significant experimental error arise in Table 12: 5) variations in impregnation solvent density; 6) variations in the water concentration of the impregnation solvent; and 7) variations in the quality of the linear density gradient. The correlation coefficient for the linear density gradient was calculated from the 21 randomly produced density gradients used in this research. Column height vs. bead density calibrations were based on eight glass calibration beads and suggest that error due to gradient quality was unlikely. However, the impregnation solvent density did vary considerably as a result of variations in distillation separation efficiency. Since sample equilibration was controlled by mass transfer of column solvents into the fiber structure, then random error may have also been controlled by variations in the extent of exchange between column solvents and impregnation solvents. The net result could be that a residual quantity of impregnation solvent remained in the fiber walls, thus contributing additively to average fiber density. Since the limited data of Figure 19 suggest a negative correlation between average fiber density and impregnation solvent density, variations in impregnation solvent density probably did not contribute to random error.

Table 12. Average density gradient column solvent composition.

	Impreg density g/ml	Impreg [H2O] ppm	FL [H2O] ppm	FD [H2O] ppm	FL density g/ml	FD density g/ml	Linear gradient R^2
Average	1.4884	8.6	10.4	9.3	1.5001	1.5837	0.9995
Std.deviation	0.0028	5.8	4.6	3.6	0.0020	0.0060	0.0006

FL and FD are standard notation for low density and high density gradient solvents, respectively[181].

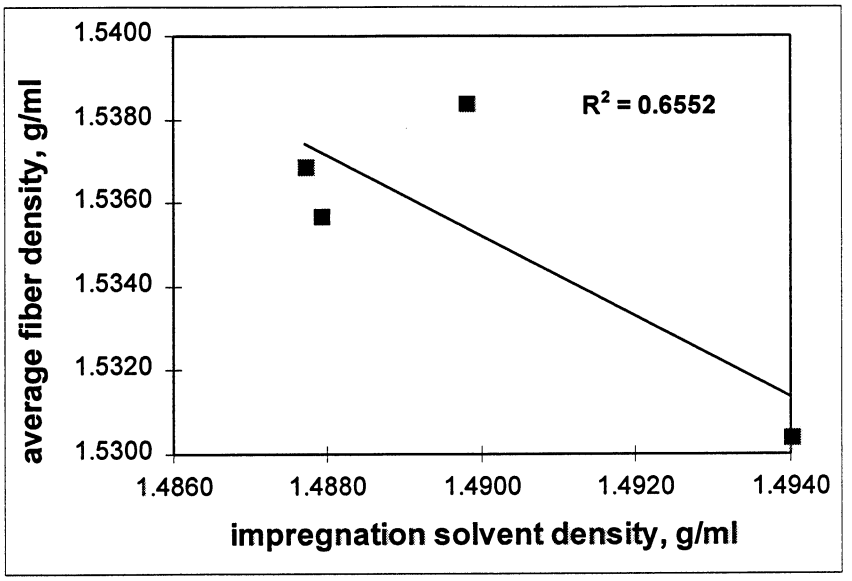

These results are for the 33.4 kappa number 10.0 thick chip pulp.

Figure 19. Average fiber density vs. impregnation solvent density.

Much Karl Fischer titration data has been obtained under a variety of conditions. This data was compiled to understand the ability of vacuum-dried-cellulose fiber in removing water from chloroform and tetrachloroethylene. Data from Table 9 showed that a positive correlation existed between % fiber water uptake and initial water concentration of the solvents. Using this correlation, an estimate was made of the amount of residual water that may be adsorbed by wood fibers during impregnation. Thus, an estimation of the effect of the variation in impregnation solvent water content on fiber density was possible, as shown in Figure 20. This was a weighted component density relationship used to estimate the reduction in fiber density from water adsorption. Calculations were based on a 30 kappa number pulp fiber with an average fiber density of 1.5345 g/ml.

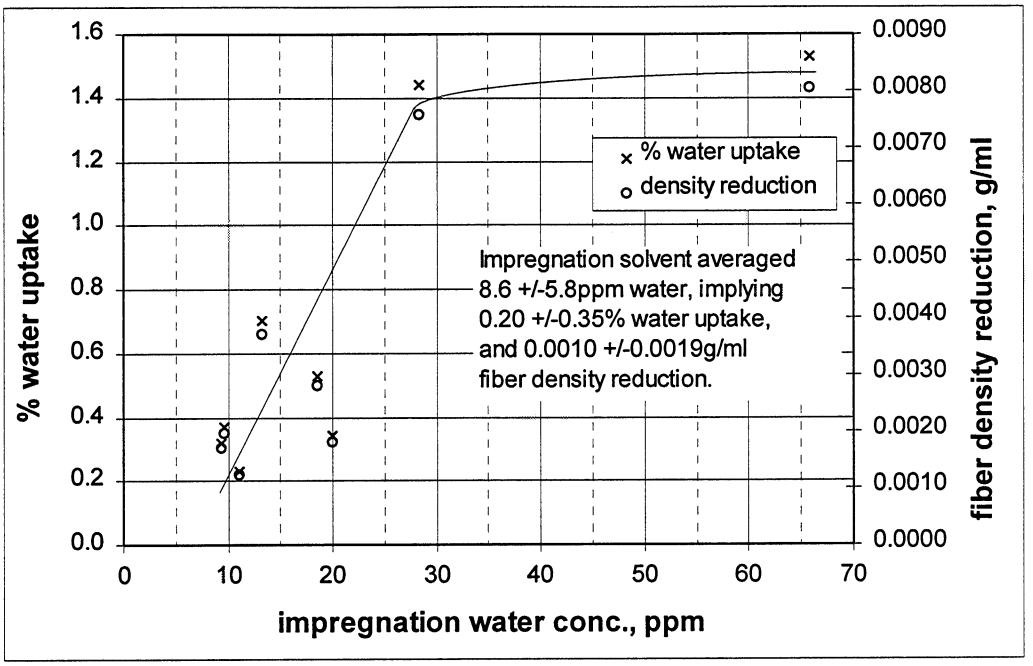

Parameters of interest in water adsorption estimation for a single vacuum-dried fiber treatment

	CHCl3	C2Cl4
Average % reduction in water - single stage	33.2	52.9
O.D. wt. of filter paper, g	1.8	1.8
Volume of solvent, ml	2000	2000
O.D. wt. 30 kappa number fiber, μg (50μm diameter x 30μm lumen x 3mm length)	1.45	
Average impregnation solvent water, ppm	8.6	

Note: fiber density reduction (g/ml) can be converted to DGC kappa number increase using a factor of 2478, and density reduction = $\rho_{fiber}-(x_{water}\rho_{water} + x_{fiber}\rho_{fiber})$; x=fraction determined by Table 9.

Figure 20. Estimation of error induced through water adsorption during impregnation.

Data in Figure 20 shows that a decrease in average fiber density may result from an increase in impregnation solvent water content and are based solely on additive density changes from water adsorption. The level of variation suggested in Figure 20 encompassed that of the kraft holopulp random error. However, Figure 21 provides contradictory evidence that as impregnation solvent water contents increased, so did average fiber densities. Either the presence of water creates a binding force between microfibrils to increase cell wall density, or the miscibility of water with cellulose makes fiber regions accessible that are otherwise inaccessible

to nonpolar solvents, as suggested by Hermans[168]. Thus, variations 4 and 6 appear suspect as the cause for any remaining error in the density gradient column measurements.

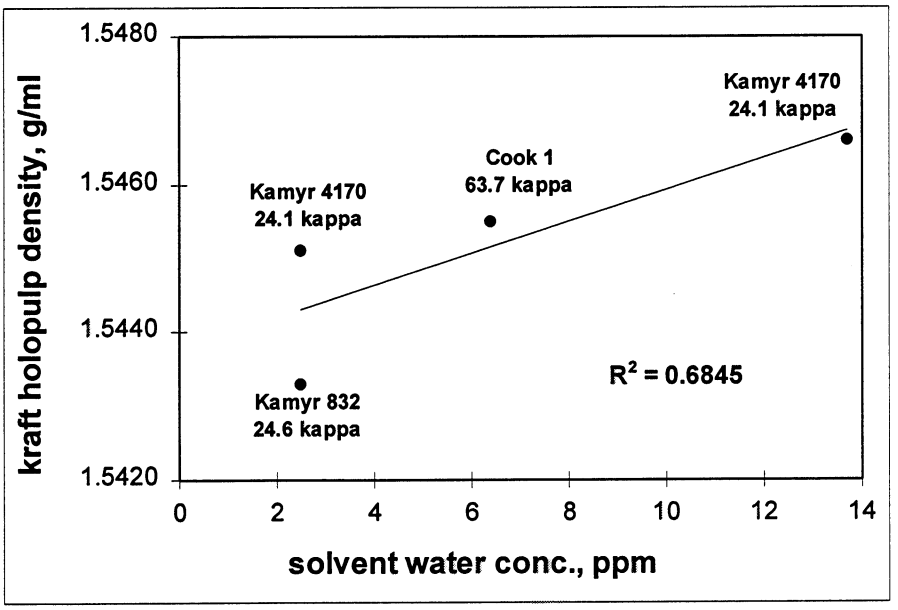

Pulps are labeled with brownstock kappa number prior to holopulping to indicate extent of cook.

Figure 21. Relationship between kraft holopulp density and solvent water concentration.

Measurement Error

The image acquisition and analysis apparatus consisted of an Electrim EDC1000U monochrome digital camera linked to a personal computer with Optimas™ image analysis software. Although the camera is of high resolution and has image averaging and integration capability, problems such as depth of field variations, artifacts from light and extraneous particles, and variations in parallax could have created error in data acquisition and parameter estimation. Imaging and image analysis began as a large source of error due to an inability to produce high contrast images on a homogeneous background. The birefringent nature of cellulose provided the physical means to produce high contrast images through cross-polarization

techniques[184,185]. Table 13 provides an estimate of measurement error inherent in the image acquisition and analysis technique. This estimate includes error from variations in depth of field, parallax, artifacts, manual threshold settings, selection of region of interest, and data manipulation.

Table 13. Calculation of measurement error in g/ml.

	kappa number	mean density (g/ml)	density std.dev. (g/ml)
Kamyr 1964 - Holo (Center Position)	0	1.54510	0.00122
Kamyr 1964 - Holo (Left of Center)	0	1.54504	0.00128
Kamyr 1964 - Holo (Right of Center)	0	1.54496	0.00133
Kamyr 1964 - BS (Center Position)	31.4	1.54054	0.00460
Kamyr 1964 - BS (Left of Center)	31.4	1.54034	0.00426
Kamyr 1964 - BS (Right of Center)	31.4	1.54015	0.00469
Average Values:			
Kamyr 1964 - Holo	0.0	1.5450	0.0013
Kamyr 1964 - BS	31.4	1.5403	0.0045
Standard Deviation in Average Values (Measurement Error):			
Kamyr 1964 - Holo	0.0	**0.0001**	**0.0001**
Kamyr 1964 - BS	31.4	**0.0002**	**0.0002**

The accuracy of the glass calibration beads have set the minimum achievable experimental error to +/-0.0002 g/ml[181]. Measurement error was relatively small for both average fiber density and standard deviation in average fiber density. In fact, measurement error was no greater than the error within the glass calibration beads. This result establishes that the determination of average fiber density and standard deviation in average fiber density are limited by random error, which is approximately one order of magnitude greater than measurement error. Therefore, current image acquisition and data analysis techniques were more than suitable for this particular application.

Verfication of the DGC Technique with Valonia Cellulose Standards

Molecular dimensions can be measured with x-ray crystallography. Likewise, the density of crystalline cellulose can be theoretically calculated on the basis of the unit cell structure[186]. The earliest attempts at characterizing the unit cell structure of cellulose were made by Sponsler and Dore in 1926, Meyer and Mark in 1928, and Meyer and Misch in 1936[174,187]. The first assumption was the single chain unit cell with (1,1) and (4,4) links. Next came the two chain unit cell, and finally, the (1,4) linkage. In each model, two glucose molecules per chain were the rule. Each unit cell was considered monoclinic and based on the structures in Figure 22.

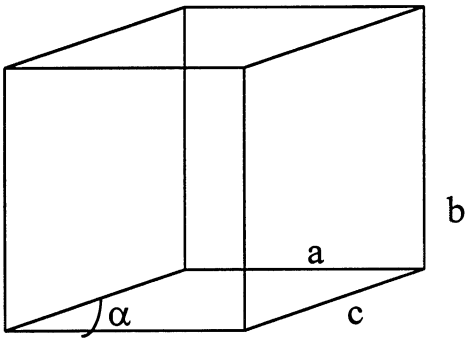

a.) monoclinic unit cell; a=8.3 angstroms b=10.3 angstroms (fiber axis) c=7.9A $\alpha=84^0$

unit cell volume=abc[sinα].

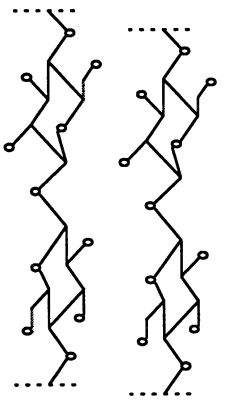

b.) 2 chain unit cell of β-D-glucopyranose; parallel arrangement of native cellulose.

Figure 22. Cellulose unit cell as depicted by Meyer and Mark, and Meyer and Misch.

Attala and VanderHart[188-190] have shown the presence of a second phase within cellulose using solid state ^{13}C NMR. Peak multiplicity indicated that cellulose Iα and cellulose Iβ coexist within cellulose crystalline structures in the proportion of 65% and 35%, respectively. Sugiyama et al.[191,192] have assigned infrared absorption bands to both phases using infrared spectroscopy, and provided unit cell dimensions using electron diffraction. Figure 23 provides a comparison of the triclinic cellulose Iα to the monoclinic cellulose Iβ.

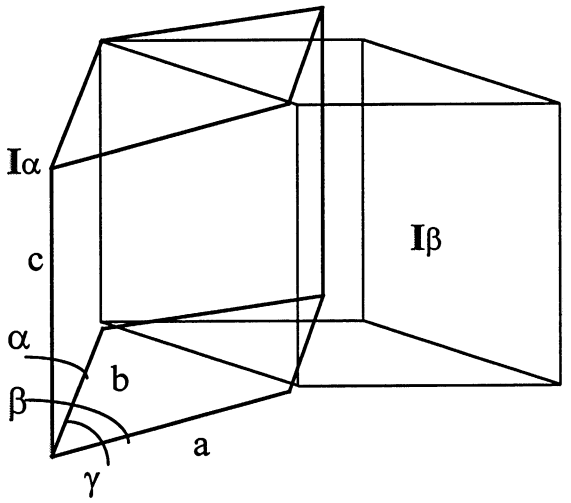

dimensions of unit cell allomorph Iα: a=6.74 angstroms b=5.93 angstroms c=10.36 angstroms (chain axis); α=117° β=113° γ=81° (triclinic); comprises 65% of the unit cell; only one chain per unit cell.

dimensions of unit cell allomorph Iβ: a=8.01 angstroms b=8.17 angstroms c=10.36 angstroms (chain axis); α=97.3° (monoclinic); comprises 35% of the unit cell; two chains per unit cell.

unit cell volume=$abc[1-\cos^2\alpha-\cos^2\beta-\cos^2\gamma+2\cos\alpha\cos\beta\cos\gamma]^{1/2}$.

Figure 23. Two distinct crystalline phases within native cellulose; dimorphism.

The developed density gradient column procedure was used to determine the density of *Valonia ventricosa* cellulose as a standard for comparison. A comparison of density gradient column measurements to x-ray diffraction based density calculations[174] can provide an estimate of the improved density gradient column accuracy. Table 14 compares values of density and

standard deviation in density for *Valonia ventricosa* as measured by x-ray diffraction and density gradient column analyses. Unit cell density calculations were based on the following relationship using diffraction values from Hermans[174] and Sugiyama et al.[191,192]:

$$unit\ cell\ density = \frac{N_g(MW_g)}{N_A(V)}$$

where N_g is the number of glucose molecules in the unit cell, MW_g is molecular weight of glucose, N_A is Avogadro's constant, and V is the unit cell volume.

Table 14. Values of *Valonia ventricosa* density as determined by density gradient column and x-ray diffraction analyses.

sample	ρ cellulose I (total) (g/ml)	σ cellulose I (total) (g/ml)	ρ cellulose Iα (65%) (g/ml)	ρ cellulose Iβ (35%) (g/ml)
valonia x-ray one-phase unit	1.60	0.01		
valonia electron diffraction two-phase unit	1.592	0.008	1.586	1.601
valonia DGC	1.5981	0.0011		
valonia DGC	1.5985	0.0011		
valonia DGC	1.5985	0.0011		
valonia DGC	1.6013	0.0011		
valonia DGC	1.6013	0.0011		
DGC number average	**1.5995**	**0.0016**		

The values obtained by the improved density gradient column technique were found to be well within the 0.5% experimental error assumed for x-ray diffraction data[174]. An equal amount of error was assumed for the electron diffraction data. Using this estimate of experimental error, the density values were not significantly different when t-tested. Thus, the density gradient

column technique does agree with the electron diffraction and x-ray diffraction referee techniques.

Secondary Analyses of DGC Kappa Number and Lignin Density

The kappa number vs. average fiber density relationship provided a method of converting individual fiber density values to "DGC kappa number," which is an estimated density gradient column kappa number equivalent. However, it was first necessary to carefully model the relationship to avoid making false conclusions from the secondary analysis. Figure 24 relates average fiber density to kappa number and provided the basis for all secondary analyses of delignification diversity in terms of DGC kappa number.

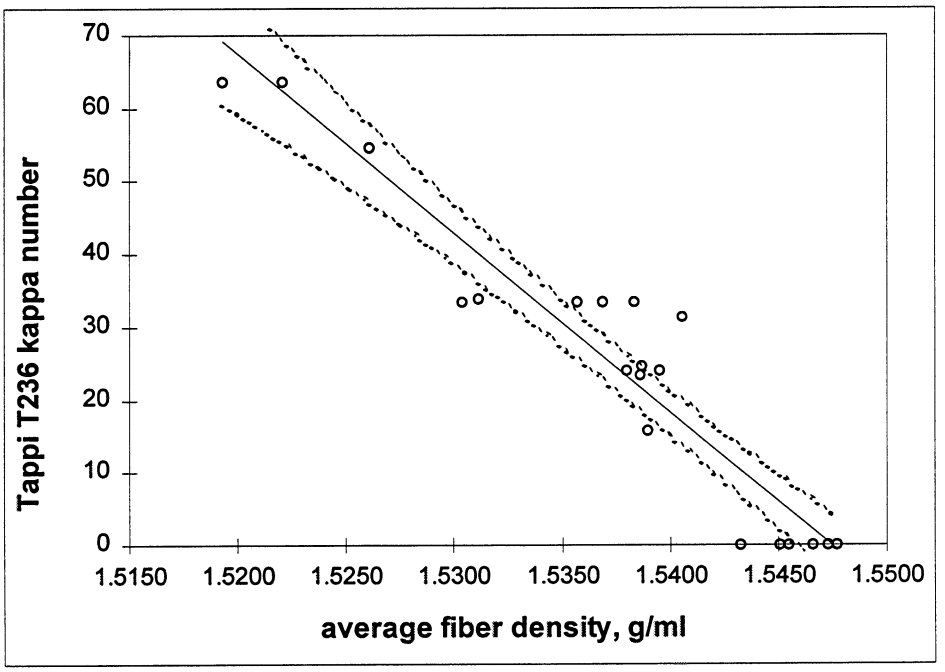

slope	intercept	R^2	std. error in kappa number
-2.46E+03	3.80E+03	0.907	6.5

Figure 24. Tappi T236 kappa number vs. average fiber density.

The large random error in Table 11 made it statistically necessary to use the linear relationship given in Figure 24. The 95% confidence bands show that the mean response for kappa number varies 6-10 kappa number in the range of this secondary analysis. The choice of the model was based on the premise that the simplest model be used. A plot of average class values, a residual plot, a lack-of-fit analysis, and an analysis of the contribution of a quadratic term are given in APPENDIX B. In addition, it is also shown how a quadratic relationship between fiber density and kappa number implies that lignin density increases with extent of cook, when assuming a constant holopulp density. Although statistics do not fully support a quadratic relationship at this time, it is conceivable that changes in lignin density do occur, given our knowlege of changes in lignin structure with extent of cook. As a result, the pulp component densities listed in Table 15 were calculated using the linear model, along with the average holopulp density of Table 10.

Table 15. Density of holocellulose and lignin.

component	density (g/ml)	std. deviation (g/ml)
holocellulose	1.5458	0.0011
lignin	1.2719	0.0090

The lignin density of 1.2719 g/ml given in Table 15 is different than the calculated 1.335 g/ml of Stamm and Sanders[173] in toluene, CCl_4, and C_2Br_4, as well as the calculated 1.375 g/ml of Tichy and Proctor[6] in CCl_4 and $CHCl_3$. However, it is consistent with the direct lignin pellet density measurements of Yoshida, et al[193] in CCl_4 and n-heptane.

MEASUREMENT OF DELIGNIFICATION DIVERSITY

The premise of this thesis is based on earlier research that provided measures of mass transfer limitations as a function of cooking condition and chip size. These earlier contributions suggested that valuable information may be obtained on an interfiber level. This research contributes interfiber lignin content measurements in a novel manner using modified traditional techniques. Figure 25 illustrates delignification diversity in terms of the overall standard deviation in DGC kappa number for 2.5-mm-thick chip pulps, 10.0-mm-thick chip pulps, and mill-produced pulps. This particular relationship is significant in that it defines delignification diversity in one term, and the term is a pure calculation for all types of numerical distributions. The composite normal distribution provided the means to look further into delignification diversity.

Figure 26, Figure 27, and Figure 28 represent the delignification diversity histograms obtained from 10.0-mm-thick chip laboratory pulps, 2.5-mm-thick laboratory pulps, and continuous digester mill pulps, respectively. The complete collection of density gradient column histograms is contained in APPENDIX B. The composite normal distribution provides further insight into the differences between the distributions.

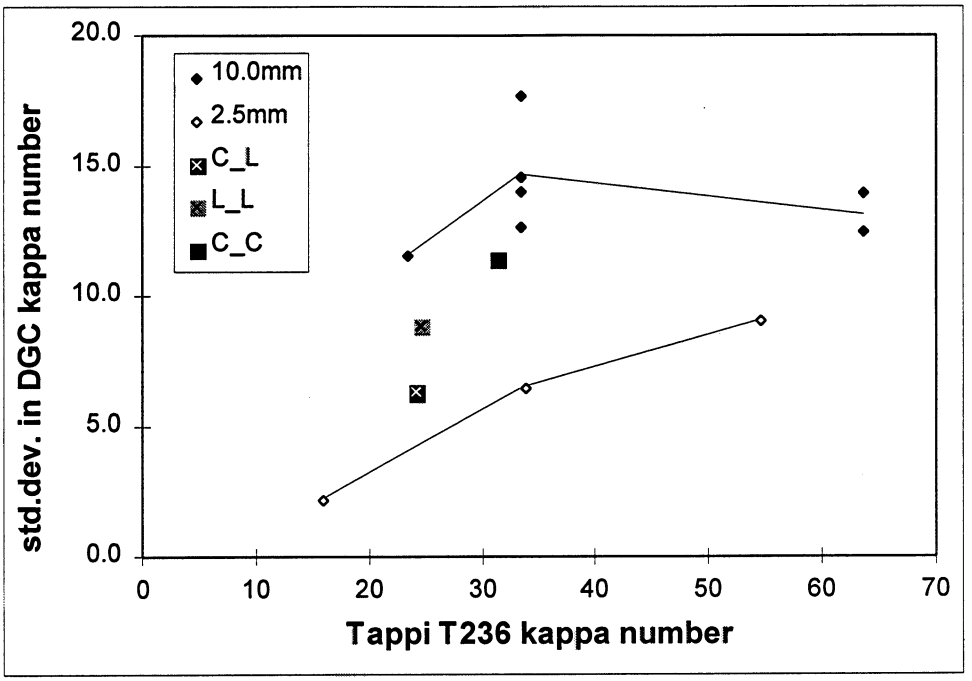

C_L refers to Kamyr conventional feed and Lo-solids™ cooking.
L_L refers to Kamyr Lo-level™ feed and Lo-solids™ cooking.
C_C refers to Kamyr conventional feed and conventional cooking.
2.5-mm and 10.0-mm refer to chip thicknesses of laboratory kraft pulps.

Figure 25. Delignification diversity vs. Tappi T236 kappa number.

DISCUSSION

It was found that two normal distributions fit well to data within the constraints of the χ^2 goodness-of-fit test. The model was termed a composite normal distribution, and the two distributions were termed distribution A and distribution B. Concurrently, it was found that lignin density is on the order of 1.2719 g/ml for all pulp samples. Although it is known that lignin structure changes with the extent of kraft cooking[202-206], and lignin density may be assumed to vary with changes in lignin structure[193], lignin density variations could not be statistically verified with the current level of random error. However, some qualitative evidence does exist to the contrary and is shown in APPENDIX B.

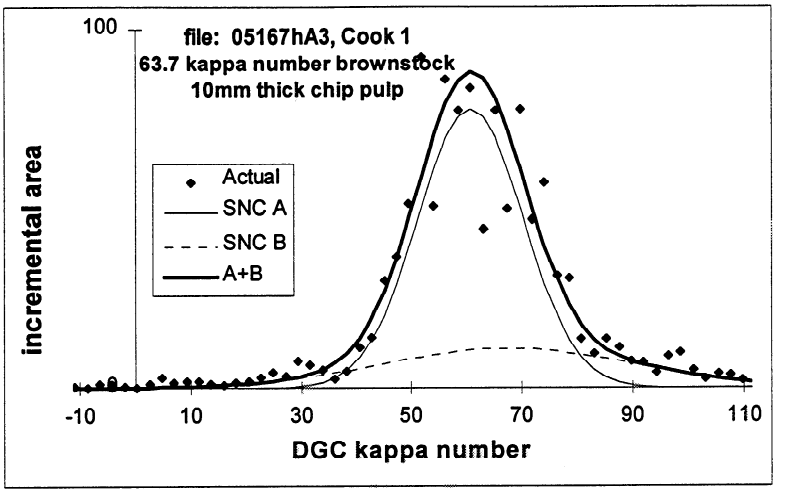

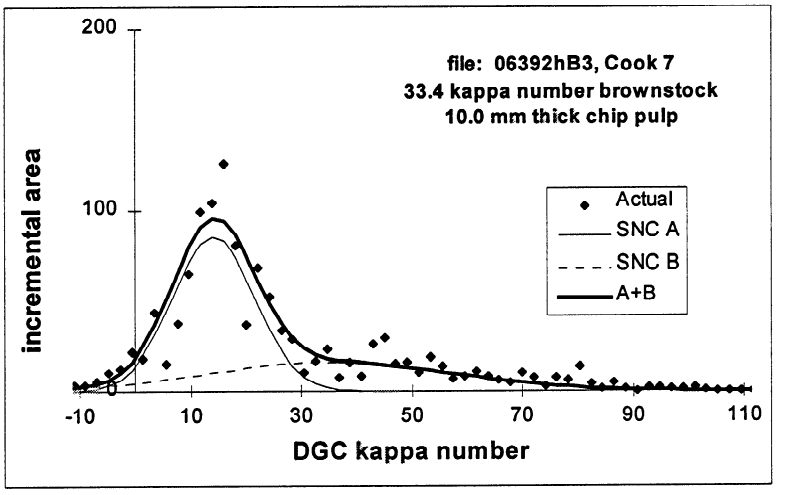

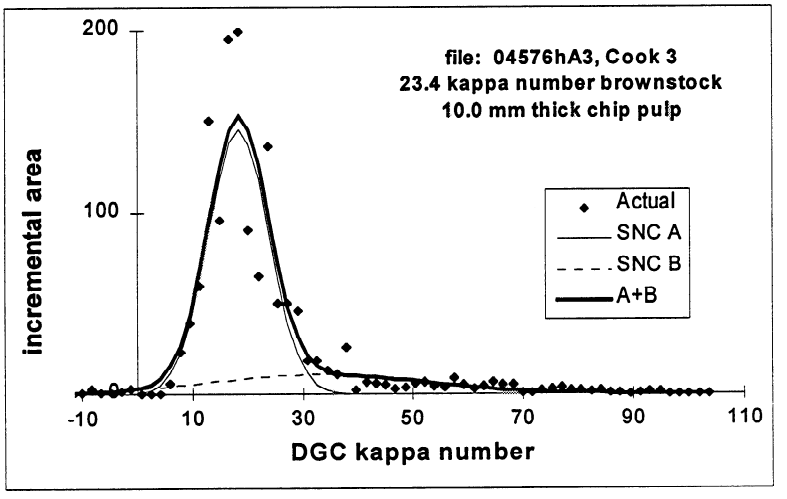

"Actual" refers to original data, "SNC" refers to standard normal curve, and "A+B" refers to the composite normal distribution fit.

Figure 26. DGC kappa number distributions in thick chip laboratory cooks.

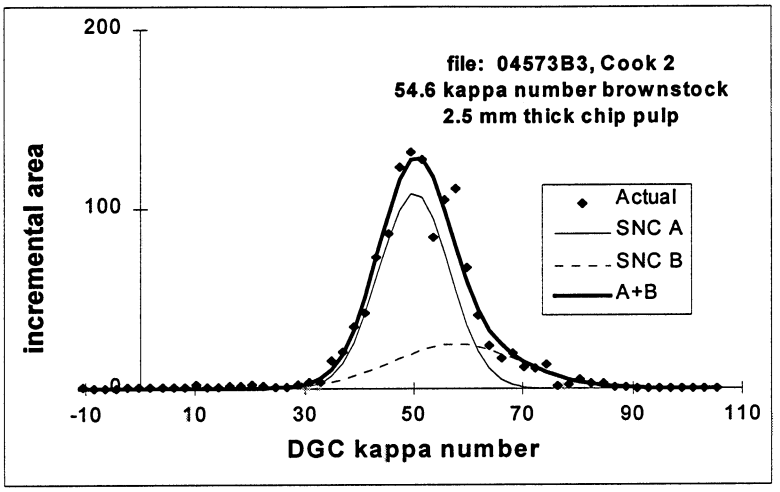

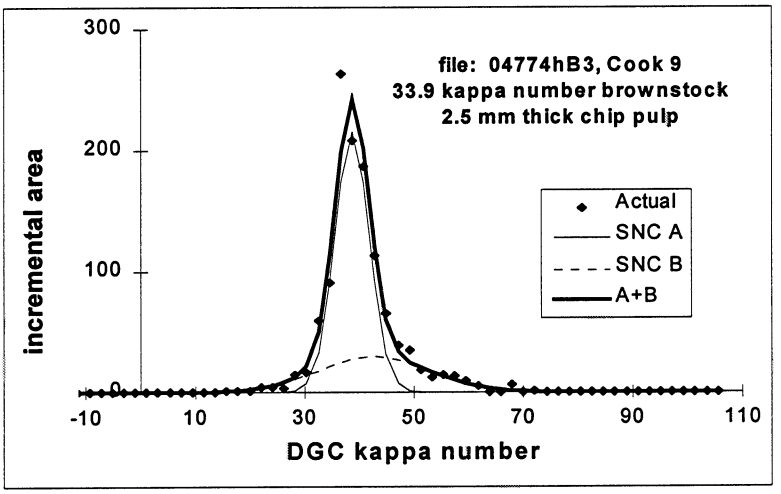

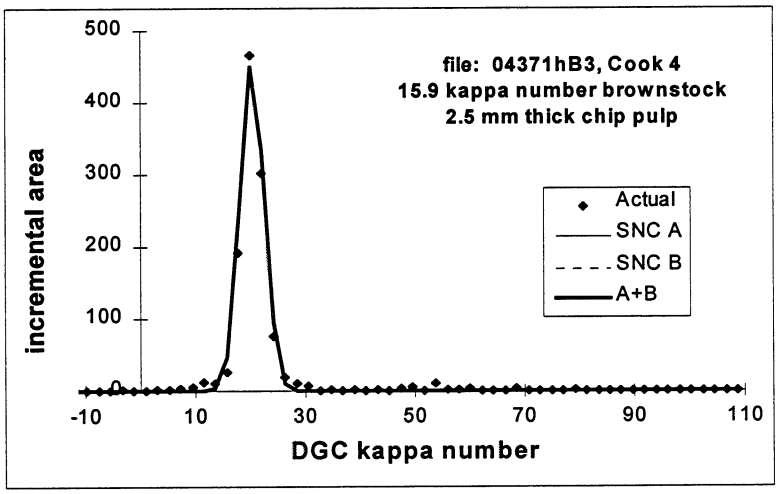

"Actual" refers to original data, "SNC" refers to standard normal curve, and "A+B" refers to the composite normal distribution fit.

Figure 27. DGC kappa number distributions in thin chip laboratory cooks.

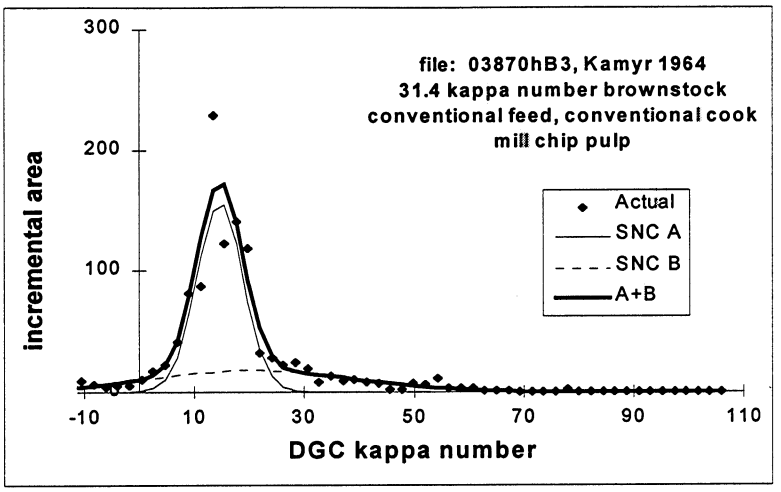

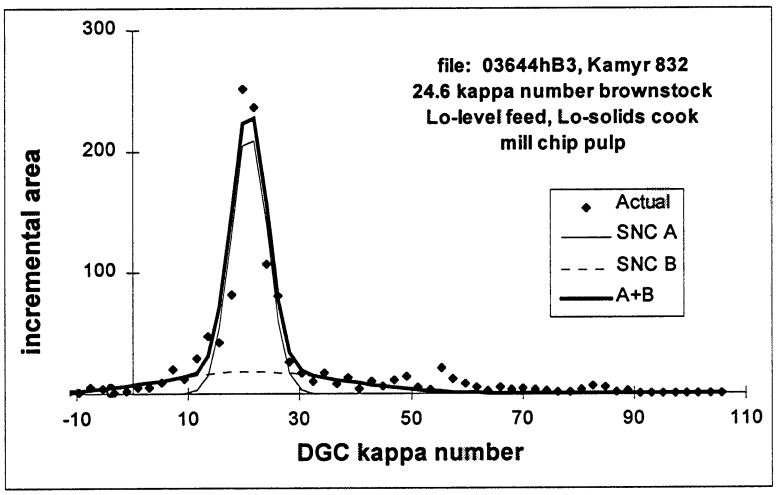

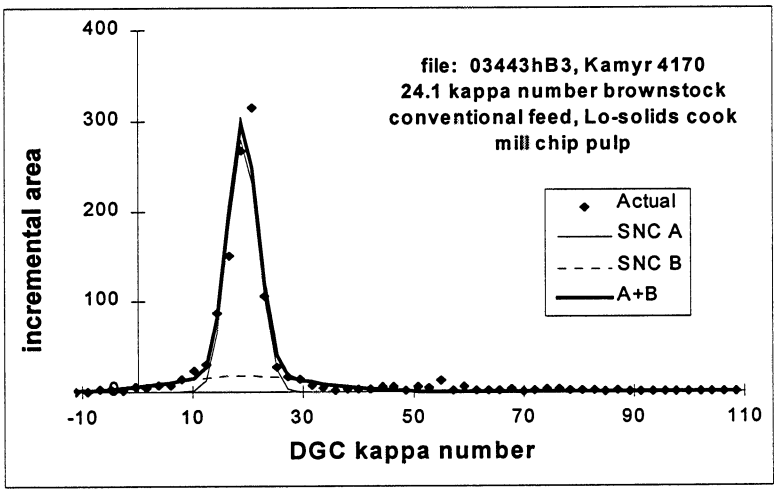

"Actual" refers to original data, "SNC" refers to standard normal curve, and "A+B" refers to the composite normal distribution fit.

Figure 28. DGC kappa number distributions in mill cooks.

Figure 25 was an early indication that the density gradient column technique was successful. The 10.0-mm-thick chip pulps were much higher in overall standard deviation in DGC kappa number than the 2.5-mm-thick chip pulps. As expected, the continuous digester mill pulps exhibited values that were intermediate. Furthermore, the conventional feed/conventional cook continous digester pulp appeared more like the 10.0-mm-thick pulps than did the Lo-level™ feed/Lo-solids™ cook or the conventional feed/Lo-solids™ cook.

Figure 26, Figure 27, and Figure 28 illustrated relationships between distributions A and B as a function of process conditions. The shifting and narrowing of distribution A relative to distribution B was most prominent in the 10.0-mm-thick chip pulps. Interestingly, the conventional feed/conventional cook mill pulp again appeared most similar to 10.0-mm-thick chip pulps. However, it should be noted that the error inherent in the secondary analysis procedure reduces the accuracy of average kappa number predictions. Figure 29 shows the 95% confidence limits for the 15.9 kappa number thin chip pulp.

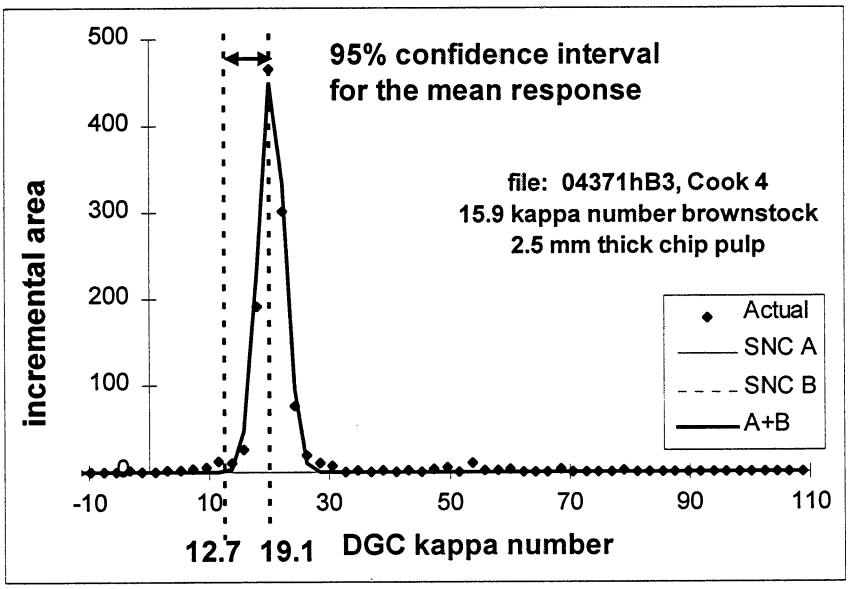

Figure 29. Example of 95% confidence limits for the mean response of DGC kappa number determinations.

The 95% confidence interval shown in Figure 29 indicates that the density gradient column technique is a weak predictor of average kappa number. However, the technique does appear to provide good measures of single fiber kappa number distributions. For example, the thick chip pulps of Figure 26 suggest that mass transfer limited conditions may produce an inner core, resulting in a second distribution.

Other than the pure calculations of the overall mean and standard deviation in average fiber densities, a total of five parameters have been calculated for each composite normal distribution. These parameters are distribution A average DGC kappa number, distribution A standard deviation in DGC kappa number, distribution B average DGC kappa number, distribution B standard deviation in DGC kappa number, and finally, the distribution A and distribution B fractional contributions. The manner in which these variables interrelate describe pulping behavior as a function of process conditions. It appears that distribution B represents 20-38% of the total pulp, as shown in Figure 30.

Figure 25 provided standard deviation information expressed in terms of overall delignification diversity. However, the composite model approach has provided an extra tool to understand more about kraft pulping. For instance, Figure 30 compares fractional contributions from distributions A and B to the overall distributions. Contributions of distribution B from 10.0-mm-thick chip pulps were approximately 8% higher than contributions of distribution B from 2.5-mm-thick chip pulps.

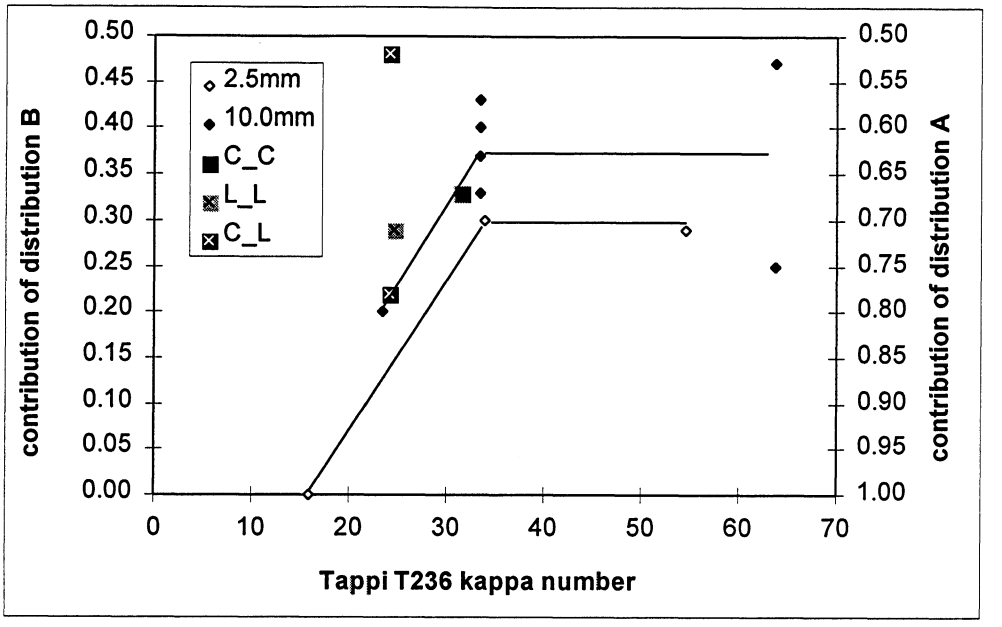

C_L refers to Kamyr conventional feed and Lo-solids™ cooking.
L_L refers to Kamyr Lo-level™ feed and Lo-solids™ cooking.
C_C refers to Kamyr conventional feed and conventional cooking.
2.5-mm and 10.0-mm refer to chip thicknesses of laboratory kraft pulps.
The relationships are hand-drawn and not supported statistically.

Figure 30. Contribution from distributions A and B vs. Tappi T236 kappa number.

Individual component histograms were compared for component distribution A, since distribution A typically constitutes the majority of the composite distribution. Furthermore, it was postulated that distribution A represents the outer portion of the chips. This portion may be subject to overcooking to obtain the target kappa number. Therefore, the nature of distribution B appears to establish delignification limitations. Figure 31 and Figure 32 illustrate distribution A for various 2.5-mm-thick chip pulps, 10.0-mm-thick chip pulps, and mill-produced pulps. Figure 33 compares distribution A from the most uniform laboratory pulp to distribution A from the most uniform mill pulp. The uniform laboratory pulp did not have a second distribution, whereas the mill pulp still contained 22% distribution B.

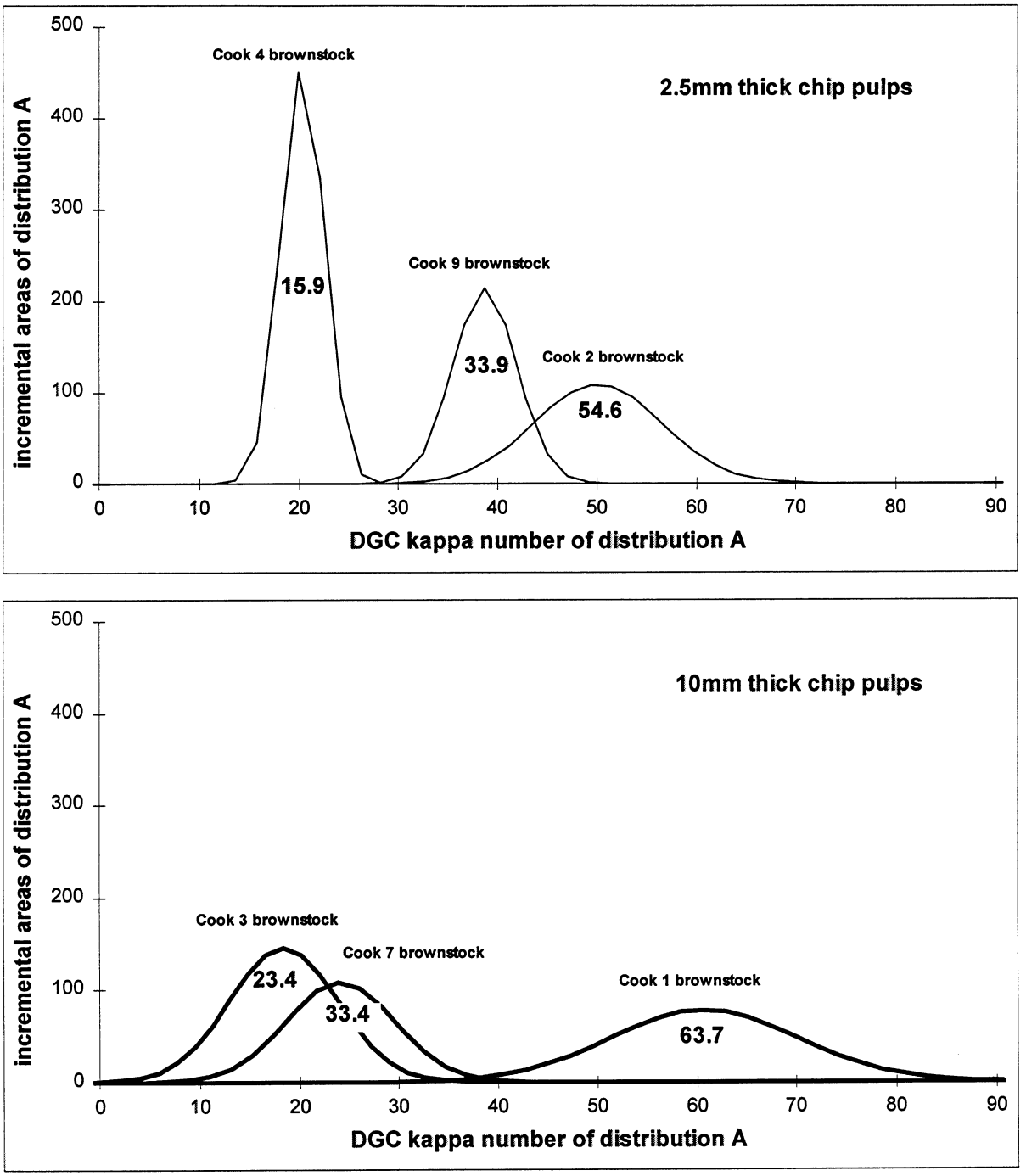

Tappi T236 kappa numbers for the overall sample are given within each histogram.

Figure 31. Distribution A from 2.5-mm-thick chip pulps and 10.0-mm-thick chip pulps.

Figure 31 shows how distribution A decreased in standard deviation and increased in percent contribution with extent of cook, especially in pulps from 2.5-mm-thick chips. Distribution A shows a larger standard deviation in DGC kappa number in pulps from 10.0-mm-thick chips. The difference between the DGC kappa number for distribution A and the Tappi T236 kappa number was larger in the case of the 33.4 kappa number pulp from 10.0-mm-thick chips.

Figure 32 suggests that the conventional feed/conventional cook had the worst uniformity of all mill pulps. In contrast, the conventional feed/Lo-solids™ cook was the best. This would imply that pressurized presteaming may be superior to the atmospheric Lo-level™ feed system.

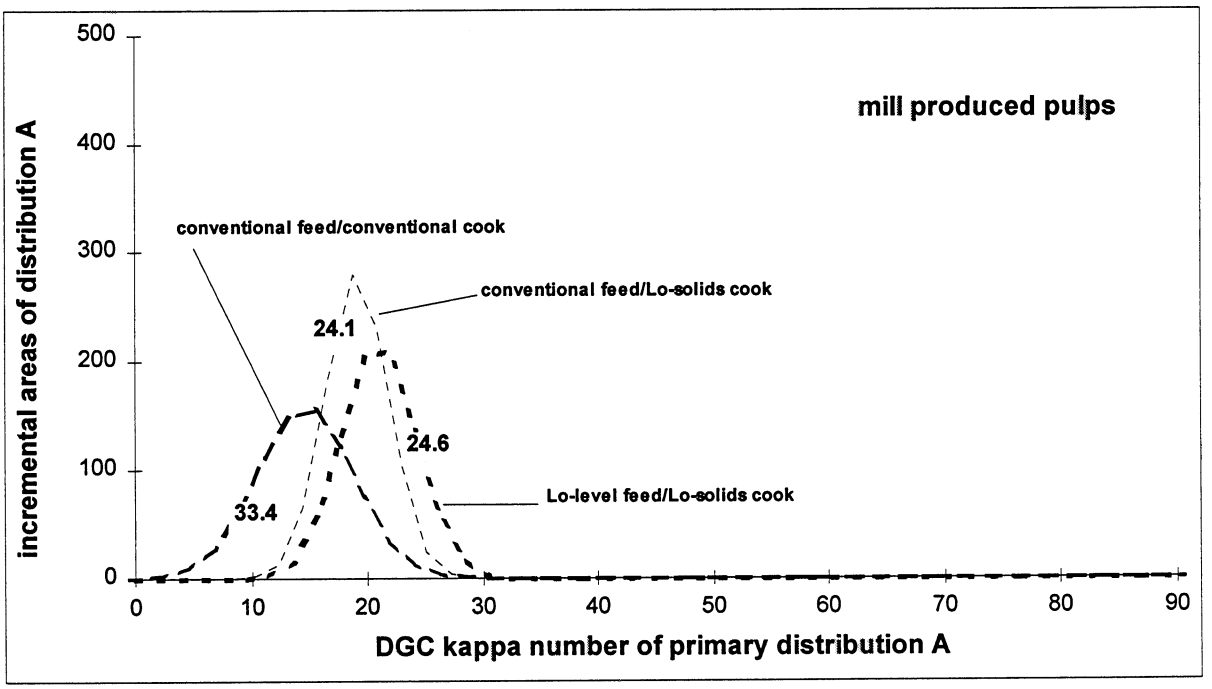

Tappi T236 kappa numbers for the overall sample are given within each histogram.

Figure 32. Distribution A from mill pulps.

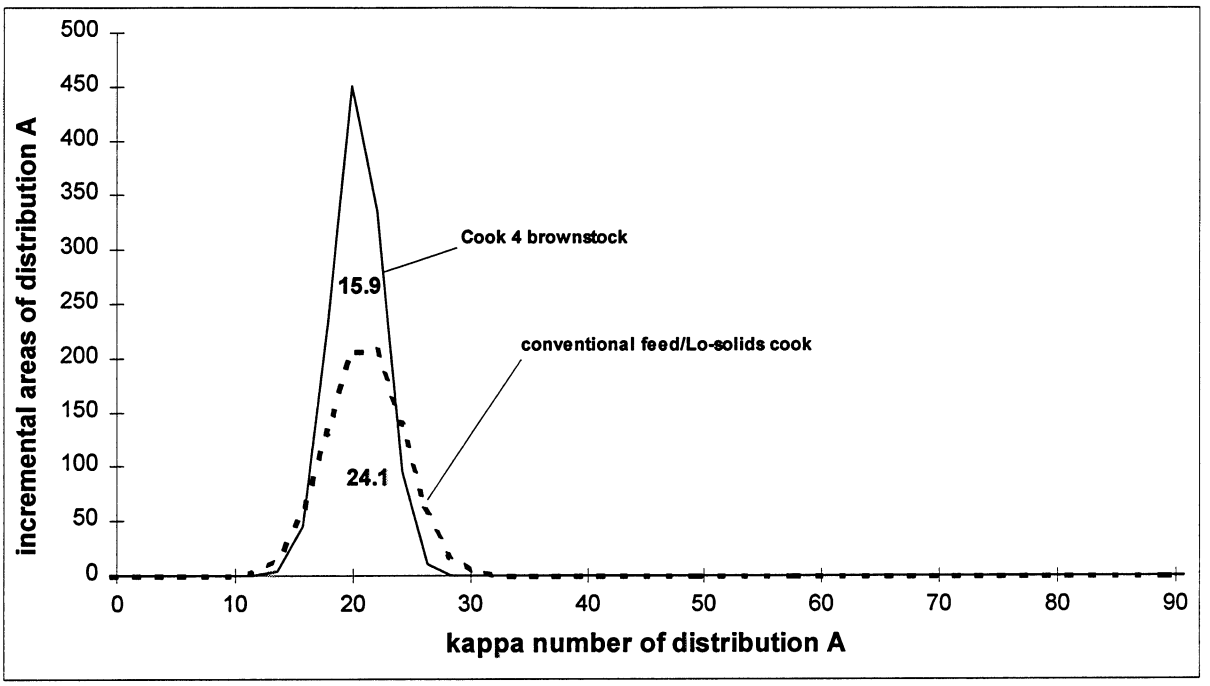

Tappi T236 kappa numbers for the overall sample are given within each histogram.

Figure 33. Distribution A from the most uniform lab pulp and the most uniform mill pulp.

Figure 34 suggests relative overcooking of distribution A in the 10.0-mm-thick chip pulps. Distribution B in both chip thicknesses appears to contain equal average DGC kappa numbers for a given Tappi T236 kappa number. The lower distribution A kappa number indicates that the chip perimeter was overcooked relative to the chip center in order to achieve the target kappa number.

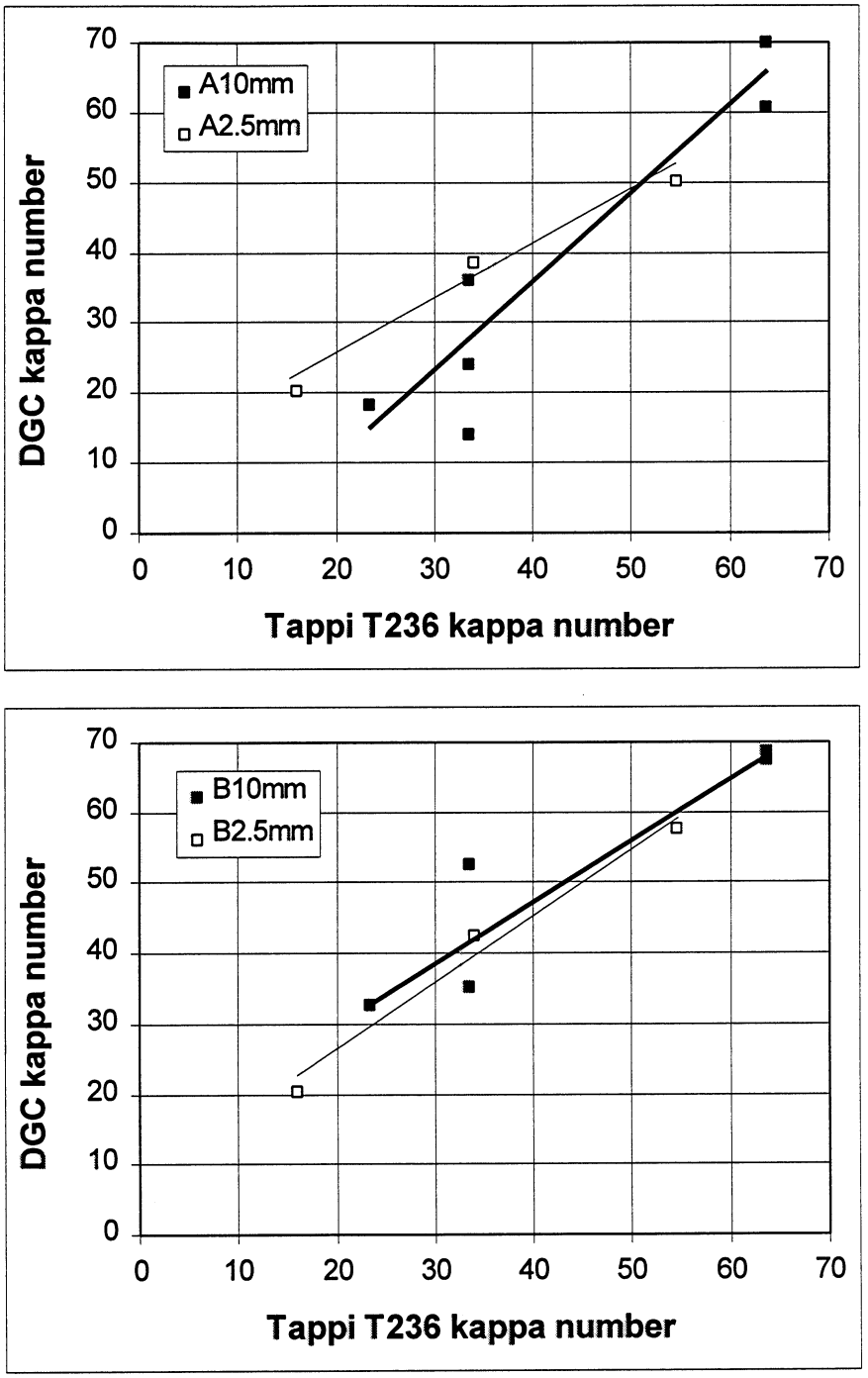

Figure 34. Comparison of component distribution DGC kappa numbers between pulps from 2.5-mm-thick chip and 10.0-mm-thick chips.

Figure 35 shows that component kappa number differences only existed under conventional cooking conditions. The Lo-solids™ pulps were more uniform in this regard.

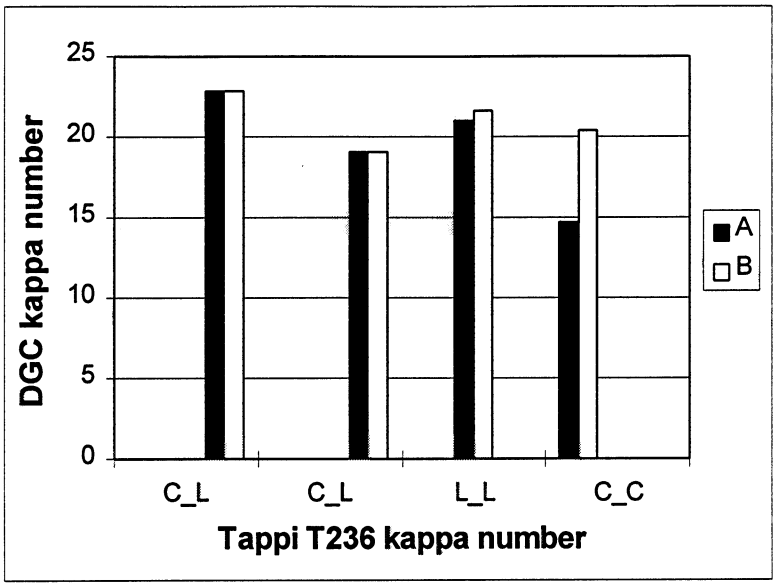

C_C refers to Kamyr conventional feed and conventional cooking.
L_L refers to Kamyr Lo-level™ feed and Lo-solids™ cooking.
C_L refers to Kamyr conventional feed and Lo-solids™ cooking.

Figure 35. Density gradient column kappa number vs. Tappi T236 kappa number for mill pulps.

Figure 36 looks only at differences between distribution A and distribution B kappa numbers to estimate differences in component pulping rates. Both thin and thick chip pulps show comparable internal component differences at high kappa numbers. Component kappa number differences for pulps from 2.5-mm-thick chips diminish to zero upon extended delignification. In contrast, component kappa number differences for thick chip pulps appear to increase to a plateau difference of approximately 15 kappa number with extended delignification.

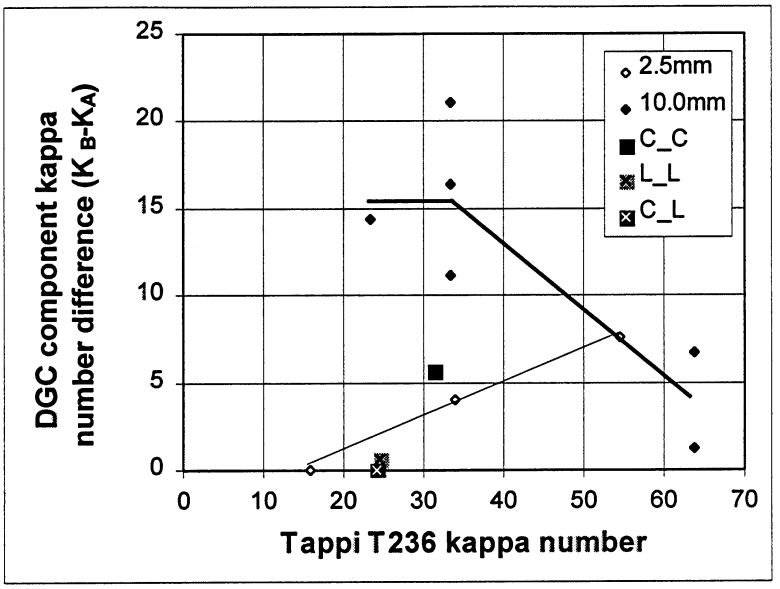

C_L refers to Kamyr conventional feed and Lo-solids™ cooking.
L_L refers to Kamyr Lo-level™ feed and Lo-solids™ cooking.
C_C refers to Kamyr conventional feed and conventional cooking.
2.5-mm and 10.0-mm refer to chip thicknesses of laboratory kraft pulps.

Figure 36. Component kappa number differences vs. Tappi T236 kappa number for laboratory and mill pulps.

Component standard deviations in DGC kappa number were markedly different within pulps from 10.0-mm-thick chips. In contrast, component standard deviations in pulps from the 2.5-mm-thick chips were initially smaller and appeared to converge with extended cooks, as shown in Figure 37.

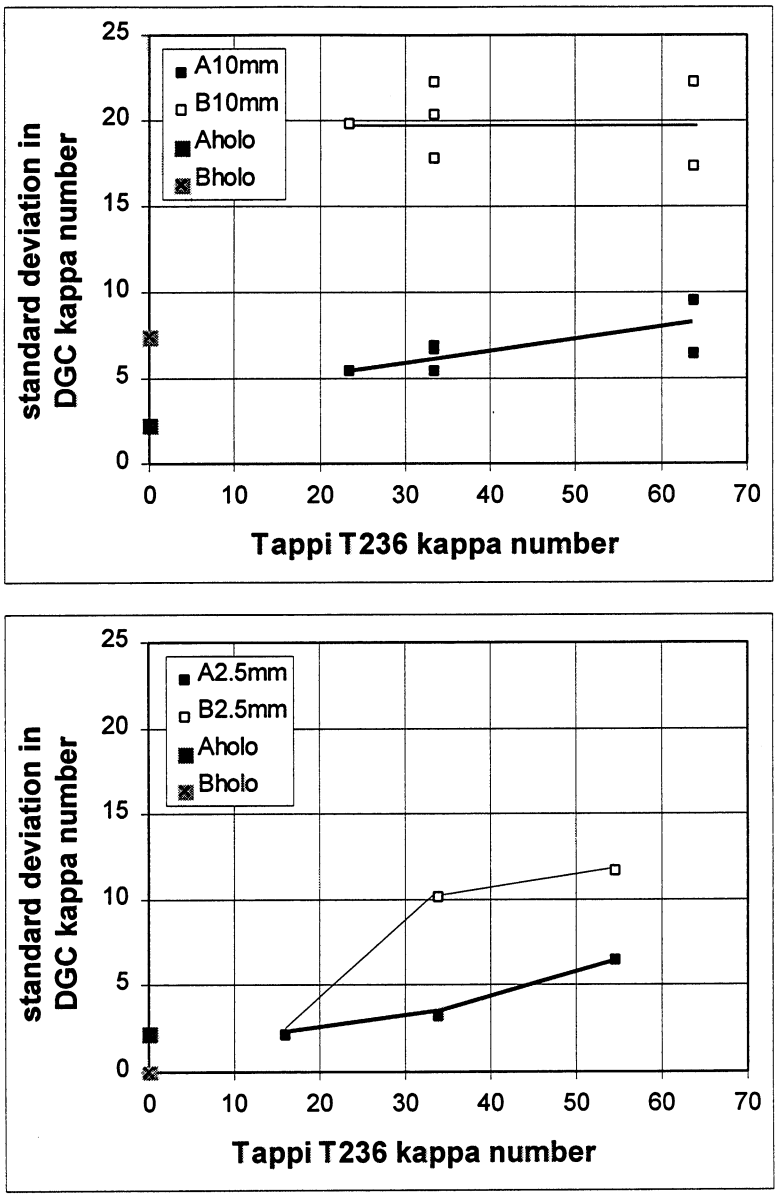

2.5-mm and 10.0-mm refer to chip thicknesses of laboratory kraft pulps.
Holo refers to the standard deviation in average fiber density for all kraft holopulps.

Figure 37. Comparison of component standard deviations in DGC kappa numbers within pulps from 2.5-mm-thick chip and 10.0-mm-thick chips.

Figure 38 relates standard deviations in component DGC kappa numbers to chip thickness. The standard deviation values were higher for both distributions in 10.0-mm-thick chip pulps.

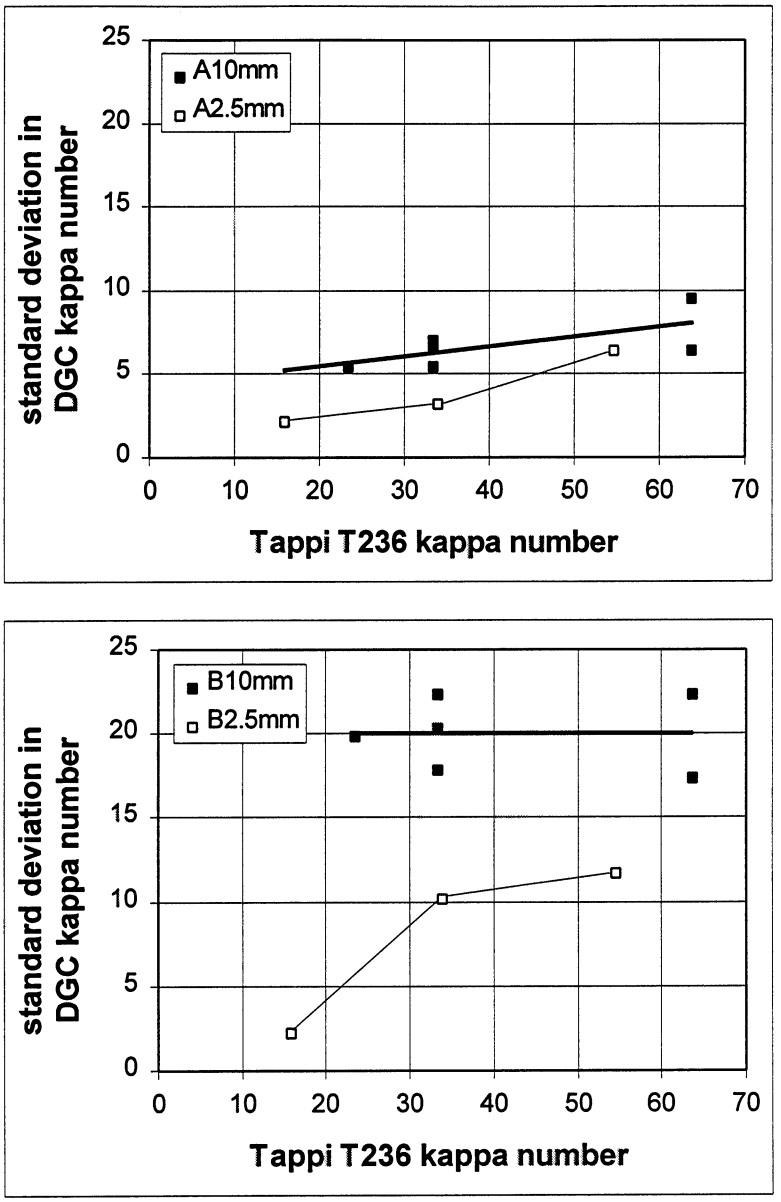

2.5-mm and 10.0-mm refer to chip thicknesses of laboratory kraft pulps.
Holo refers to the standard deviation in average fiber density for all kraft holopulps.

Figure 38. Comparison of component standard deviations in DGC kappa numbers between pulps from 2.5-mm-thick chip and 10.0-mm-thick chips.

It is again evident that the 2.5-mm-thick chip pulps were not as delignification limited as the 10.0-mm-thick chip pulps. The distribution B average and standard deviation in DGC kappa number persists in the thick chip pulps. The mill pulps showed nearly equal differences between component standard deviations in Figure 39.

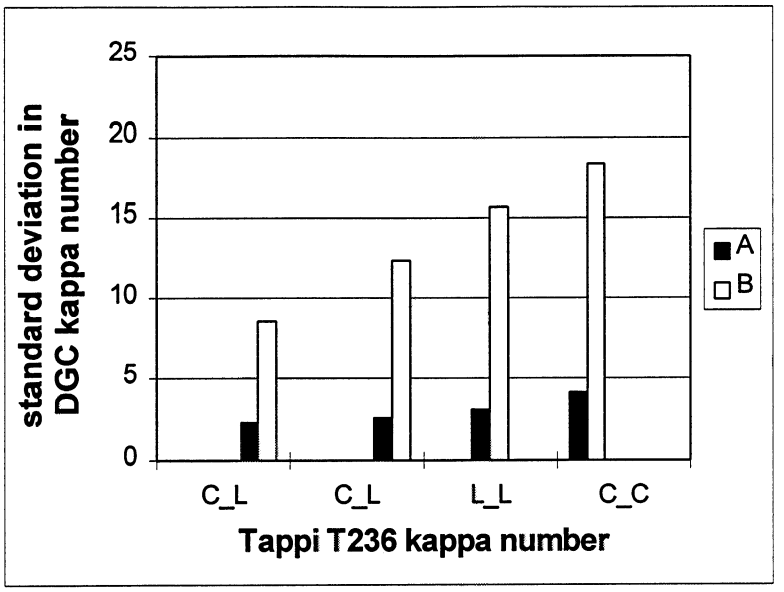

C_L refers to Kamyr conventional feed and Lo-solids™ cooking.
L_L refers to Kamyr Lo-level™ feed and Lo-solids™ cooking.
C_C refers to Kamyr conventional feed and conventional cooking.

Figure 39. Standard deviation in DGC kappa number vs Tappi T236 kappa number for component distributions in mill pulps.

It has been shown that the resolution of the density gradient column technique can be dramatically improved through modification of sampling technique. As a result, random error may be reduced enough to conclude that lignin density does change as a function of extent-of-cook. Furthermore, the UV absorption properties of lignin may assist in producing and analyzing images of dioxane lignin density distributions. Thus, the density gradient column may have the ability to provide the pulp and paper industry with a secondary analysis technique capable of inferring lignin structure in its native state. Yoshida et al.[193] have also shown that lignin pellet density increases with an increase in molecular weight. In turn, this increased molecular weight reflected an increase in thermal stability, as determined by GPC and TGA/DSC. This increase in thermal stability was postulated to come from an increase in degree of branching and condensation. Structural changes of this type have long been assumed to exist in kraft pulps as a result of known chemistry and process conditions[194-199], identified and related

to extent-of-cook[200-206] and bleachability[195-198,206-211]. Thus, a change in lignin density with extent of cook is supported by prior research. A proposed linear variation in lignin density with extent of cook is shown in APPENDIX B.

This density gradient column technique has proven to be very useful in assessing delignification diversity. Although the 95% confidence interval can be quite large at both ends of the secondary analysis calibration, the composite normal model was able to provide novel information with regard to interfiber uniformity. The process was able to provide information on up to four samples per week.

Possible Interpretations of the Composite Normal Distribution

It has been proven that delignification diversity exists on an interfiber basis and is modeled well through a composite normal distribution. However, the origin of this distribution is still subject to debate. The following three fundamental pulping parameters are suspect in the creation of the composite normal distribution: chip thickness, wood structure, and wood chemistry. Chip thickness is mass transfer associated; diffusion of chemicals in and diffusion of reaction products out rely upon chip thickness. Wood structure is highly complex, but this would be inconsequential if the complexity was equivalent between sample sets. Wood chemistry variations rely upon liquor flux, alkali charge, temperature, dissolved lignin, and dissolved sodium.[3,16,30,134,137]. All of these parameters control the relative occurrence of competing reactions that lead to increasing amounts of difficult to remove lignin. The production of two distinct distributions must result from two distinct delignification regimes within the chip.

Delignification limitations in distribution B were greater in 10.0-mm-thick chip pulps as evidenced by the increased component kappa number differences within pulps with extent of cook. The DGC kappa numbers of distributions A and B were significantly different in the 10.0-mm-thick chip pulps that were pulped to lower lignin contents, and the F-ratios for comparing component standard deviations of DGC kappa numbers were significant in every case as tabulated in APPENDIX B. Thus, distributions A and B were statistically proven to be from different populations.

In this study, liquor flux, alkali charge, and temperature were constant between data sets. Chip thickness, dissolved lignin, and dissolved sodium were different between data sets and serve as a point of focus for this discussion. It has been identified that pulp quality increases with a decrease in chip thickness down to 1.5 mm [3], whereas earlier research has shown that 3 mm is the optimal chip thickness[87]. Furthermore, chip thickness related improvements exist beyond modified cooking improvements[134,137].

Wood structure is suspect only in the relative distribution of morphological characteristics between the two laboratory sample sets. The prime consideration is the juvenile wood/mature wood ratio, since it is known that juvenile wood delignifies faster than mature wood[46,212]. Laboratory chips for each data set came from different heights within the tree. The 2.5-mm-thick chips came from the bottom 8 ft section and do not contain pith wood, whereas the 10.0-mm-thick chips are from the adjoining 8 ft section and do contain pith wood. Pith wood is juvenile wood, and the transition from juvenile wood to mature wood is most commonly defined by a change in specific gravity. This change in specific gravity correlates with percent latwood[46], and differences in delignification rates are small, if at all existent, between earlywood and

latewood[42-45]. Zobel[46,48,49] has shown that the juvenile wood contribution decreases with tree age, and the specific gravity of juvenile wood increases with height in the tree. The 22 year old tree used in this study would have been approximately 60 ft tall, and the bottom 16 ft section should contain a relatively small difference in juvenile wood contribution between its upper and lower halves[46]. Both the upper and lower 8 ft sections were assumed to average 14 inches in diameter. Furthermore, the outer annulus subject to veneer cutting was assumed to contain 40% latewood, and the 4-inch core was assumed to contain 20% latewood[212]. Using these assumptions, an estimate was made of the latewood contents of the 2.5 and 10.0-mm-thick chips. The 10.0-mm-thick chips were estimated to contain approximately 37% latewood, whereas the 2.5-mm-thick chips were estimated to contain approximately 40% latewood. As a result, it has been assumed that component pulping behavior differences due to juvenile wood were not significantly different between the 2.5- and 10.0-mm-thick chip furnishes.

Wood chemistry must differ with respect to frequency of competing reactions within thin and thick chip delignification. Increases in chip thickness create alkali depleted conditions[72,87]. Under alkali depleted conditions, the amount of dissolved lignin becomes high relative to alkali. The net result is an increase in products from competing reactions. In addition, an increase in the molecular size and degree of cross-linking in the residual lignin may increase the occurrence of competing reactions by limiting leaching and hindering delignification rates. Lignin has been divided into molecular weight fractions and evidence of cross-linking has been observed[193]. Formation of condensed lignin structures has been observed and related to extent of cook[194,202,204-207]. Increased base reactions such as carbohydrate peeling, stilbene formation, and other competing reactions result in increased dissolved sodium concentrations. Decreased fiber

swelling and a higher molecular weight lignin may result and establish the delignification limitation present in distribution B.

Whiting et al.[63] have calculated the quantity of residual lignin present in cell wall tissue fractions. The quantity of liqnin that did not follow first-order kinetics was considered L_D, or lignin that was "difficult to remove." In whole wood fractions, approximately 3.51% lignin was measured as L_D, or residual phase lignin in spruce. This value is supported by others[54], and represents 13% of the total lignin in spruce[63]. If all fibers are uniformly delignified, then this quantity of 3.51% L_D should be equal on a fiber to fiber basis. This corresponds to approximately 24 kappa number [252].

Distribution A and distribution B appear to represent the outer chip perimeter and the inner chip core, where transfer of chemical in and transfer of dissolved lignin out is impeded during pulping of 10.0-mm-thick chips. Viscosity dropped steeply in 2.5-mm-thick chip pulps in the 24 kappa number range. This limitation appeared related to the native quantity of difficult to remove lignin rather than distribution B. Viscosity dropped in 10.0-mm-thick pulps in the 50-60 kappa number range. This corresponded with differences between delignification levels in distribution A between thick and thin chip pulps. As kappa number decreased, distribution A increased in percent contribution and decreased in standard deviation. Beyond 30 kappa number in 10.0-mm-thick chip pulps, distribution A was forced to delignify further to offset the delignification limitation in distribution B. In both thin and thick chips, viscosity loss was related to overcooking of the pulp at the delignification limitation.

Distribution B contains a higher variation in lignin content and a higher resistance to delignification within 10.0-mm-thick chip pulps. Density gradient column results suggest that

delignification limitations within 10.0-mm-thick chips were primarily due to difficult to remove lignin in distribution B. Distribution B in thick chips appears to have arisen from reprecipitation of dissolved lignin or condensation of residual lignin as a result of mass transfer limitations and associated competing reactions.

Distribution B from thin chip pulps did not appear delignification limited. The standard deviation in distribution B remained the same throughout the cook for 10.0-mm-thick chip pulps, whereas it diminished in pulps from 2.5-mm-thick chips. The diversity present in the 2.5-mm-thick chip pulps may be due to delignification differences between juvenile wood and mature wood[212]. This hypothesis is further reinforced by past research on earlywood and latewood pin chip pulping[45]. Small differences have been observed in delignification rates between earlywood and latewood when pulping each increment separately in the form of pin chips. In addition, Lo-solids™ pulping conditions appear to minimize competing reactions that may create delignification limitations in distribution B. In this study, Lo-solids™ pulps are similar to laboratory produced uniform pulp standards. In contrast, laboratory produced 10.0-mm-thick chip pulps were similar to the conventional feed/conventional cook mill pulp. The overall standard deviation in kappa number appears to correlate reasonably well with chip thickness.

In summary, diffusion limitations appeared to create delignification limitations in distribution B for 10.0-mm-thick chip pulps. Distribution B in the 2.5-mm-thick chip pulps did not appear delignification limited. The origin of distribution B may have been related to quantities of juvenile wood and mature wood, but this is not clear. For example, if distribution B does not exist in chips thinner than 2.5-mm, then it may simply originate from chip thickness derived mass transfer limitations. The delignification limitations that developed within 10.0-

mm-thick chip pulps were most likely from the alkali depleted conditions and high dissolved lignin content in the chip center.

Although it is not clear where diffusion limitations end and chemical reaction limitations begin in this study, it appears that distribution A represents the outer portion of the chip and distribution B represents the core. Correlations between the drop in distribution A kappa number and overall viscosity suggest overcooking of the chip perimeter in 10.0-mm-thick chip pulps. Viscosity was maintained until the theoretical 24 kappa number limit in 2.5-mm-thick pulps. Chip thickness appears to be the controlling factor in delignification diversity. The improved uniformity from the Lo-solids™ process suggests that reductions dissolved lignin and dissolved sodium offset the dependence of uniformity on chip thickness.

CHAPTER FOUR: INFRARED SPECTROSCOPY

PRINCIPLES

Theory

Infrared spectroscopy has been extremely useful to the study of cellulose and lignin for many years. Modern interferometers are based on the Michelson two beam interferometer designed in 1891, and later improved by the advent of the fast Fourier transform, minicomputers, and helium-neon lasers in the 1960s[213]. Although use of infrared spectroscopy prior to this period required much time and effort, extensive information was still obtained for complex molecules.

Infrared spectra of organic substances can be highly complex. This is due to the fact that the amount of possible fundamental vibration modes for nonlinear molecules containing n atoms is $3n$-6. Many of the energy absorptions associated with these vibrational modes occur at the same frequency, and not all of the absorptions are independent. In addition, there are also overtone frequencies corresponding to excitation of molecules to the next vibrational state[214]. Thus, the investigation of lignocellulosics has been ongoing for many years. A brief description of some major contributions leading to quantitative determinations of lignin in wood pulp will now follow.

Spectroscopy of Cellulose, Lignin, and Lignocellulose

Several infrared techniques have been used to examine cellulose and lignin. As a result, these studies have led to many attempts at identifying and quantifying wood pulp components[215-

[230]. Fortunately, early research by Marrinan and Mann[231-233], Liang and Marchessault[215,234-238], Higgins, Stewart, and Harrington[239], and O'Connor[240] have provided information essential to the understanding of cellulose infrared absorptions and their relation to cellulose structure[241]. In addition to contributing to the understanding of cellulose absorption band assignments, deuteration of amorphous regions helped to resolve diffuse bands[231], use of plane-polarization helped to estimate molecular chain orientation[232,235-237], and peak ratios were used to estimate degree of crystallinity[240]. Band assignments for cellulose have been conveniently tabulated in standard reference materials[242].

Subtraction techniques can be used to simplify a complex spectrum by subtracting a reference spectrum until there is a growth of negative peaks in the original spectrum[213]. Although this method may be fine for qualitative work, quantitative analyses should use a less subjective subtraction technique to ensure reproducibility. Component ratios or regression analyses have been used objectively to acquire reproducible information from multicomponent spectra. Component ratios make the assumption that component spectra are orthogonal, where the overall matrix does not have an effect on individual absorbencies. Regression analyses determine the most significant peak correlations between some accepted measure and the secondary measure determined by the infrared spectra calibration set. The following researchers used a variety of methods over a 30 year period to estimate component concentrations within wood pulps.

In 1962, Kolboe and Ellefsen[218] concluded that Norwegian spruce contains 28-29% lignin. Difference spectra were taken by analyzing 10 mg O.D. wood in KBr against varying

quantities of lignin in KBr. Complete elimination of the absorption peak at 1515 cm^{-1} occurred using 2.8-2.9 mg lignin in the reference beam.

In 1967, Marton and Spark[219] used the attenuated total reflectance of a multiple internal reflectance prism to enable examination of low lignin pulps. Secondary analyses were performed using 1510 cm^{-1}/1310 cm^{-1} peak ratios against acetyl bromide estimations of lignin content. The procedure was found to be accurate within ±4% above 30 kappa number. A similar secondary analysis procedure was used in 1969 by O'Connor[240] to determine percentages of synthetic fiber in cotton blends.

In 1980, Saad, Issa, and Fahmy[220] used KBr pellet spectra to ratio peaks at 1600 cm^{-1}, 1595 cm^{-1}, and 1510 cm^{-1} against the peak at 893 cm^{-1}. Baseline correction techniques were varied and two linear regions corresponding to 13.8-15.8% and 8.8-11.8% lignin were identified. However, this study agreed with that of Bolker and Somerville[215]; infrared spectroscopy was not suggested for lignin contents less than 10%.

In 1987, Berben et al.[221] used DRIFT (diffuse reflectance fourier transform) spectroscopy to acquire infrared spectra from pulps containing 1-20% lignin. Lignin difference spectra were produced by subtracting a cotton linters spectra from brownstock pulp spectra. The area under the 1510 cm^{-1} peak was regressed against klason lignin, and the standard error of analysis was approximately ±10 kappa number, or ±1.8% klason lignin.

In 1990, Schultz and Burns[215] used four peaks to determine lignin, hemicellulose, and cellulose composition with FTIR by secondary analysis combined with stepwise regression. Standard KBr pellet techniques were combined with first-derivative spectra to avoid difficulties

in baseline shift and accentuate small spectral differences. Since first derivative spectra give negative peaks, the absolute value of the first-derivative was used in the 1600-900 cm^{-1} spectral region. The R^2 values for softwood were 0.98 and 0.83 for lignin and cellulose, respectively. The fit for hemicellulose was too poor for consideration. The R^2 values for hardwood were 0.97, 0.91, and 0.90 for lignin, cellulose, and hemicellulose, respectively.

In 1991, Backa and Brolin[220] used DRIFT in combination with partial least squares analysis. A total of 232 peaks were selected outside the range of 2800 and 1750 cm^{-1}, and between 3300 cm^{-1} and 450 cm^{-1}. A few peaks were chosen in accordance with the works of Faix[222] and Schultz et al.[221], and all were approximately 10 cm^{-1} apart. The standard error provided by this technique was ±2.75% for lignin content determination. Wallbacks et al.[226] used a similar procedure and obtained a standard error of ±3.3% for lignin determination.

Later in 1991, Friese and Banerjee[227] developed upon a unique computational method to determine pulp lignin content. DRIFT spectra were obtained using disks that were cut from air-dried pulps and stacked in a sample cup. The premise of this procedure was that spectral complexity decreases as constituent spectra are subtracted. One measure of complexity is the integrated positive and negative area of first-derivative spectra. If a fraction of a component spectrum is subtracted stepwise from the multi-component spectrum, and the area of the first-derivative spectra is obtained, the component spectrum will be factored out when the first-derivative area minimizes. This procedure was used by subtracting individual lignin and cellulose component spectra from brownstock pulp, where the cellulose component served as an internal standard. The lignin:cellulose ratio was linearly regressed against kappa number for a variety of kraft softwood pulps. The uncertainty of this secondary analysis technique was

approximatley ±2 kappa units in the 10-40 kappa number range. The apparent high precision and sensivity of these data led to further investigation in the development of this thesis work.

Microspectroscopy

Infrared microspectroscopy is a technique that began development over three decades ago[243]; however, there have been few publications in this area of research since that time[244-249]. Nevertheless, the technique has proven to be very useful in determining compositions of small samples. Unfortunately, specular distortions from sample size and shape create experimental limitations. The technique is considered to be relatively mature in terms of qualitative determinations, however, its limitations in quantitative analyses are not fully understood[247].

Either reflectance/absorbance or transmission modes can be used to analyze samples. Reflectance/absorbance infrared spectra are obtained by collecting reflected and transmitted radiation from a reflective surface below the sample. An ATR (attenuated total reflectance) objective is used to collect and focus the refracted radiation for the detector, and only the upper collimator is required. Transmission spectra were used in this thesis, and the complications associated with transmission microspectroscopy will be discussed according to the optical arrangement shown in Figure 40.

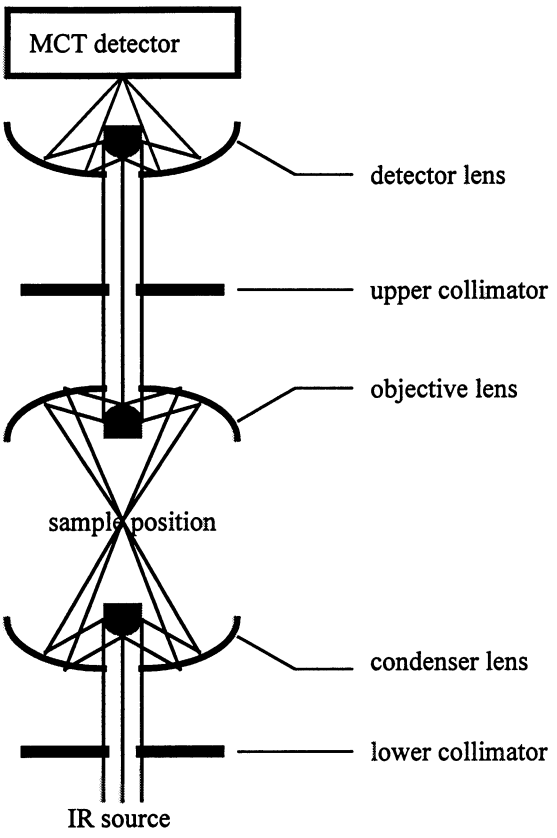

Figure 40. Diagram of infrared microscope optics.

The mercury-cadmium-telluride detector is cooled by liquid nitrogen, and the detector lens is prepositioned by the manufacturer. However, positioning of the objective lens and condenser lens are critical to spectral quality and vary from sample to sample. In fact, positioning of the condenser lens must be checked periodically, since even the slightest disturbance can affect its position and create specular distortions. The upper and lower collimators are adjusted in an effort to restrict incident and transmitted radiation to the particular area of interest. Irregularities in the sample structure, diffraction of radiation from collimator edges, or inaccuracies in lens adjustment cause degradation of spectral quality[249].

Complications due to sample structure were of most concern in this study. Wood pulp fibers are highly complex polymer networks that are also geometrically nonuniform. The optical

configuration of the infrared microscope is designed to reproducibly send accurate and quantitative information from the sample to the detector. However, the presence of a cylindrical fiber can create lensing effects and cause the transmitted radiation to stray from its intended path[244]. Furthermore, any irregularities in the fiber surface can cause further straying of transmitted radiation. To gain control over irregularities in physical structure, pliable fibers can be compressed to form thin films[249]. Unfortunately, these compressed fibers are subject to changes in molecular interaction, thus resulting in spectral differences that may be due to factors such as increased crystallinity[250].

TASK OBJECTIVES

The experimental approach to measure lignin content in individual fibers used the spectral subtraction procedure of Friese and Banerjee[227]. The following objectives were met in this portion of the thesis work: 1) determine the flexibility of the spectral subtraction procedure with respect to changes in band width using a simple spreadsheet model; 2) assess the accuracy and sensitivity of the spectral subtraction procedure using a liquid-cell system; and 3) develop a means of comparing KBr pellet spectra with microcompression cell spectra. Quantitative analyses may be seriously hindered by differences between KBr pellet spectra and compression cell spectra. This problem was addressed by attempting to locate bands that were not measurably affected by compression cell pressure.

MATERIALS

Chemicals

Table 16 lists the necessary chemicals. For common analyses, such as kappa number, viscosity, and ABC titrations, chemicals from the common laboratory supply were used.

Table 16. Chemical listing for infrared spectroscopy.

Chemical	Vendor
carbon tetrachloride, technical grade	VWR
tetrachloroethylene, technical grade	VWR, Fischer
chloroform, technical grade	VWR, Fischer
potassium bromide, analytical grade	VWR
acetophenone	VWR
toluene	VWR
liquid nitrogen	Air Products

Laboratory Pulps

Table 17 summarizes the laboratory-produced kraft pulps used in FTIR analyses. The wood source was southern yellow pine, 3.0-mm-thick, rotary-cut veneer.

Table 17. Description of laboratory pulps used in FTIR analyses.

Parameter	A	B	C	D	E
chip thickness, mm	3.0	3.0	3.0	3.0	3.0
temperature, C	165	165	165	165	165
effective alkali, gpl	40	40	40	40	40
sulfidity, %	30	30	30	30	30
target H-factor	2000	1500	1000	750	400
kappa number	11.9	17.6	21.5	32.9	78.0
% unscreened yield	42.7	44.8	48.0	49.4	59.5
% screened yield	42.7	44.8	48.0	49.4	52.1
time to temperature, min.	60	60	60	60	60
time at temperature, min.	180	137	83	63	24
L:W=6:1, EA=24% on wood 30% sulfidity, based on AA					

EQUIPMENT

FTIR Instrumentation

A Nicolet infrared spectrometer with a Nic-Plan™ microscope attachment was used to obtain FTIR spectra. A demountable liquid transmission cell and pellet press were used to produce liquid-cell spectra and KBr pellet spectra, respectively. In addition, a Spectra-Tech Microcompression Diamond Cell™ was used to mount individual fibers and obtain single fiber spectra. Grams 386™ spectral analysis software from Galactic Industries was used for spectral manipulation, component subtractions, and displaying of results.

METHODS

Liquid-cell Spectroscopy

Liquid-cell results were obtained using 0.025-mm-thick teflon spacing between KCl salt plates in the cell. Sample spectra were compiled from 128 scans at 8 cm^{-1} resolution, and background spectra were taken with the KCl salt plates in direct contact.

KBr Pellet Spectroscopy

All fiber samples were freeze-dried and stored in a dessicator filled with $CaSO_4$ prior to analysis. Each sample was then cryocrushed with liquid nitrogen and mixed with KBr at a concentration of 0.5-1.0%. Cotton fiber was used for the cellulose subtraction standard, whereas dioxane lignin from a 28 kappa number conventional softwood kraft pulp was used for the lignin subtraction standard. A dry air purge system was used and spectra were taken from 128 scans at 4 cm^{-1} resolution.

Single Fiber Spectroscopy

Individual fiber spectra were taken in a Spectra-Tech™ diamond compression cell. Each fiber was individually mounted under a light microscope with a small quantity of KBr mounted next to each fiber for background corrections. Variable aperture size was used with an average aperture size of approximately 20 μm x 20 μm. Spectra were acquired from 128 scans at 4 cm^{-1} resolution.

RESULTS

Subtraction Algorithm

The subtraction algorithm approach of Friese and Banerjee[227] has been proven to serve as a powerful spectral subtraction procedure. However, it is not limitless in its application. Problems due to component band overlap, specular distortions, and differences between calibration spectra and single fiber spectra were suspected and subject to investigation.

This particular subtraction technique is based on the premise that as spectral complexity decreases, so does the area under the first derivative curve of the given spectra. In effect, complexity is reduced as individual component spectra are subtracted from their mixed component spectra. Thus, component concentrations can be derived using this technique. Unfortunately, band overlap can create inaccuracies in these quantitative analyses. Furthermore, it is sometimes difficult to obtain representative component spectra to use as subtraction standards, or subtrahends. In an effort to acquire an understanding of the limitations of this spectral subtraction technique, a spreadsheet model was developed. All the results are shown in APPENDIX C, however, a summary of the results now follows.

Figure 41 describes the way in which optimum "subtraction factors" are chosen. The optimum subtraction factor is that which minimizes the area under the first derivative curve of the subtraction result. However, the component subtraction standard, or subtrahend, may have spectral characteristics different from the actual component being quantified. This may be due to a poor choice of the standard from a misunderstanding of chemical structure, limitations in isolating a standard free from chemical modification, or possibly from impurities.

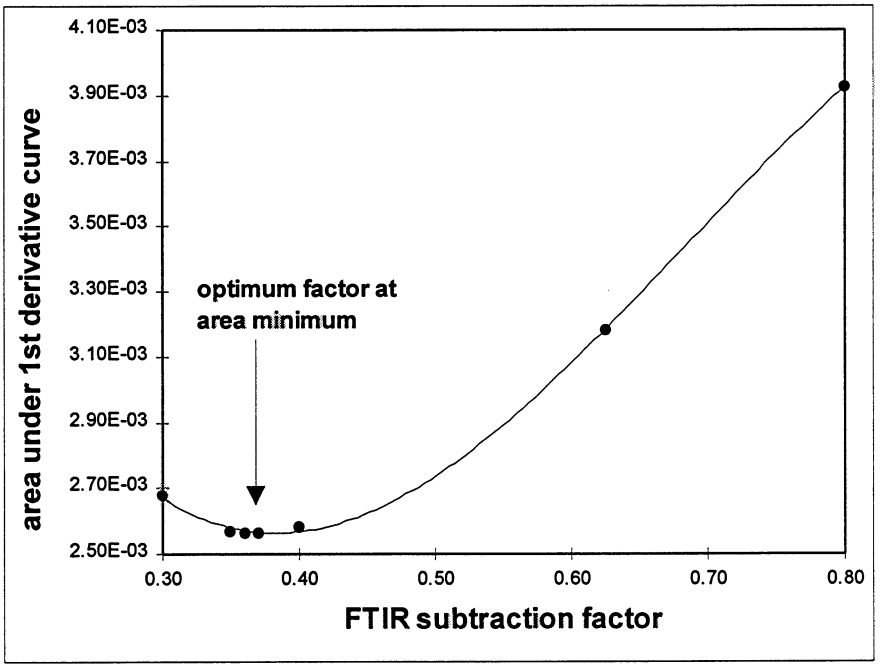

Figure 41. Selection of an optimum FTIR subtraction factor.

A spreadsheet model was used to determine the effect of differences in spectral character. Normal curves were produced and manipulated by varying the average and standard deviation of component curves according to the needs of this investigation. A simplified system analogous to the lignin/holocellulose system was used, where "perfect" and "imperfect" subtraction routines proved that slight deviations in spectral character can create large deviations in subtraction results.

A perfect subtraction routine would include subtrahends that are identical to the component that is being removed from an overall spectrum. Unfortunately, it is sometimes very difficult to obtain such subtrahends. Infrared spectra are very sensitive to the state of the sample[213]. Changes in the state of the sample relate to changes in molecular vibrations and can be due to many factors such as differences between sample analysis techniques[213,249] and differences within sample analysis techniques[251]. Figure 42 compares the slope of calibration curves obtained using ideal and nonideal component standards.

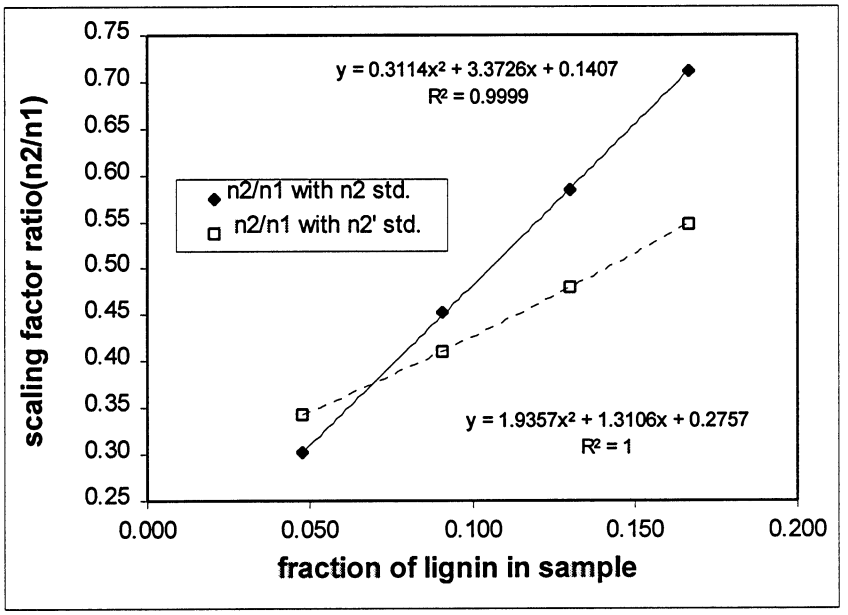

Figure 42. Calibration curves from perfect and imperfect subtraction standards.

Component n1 serves as the cellulose analog and is perfect in both calibration curves. Components n2 and n2' are perfect and imperfect lignin analog standards, respectively. Any errors inherent in this secondary analysis technique become more critical when the slope of the calibration curve decreases. Component n2' was slightly narrower than the perfect standard n2.

Figure 43 provides a simplified example of how slight imperfections in component standards affect subtraction results. In this case, the subtraction component n1' has a sharper distribution than component n1. The subtraction result is not a pure component representing 20% of n2, but rather a mixture of n1 and n2. Despite this limitation, the secondary analysis procedure is still very powerful under controlled conditions. However, it becomes important to restrict interpretations to spectra within specific sample sets. Thus, the technique becomes less robust. Furthermore, the precision of the technique suffers when imperfect subtraction standards are used to estimate component composition.

Changes in spectral character have been shown to adversely affect subtraction results and limit the applicability of the subtraction algorithm. These changes can occur from a variety of sources, however, deliberate changes in experimental technique and technique limitations are of most interest in this study. Unfortunately, this interest takes the study away from a specific sample set and forces a merger between two different types of infrared spectra. Likewise, variations in the amount of band overlap can adversely affect results. In order to isolate the affect of band overlap on the subtraction algorithm, liquid-cell spectra were acquired from four separate organic components. The goal was to determine if individual concentrations could be resolved from volumetrically determined mixtures.

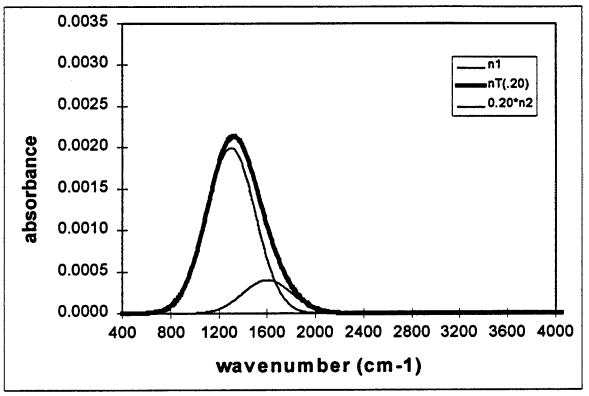

components n1, n2, and overall nT

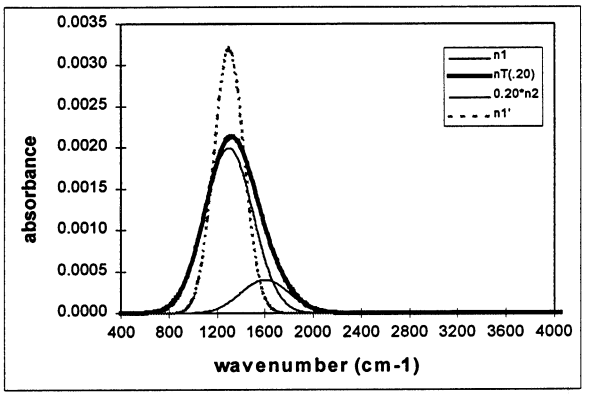

components n1, n1', n2, and overall nT

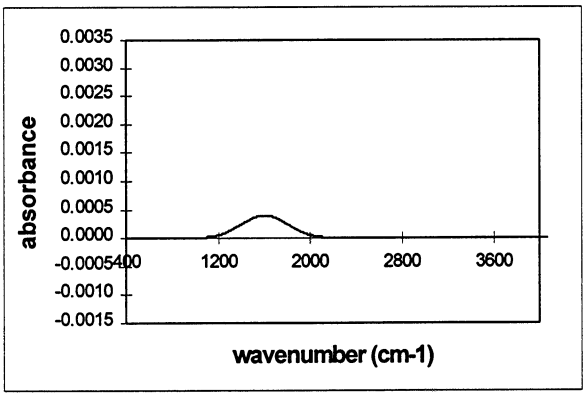

subtraction result using perfect standard n1

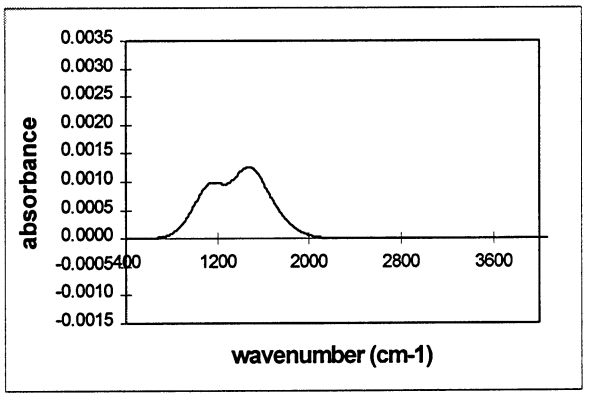

subtraction result using imperfect standard n1'

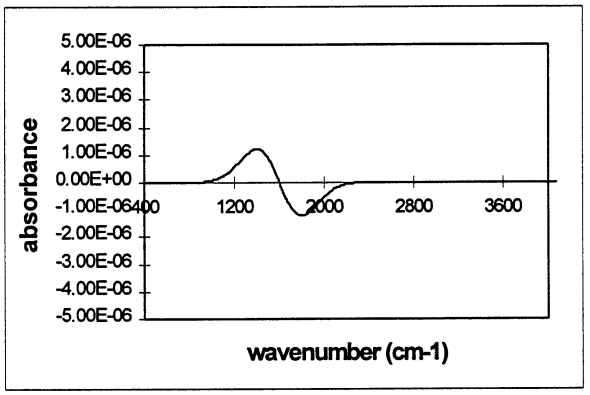

area under 1st derivative curve of subtraction result

a.) perfect subtraction standard

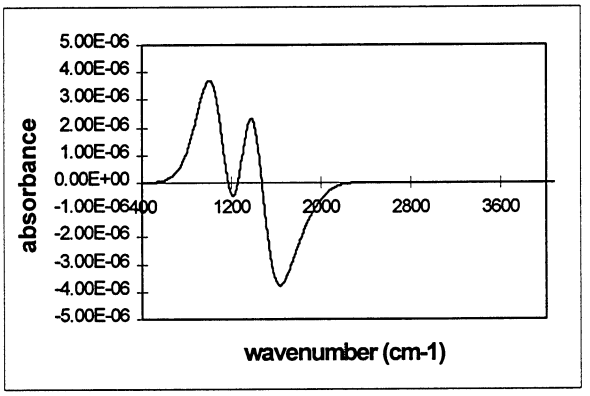

area under 1st derivative curve of subtraction result

b.) imperfect "sharp" subtraction standard

Figure 43. Comparison of results from perfect and imperfect subtraction standards.

The Liquid-cell Model System

A four component organic solvent mixture was used to test the versatility of the spectral subtraction technique within a simple system. A liquid-cell method was chosen for the reproducibility and simplicity of liquid state infrared spectra to eliminate problems due to variation in molecular vibrations. Furthermore, mixtures of any number of organic liquids could easily be produced. Figure 44 shows the infrared spectra of the four organic compounds selected for use in this study. Toluene (A), tetrachloroethylene (B), and acetophenone (C) were combined volumetrically in a carbon tetrachloride (D) background. Carbon tetrachloride served as a diluent because of its relatively nonabsorbing character. For example, the high absorbance of the carbonyl group in acetophenone required that it be mixed in a relatively nonabsorbing background at lower concentrations.

Each component was combined volumetrically with carbon tetrachloride to form individual calibration curves. Subtractions were performed in select spectral regions to emphasize individual component characteristics outside of the range of CCl_4 absorptions. Toluene (A) was quantified using the region from 1000-1650 cm^{-1}, and tetrachloroethylene (B) was quantified using the region from 850-1825 cm^{-1}, and acetophenone (C) was quantified using the region from 1200-1725 cm^{-1}. The overtone region was excluded, in general, because it would also be excluded in the wood matrix system in an effort to avoid error from variations in water content. Furthermore, the strong absorption from the acetophenone (C) carbonyl group in the 1700 cm^{-1} region makes its aromatic absorption region appear insignificant in comparison to same region for toluene (A).

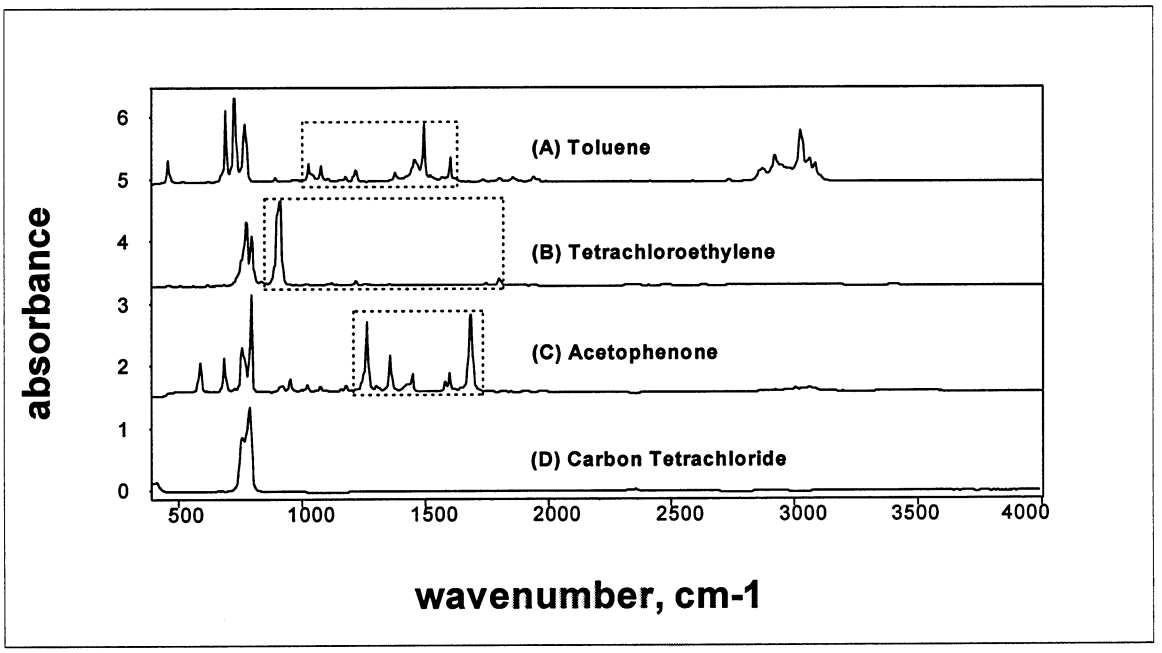

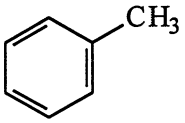

A.) Toluene

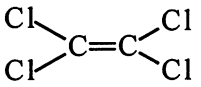

B.) Tetrachloroethylene

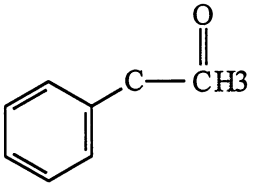

C.) Acetophenone

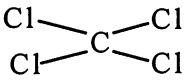

D.) Carbon Tetrachloride

Select subtraction regions for each component are outlined above.

Figure 44. Infrared spectra and chemical structure of liquid-cell model components.

The pathlength of the liquid cell was constant and linear relationships existed between FTIR scaling factors and known percent compositions. Figure 45 suggested that the subtraction algorithm worked very well for mixtures of single components in CCl_4. However, a more valid test should involve subtractions performed under conditions of band overlap.

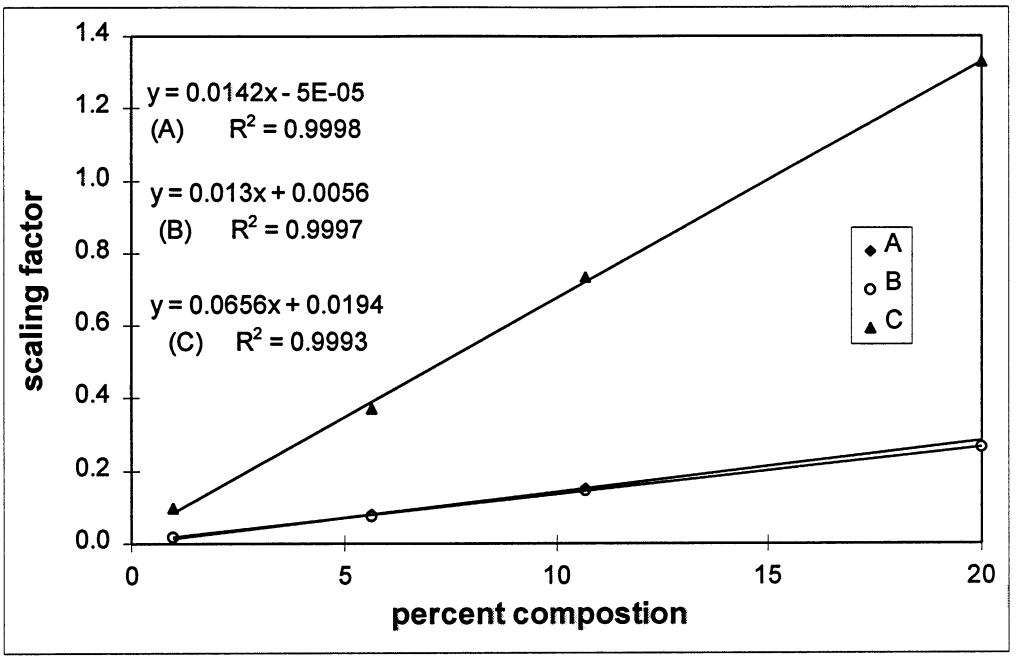

Figure 45. Calibration curves for the liquid-cell model subtraction system: toluene (A), tetrachloroethylene (B), acetophenone (C).

Figure 46 provides an example of one of many four component mixtures from which the subtraction algorithm was able to quantify individual component concentrations. APPENDIX C contains a statistical analysis of liquid cell subtractions using a 2^3 factorial analysis with an analysis of variance for systems of complex mixtures. Yates' algorithm was used to separate effects of high and low component concentrations within and between the three individual components mixed with CCl_4. In addition, it was possible to assess component interactions with this statistical technique. The dependent variable was measurement accuracy using volumetrically determined compositions as the referee technique. The sums of squares of the differences between volumetrically determined concentrations and spectroscopically determined concentrations represented measurement accuracy.

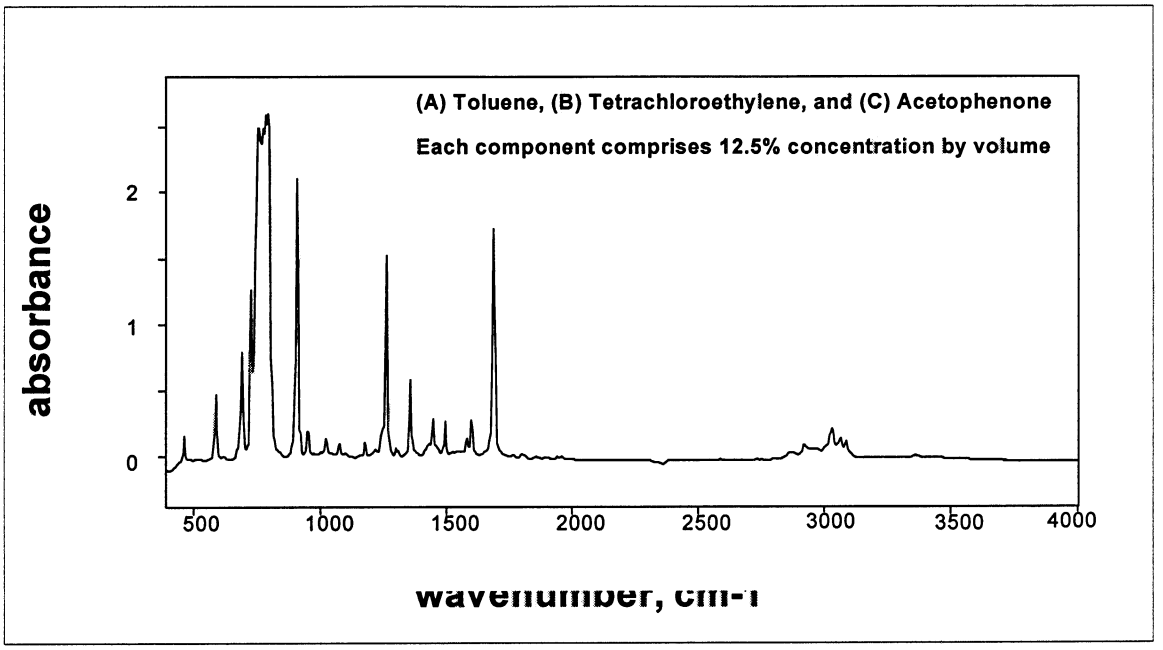

Figure 46. Liquid-cell model component mixture in a CCl_4 base.

The F-ratios for all interactions never exceeded the critical F-ratio at the α=0.05 level of confidence. Therefore, the technique worked for this liquid-cell system. However, a small negative interaction effect, along with an increased F-ratio, did exist when the concentration of toluene was at its high level in the presence of tetrachloroethylene and/or acetophenone. In other words, the accuracy of the technique can diminish from component interactions.

In summary, the liquid-cell model has demonstrated that the subtraction technique has the ability to resolve fairly complex mixtures into individual component concentrations. However, band overlap and component interaction difficulties can arise. To minimize band overlap problems, each component under analysis should contain distinct spectral information. Component interaction difficulties did not appreciably affect the accuracy of the spectral subtraction technique in this particular application.

Kraft Pulp Brownstock Calibration Set

Confidence in the subtraction algorithm and liquid-cell data led to the analysis of the more complex solid phase samples. Spectra from KBr pellets were chosen as the calibration set for the secondary analysis of infrared data. Approximately 1 mg of fiber, or 1000 fibers, were cryocrushed and mixed with KBr to form pellets and represent a spectral average for a given pulp sample. As shown in Figure 47, pellet spectra from cryocrushed fibers were easy to reproduce, thus serving as good calibration standards.

Past research has shown that variations in sample preparation create variations in spectral results[251]. APPENDIX C illustrates spectral variations due to the presence of water, the effect of oven drying, and the effect of grinding cellulose samples in a Wiley mill™ and Wig-L-Bug™. A Wiley mill is a centrifugal cutting device that repeats cutting until the fibers pass through a screen of specific size. The Wig-L-Bug™ is a device that is used to ball-mill particles into a powder.

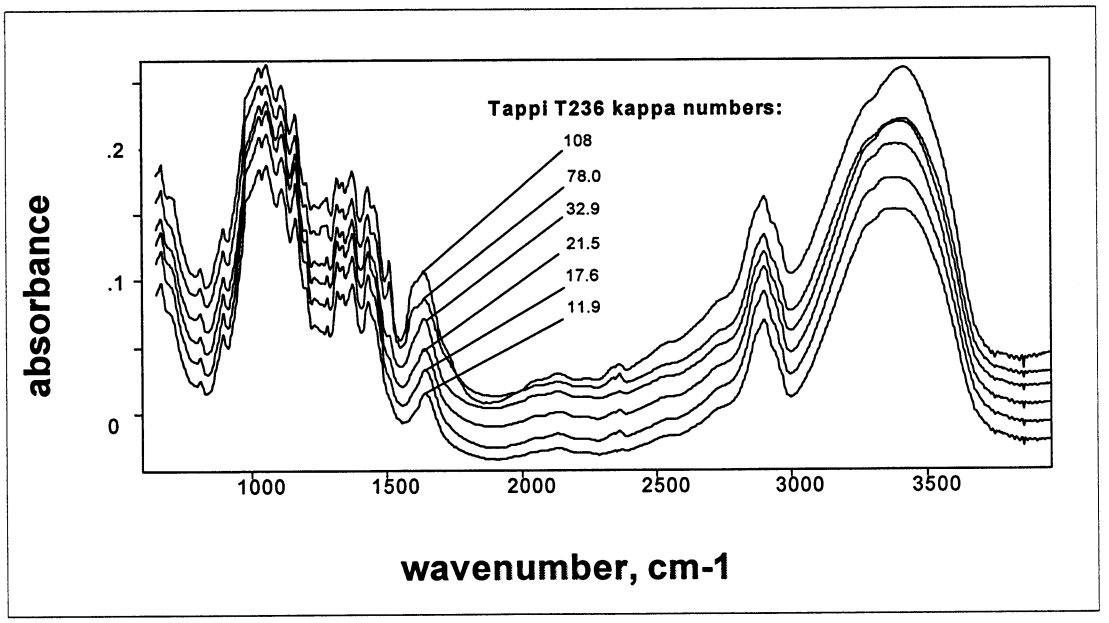

Figure 47. Infrared KBr pellet spectra of a kraft brownstock pulp calibration set.

Figure 48 illustrates the excellent calibration curve obtained from KBr pellet spectra. The 95% confidence band for the mean response indicates that very little error can be assumed from this secondary analysis. Cotton fiber was used for the cellulose subtraction standard, and 28 kappa softwood dioxane lignin was used for the lignin subtraction standard. One aspect unique to this study was that select subtraction regions of 1300-1475 cm^{-1} and 1225-1525 cm^{-1} were used for cellulose and lignin, respectively. These regions were chosen on the basis of pellet spectra and microcompression cell spectral similarities. A way of obtaining a measure of "percent similarity" will be discussed in the following section.

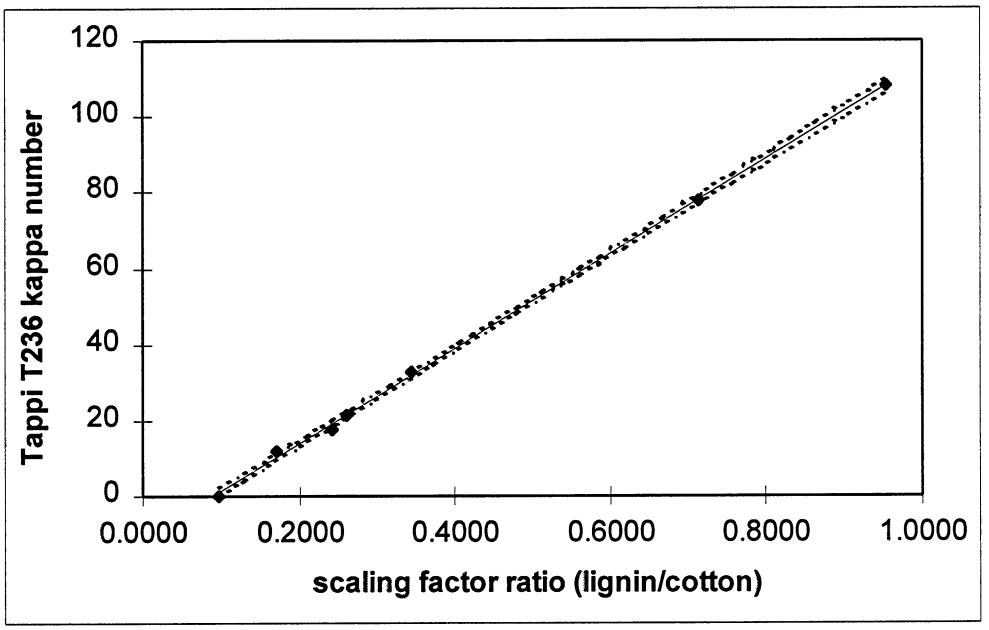

slope	intercept	R^2	std. error in kappa number
124.9	-11.05	0.9992	1.2

Figure 48. Calibration curve for FTIR secondary analysis.

Infrared microspectroscopy with a diamond compression cell was chosen to acquire and relate single fiber spectra to the KBr pellet calibration spectra. Unfortunately, microcompression cell cellulose spectra were appreciably different in character than pellet cellulose spectra, as

shown in Figure 49. This was anticipated due to expected changes in molecular vibration within the fiber when pressure is applied. Furthermore, it can be seen that the relative amount of lignin being measured was very small.

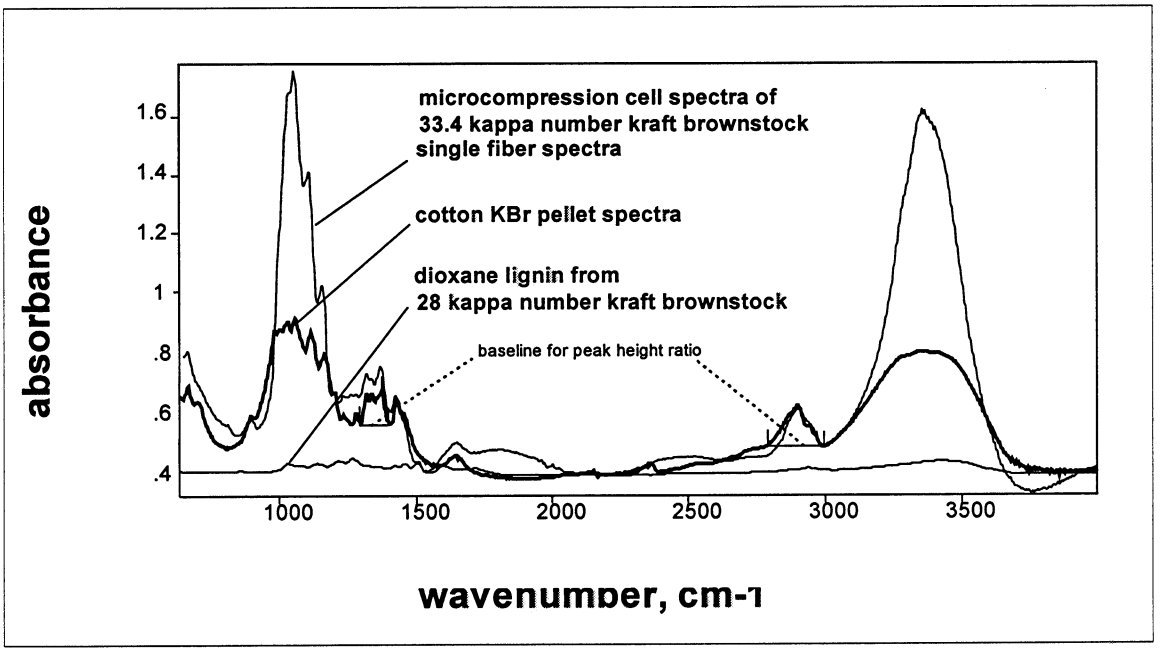

Figure 49. Comparison of spectra: micrompressed fiber and pellet cellulose relative to pellet lignin.

Only a 10.7% similarity existed between microcompression cell spectra and pellet spectra in the range of 850-1525 cm^{-1}. An estimate of percent similarity was calculated by producing a difference spectrum from a microcompression cell sample and a pellet sample from the same source. The difference spectrum represents a fraction of the original microcompression cell spectrum, and this fraction is estimated using the subtraction algorithm as follows:

(1) microcompression cell spectrum-(fraction$_1$)(pellet spectrum) = difference spectrum$_1$

(2) difference spectrum$_1$-**(fraction$_2$)**(microcompression cell spectrum) = difference spectrum$_2$

(3) (1-**fraction$_2$**)100 = **percent similarity**

Difference spectrum$_1$ is automatically scaled to the microcompression cell spectrum from subtraction (1). The fraction from subtraction (2) represents dissimilar spectral character

between difference spectrum$_1$ and the microcompression cell spectrum. Percent similarity was then calculated from (3). Using this method, the percent similarity values in Table 18 have been chosen to correct subtraction factors obtained from the select regions of microcompression cell fiber spectra. Minor differences existed between microcompression cell lignin spectra and KBr pellet lignin spectra, as shown in Figure 50. Subtraction factors for lignin were also corrected according to values in Table 18.

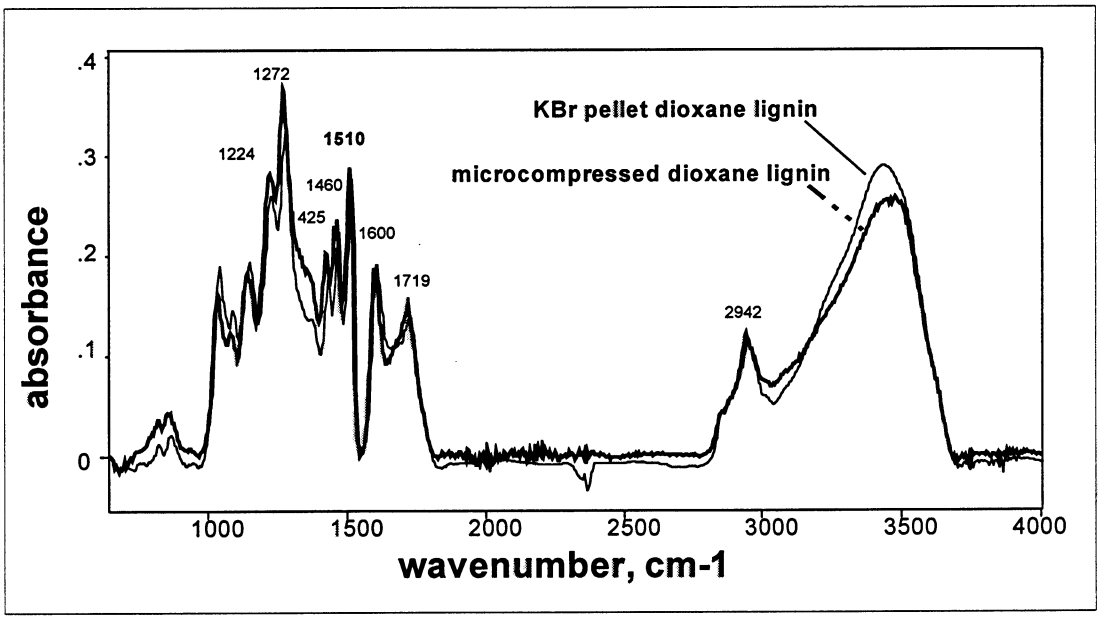

Figure 50. Comparison of micrompression cell lignin and pellet lignin FTIR spectra.

APPENDIX C contains an explanation of how and why the percent similarities were used with peak height ratios to correct for spectral changes due to microcompression cell pressure. Figure 51 describes how baselines were chosen to measure peak height ratios. O'Connor[240] has shown that cellulose crystallinity can be measured through the 2900 cm^{-1}/1372 cm^{-1} peak ratio. A decrease in peak ratio was shown to correlate well with an increase in cellulose crystallinity as determined by x-ray diffraction. Compression cells have also been shown to increase

crystallinity within fiber samples[250]. It was proposed here that compression effects could be corrected using measurement of changes in select peak intensities.

Table 18. Percent similarity measurements with associated error.

sample description	select region:	%similarity 1225-1525 (cm-1)	1300-1475 (cm-1)
microcompression cotton and cryocotton pellet			
cotmc1bc and cot12bc			76.48
cotmc2bc and cot12bc			81.96
cotmc3bc and cot12bc			78.25
cotmc4bc and cot12bc			84.94
microcompressed lignin and lignin pellet			
dlgmcbc1 and dlig1_bc		81.79	
dlgmcbc2 and dlig1_bc		82.81	
dlgmcbc3 and dlig1_bc		87.00	
average		**83.87**	**80.41**
stdev.		**2.76**	**3.79**
CV		**0.0329**	**0.0471**

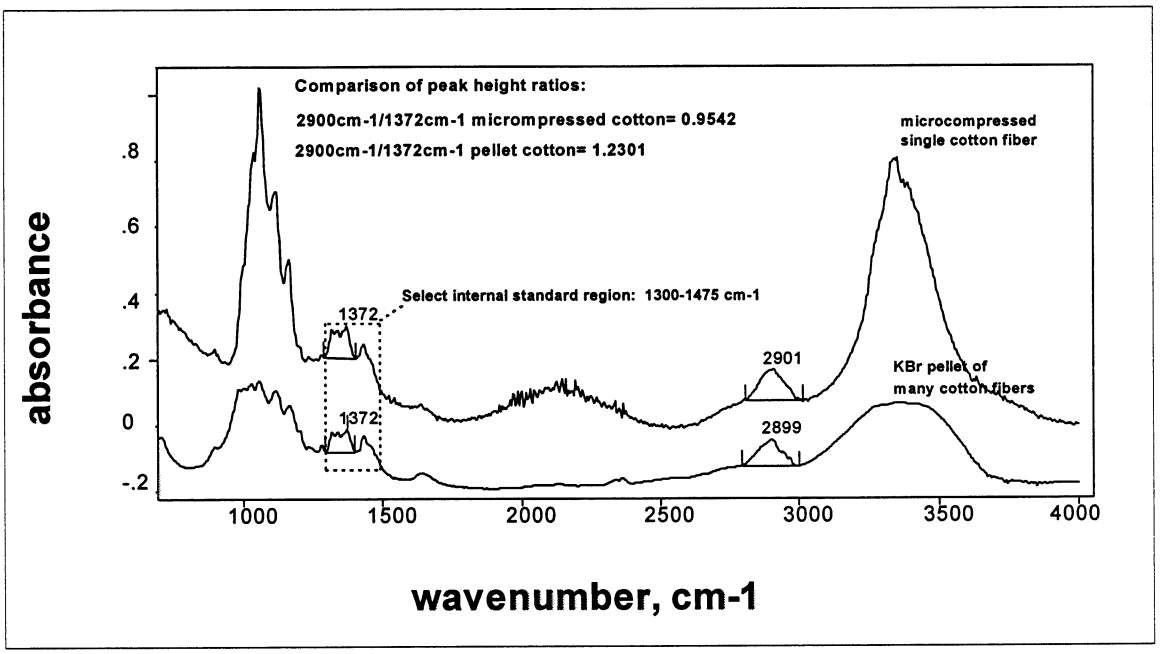

Figure 51. Comparison of peak height ratios and the select cellulose spectral region.

Table 19 contains results of individual fiber FTIR kappa number determinations of five different pulp samples. Although the relative values of the five data sets appear fairly consistent

with expectations, the accuracy of the data is poor. The most obvious error was the negative kappa number of cook 7m. Aromatic peaks were obviously present in the 1510 cm^{-1} region for this data set, but this was not evident from the spectral subtractions. However, the standard deviations in average kappa number values were relatively close to expected values. Therefore, the procedure had some merit, but the variability in individual fiber spectra created too much variability in the subtraction results.

Table 19. FTIR kappa number results using percent similarity and pressure corrections.

file	fiber location	chip thickness(cm)	Tappi T236 kappa	FTIR kappa	FTIR stdev
Cook 7m	middle	10.0	33.4	-6.42	19.28
Cook 7e	end	10.0	33.4	41.68	18.38
Cook 9m	middle	2.5	33.9	26.07	14.43
Cook 9e	end	2.5	33.9	31.35	14.67
78 kappa	middle	2.5	78.0	99.96	16.33

APPENDIX C describes development of the FTIR spectral analysis techniques and discusses procedures and results in more detail.

The quality of the microcompression cell spectra is diminished by specular distortions and variations in state. Spectral quality should be improved prior to further investigation. Figure 52 provides an example of typical spectral variation obtained with the microcompression cell.

When evaluating the spectra in Figure 52 from front to back, the first three spectra show a small peak in the 1510 cm^{-1} region; this is an aromatic ring stretching absorption that correlates well with overall lignin content. The fourth spectrum would be discarded due to specular distortion, and the fifth spectrum shows how specular distortion can completely mask the 1510 cm^{-1} region. Reasonable calibration curve spectra did result using a select spectral region of 975-

1475 cm^{-1} for lignin. However, the variations in band overlap from variations in pressure resulted in meaningless subtraction results for compression cell spectra.

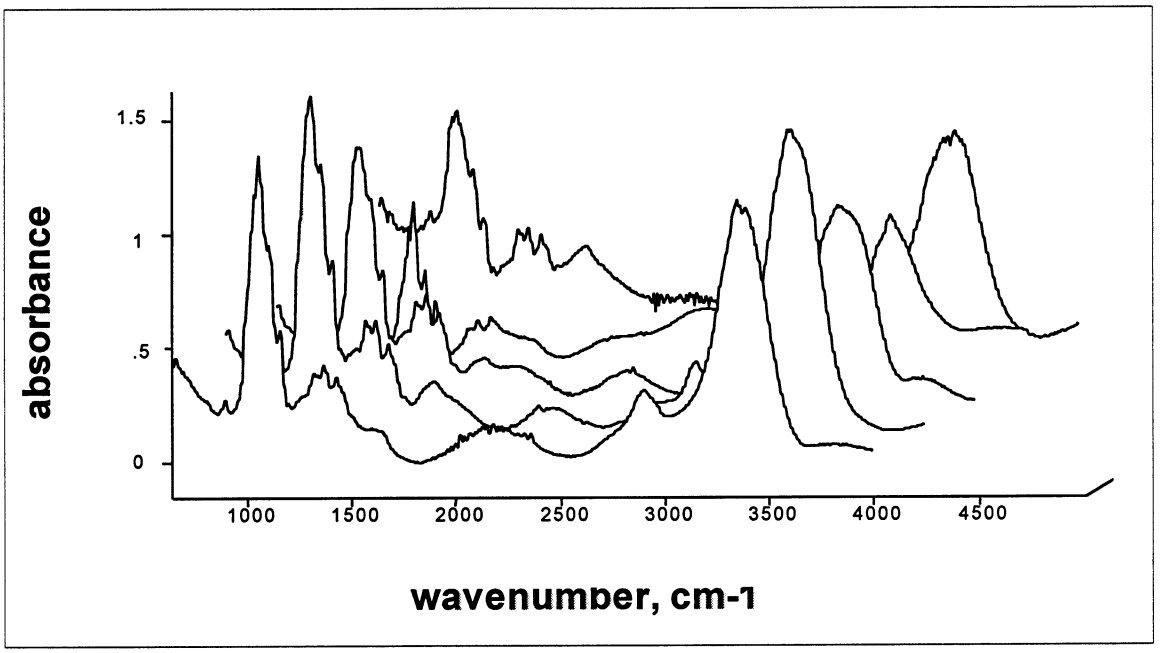

Figure 52. Spectra from Cook 7m illustrating variability of compression cell spectra.

Difference spectra from the KBr pellet calibration set were investigated to understand spectral changes that occur in lignin throughout a kraft cook. Functional group changes are known to occur as the cook proceeds, but the effect of these changes on the infrared spectra were of the most interest in this study.

According to Hergert[54], ring deuteration studies have shown that the 1510 cm^{-1} and 1425 cm^{-1} bands are due to aromatic ring stretching that is strongly coupled by C-H in-plane deformations. However, the intensity of the 1425 cm^{-1} band has been shown to be very sensitive to ring substitution. The 1460 cm^{-1} band has been attributed to C-H bonds and methoxyl groups on aromatic rings. Combining these early results with other results from extended kraft cooking, an increase in ring substitution should decrease the 1460 cm^{-1} band due to a loss of C-H bonds

and methoxyl groups due to condensation reactions and demethoxylation. Furthermore, the 1425 cm^{-1} band should increase due to an increase in ring substitution from condensation and hydroxylation. These types of changes may be detectable in the difference spectra.

Difference spectra were produced using the 78 kappa number kraft pulp as the term file. The results are given in Figure 53 and show a relative increase in the 1510 cm^{-1} band in the difference spectra. In addition, the difference spectra produced by subtraction of the 33 kappa number pulp from the 78 kappa number pulp was similar to the dioxane lignin spectra from a 28 kappa conventional kraft pulp. Ring substitution effects appear to exist below the 33 kappa number range.

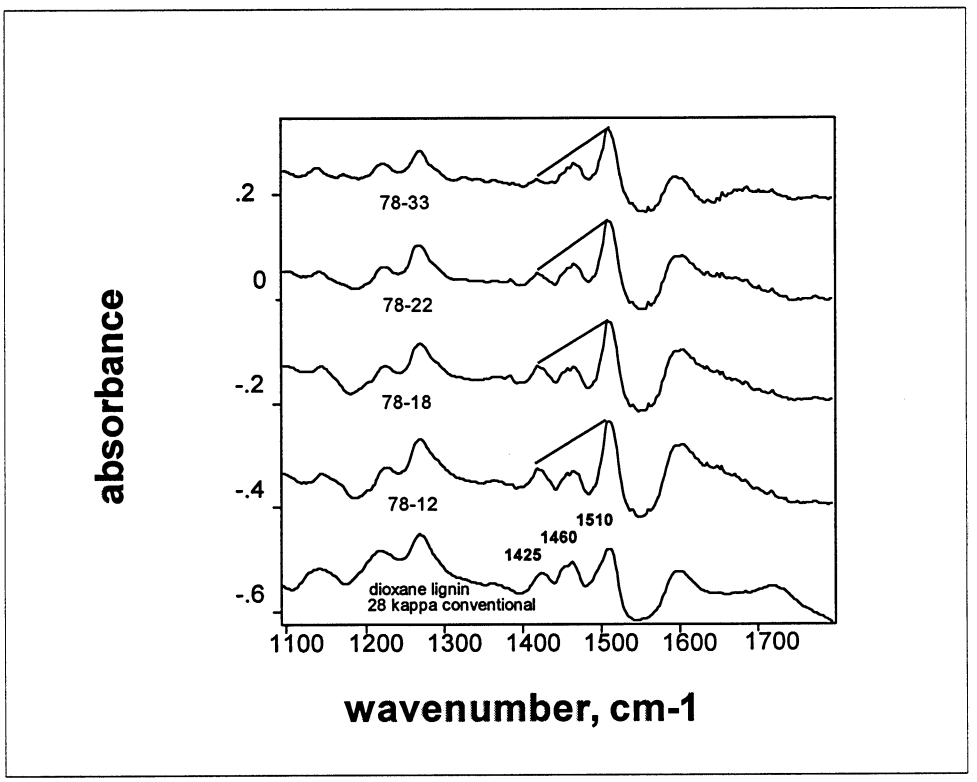

Note: bars are added to accentuate relative spectral changes

Figure 53. Difference spectra for the calibration set: 78 kappa number term file.

These results raised interest in determining the type of lignin that is being removed during successive stages in the delignification process. The difference spectra obtained using the higher kappa number kraft pulp for the term file appear to be comprised mainly of unsubstituted lignin. This high concentration of "bulk phase" lignin in the difference spectra may have masked otherwise apparent spectral changes. In an attempt to unveil these spectral changes, Figure 54 provides difference spectra for successive delignification stages within the "residual phase" lignin that was removed in prolonged cooks.

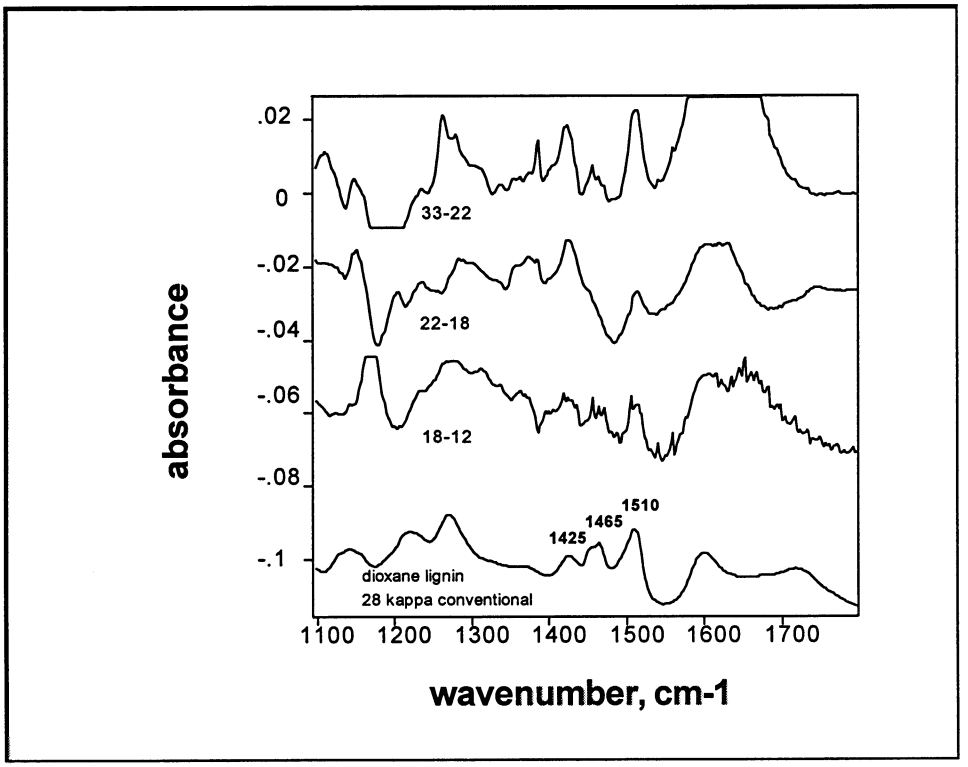

Figure 54. Difference spectra for the calibration set: residual phase stepwise subtractions.

Interestingly, some distinct changes do appear to exist when prolonging delignification beyond 33 kappa number. The difference spectra obtained by subtraction of the 22 kappa number pulp from the 33 kappa number pulp suggests removal of lignin with a high degree of

ring substitution. Furthermore, the difference spectra obtained by subtracting the 18 kappa number pulp from the 22 kappa number pulp suggests removal of an even more highly substituted lignin. However, the aromatic ring stretching band was strongly diminished in this case. Perhaps, normal ring stretching was hindered by the high degree of substitution. In support of this postulation, the 1460 cm^{-1} band diminished to a slight shoulder, suggesting that only minor amounts of aromatic C-H groups or methoxyl groups existed in lignin that was removed during this portion of delignification. A reduction in the removal of substituted aromatic rings was suggested by the difference spectra obtained when subtracting the 12 kappa number pulp from the 18 kappa number pulp.

It becomes difficult to derive firm conclusions from these single difference spectra, especially since they were produced from small differences in lignin content. Lignin is not the only component removed during prolonged delignification; hemicellulose and cellulose are also being removed. Furthermore, the observed "peaks" may simply represent random noise. Additional difference spectra were produced to verify whether the peaks are real. The 12 kappa number pulp was subtracted from the 33 kappa number pulp, and the 12 kappa number pulp was subtracted from the 22 kappa number pulp. These difference spectra contain a relatively higher quantity of lignin, as compared to the difference spectra of Figure 54. Figure 55 supports the observation in Figure 54: the 1425 cm^{-1} band increased while the 1460 cm^{-1} band decreased beyond 33 kappa number in both additional cases. In effect, lignin removed below 33 kappa number does appear to contain a high degree of aromatic ring substitution. The thrust of this observation is that the extent of aromatic ring substitution may be monitored by infrared difference spectra.

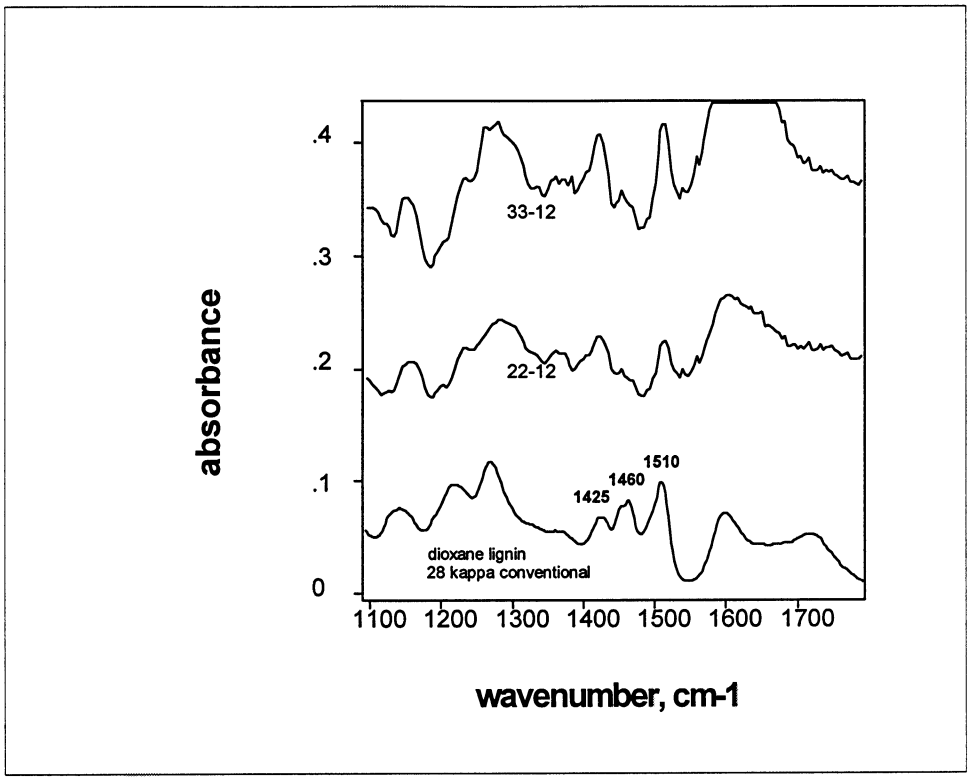

Figure 55. Difference spectra for the calibration set: residual phase subtractions verified.

DISCUSSION

The infrared microspectroscopy data was unsuccessful in determining single fiber lignin content. However, techniques were developed that may have merit once the spectral variability is controlled. Spectral variability resulted mainly from specular distortions and variations in microcompression cell pressure.

A secondary calibration curve was based on a KBr pellet technique and showed excellent reproducibility. As a result, the technique was highly accurate and precise. In fact, this calibration was at least as precise as any found thus far in the literature. Furthermore, the subtraction algorithm is flexible and easy to use.

Infrared difference spectra were produced in an attempt to better understand component subtraction spectra. Difference spectra of lignin were produced at various levels of kraft delignification. The results suggest that the extent of ring substitution may easily be monitored with KBr pellet difference spectra by comparing relative peak heights for the 1425 cm^{-1}, 1460 cm^{-1}, and 1510 cm^{-1} absorption bands.

The main conclusions from the infrared spectroscopy portion of this thesis are as follows:

- The infrared microspectroscopy technique produced highly variable spectra that were not sufficient in providing accurate and reproducible measurements of interfiber lignin content.

- The 95% confidence interval for the mean response of FTIR kappa number as a function of Tappi T236 kappa number spanned 1.6 kappa number to 2.3 kappa number units.

- Lignin difference spectra were produced from KBr pellet spectra to identify variability in subtraction component spectra. Comparison of specific peak heights suggested that aromatic ring substitution increased with extent of cook. Beyond 22 kappa number, an even higher level of ring substitution appeared to exist.

CHAPTER FIVE: CONCLUSION

Prior research with regard to delignification diversity has been limited by the availability of a reliable measurement technique. A custom density gradient column was designed, and experimental techniques were modified. Therefore, it is now possible to reproducibly obtain interfiber density measurements and relate them to interfiber lignin content diversity. Development of an anhydrous fiber preparation method, along with solvent purification and anhydrous column production techniques, provided a reliable and useful measurement technique. High contrast images were acquired using cross-polarization techniques with digital image averaging.

Laboratory kraft pulps were produced from 2.5-mm-thick chips and 10.0-mm-thick chips. Mill-produced pulps were obtained from a conventional continuous digester that was modified to Lo-solids™ pulping and Lo-level™ feed process conditions. Interfiber kraft pulping uniformity data were obtained using the improved density gradient column techniques with nonpolar solvents.

Density gradient column techniques were modified to increase measurement accuracy and precision. Anhydrous techniques were used in fiber preparation, solvent purification, and column production to avoid fluctuations in fiber density. Equilibrium time was reduced and precision was increased using dry conditions with vacuum impregnation at better than $5x10^{-3}$ torr. Kraft holopulps were produced to diagnose possible sources of experimental error, and it was discovered that kraft holopulp density was independent of extent of cook and chip thickness within the current level of random error. The major source of experimental error was an

improper sampling technique. Density gradient column measurements were accurate; Valonia cellulose density determinations were not statistically different than x-ray and electron diffraction estimates of Valonia cellulose unit cell density.

The pooled random error was ±5.58 kappa number, and the standard error of prediction was 6.5 kappa number for single fiber kappa number analyses. The 95% confidence bands show that the mean response for kappa number varies 6-10 kappa number in the range of this secondary analysis. Measurement error was insignificant. The average kraft holocellulose density was 1.5458 ±0.0015 g/ml, and the calculated lignin density was 1.2719 ±0.0090 g/ml.

Lignin content distributions were modeled using a composite of two normal distributions, A and B. Variations in interfiber density were due to lignin content, as proven by the comparitively low standard deviation in kraft holopulp DGC kappa number. Distribution A was limited to a delignification minimum of approximately 20 kappa number, whereas distribution B was limited to a delignification minimum of approximately 35 kappa number. The quantity of distribution B from the 10.0-mm-thick chips was typically 8% higher than the quantity of distribution B from 2.5-mm-thick chips. Distribution B contributed a maximum of 35-40%, regardless of chip thickness or process condition. The overall standard deviation in kappa number ranged from 11.5 to 17.7 in 10.0-mm-thick chip pulps and from 2.2 to 9.0 in 2.5-mm-thick chip pulps. Standard deviations for component distributions were statistically different within each pulp sample, proving that distributions A and B were from different populations. Distribution B disappeared with extended delignification in 2.5-mm-thick chips. Mill-produced pulps were intermediate in delignification diversity. However, the Lo-solids™ pulping with pressurized presteaming provided the most uniform pulp. Diffusion limitations appeared to

create delignification limitations in distribution B for 10.0-mm-thick chip pulps. Distribution B in the 2.5-mm-thick chip pulps did not appear delignification limited. The origin of distribution B may have been related to quantities of juvenile wood and mature wood, but this is not clear. For example, if distribution B does not exist in chips thinner than 2.5-mm, then it may simply originate from chip thickness derived mass transfer limitations. The delignification limitations that developed within 10.0-mm-thick chip pulps were most likely from the alkali depleted conditions and high dissolved lignin content in the chip center.

Although it is not clear where diffusion limitations end and chemical reaction limitations begin in this study, it appears that distribution A represents the outer portion of the chip and distribution B represents the core. Correlations between the drop in distribution A kappa number and overall viscosity suggest overcooking of the chip perimeter in 10.0-mm-thick chip pulps. Viscosity was maintained until the theoretical 24 kappa number limit in 2.5-mm-thick pulps. Chip thickness appears to be the controlling factor in delignification diversity. The improved uniformity from the Lo-solids™ process suggests that reductions in dissolved lignin and dissolved sodium offset the dependence of uniformity on chip thickness.

Infrared microspectroscopy was unsuccessful in providing interfiber uniformity measurements as a result of spectral variability. The reproducibility of single fiber spectra suffered because of uncontrollable microcompression cell pressure. Therefore, differences between the KBr pellet calibration spectra and microcompression cell spectra could not be resolved. The flexibility of the infrared quantitative technique was investigated using a simple spreadsheet model and liquid-cell infrared data. The technique was shown to be somewhat sensitive to component interactions. However, these effects were not significant within the

model liquid-cell system. Band overlap can also present a problem, especially when spectral reproducibility is poor. The technique was found to be accurate and sensitive, where a standard error of prediction of 1.2 kappa number resulted for the kraft pulp KBr pellet calibration set. The 95% confidence band shows that the mean response can be determined with very little error through this secondary analysis. This technique was used to produce lignin difference spectra at each stage of delignification. These difference spectra suggest that lignin becomes highly substituted beyond 30 kappa number. Normal ring stretching appears hindered beyond 22 kappa number, suggesting an even higher level of ring substitution.

SUGGESTIONS FOR FUTURE RESEARCH

I.

The most obvious next step would be a pulp strength and bleachability analysis of pulps that contain various levels of uniformity and condensed lignin. Laboratory-produced uniform pulps could be mixed to simulate varying degrees of nonuniformity to isolate possible causes for differences in strength and bleachability. Strength and bleachability analyses could then be compared to mill pulps. Factors such as interfiber lignin variability without a high level of lignin condensation and alkaline hydrolysis, interfiber lignin variability with a suspected high level of lignin condensation and alkaline hydrolysis, and physical damage from mill operating conditions can be isolated for a better understanding of what affects pulp quality.

II.

The density gradient column is a highly sensitive instrument capable of measuring the density of extremely small samples[157]. This research involved production of a custom density gradient column and imaging procedure that may prove useful in secondary analyses of lignin. Lignin isolation techniques have proven useful in the identification of functional group changes during kraft cooking[210]. However, all lignin isolation techniques are subject to question, because chemical alteration may take place within lignin as a result of the isolation process[54]. Therefore, a secondary analysis of lignin structure in its native state may be possible using NMR and FTIR in conjuction with density gradient column analyses. The following experimental approach should be considered:

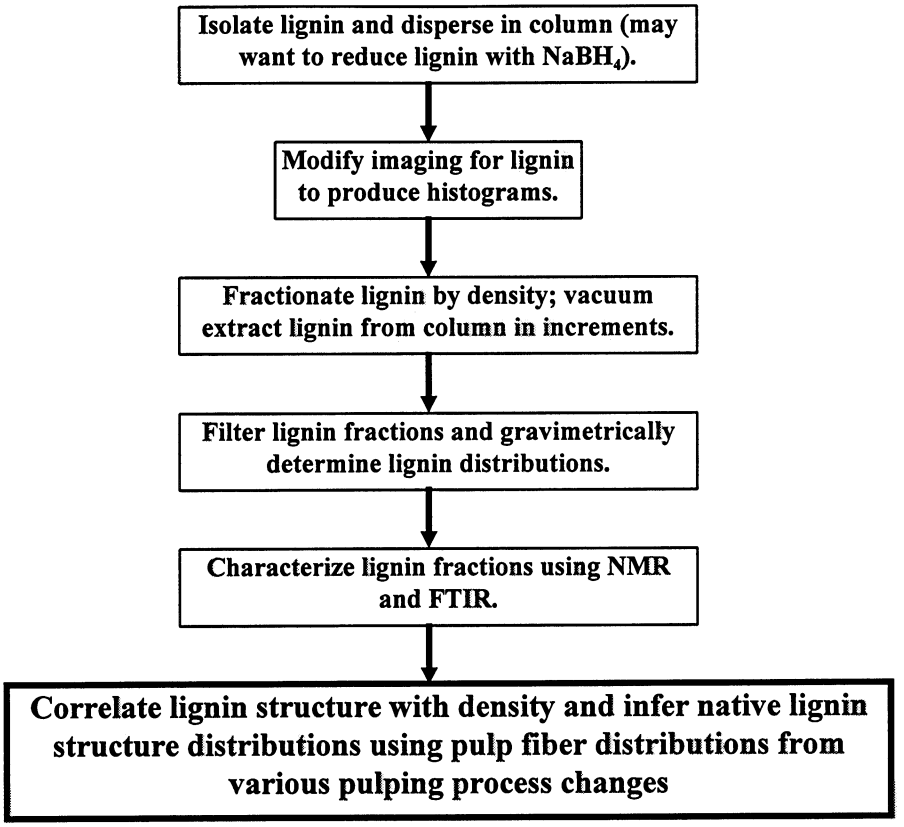

This procedure may also prove useful in isolating specific types of lignins for chemical reactivity studies.

III.

It may also be of interest to determine the density of recycled fibers. As the fiber is beaten, pressed into a sheet, repulped, etc., changes in the molecular orientation within the fiber wall may be expected. A better understanding of the life span of recycled fiber may evolve, since the point of fiber failure should relate to a reduction in cell wall density.

IV.

The infrared microspectroscopy technique would benefit from microcompression cell pressure control. Use of the peak ratio technique given in APPENDIX B may then provide accurate determinations of interfiber lignin content. In addition, the infrared microspectroscopy technique would also have the unique ability to map lignin concentrations within fibers as well as between fibers. It may also be possible to average multiple single fiber spectra for each point in the calibration set. Although time consuming, this technique should work if the spectral quality is sufficient.

Another way of approaching the problem of pressure variation would be to eliminate use of the microcompression cell. It may be possible to compare reflectance/absorbance spectra to KBr pellet calibration spectra. However, this procedure does involve pressing the fiber with a roller pen prior to analysis and may not be quantitative due to loss of stray radiation.

Perhaps the best approach would involve use of an embedding techniqe. Single fibers could be carefully placed in a nonabsorbing background material with an index of refraction near that of cellulose. Of course, KBr is typically used for this purpose, but the microscope may not be able to focus on a fiber within a KBr pellet. Since atmospheric moisture can create an opaque pellet, perhaps pellets can be carefully formed in a dry box. This procedure would seem to solve all problems if the optical difficulties could be surpassed; the spectra would be acquired as an average spectra from the bench spectrometer and as single fiber spectra from the microspectrometer. Effectively, they would be from the same sample set and should not be subject to differences in molecular vibrational response.

ACKNOWLEDGEMENTS

I would like to thank the Institute of Paper Science and Technology, the Board of Trustees, all member companies, and individual contributors who have made it possible for me to focus on my education for nearly seven years at the Institute. I am especially grateful for the help and guidance provided by my advisor, Dr. Alan Rudie, and research committee members, Dr. Earl Malcolm and Dr. Thomas McDonough.

I would also like to acknowledge the following individuals for contributions to my research: defense committee members Dr. Hiroki Nanko and Dr. Jian Li, machinist Joseph Nadeau, Dr. Bruno Marcoccia of Ahlstrom-Machinery, faculty member Dr. Derek Page, Don and Thom Lillie of Lillie's Glassblowers, Georgia Tech Glassblowers, Ken Gresham of EM Science, and fellow students, staff, and faculty members.

Special thanks go to those individuals that have made my stay at the Institute enjoyable. You know who you are. I have made many friends over the years in Atlanta, but my most trustworthy friend is my dog King. He has been with me for eleven years and has been the only one to not complain, despite many long days without a pit stop.

I am most grateful to my family, especially my wife Birim and my son Trevor. Although Birim has only been exposed to the last portion of this work, her patience, love, and encouragement have allowed me to fully focus on the completion of this thesis. Most importantly, she has taught me how to trust in others once again. Trevor has simply been the reason why.

APPENDIX A

Pulping Data

All data obtained from laboratory pulping is tabulated in this appendix. Table A 1 contains pulping data for 2.5-mm-thick chips and 10.0-mm-thick chips. These pulps were used in density gradient column analyses. Table A 2 contains pulping data for 3.0-mm-thick chips. These pulps were used in the FTIR microspectroscopy analyses.

All pulps were produced using southern yellow pine. The pulps in Table A 1 were from a 22 year old loblolly pine *(Pinus taeda)*. The bottom 8ft. section was rotary veneer cut to 0.100in (2.5-mm) thickness for thin chip studies. The middle 8ft section was cut to 10-mm-thickness in the radial direction, and 25-mm in both the tangential and longitudinal directions. Table A 2 contains pulps that were produced from a similar wood source that was described as southern yellow pine. All wood was provided by Georgia Pacific of Madison, Georgia.

Table A 1. Complete pulping data for density gradient column analyses.

Parameter	Cook# 1	2	3	3R	4	4R	5	5R	6	7	7R	8	8R	9	9R	10	10R	11	12
chip thickness, mm	**10.0**	**2.5**	**10.0**	**10.0**	**2.5**	**2.5**	**10.0**	**10.0**	**2.5**	**10.0**	**10.0**	**2.5**	**2.5**	**2.5**	**2.5**	**2.5**	**2.5**	**2.5**	**2.5**
temperature, C	**150**	**150**	**170**	**170**	**165**	**165**	**165**	**165**	**160**	**160**	**160**	**155**	**155**	**154**	**154**	**158**	**158**	**159**	**160**
H-factor	**548**	**548**	**2803**	**2803**	**1892**	**1892**	**1892**	**1892**	**1274**	**1274**	**1274**	**845**	**845**	**786**	**786**	**1140**	**1140**	**1200**	**1400**
kappa number	**63.7**	**54.6**	**23.4**	**22.7**	**15.9**	**14.0**	**25.9**	**29.1**	**18.9**	**33.4**	**36.7**	**28.3**	**35.2**	**33.9**	**32.0**	**24.2**	**27.8**	**27.5**	**23.0**
viscosity, cP	**46.07**	**44.97**	**16.88**		**17.19**		**25.07**		**26.89**	**37.58**		**43.41**							
yield, unscreened	**0.520**	**0.442**	**0.423**	**0.408**	**0.394**	**0.410**	**0.457**	**0.448**	**0.402**	**0.482**	**0.446**	**0.443**	**0.448**	**0.455**	**0.439**				
yield, screened	**0.515**	**0.442**	**0.413**	**0.400**	**0.394**	**0.410**	**0.451**	**0.439**	**0.402**	**0.474**	**0.441**	**0.443**	**0.448**	**0.455**	**0.439**				
time to temperature, min.	**60**	**60**	**60**	**60**	**60**	**60**	**60**	**60**	**60**	**60**	**60**	**60**	**60**	**60**	**60**	**60**	**60**	**60**	**60**
time at temperature, min.	**240**	**240**	**240**	**240**	**240**	**240**	**240**	**240**	**240**	**240**	**240**	**240**	**240**	**240**	**240**	**240**	**240**	**248**	**258**
L:W=6:1, EA=24% on wood																			
Computer H-factor:																			
100C-Tmax to time			2783	2856	1900	1945		1926	1270		1258	869	824	752	754	1141	1140	1203	
Tmax to 100C; cool			*23*	*23*	*21*	65		21	18		12	14	15	12	12	16	7	*15*	
total computer H-factor			*2806*	*2879*	*1921*	2010		1947	1288		1269	883	839	764	766	1157	1147	*1220*	*1420*
Italics are an estimate																			
Pulp Available, (g)	**291.4**	**203.4**	**236.9**	**200.3**	**181.5**	**205.3**	**201.0**	**219.4**	**185.0**	**270.2**	**220.6**	**235.9**	**224.6**	**227.8**	**219.6**				
White Liquor:																			
A	12.67	12.37	12.46	12.90	12.58	12.88	12.92	12.90	12.35	12.30	12.92	12.49	12.98	12.87	12.76	12.05	12.20	12.33	12.20
B	15.00	14.61	14.77	15.25	14.85	15.08	14.82	15.24	14.63	14.56	15.26	14.66	15.34	15.09	14.95	14.02	14.35	14.31	14.30
C																			
NaOH, gpl Na2O	32.05	31.40	31.47	32.71	31.96	33.11	34.16	32.74	31.22	31.12	32.80	31.99	32.92	33.02	32.77	31.25	31.16	32.10	31.31
Na2S, gpl Na2O	14.45	13.89	14.32	14.57	14.07	13.64	11.78	14.51	14.14	14.01	14.51	13.45	14.63	13.76	13.58	12.21	13.33	12.25	13.02
Na2CO3, gpl Na2O																			
EA, gpl Na2O	**39.28**	**38.35**	**38.63**	**39.99**	**39.00**	**39.93**	**40.05**	**39.99**	**38.29**	**38.13**	**40.05**	**38.72**	**40.24**	**39.90**	**39.56**	**37.36**	**37.82**	**38.22**	**37.82**
% Sulfidity	**31.07**	**30.66**	**31.28**	**30.82**	**30.57**	**29.18**	**25.64**	**30.71**	**31.17**	**31.04**	**30.67**	**29.60**	**30.77**	**29.42**	**29.30**	**28.10**	**29.97**	**27.61**	**29.37**
Post-impreg. Liquor:																			
A	7.49		9.64	11.41	8.49	9.76	10.21	10.47	9.22	9.61	10.53	9.27	9.10	9.63	9.20	8.50	8.90	8.63	
B	9.13		11.79	13.56	10.29	11.65	12.20	12.50	10.80	11.53	12.54	11.20	10.88	11.58	11.04	10.30	10.65	10.30	
C																			
NaOH, gpl Na2O	18.14		23.22	28.71	20.74	24.40	25.48	26.16	23.68	23.84	26.41	22.75	22.69	23.81	22.82	20.77	22.17	21.58	
Na2S, gpl Na2O	10.17		13.33	13.33	11.16	11.72	12.34	12.59	9.80	11.90	12.46	11.97	11.04	12.09	11.41	11.16	10.85	10.35	
Na2CO3, gpl Na2O																			
EA	**23.22**		**29.88**	**35.37**	**26.32**	**30.26**	**31.65**	**32.46**	**28.58**	**29.79**	**32.64**	**28.74**	**28.21**	**29.85**	**28.52**	**26.35**	**27.59**	**26.75**	
% Sulfidity	**35.93**		**36.47**	**31.71**	**34.99**	**32.45**	**32.62**	**32.48**	**29.26**	**33.30**	**32.06**	**34.46**	**32.72**	**33.68**	**33.33**	**34.95**	**32.86**	**32.43**	
Steaming time(hrs)	2.0	2.0	2.0		2.0	1.0	2.0	2.0	2.0	1.0	2.0	2.0	1.0	2.0	2.0	4.0	5.0	1.0	1.0
Impreg.time+soak(hrs)	21.0	17.0	2.0		12.0	4.0	1.5	2.0	64.0	2.0	2.0	12.0	4.5	3.0	3.0	4.0	4.0	2.0	2.0
Residual Alkali																			
A	5.45	6.98	4.59	4.68	5.64	6.05	5.78	5.25	6.67	4.54	5.71	6.36	6.37	7.23	7.18	5.85		5.52	5.90
B	6.58	8.11	5.29	5.57	6.90	7.11	6.91	5.86	7.85	5.72	6.86	7.57	7.50	8.52	8.66	7.10		6.55	7.25
C	9.02	10.03	7.32																
NaOH, gpl Na2O	13.39	18.14	12.06	11.75	13.58	15.47	14.42	14.38	17.02	10.42	14.14	15.97	16.24	18.41	17.67	14.26		13.92	14.11
Na2S, gpl Na2O	7.01	7.01	4.34	5.52	7.81	6.57	7.01	3.78	7.32	7.32	7.13	7.50	7.01	8.00	9.18	7.75		6.39	8.37
Na2CO3, gpl Na2O	7.56	5.95	6.29																
EA	**16.90**	**21.64**	**14.23**	**14.51**	**17.48**	**18.76**	**17.92**	**16.28**	**20.68**	**14.07**	**17.70**	**19.72**	**19.75**	**22.41**	**22.26**	**18.14**		**17.11**	**18.29**
% Sulfidity	**34.35**	**27.87**	**26.47**	**31.96**	**36.52**	**29.82**	**32.71**	**20.82**	**30.06**	**41.26**	**33.53**	**31.97**	**30.13**	**30.28**	**34.18**	**35.21**		**31.45**	**37.24**
%Alkali Consumed																			
post-impregnation	**40.88**		**22.63**	**11.55**	**32.51**	**24.22**	**20.98**	**18.84**	**25.34**	**21.87**	**18.50**	**25.78**	**29.89**	**25.17**	**27.90**	**29.46**	**27.05**	**30.01**	
residual alkali	**56.99**	**43.57**	**63.16**	**63.72**	**55.17**	**53.03**	**55.26**	**59.30**	**45.99**	**63.09**	**55.80**	**49.08**	**50.92**	**43.82**	**43.73**	**51.45**		**55.23**	**51.64**

Table A 2. Complete pulping data for infrared spectroscopy analyses.

Cook	A	B	C	D	E
chip thickness, mm	**3.0**	**3.0**	**3.0**	**3.0**	**3.0**
temperature, C	**165**	**165**	**165**	**165**	**165**
effective alkali, gpl	**40**	**40**	**40**	**40**	**40**
sulfidity, %	**30**	**30**	**30**	**30**	**30**
target H-factor	**2000**	**1500**	**1000**	**750**	**400**
kappa number	**11.9**	**17.6**	**21.5**	**32.9**	**78.0**
% unscreened yield	**42.7**	**44.8**	**48.0**	**49.4**	**59.5**
% screened yield	**42.7**	**44.8**	**48.0**	**49.4**	**52.1**
time to temperature, min.	**60**	**60**	**60**	**60**	**60**
time at temperature, min.	**180**	**137**	**83**	**63**	**24**
L:W=6:1, EA=24% on wood					
White Liquor:					
A	14.75	12.80		13.25	14.01
B	17.21	14.58		15.51	15.93
C	17.58	15.06		15.80	16.33
NaOH, gpl Na2O	38.11	34.16		34.08	37.45
Na2S, gpl Na2O	15.22	11.04		13.99	11.94
Na2CO3, gpl Na2O	1.16	1.49		0.91	1.24
EA, gpl Na2O	**45.73**	**39.68**		**41.08**	**43.42**
% Sulfidity	**28.54**	**24.42**		**29.11**	**24.17**
Post-impreg. Liquor:					
A	11.11	9.54	9.23	9.77	9.98
B	13.04	10.90	10.86	11.68	11.66
C	13.99	11.73	11.56	13.51	12.36
NaOH, gpl Na2O	28.44	25.36	23.58	24.37	25.70
Na2S, gpl Na2O	11.97	8.43	10.08	11.84	10.45
Na2CO3, gpl Na2O	2.96	2.57	2.17	5.67	2.17
EA	**34.43**	**29.57**	**28.61**	**30.29**	**30.92**
% Sulfidity	**29.61**	**24.95**	**29.94**	**32.71**	**28.90**
Steaming time(hrs)	3.50	1.50	2.50	2.00	2.00
Impreg.time+soak(hrs)	72.00	14.00	21.00	40.50	20.50
Residual Alkali					
A	6.04	5.69	5.95	6.95	7.26
B	7.25	6.85	7.13	8.41	8.79
C	10.14	9.45	9.36	11.04	10.69
NaOH, gpl Na2O	14.94	14.06	14.76	17.02	17.76
Na2S, gpl Na2O	7.53	7.16	7.35	9.05	9.49
Na2CO3, gpl Na2O	8.96	8.08	6.90	8.15	5.87
EA	**18.71**	**17.64**	**18.43**	**21.55**	**22.51**
% Sulfidity	**33.52**	**33.75**	**33.24**	**34.72**	**34.81**
%Alkali Consumed					
post-impregnation	**24.71**	**25.47**		**26.26**	**28.78**
residual alkali	**59.08**	**55.55**		**47.55**	**48.16**

APPENDIX B

Karl Fischer Titration and Water Analysis

The Karl Fischer titration procedure is the most sensitive procedure to determine the presence of water in organic solvents[178]. The procedure traditionally uses a reagent solution of iodine, sulfur dioxide, and pyridine in methanol. However, nonpyridine based solvents are now marketed under various trade names[182]. A coulometric titrator was used in this application, where a charge is established across two platinum electrodes in a reaction cell. The free iodine in the reagent is reduced to iodide in the presence of water. The voltage increases to maintain the constant charge, and the extent of the voltage increase determines the level of water present.

A glass syringe and stainless steel needles were necessary for the chloroform and tetrachloroethylene used in this study. The apparatus is highly sensitive to water and must be carefully installed to ensure reaction cell dryness. Water that has been adsorbed within the reaction cell should equilibrate with the coulometric solution, however, this equilibration can take days and should be avoided.

Karl Fischer measurements were taken throughout the solvent preparation procedure to initially diagnose trouble areas in technique development. The procedure served as a monitor of solvent dryness prior to beginning the tedious process of fiber preparation, impregnation, and column development. Variations in solvent water content were controlled and density gradient column measurement reproducibility was improved. Table B 1 provides the titration data for the 21 columns analyzed in the density gradient column portion of this thesis.

Table B 1. Karl Fischer titration data for density gradient column analyses.

File #	Description	Kappa Number	[H2O] CHCl3 post-distill	[H2O] C2Cl4 post-distill	[H2O] CHCl3 post-VF	[H2O] C2Cl4 post-VF	[H2O] CHCl3 % red.	[H2O] C2Cl4 % red.	[H2O] FL	[H2O] FD	density FL	density FD	calibration R^2	Impreg density
02868hA3	**Kamyr 4170 - Holo**	**0**	18.5	15.3	13.7	6.4	25.9	58.2	15.9	8.1	1.4984	1.5962	0.9997	
03647hA3	**Cook 1 - Holo**	**0**	9.7		6.4		34.0		14.4	13.6	1.5025	1.5848	0.9998	
03870hA3	**Kamyr 1964 - Holo**	**0**							7.9	5.9	1.4991	1.5833	0.9990	
04067hA3	**Kamyr 4170 - Holo**	**0**			2.5	6			4.7	8.5	1.5020	1.5829	0.9993	1.4851
04065hB3	**Kamyr 832 - Holo**	**0**			2.5	6			6.5	6.9	1.4983	1.5826	0.9995	1.4851
05965hA3	**Cook 3 - Holo**	**0**											0.9998	1.4879
06392hA3	**Cook 2 - Holo**	**0**	28.3	13.2	15.3	6.9	45.9	47.7					0.9995	
04371hB3	**Cook 4 - BS**	**15.9**			4.7	6.4			11	6.7	1.5022	1.5815	0.9996	1.4874
04576hA3	**Cook 3 - BS**	**23.4**							12.4	8.6	1.5030	1.5705	0.9999	1.4874
02866hB3	**Kamyr 4170 - BS**	**24.1**	18.5		13.7	6.4	25.9		14.7	10.1	1.4980	1.5939	0.9971	
03443hB3	**Kamyr 4170 - BS**	**24.1**	15.6	10.2	13.6								0.9997	
03644hB3	**Kamyr 832 - BS**	**24.6**	9.7		6.4		34.0		10.8	13.6	1.4989	1.5848	0.9997	
03870hB3	**Kamyr 1964 - BS**	**31.4**							6.8	11.4	1.5007	1.5829	0.9996	
04772hA3	**Cook 7 - BS**	**33.4**											0.9998	1.4877
05963hB3	**Cook 7 - BS**	**33.4**											0.9998	1.4879
06392hB3	**Cook 7 - BS**	**33.4**			18.2								0.9995	1.4898
05169hA3	**Cook 7 - BS**	**33.4**			1.8	3.5			0.7	2.7	1.5000	1.5820	0.9998	1.4940
04774hB3	**Cook 9 - BS**	**33.9**							14.8	15.5	1.5007	1.5836	0.9998	1.4877
04573hB3	**Cook 2 - BS**	**54.6**							15.5	12.2	1.5011	1.5796	0.9996	1.4874
04366hA3	**Cook 1 - BS**	**63.7**			4.7	6.4			9.2	6.5	1.4963	1.5831	0.9996	1.4874
05167hB3	**Cook 1 - BS**	**63.7**											0.9998	1.4940
	AVERAGE		**16.7**	**12.9**	**8.6**	**6.0**	**33.2**	**52.9**	**10.4**	**9.3**	**1.5001**	**1.5837**	**0.9995**	**1.4884**
	STD.DEV.		**6.9**	**2.6**	**5.8**	**1.0**	**8.2**	**7.4**	**4.6**	**3.6**	**0.0020**	**0.0060**	**0.0006**	**0.0028**

Verification of the Composite Normal Model for Histograms

The composite normal model was chosen on the basis of simplicity, flexibility, and the knowledge that the physical and chemical pulping limitations could lead to at least two individual pulping rates within a given pulp sample. Application of this model to each sample required that some criteria be used to statistically verify each model fit. Without such verification, the model would have little merit. Therefore, the method of choice was the Chi-square (χ^2) goodness-of-fit test[253].

Table B 2 provides a list of density related parameters for 3 point moving averages of all distributions included in this thesis. Fractional contributions, average fiber density, and standard deviation in average fiber density for distribution A and distribution B are shown with respect to the degrees of freedom set by the modeling equation. Tabulated statistical values for the Chi-square goodness-of-fit test are given at the α=0.01 and α=0.05 probability levels. The last column in Table B 2 provides a "false" statement for acceptable Chi-square values that are within α=0.01 and α=0.05 probability limits, whereas unacceptable Chi-square values are given for distributions that did not fit within stated limits.

The moving average can add error to estimated parameters by artificially broadening the narrower kraft holopulp distributions. Table B 3 provides the entire data set, as calculated with the composite normal distribution fit method on actual data. Use of actual data provides Chi-square values that are much higher than that obtained from data modified by a three-point moving average. However, the model does fit the trends well, as verified by Table B 2. All data analyses were performed on this data set. Transformations of density and standard deviation in density to kappa number were linear, as verified in this appendix.

Table B 2. Parameters estimated using centered three-point moving averages, as verified by Chi-Square analyses.

File #	Description	Comp. A Fxn	Comp. B Fxn	Comp. A Density	Comp. B Density	Comp. A StDev	Comp. B StDev	Actual df	Tabulated $\chi^2(0.05)$	Tabulated $\chi^2(0.01)$	Actual Fit χ^2	χ^2 $\alpha<0.01$
02868hA3	Kamyr 4170 - Holo	1.00	0.00	1.5467		0.0014		6	12.592	16.810	9.6	FALSE
02866hB3	Kamyr 4170 - BS	0.56	0.44	1.5380	1.5380	0.0015	0.0030	10	15.507	20.090	7.0	FALSE
03443hB3	Kamyr 4170 - BS	0.82	0.18	1.5395	1.5395	0.0014	0.0055	14	23.685	29.141	14.4	FALSE
03647hA3	Cook 1 - Holo	1.00	0.00	1.5455		0.0011		7	14.067	18.475	5.8	FALSE
03644hB3	Kamyr 832 - BS	0.72	0.28	1.5389	1.5385	0.0015	0.0065	20	31.410	37.566	27.5	FALSE
03870hA3	Kamyr 1964 - Holo	0.82	0.18	1.5453	1.5446	0.0011	0.0017	7	14.067	18.475	18.8	18.8
03870hB3	Kamyr 1964 - BS	0.68	0.32	1.5412	1.5380	0.0019	0.0080	23	35.172	41.638	13.2	FALSE
04067hA3	Kamyr 4170 - Holo	1.00	0.00	1.5451		0.0012		6	12.592	16.812	11.9	FALSE
04065hB3	Kamyr 832 - Holo	0.87	0.13	1.5435	1.5415	0.0011	0.0026	10	18.307	23.209	28.8	28.8
04366hA3	Cook 1 - BS	0.40	0.60	1.5190	1.5188	0.0028	0.0063	25	37.652	44.314	27.9	FALSE
04371hB3	Cook 4 - BS	1.00	0.00	1.5390		0.0012		7	14.067	18.475	12.5	FALSE
04576hA3	Cook 3 - BS	0.80	0.20	1.5398	1.5340	0.0023	0.0080	23	35.172	41.638	37.9	FALSE
04573hB3	Cook 2 - BS	0.71	0.29	1.5270	1.5239	0.0026	0.0047	21	32.671	38.932	14.0	FALSE
04772hA3	Cook 7 - BS	0.58	0.42	1.5363	1.5378	0.0062	0.0028	28	41.337	48.278	42.1	FALSE
04774hB3	Cook 9 - BS	0.70	0.30	1.5316	1.5300	0.0015	0.0042	16	26.296	32.000	8.9	FALSE
05169hA3	Cook 7 - BS	0.72	0.28	1.5326	1.5260	0.0030	0.0070	27	40.113	46.963	44.2	FALSE
05167hB3	Cook 1 - BS	0.75	0.25	1.5227	1.5200	0.0040	0.0090	25	37.652	44.314	26.7	FALSE
05965hA3	Cook 3 - Holo	0.90	0.10	1.5473	1.5472	0.0012	0.0030	9	16.919	21.666	16.0	FALSE
05963hB3	Cook 7 - BS	0.61	0.39	1.5375	1.5330	0.0022	0.0080	27	40.113	46.961	23.5	FALSE
06392hA3	Cook 2 - Holo	1.00	0.00	1.5477		0.0013		7	14.067	18.475	14.1	FALSE
06392hB3	Cook 7 - BS	0.64	0.36	1.5415	1.5330	0.0030	0.0090	35	49.802	57.342	51.4	FALSE
EQUILIBRIUM TIME STUDY (ADDITIONAL DATA):												
04324hA3	Cook 1 - BS (24hr)	0.70	0.30	1.5185	1.5100	0.0039	0.0100	27	40.113	46.963	41.0	FALSE
04339hA3	Cook 1 - BS (39 hr)	0.67	0.33	1.5190	1.5190	0.0060	0.0025	26	38.885	45.642	23.6	FALSE
04348hA3	Cook 1 - BS (48hr)	0.67	0.33	1.5190	1.5190	0.0060	0.0025	26	38.885	45.642	17.5	FALSE
043186hA3	Cook 1 - BS (186hr)	0.60	0.40	1.5200	1.5200	0.0029	0.0062	25	37.652	44.314	22.4	FALSE
04329hB3	Cook 4 - BS (29hr)	1.00	0.00	1.5383		0.0011		6	12.592	16.810	17.6	17.6
04344hB3	Cook 4 - BS (44hr)	1.00	0.00	1.5386		0.0011		7	14.067	18.475	9.7	FALSE
04353hB3	Cook 4 - BS (53hr)	0.88	0.12	1.5388	1.5387	0.0011	0.0020	7	14.067	18.475	7.4	FALSE
043191hB3	Cook 4 - BS (191hr)	0.70	0.30	1.5392	1.5392	0.0017	0.0009	10	18.307	23.209	15.9	FALSE
05943hB3	Cook 7 - BS (43hr)	0.65	0.35	1.5374	1.5350	0.0025	0.0090	27	40.113	46.963	15.8	FALSE
05949hB3	Cook 7 - BS (49hr)	0.65	0.35	1.5373	1.5350	0.0022	0.0090	27	40.113	46.963	15.3	FALSE
05975hB3	Cook 7 - BS (75hr)	0.60	0.40	1.5375	1.5340	0.0024	0.0060	26	38.885	45.642	13.8	FALSE
05994hB3	Cook 7 - BS (94hr)	0.57	0.43	1.5375	1.5340	0.0024	0.0081	26	38.885	45.624	9.6	FALSE
ASSESSMENT OF MEASUREMENT ERROR (REPEATING PHOTOGRAPHY AND ANALYSIS ONLY):												
03870hA3a	Kamyr 1964 - Holo	0.60	0.40	1.5452	1.5452	0.0009	0.0019	8	18.307	23.209	25.7	25.7
03870hA3b	Kamyr 1964 - Holo	0.55	0.45	1.5449	1.5454	0.0014	0.0012	7	14.067	18.475	23.0	23.0
03870hB3a	Kamyr 1964 - BS	0.70	0.30	1.5412	1.5380	0.0020	0.0070	22	33.924	40.289	11.9	FALSE
03870hB3b	Kamyr 1964 - BS	0.62	0.38	1.5412	1.5385	0.0021	0.0068	25	37.652	44.314	10.4	FALSE

Table B 3. Parameters estimated using actual data only, as verified by Chi-square analyses

File #	Description	Kappa Number	Comp. A Fxn	Comp. B Fxn	Comp. A Density	Comp. B Density	Comp. A StDev	Comp. B StDev	Actual df	Tabulated $\chi^2(0.05)$	Tabulated $\chi^2(0.01)$	Actual Fit χ^2
02868hA3	Kamyr 4170 - Holo	0	1.00	0.00	1.5466		0.0010		4	9.488	13.277	29.4
03647hA3	Cook 1 - Holo	0	1.00	0.00	1.5455		0.0009		5	11.070	15.090	19.9
03870hA3	Kamyr 1964 - Holo	0	0.82	0.18	1.5453	1.5442	0.0007	0.0022	8	15.507	20.090	24.2
04067hA3	Kamyr 4170 - Holo	0	1.00	0.00	1.5451		0.0010		6	12.592	16.812	80.1
04065hB3	Kamyr 832 - Holo	0	0.80	0.20	1.5435	1.5425	0.0007	0.0031	10	18.307	23.209	37.9
05965hA3	Cook 3 - Holo	0	0.90	0.10	1.5473	1.5472	0.0010	0.0030	8	15.507	20.090	51.8
06392hA3	Cook 2 - Holo	0	1.00	0.00	1.5477		0.0009		5	11.071	15.086	41.9
04371hB3	Cook 4 - BS	15.9	1.00	0.00	1.5390		0.0009		5	11.071	15.086	31.8
04576hA3	Cook 3 - BS	23.4	0.80	0.20	1.5398	1.5340	0.0022	0.0080	22	33.924	40.289	182.0
02866hB3	Kamyr 4170 - BS	24.1	0.52	0.48	1.5380	1.5380	0.0010	0.0035	12	21.026	26.217	32.3
03443hB3	Kamyr 4170 - BS	24.1	0.78	0.22	1.5395	1.5395	0.0011	0.0050	14	23.685	29.141	47.3
03644hB3	Kamyr 832 - BS	24.6	0.71	0.29	1.5388	1.5385	0.0013	0.0063	19	30.144	36.191	92.9
03870hB3	Kamyr 1964 - BS	31.4	0.67	0.33	1.5413	1.5390	0.0017	0.0074	23	35.172	41.638	75.3
04772hA3	Cook 7 - BS	33.4	0.57	0.43	1.5363	1.5378	0.0062	0.0028	27	40.113	46.963	96.5
05169hA3	Cook 7 - BS	33.4	0.67	0.33	1.5326	1.5260	0.0028	0.0072	26	38.885	45.642	83.4
05963hB3	Cook 7 - BS	33.4	0.60	0.40	1.5375	1.5330	0.0022	0.0082	25	37.652	44.314	69.0
06392hB3	Cook 7 - BS	33.4	0.63	0.37	1.5415	1.5330	0.0027	0.0090	33	47.400	54.776	126.4
04774hB3	Cook 9 - BS	33.9	0.70	0.30	1.5316	1.5300	0.0013	0.0041	16	26.296	32.000	43.7
04573hB3	Cook 2 - BS	54.6	0.71	0.29	1.5270	1.5239	0.0026	0.0047	19	30.144	36.191	36.8
04366hA3	Cook 1 - BS	63.7	0.53	0.47	1.5190	1.5195	0.0026	0.0070	22	33.924	40.289	86.1
05167hB3	Cook 1 - BS	63.7	0.75	0.25	1.5227	1.5200	0.0039	0.0090	23	35.172	41.638	74.4
EQUILIBRIUM TIME STUDY (ADDITIONAL DATA):												
04324hA3	Cook 1 - BS (24hr)	63.7	0.70	0.30	1.5185	1.5100	0.0039	0.0100	27	40.113	46.963	105.7
04339hA3	Cook 1 - BS (39 hr)	63.7	0.33	0.67	1.5190	1.5190	0.0021	0.0060	23	35.172	41.638	68.3
04348hA3	Cook 1 - BS (48hr)	63.7	0.28	0.72	1.5190	1.5190	0.0025	0.0060	24	36.415	42.980	84.1
043186hA3	Cook 1 - BS (186hr	63.7	0.45	0.55	1.5200	1.5210	0.0029	0.0070	24	36.415	42.980	82.6
04329hB3	Cook 4 - BS (29hr)	15.9	1.00	0.00	1.5383		0.0008		4	9.488	13.277	25.3
04344hB3	Cook 4 - BS (44hr)	15.9	1.00	0.00	1.5386		0.0008		5	11.071	15.086	13.4
04353hB3	Cook 4 - BS (53hr)	15.9	0.88	0.12	1.5387	1.5388	0.0008	0.0020	7	14.067	18.475	19.0
043191hB3	Cook 4 - BS (191hr	15.9	0.30	0.70	1.5393	1.5392	0.0005	0.0015	8	15.507	20.090	29.7
05943hB3	Cook 7 - BS (43hr)	33.4	0.64	0.36	1.5374	1.5350	0.0025	0.0090	25	37.652	44.314	69.4
05949hB3	Cook 7 - BS (49hr)	33.4	0.63	0.37	1.5373	1.5350	0.0022	0.0090	24	36.415	42.980	52.5
05975hB3	Cook 7 - BS (75hr)	33.4	0.59	0.41	1.5375	1.5324	0.0024	0.0076	24	36.415	42.980	59.2
05994hB3	Cook 7 - BS (94hr)	33.4	0.57	0.43	1.5375	1.5340	0.0023	0.0089	24	36.415	42.980	50.4
ASSESSMENT OF MEASUREMENT ERROR (REPEATING PHOTOGRAPHY AND ANALYSIS ONLY):												
03870hA3a	Kamyr 1964 - Holo	0	0.61	0.39	1.5452	1.5448	0.0006	0.0019	7	14.067	18.475	22.8
03870hA3b	Kamyr 1964 - Holo	0	0.70	0.30	1.5449	1.5451	0.0009	0.0020	8	15.507	20.090	105.1
03870hB3a	Kamyr 1964 - BS	31.4	0.73	0.27	1.5412	1.5380	0.0020	0.0070	21	32.671	38.932	63.5
03870hB3b	Kamyr 1964 - BS	31.4	0.61	0.39	1.5412	1.5385	0.0019	0.0068	22	33.924	40.289	76.6

Complete Set of Histograms

In an effort to achieve a concise and readable thesis, efforts were taken to reduce the number of figures required for explanations. Likewise, it is also important to provide the reader with all information used to develop the defense of this project. The following figures provide qualitative evidence of the second distribution, along with comparisons of replicate samples.

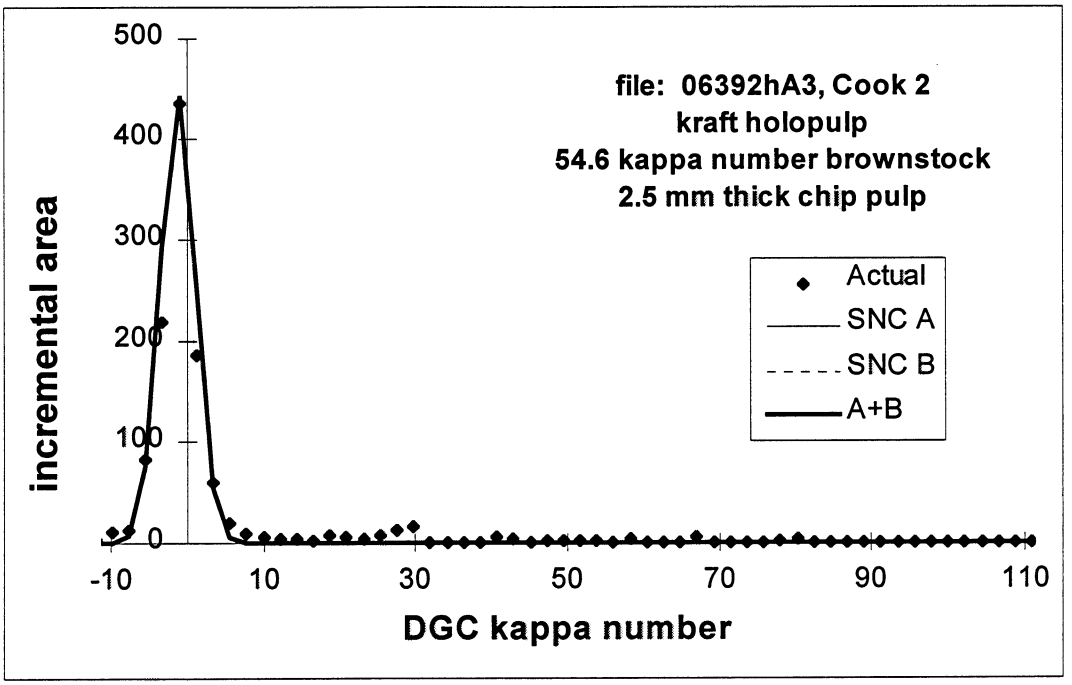

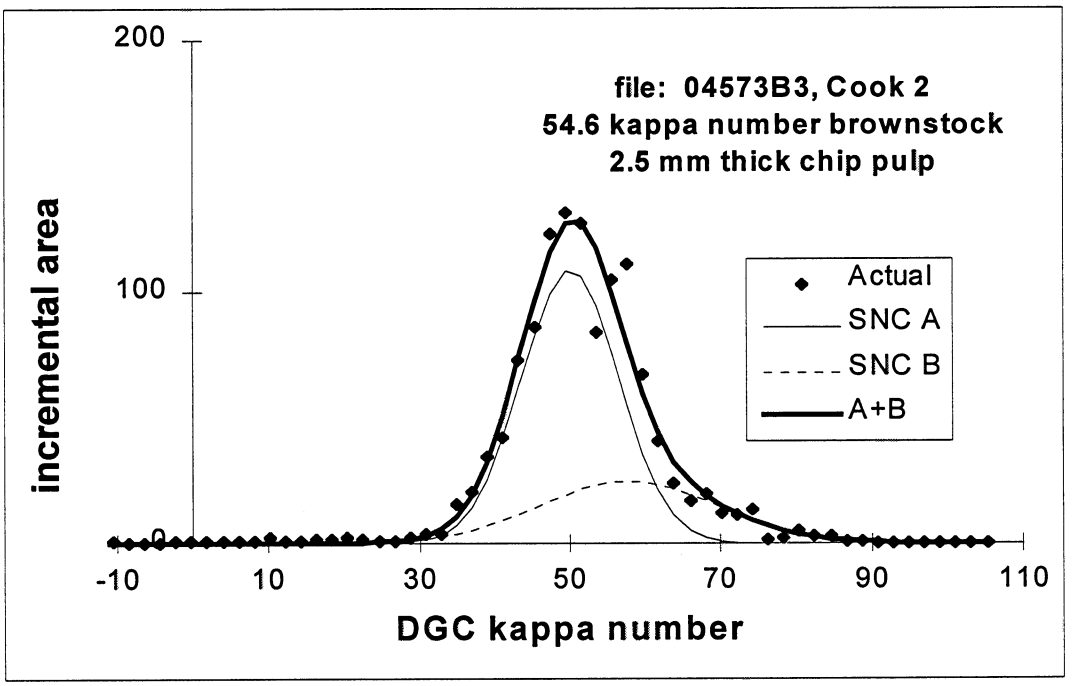

Figure B 1. Holopulp and brownstock distributions for 54.6 kappa number kraft pulp from 2.5-mm-thick chips.

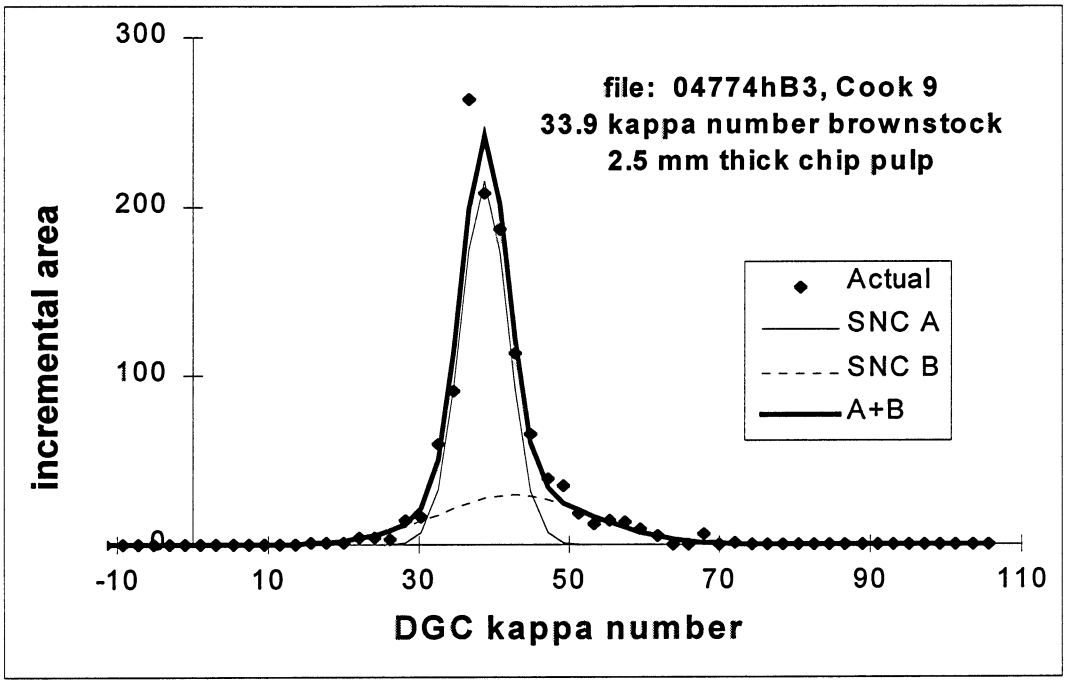

Figure B 2. Brownstock distributions for 33.9 kappa number kraft pulp from 2.5-mm-thick chips.

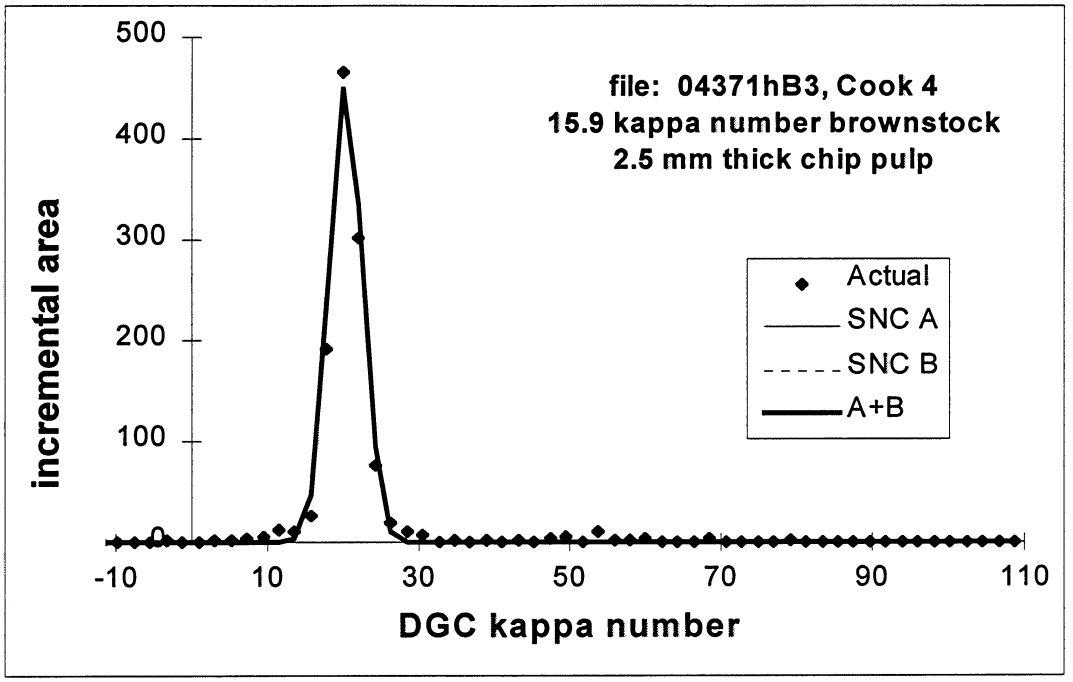

Figure B 3. Brownstock distributions for 15.9 kappa number kraft pulp from 2.5-mm-thick chips.

Thick Chip Pulps

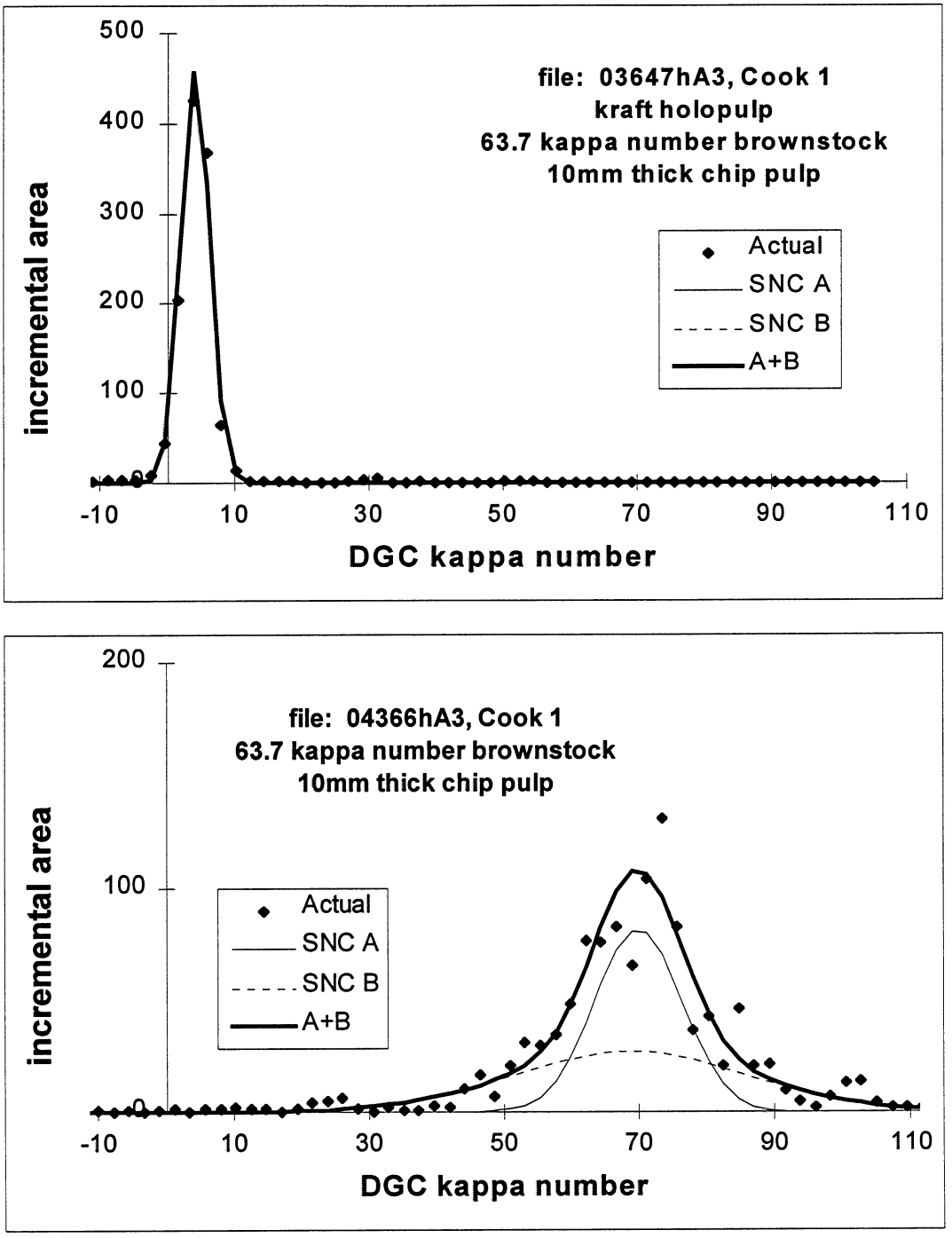

Figure B 4. Holopulp and brownstock distributions for 63.7 kappa number kraft pulp from 10.0-mm-thick chips.

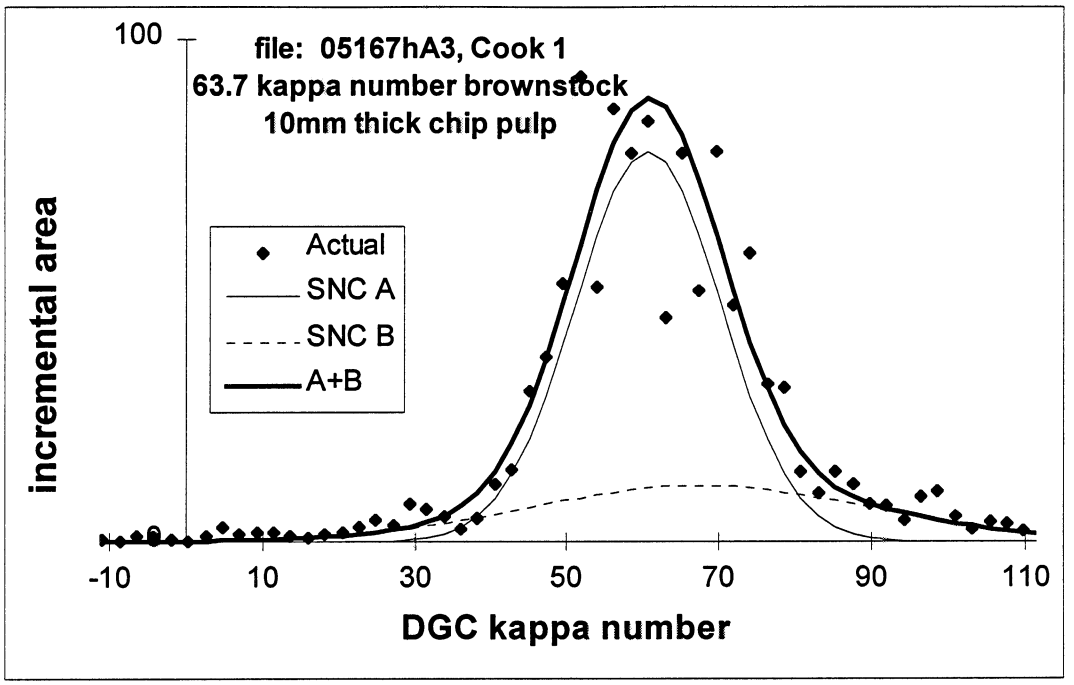

Figure B 5. Brownstock distributions for 63.7 kappa number kraft pulp from 10.0-mm-thick chips.

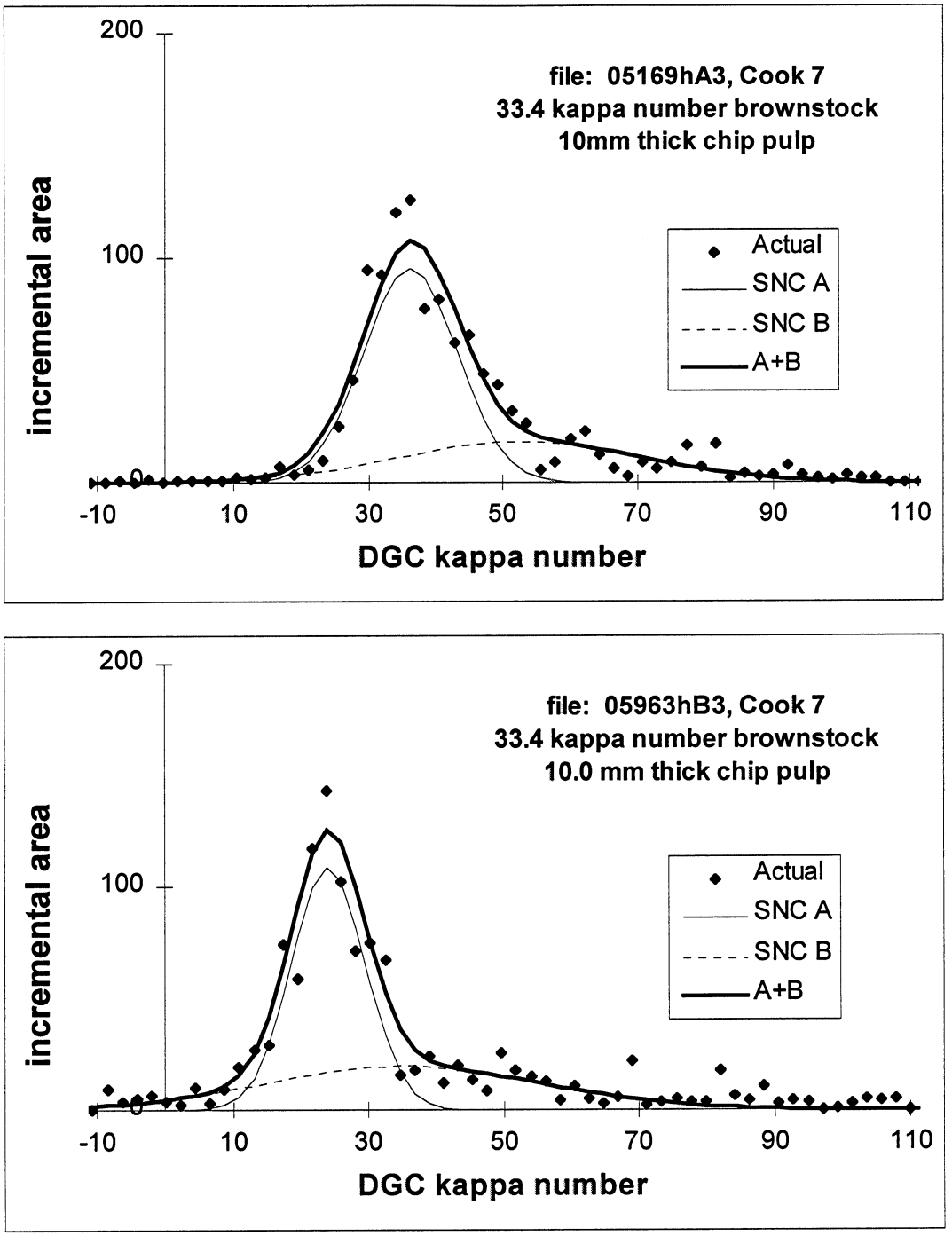

Figure B 6. Brownstock distributions for 33.4 kappa number kraft pulp from 10.0-mm-thick chips.

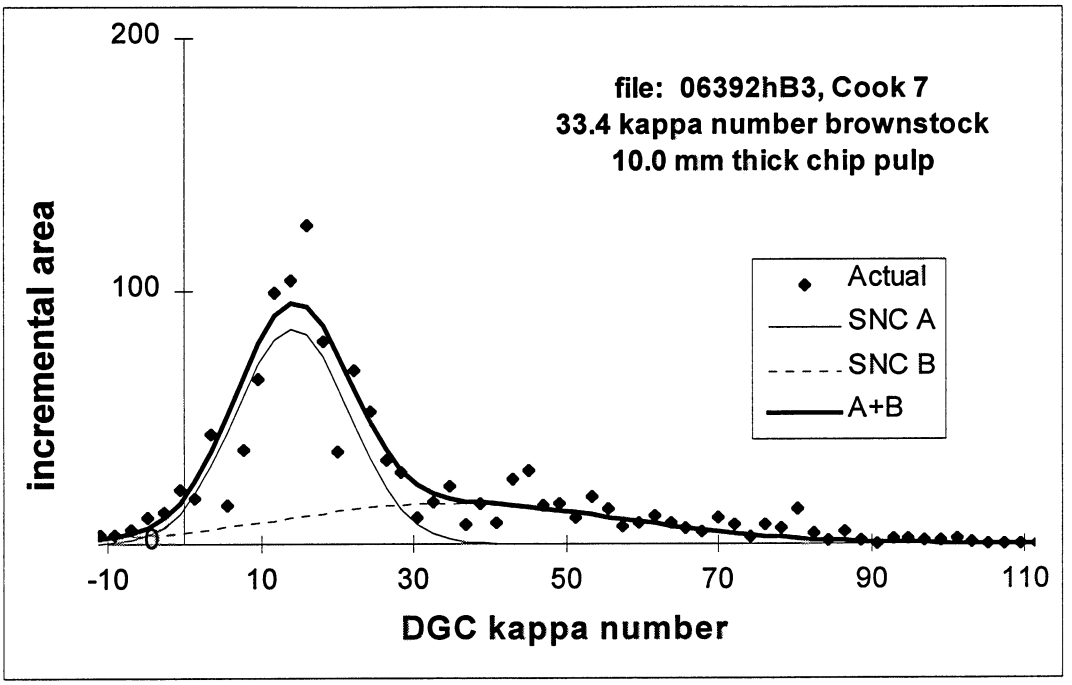

Figure B 7. Brownstock distributions for 33.4 kappa number kraft pulp from 10.0-mm-thick chips.

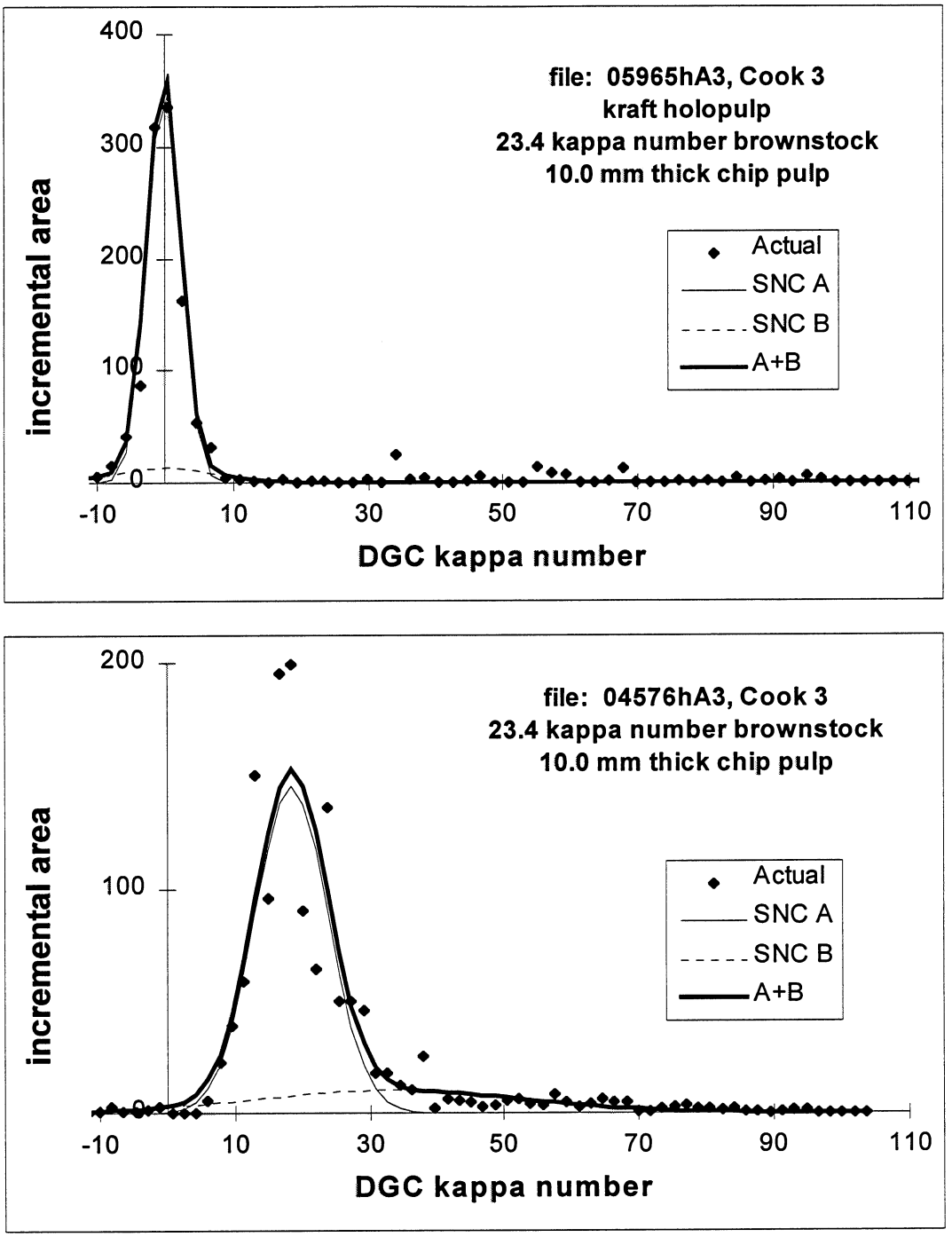

Figure B 8. Holopulp and brownstock distributions for 23.4 kappa number kraft pulp from 10.0-mm-thick chips.

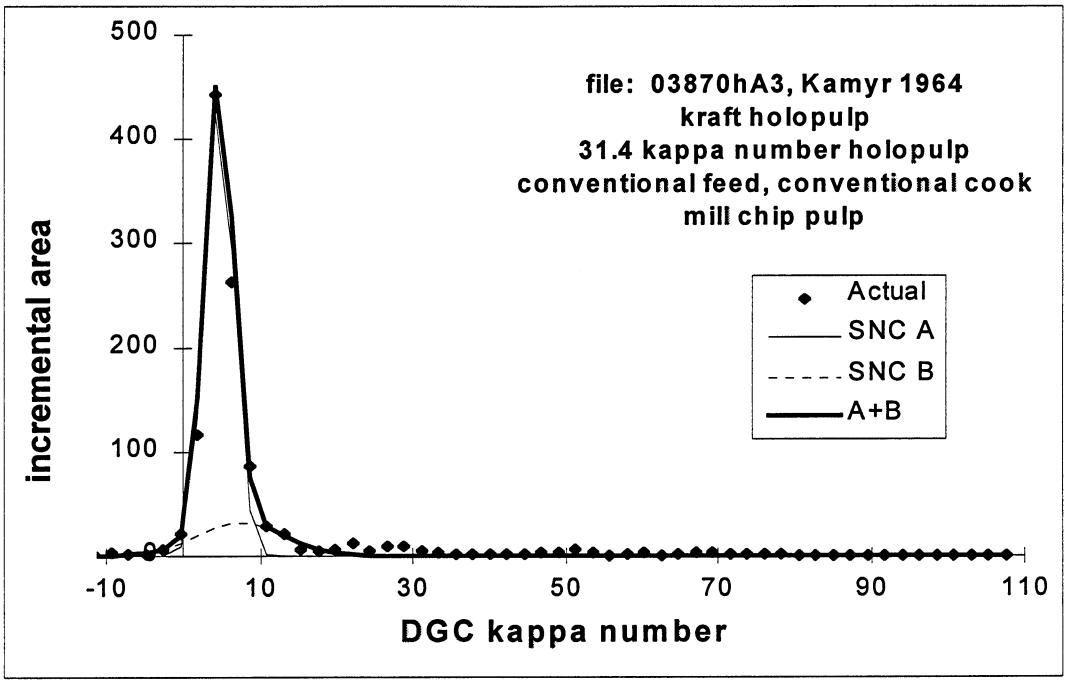

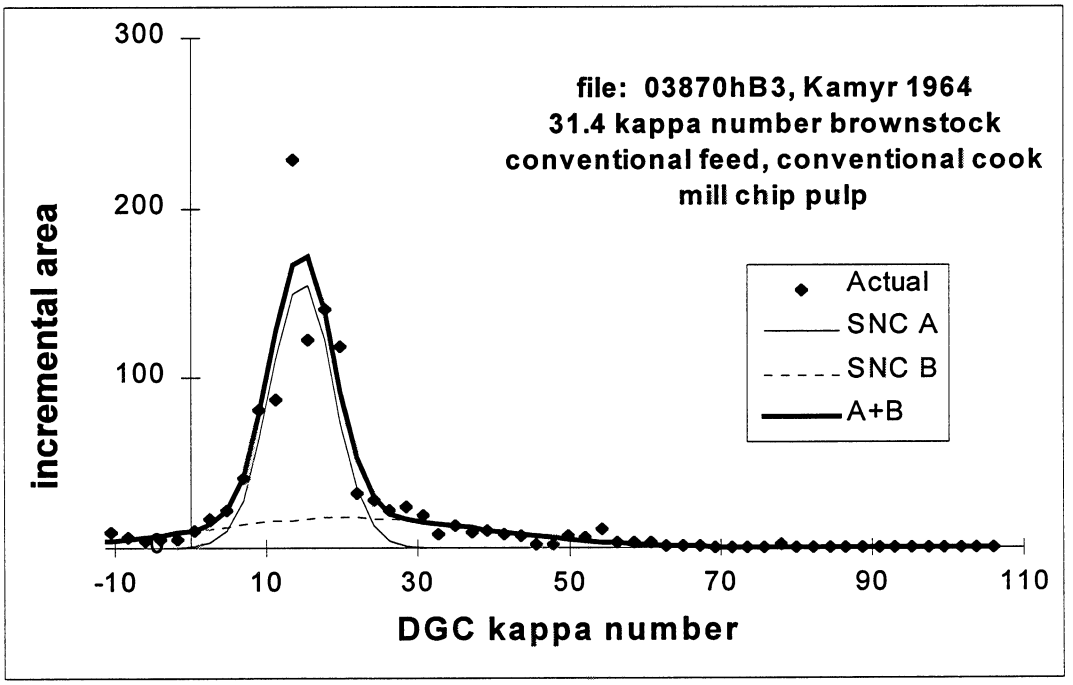

Figure B 9. Holopulp and brownstock distributions for 31.4 kappa number kraft pulp from mill chips.

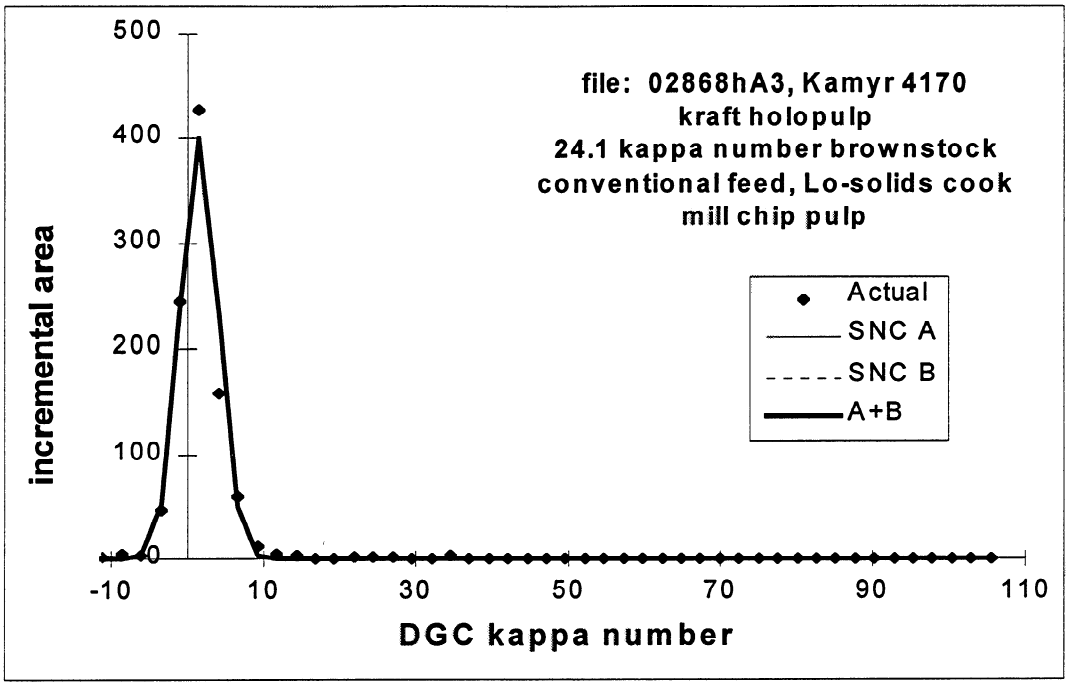

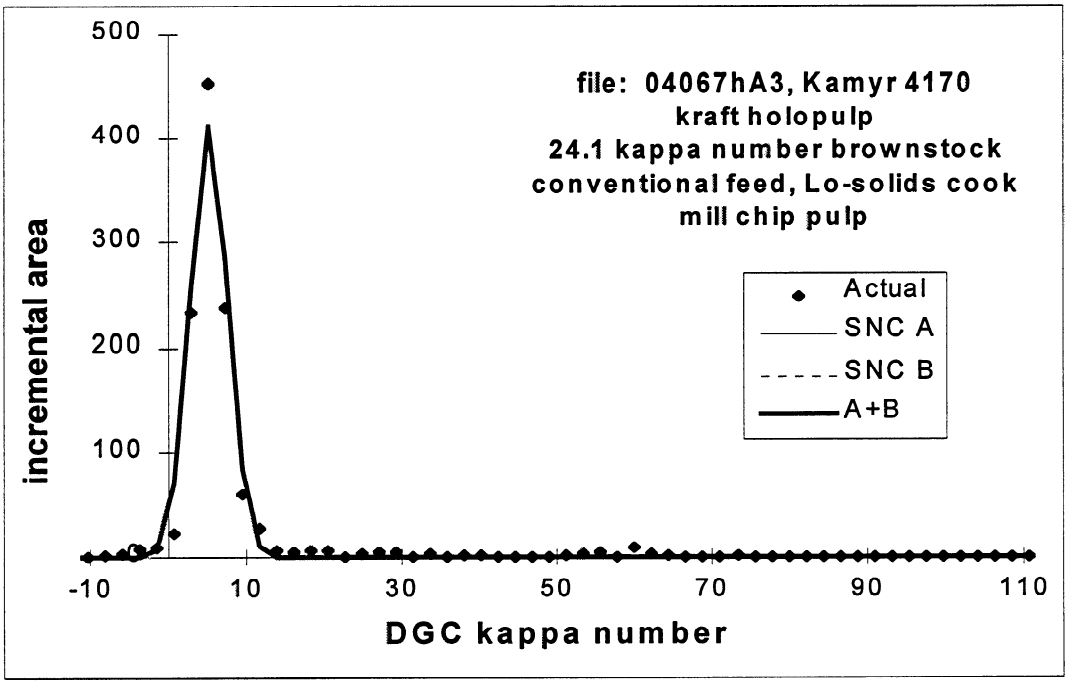

Figure B 10. Holopulp distributions for 24.1 kappa number kraft pulp from mill chips.

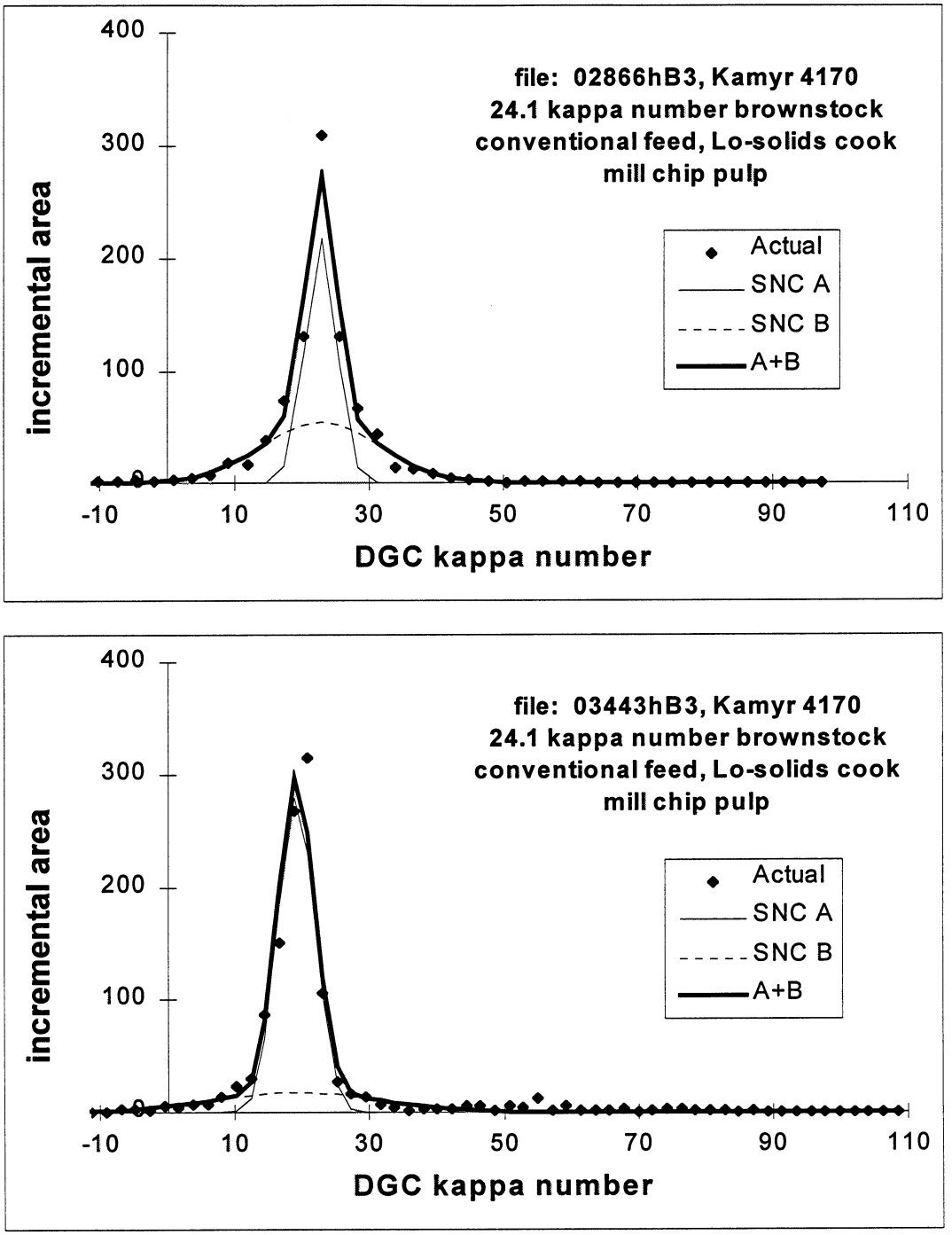

Figure B 11. Brownstock distributions for 24.1 kappa number kraft pulp from mill chips.

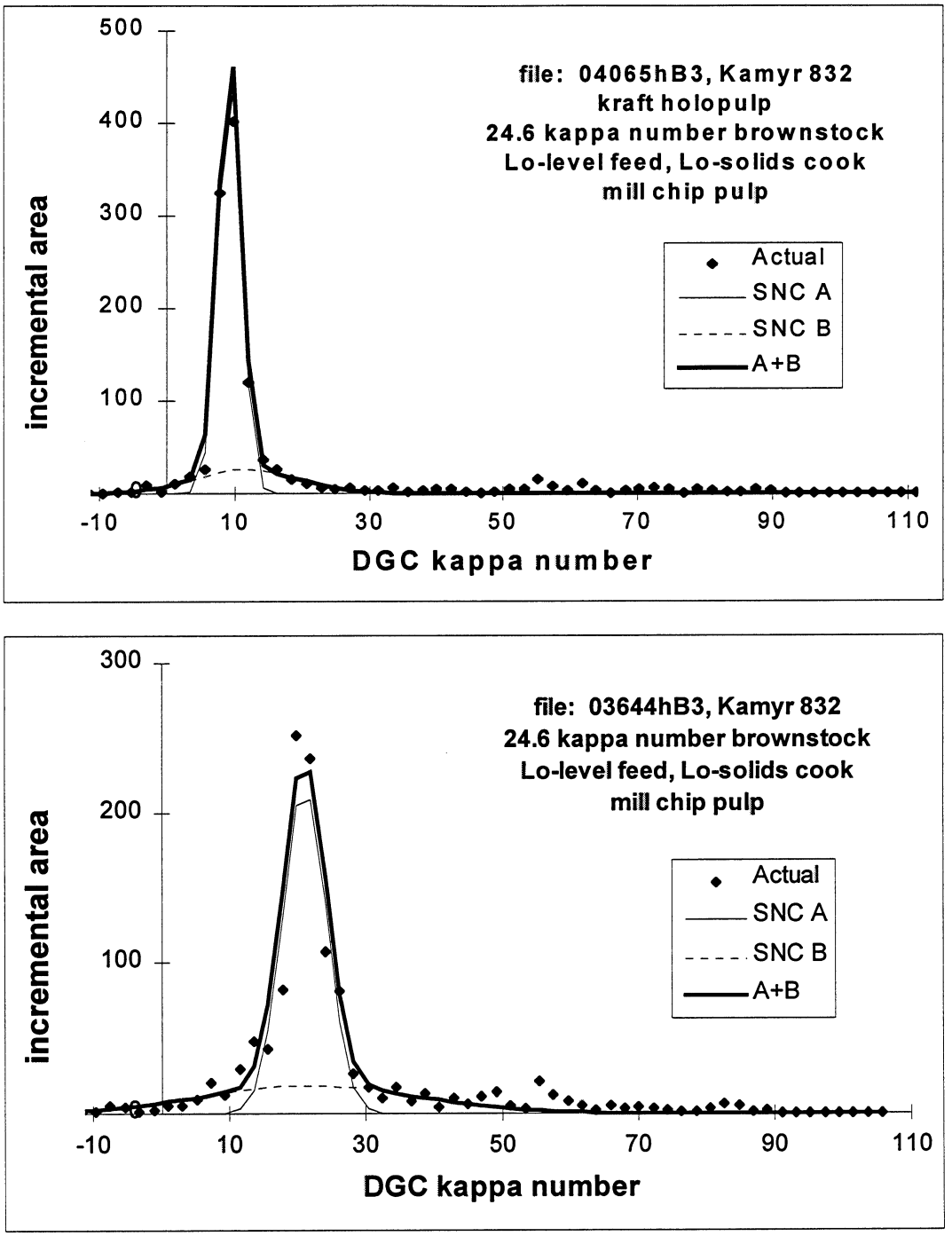

Figure B 12. Holopulp and brownstock distributions for 24.6 kappa number kraft pulp from mill chips.

Verification of the Average Fiber Density vs. Kappa Number Model

The relationship between average fiber density and Tappi T236 kappa number appeared slightly quadratic in character, especially when plotting average class values for comparison purposes. Therefore, a qualitative and quantitative statistical analysis was necessary to determine which model was most appropriate. Figure B 13 describes the correlations of interest.

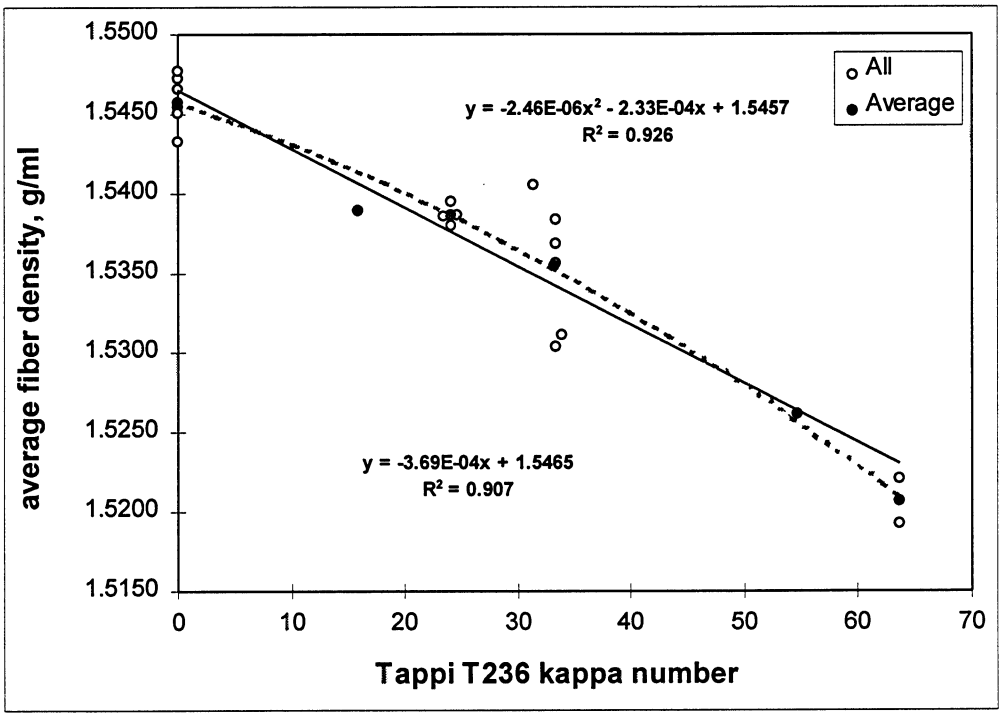

Figure B 13. Average fiber density vs. Tappi T236 kappa number; model for secondary analyses.

At first glance, it is not obvious which model is most appropriate. In fact, it may not be clear what the linear and quadratic models imply about lignin density as a function of extending delignification. Using the assumption of a constant kraft holopulp average fiber density from Table 10, the remaining contribution to fiber density is from lignin. It can be mathematically

shown that the linear model implies a constant lignin density, whereas the quadratic model implies a linear change in lignin density throughout the kraft cook. Additivity shows that

$$\rho_T = \rho_L(x) + \rho_H(1-x), \text{ where}$$

ρ_T = total fiber density, g/ml
ρ_H = kraft holocellulose fiber density, g/ml
ρ_L = kraft lignin density, g/ml
and
x = weight fraction lignin = (0.1338)(kappa number).[252]

The relationship between ρ_T and kappa number is used to obtain a value of ρ_T at a particular value of x. Thus, generic forms of both linear and quadratic models can be substituted for ρ_T in the additivity relationship. This purely empirical approach provides a mathematical method for understanding what each model implies about the effect of kraft cooking on lignin density. Differentiating for ρ_L with respect to x eliminates terms in each model assumption. Using the differentiated form of each assumption and integrating for ρ_L gives

$$\int d(\rho_L) = \int\left(a + \frac{(\rho_H - c)}{x^2}\right)dx = ax + \frac{(c-\rho_H)}{x} + constant$$

for ρ_T as a function of $ax^2 + bx + c$, and

$$\int d(\rho_L) = \int\left(\frac{(\rho_H - c)}{x^2}\right)dx = \frac{(c-\rho_H)}{x} + constant$$

for ρ_T as a function of bx + c.

Both models predict a value of ρ_H from the intercept, c, thereby eliminating a term from each of the integrated expressions. Therefore, the linear model implies a constant lignin density throughout the kraft pulping process, whereas the quadratic model implies a linear change in lignin density with extent of cook.

Intuitively, it may be expected that the relationship would be nonlinear, assuming that structural changes in lignin are measurable through changes in lignin density. Structural changes in lignin, as a result of condensation reactions, are known to occur as the cook proceeds. Interestingly, a comparison of the correlation coefficients supports curvilinearity, as does the apparent curvature of the average class values of average fiber density vs. kappa number. Furthermore, a residual plot provides some qualitative evidence of the quadratic trend, as shown in Figure B 14.

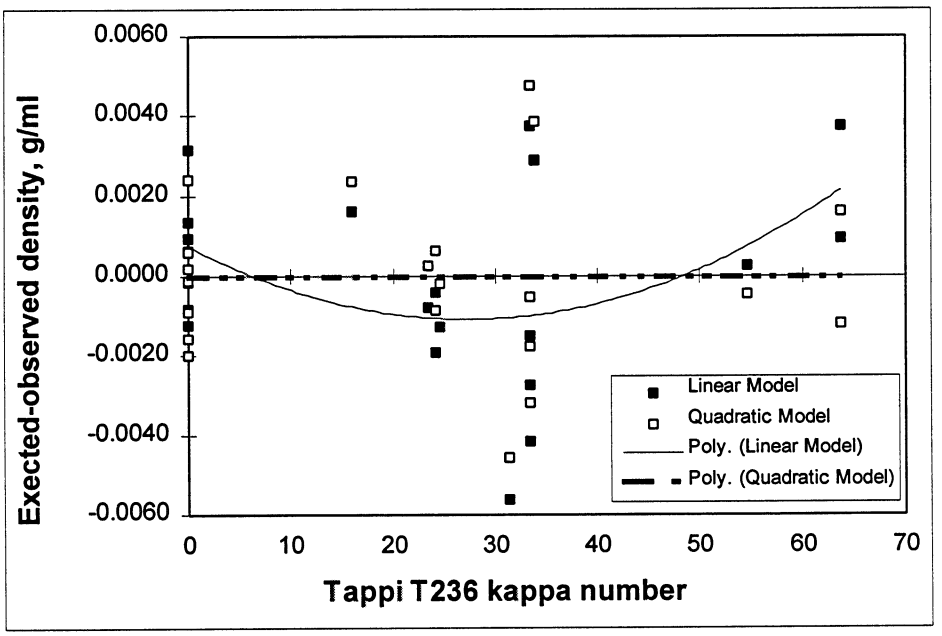

Figure B 14. Residual plot of kappa number determinations from density measurements.

The residual plot suggests a curvilinear trend rather than a linear trend. For both linear and quadratic secondary analysis models, a second order equation was fit to the residuals. An even distribution of residuals around the quadratic model produced random scatter around the value of zero in the residual plot, resulting in the horizontal dashed line of Figure B 14. Conversely, an uneven distribution of residuals around the linear model indicated a systematic relationship in the residual plot, resulting in the parabolic solid line of Figure B 14. Thus, the qualitative relationships and correlation coefficients suggest that the quadratic model may be most appropriate. However, a more rigorous quantitative analysis indicated that there is really no statistical evidence to reject the linear secondary analysis model.

Table B 4. Lack-of-fit and sums of squares analyses; linear vs. quadratic models of average fiber density vs. kappa number.

	Linear	Quadratic	SS lin.-SS quad.
	F LOF	F LOF	F contr.
α,v1,v2=fcrit	0.01,8,11=4.74	0.01,7,11=4.08	0.01,1,11=6081
α,v1,v2=fcrit	0.05,8,11=2.95	0.05,7,11=3.01	0.05,1,11=242.9
f-ratio	**1.688**	**1.193**	**5.153**

Under the premise that the simplest model be used, it becomes important to know the statistical significance of adding higher order terms to an assumed model. Table B 4 compares F-ratios for linear and quadratic models. Both models are given an F-ratio to determine "lack-of-fit", or systematic error, for a more rigorous test of curvilinearity.

The lack-of-fit test involves separating the residual sum of squares into a pure error term and a systematic "lack-of-fit" term, where

$$\Sigma\Sigma(y_{ju}-y_{jexp})^2 = \Sigma\Sigma(y_{ju}-y_{javg})^2 + \Sigma n_j(y_{jexp}-y_{javg})^2, \text{ or}$$

$$SS_{residuals} = SS_{pure\ error} + SS_{lack\text{-}of\text{-}fit}, \text{ and}$$

y_{ju} = "u^{th}" observation from the "j^{th}" class,
y_{javg} = average of all observations in the "j^{th}" class,
y_{jexp} = expected value from the model for the "j^{th}" class, and
SS = sum of squares, or sum of the squares of the deviations.

The F-ratio for lack-of-fit is simply the ratio of the mean square for lack-of-fit to the pooled mean square for pure error[253]. Table B 5 lists the data used in calculating the F-ratios given in Table B 4.

Although the F-ratio for systematic error was reduced in the case of the quadratic model, the corresponding F-ratio for the linear model could not reject linearity at the α=0.05 level. Similarly, the significance of contributing a quadratic term to the linear model could be tested through an additional F-ratio, termed F_{contr} in Table B 4. The difference between the residual sum of squares from the linear model and residual sum of squares from the quadratic model represents the significance of the quadratic term in reducing the total residual sum of squares. A significant reduction would result in a corresponding significant F-ratio for that reduction. Since the F-ratio for the reduction was insignificant, the contribution of the quadratic term was insignificant.

Table B 5. Lack of fit analysis for choice of kappa vs. density model.

Density	Actual Kappa	Expected density (Quad.)	Expected density (Linear)	act-exp density Resid. (Quad.)	act-exp density Resid. (Linear)	Class kappa number	(pool pure error) ΣΣ(Yju-Yjavg)^2 n(u) point, m(j) class	MSE (ΣΣ(Yju-μYj)^2)/d.f. n(u) point, m(j) class d.f.=Σnj - m=11	MS res ΣΣ(Yju-Yjfit)^2/d.f. df=n-p=n-2=19 (Linear)	MS LOF (SSres-SSE)/d.f. d.f.=n-2-nE=8 (Linear)	MS res ΣΣ(Yju-Yjfit)^2 df=n-p=n-3=18 (Quad.)	MS LOF d.f.=n-3-nE 7.0 (Quad.)
								5.05E-06	**6.52E-06**	**8.53E-06**	**5.43E-06**	**6.03E-06**
1.5466	0.0	1.5457	1.5465	0.0009	0.0001	0.0	1.38E-05		1.88E-08		8.15E-07	
1.5455	0.0	1.5457	1.5465	-0.0002	-0.0010	24.1	1.13E-06		9.27E-07		3.90E-08	
1.5451	0.0	1.5457	1.5465	-0.0006	-0.0014	33.4	3.59E-05		1.86E-06		3.57E-07	
1.5451	0.0	1.5457	1.5465	-0.0006	-0.0014	63.7	4.74E-06		1.86E-06		3.57E-07	
1.5433	0.0	1.5457	1.5465	-0.0024	-0.0032				1.00E-05		5.75E-06	
1.5473	0.0	1.5457	1.5465	0.0016	0.0008				6.84E-07		2.54E-06	
1.5477	0.0	1.5457	1.5465	0.0020	0.0012				1.53E-06		4.01E-06	
1.5390	15.9	1.5414	1.5406	-0.0024	-0.0016				2.57E-06		5.68E-06	
1.5386	23.4	1.5389	1.5378	-0.0003	0.0008				6.27E-07		7.78E-08	
1.5380	24.1	1.5387	1.5376	-0.0007	0.0004				1.76E-07		4.40E-07	
1.5395	24.1	1.5387	1.5376	0.0008	0.0019				3.69E-06		7.00E-07	
1.5387	24.6	1.5385	1.5374	0.0002	0.0013				1.65E-06		3.73E-08	
1.5405	31.4	1.5360	1.5349	0.0046	0.0057				3.19E-05		2.10E-05	
1.5369	33.4	1.5352	1.5342	0.0018	0.0028				7.71E-06		3.09E-06	
1.5304	33.4	1.5352	1.5342	-0.0048	-0.0037				1.39E-05		2.26E-05	
1.5357	33.4	1.5352	1.5342	0.0005	0.0015				2.36E-06		2.69E-07	
1.5384	33.4	1.5352	1.5342	0.0032	0.0042				1.76E-05		1.01E-05	
1.5311	33.9	1.5350	1.5340	-0.0039	-0.0028				8.11E-06		1.48E-05	
1.5261	54.6	1.5256	1.5263	0.0005	-0.0002				5.25E-08		2.67E-07	
1.5190	63.7	1.5208	1.5230	-0.0018	-0.0040				1.57E-05		3.14E-06	
1.5221	63.7	1.5208	1.5230	0.0013	-0.0009				7.84E-07		1.71E-06	
1.5458												
1.5390						TOTAL	5.56E-05		**SSres(lin.)-SSres(quad.)**	**F LOF**	**F LOF**	
1.5387									**=SScontr(quad.) d.f.=1**	0.01,8,11=4.74	0.01,7,11=4.08	
1.5355									**(contribution of quad.term)**	0.05,8,11=2.95	0.05,7,11=3.01	
1.5261										**(Linear)**	**(Quad.)**	
1.5206									**2.60E-05**	**1.688**	**1.193**	

It was statistically necessary to assume the linear model. This was understandable, since the large pooled mean square error that controlled the quantitative statistics also controlled the strength of the qualitative statistics. As a result, available data was unable to prove that lignin density decreased linearly in the range of 10 kappa number to 70 kappa number, as shown in Figure B 15. However, it was already proven that the random error could be reduced from 0.0035 g/ml to 0.0015 g/ml through simple improvement of sampling technique, thus reducing the magnitude of the pooled mean square error. When the quadratic relationship is proven, a entirely new realm of fiber chemistry analysis could arise.

In summary, the density gradient column may be able to provide more exact measures of lignin density through very simple technique modification. The result is a potential secondary analysis technique with the ability to provide correlations between lignin density and another chemical characterization technique of choice, such as NMR. The ability to analyze lignin in its native state would have an application superior to that of its referee technique, at this point in time. It may also prove useful in model bleaching chemistry studies to derive model compounds through density gradient column fractionations of isolated lignin. Figure B 15 describes the proposed relationship between lignin density and extent of cook. Note that these results are nearly identical to the lignin fractionation results of Yoshida et al[193].

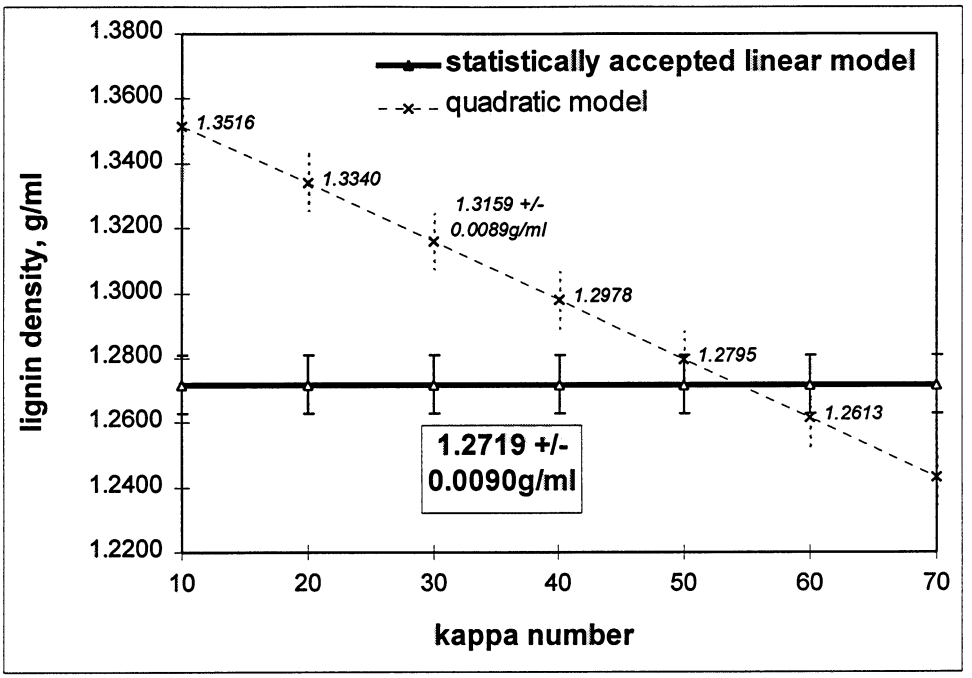

Figure B 15. Lignin density vs Tappi T236 kappa number.

Table B 6. Data converted to DGC kappa number including z-test of means and f-test of standard deviations in kappa number.

File #	Description	Kappa Number	Chip Thick. (mm)	A Fxn	B Fxn	A $X\rho$	B $X\rho$	A $s\rho$	B $s\rho$	A+B $X\rho$	A+B $s\rho$	A X kappa	B X kappa	A s kappa	B s kappa	A+B X kappa	A+B s kappa
02868hA3	**Kamyr 4170 - Holo**	**0**	mill	1.00	0.00	1.5466		0.0010		1.5466	0.0010	**1.5**		**2.5**		**1.5**	**2.5**
03647hA3	**Cook 1 - Holo**	**0**	10.0	1.00	0.00	1.5455		0.0009		1.5455	0.0009	**4.3**		**2.1**		**4.3**	**2.1**
03870hA3	**Kamyr 1964 - Holo**	**0**	mill	0.82	0.18	1.5453	1.5442	0.0007	0.0022	1.5451	0.0012	**4.7**	**7.5**	**1.8**	**5.5**	**5.2**	**3.0**
04067hA3	**Kamyr 4170 - Holo**	**0**	mill	1.00	0.00	1.5451		0.0010		1.5451	0.0010	**5.2**		**2.4**		**5.2**	**2.4**
04065hB3	**Kamyr 832 - Holo**	**0**	mill	0.80	0.20	1.5435	1.5425	0.0007	0.0031	1.5433	0.0016	**9.2**	**11.7**	**1.7**	**7.7**	**9.7**	**3.9**
05965hA3	**Cook 3 - Holo**	**0**	10.0	0.90	0.10	1.5473	1.5472	0.0010	0.0030	1.5473	0.0013	**-0.2**	**0.0**	**2.5**	**7.4**	**-0.2**	**3.3**
06392hA3	**Cook 2 - Holo**	**0**	2.5	1.00	0.00	1.5477		0.0009		1.5477	0.0009	**-1.2**		**2.2**		**-1.2**	**2.2**
04371hB3	**Cook 4 - BS**	**15.9**	2.5	1.00	0.00	1.5390		0.0009		1.5390	0.0009	**20.4**		**2.2**		**20.4**	**2.2**
04576hA3	**Cook 3 - BS**	**23.4**	10.0	0.80	0.20	1.5398	1.5340	0.0022	0.0080	1.5386	0.0047	**18.4**	**32.7**	**5.5**	**19.8**	**21.3**	**11.5**
02866hB3	**Kamyr 4170 - BS**	**24.1**	mill	0.52	0.48	1.5380	1.5380	0.0010	0.0035	1.5380	0.0025	**22.8**	**22.8**	**2.4**	**8.7**	**22.8**	**6.2**
03443hB3	**Kamyr 4170 - BS**	**24.1**	mill	0.78	0.22	1.5395	1.5395	0.0011	0.0050	1.5395	0.0025	**19.1**	**19.1**	**2.7**	**12.4**	**19.1**	**6.3**
03644hB3	**Kamyr 832 - BS**	**24.6**	mill	0.71	0.29	1.5388	1.5385	0.0013	0.0063	1.5387	0.0036	**21.0**	**21.6**	**3.2**	**15.6**	**21.2**	**8.8**
03870hB3	**Kamyr 1964 - BS**	**31.4**	mill	0.67	0.33	1.5413	1.5390	0.0017	0.0074	1.5405	0.0046	**14.7**	**20.4**	**4.2**	**18.3**	**16.5**	**11.4**
04772hA3	**Cook 7 - BS**	**33.4**	10.0	0.57	0.43	1.5363	1.5378	0.0062	0.0028	1.5369	0.0051	**27.0**	**23.3**	**15.4**	**6.9**	**25.5**	**12.7**
05169hA3	**Cook 7 - BS**	**33.4**	10.0	0.67	0.33	1.5326	1.5260	0.0028	0.0072	1.5304	0.0057	**36.2**	**52.6**	**6.9**	**17.8**	**41.6**	**14.0**
05963hB3	**Cook 7 - BS**	**33.4**	10.0	0.60	0.40	1.5375	1.5330	0.0022	0.0082	1.5357	0.0059	**24.1**	**35.2**	**5.5**	**20.3**	**28.6**	**14.5**
06392hB3	**Cook 7 - BS**	**33.4**	10.0	0.63	0.37	1.5415	1.5330	0.0027	0.0090	1.5384	0.0071	**14.2**	**35.2**	**6.7**	**22.3**	**22.0**	**17.7**
04774hB3	**Cook 9 - BS**	**33.9**	2.5	0.70	0.30	1.5316	1.5300	0.0013	0.0041	1.5311	0.0026	**38.7**	**42.7**	**3.2**	**10.2**	**39.9**	**6.4**
04573hB3	**Cook 2 - BS**	**54.6**	2.5	0.71	0.29	1.5270	1.5239	0.0026	0.0047	1.5261	0.0036	**50.1**	**57.7**	**6.4**	**11.6**	**52.3**	**9.0**
04366hA3	**Cook 1 - BS**	**63.7**	10.0	0.53	0.47	1.5190	1.5195	0.0026	0.0070	1.5193	0.0050	**69.9**	**68.7**	**6.4**	**17.3**	**69.2**	**12.5**
05167hB3	**Cook 1 - BS**	**63.7**	10.0	0.75	0.25	1.5227	1.5200	0.0039	0.0090	1.5221	0.0056	**60.7**	**67.4**	**9.5**	**22.3**	**62.2**	**14.0**

			X_A, X_B z-ratio	one-sided z-crit.: 90.0%	95.0%	97.5%	% conf.	s_A, s_B f-ratio	f-crit.,70,70: 5%	1%	type I error
02868hA3	Kamyr 4170 - Holo	0		1.280	1.645	1.960	z-crit.		1.47	1.74	f-crit.
03647hA3	Cook 1 - Holo	0									
03870hA3	Kamyr 1964 - Holo	0	0.489					9.082			
04067hA3	Kamyr 4170 - Holo	0		s=+/-0.00225g/ml							
04065hB3	Kamyr 832 - Holo	0	0.444	=+/-5.58 kappa number				20.783			
05965hA3	Cook 3 - Holo	0	0.044	= pooled random erro				9.000			
06392hA3	Cook 2 - Holo	0									
04371hB3	Cook 4 - BS	15.9									
04576hA3	**Cook 3 - BS**	**23.4**	**2.578**					13.223			
02866hB3	Kamyr 4170 - BS	24.1	0.000					13.573			
03443hB3	Kamyr 4170 - BS	24.1	0.000					20.661			
03644hB3	Kamyr 832 - BS	24.6	0.111					23.485			
03870hB3	Kamyr 1964 - BS	31.4	1.022					18.948			
04772hA3	Cook 7 - BS	33.4	0.667					4.903			
05169hA3	**Cook 7 - BS**	**33.4**	**2.933**					6.612			
05963hB3	**Cook 7 - BS**	**33.4**	**2.000**					13.893			
06392hB3	**Cook 7 - BS**	**33.4**	**3.778**					11.111			
04774hB3	Cook 9 - BS	33.9	0.711					9.947			
04573hB3	Cook 2 - BS	54.6	1.364					3.268			
04366hA3	Cook 1 - BS	63.7	0.222					7.249			
05167hB3	Cook 1 - BS	63.7	1.200					5.465			

APPENDIX C

Subtraction Algorithm and the Effect of Spectral Variability

The FTIR subtraction algorithm is based on the spectral subtraction procedure of Friese and Banerjee[227]. To help identify factors that may create differences in spectral subtraction results, a simplified spreadsheet model was developed. A set of number arrays were produced using standard normal distributions by varying μ and σ, where μ is the mean of the distribution and σ is the standard deviation. By varying x from 400-4000 cm^{-1}, it became possible to use simplified peaks as analogs to individual cellulose and lignin spectra. A characteristic peak for lignin is typically found at about 1600 cm^{-1}, whereas cellulose has a comparatively stable peak at about 1300 cm^{-1}. A "standard" peak for each component was simulated using a standard deviation of 200 cm^{-1}. The small 5-20% contribution of lignin to the overall spectra was modeled by taking the desired contribution from the lignin analog spectra (n2) and adding it to the cellulose analog spectra (n1). Likewise, the peak width was altered by changing this standard deviation. In the following analysis, the "sharp" peak has a σ of 125 cm^{-1} relative to the "standard" peak σ of 200 cm^{-1}.

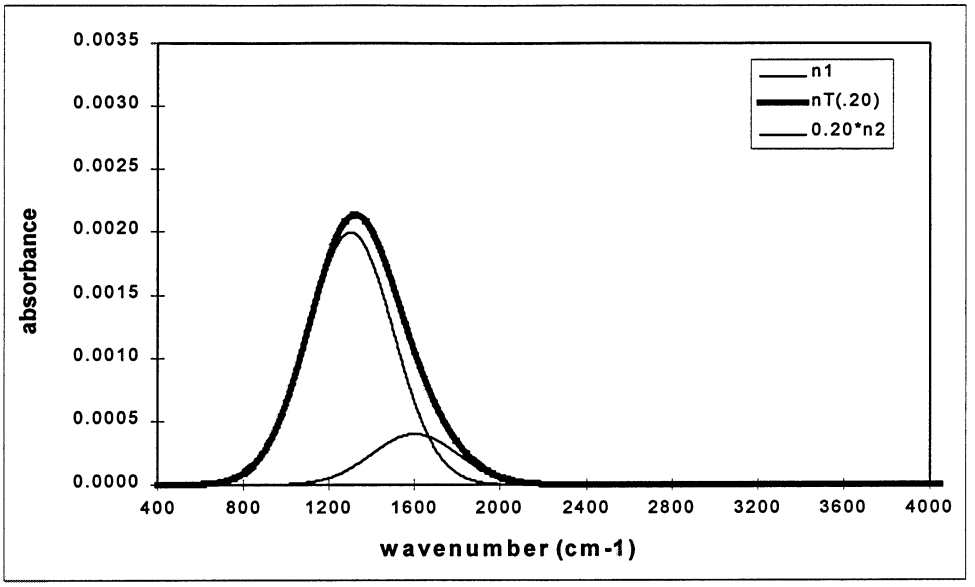

Figure C 1. Lignin analog(n2), cellulose analog(n1), and overall (nT) spectra.

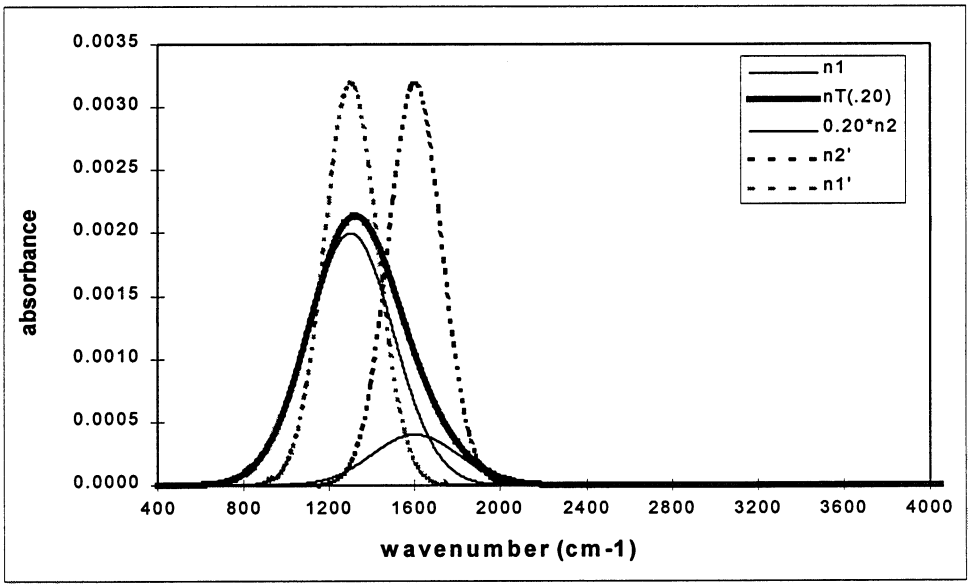

Figure C 2. "Sharp" peaks superimposed over component and total spectra.

Figure C 1 and Figure C 2 illustrate the simplicity of the model. Component n1 is the simulated cellulose component, whereas n2 is the lignin analog component at a representative 20% of the "standard" lignin spectra. The sum of n1 and n2 is nT, or the overall lignin and

cellulose composite spectra. Figure C 2 includes the "sharp" subtraction standards, n1' and n2', that will be used to simulate the effects of peak shape. The first step in this theoretical analysis is to describe the perfect subtraction routine. The standard cellulose component will be subracted from the overall spectra and should theoretically yield a perfect 20% fraction of the standard lignin spectra. Figure C 3 illustrates the comparison between sharp and standard peak, where in this case the standard cellulose subraction spectra is perfectly overlapped with the cellulose component. The lignin subtraction spectra is sharp and simulates a strong absorbance and reduced peak width.

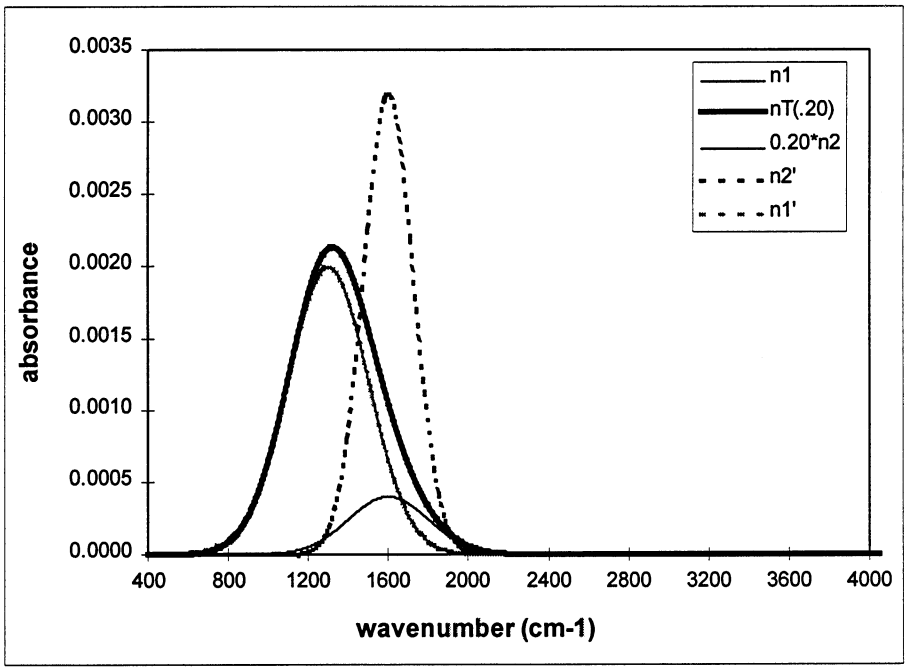

Figure C 3. Comparison of the standard peak of n1 with sharp peak of n2.

In Figure C 4, an example of the perfect subtraction routine serves to illustrate the mechanism of this spectral subtraction procedure using the ideal subtraction standard.

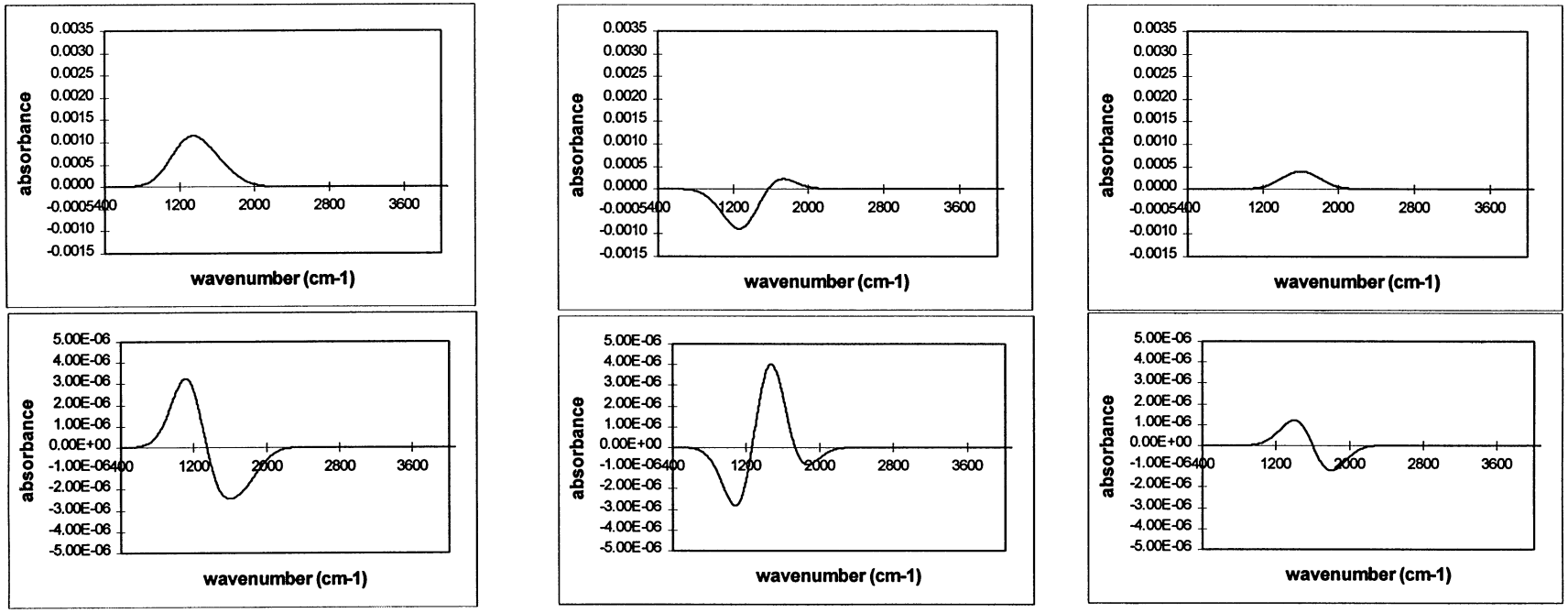

	A	B	C
FACTOR	0.50	1.50	1.00
AREA	2.30E-03	2.22E-03	7.98E-04

(NOTE: Top figure is the subtraction result, and the bottom figure is the first derivative of the subtraction result)

Figure C 4. Subtraction of n1 from nT with a perfect subtraction standard.

Figure C 4c shows that the area under the first-derivative of the subtraction result is minimized with a subtraction factor of 1. This is expected since nT, the total of n1 and n2, is comprised of exactly 1 unit of the standard cellulose analog curve. The remaining difference spectra is exactly 20% of n2. Most importantly, the area under the first derivative curve has been minimized to identify the correct scaling factor for the subtraction component.

Ultimately, subtraction standards need to dilineate differences between cellulose and lignin to the largest degree, in order to maximize the slope and produce the most useful calibration curve. Shared absorbances between cellulose and lignin will only decrease the scaling factor ratios, thereby reducing the accuracy of this secondary analysis.

Figure C 5 illustrates the same subtraction procedure using the sharp n1 spectra, where the σ was reduced from 200-125 cm^{-1} to obtain the sharper distribution. In this imperfect case, the model is identifying the appearance of the difference spectra and its associated first-derivative spectra. Clearly, the subtraction factor that minimizes the area under the first-derivative peak in this imperfect case is significantly different than its counterpart in the perfect case of Figure C 4. In fact, the n2 spectra does not come out unscathed in the difference spectra. This explains why it is difficult to obtain a good lignin subtraction standard through spectral subtraction of holocellulose from overall pulp spectra. A near perfect holocellulose match would be required to obtain a good lignin difference spectra, and may be beyond reasonable expectation due to the complexity of residual lignin.

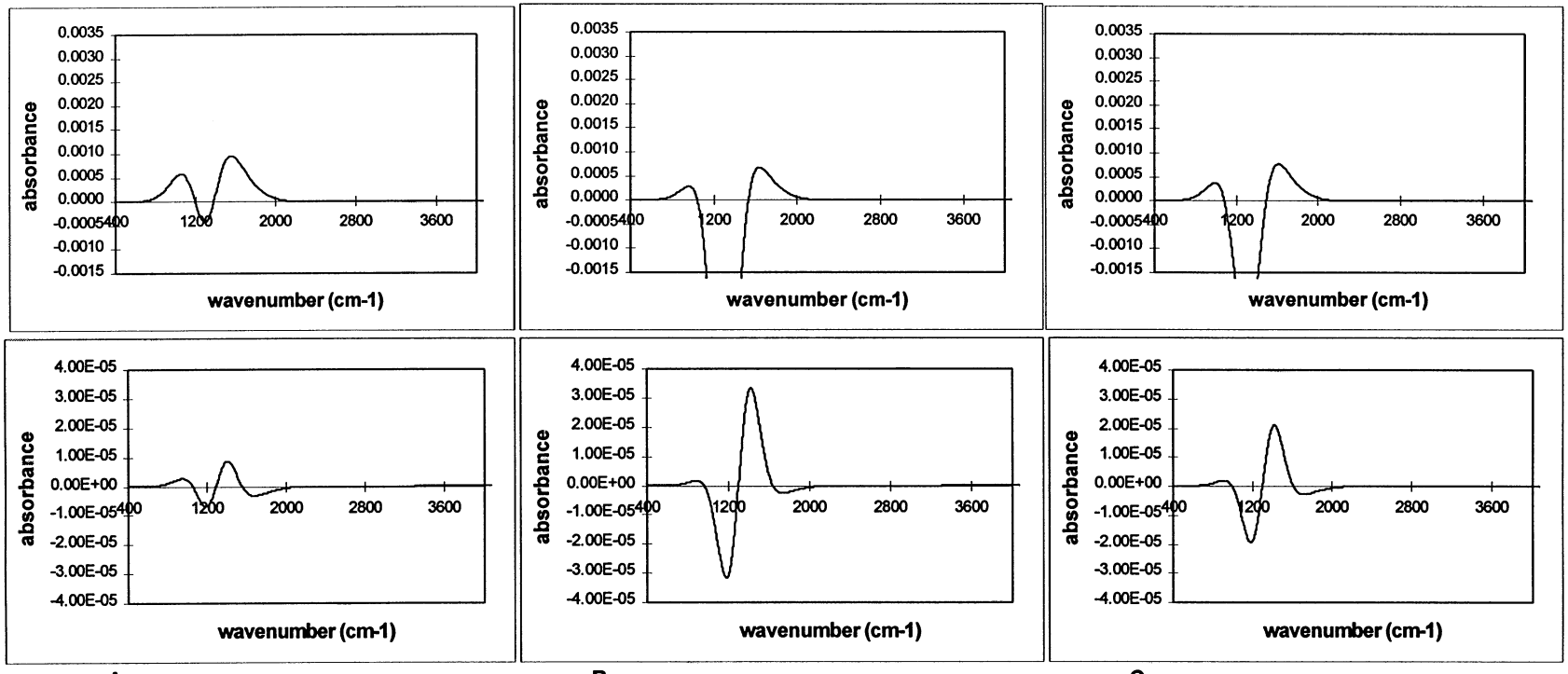

A B C

(NOTE: Top figure is the subtraction result, and the bottom figure is the first derivative of the subtraction result)

Result	Factor	Area
A	0.8	3.93E-03
B	2.4	1.30E-02
C	1.6	8.23E-03
ITERATION:		
	0.40	2.581E-03
	0.80	3.927E-03
	0.63	3.182E-03
	0.30	2.677E-03
	0.35	2.568E-03
	0.37	2.564E-03
D	0.36	2.564E-03

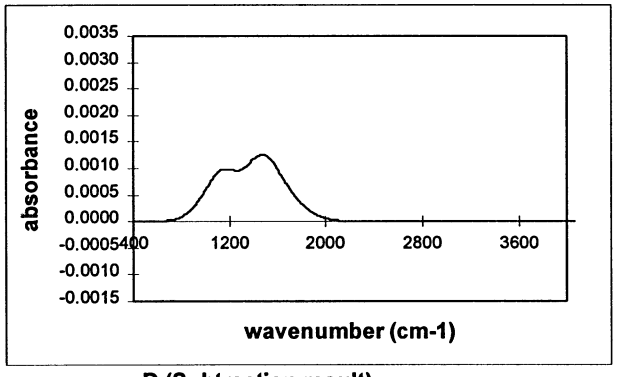

D (Subtraction result)

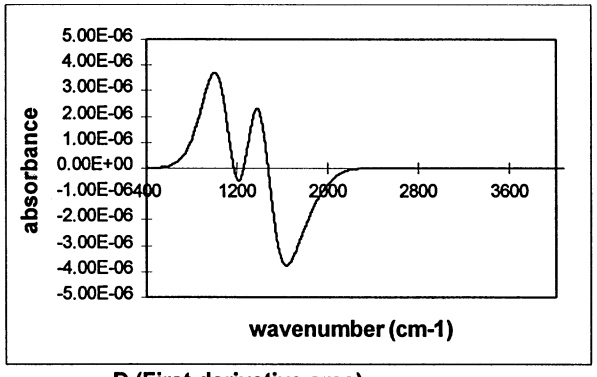

D (First-derivative area)

Figure C 5. Subtraction of n1 from nT with an imperfect "sharp" subtraction standard.

Figure C 6 describes the relationship between the area under the first derivative curve and the FTIR subtraction factor. As absorption intensities are reduced through the subtraction procedure, peaks are removed and the complexity of the infrared spectrum is reduced. The complexity of the spectrum is minimized when the area under the first derivative curve is minimized.

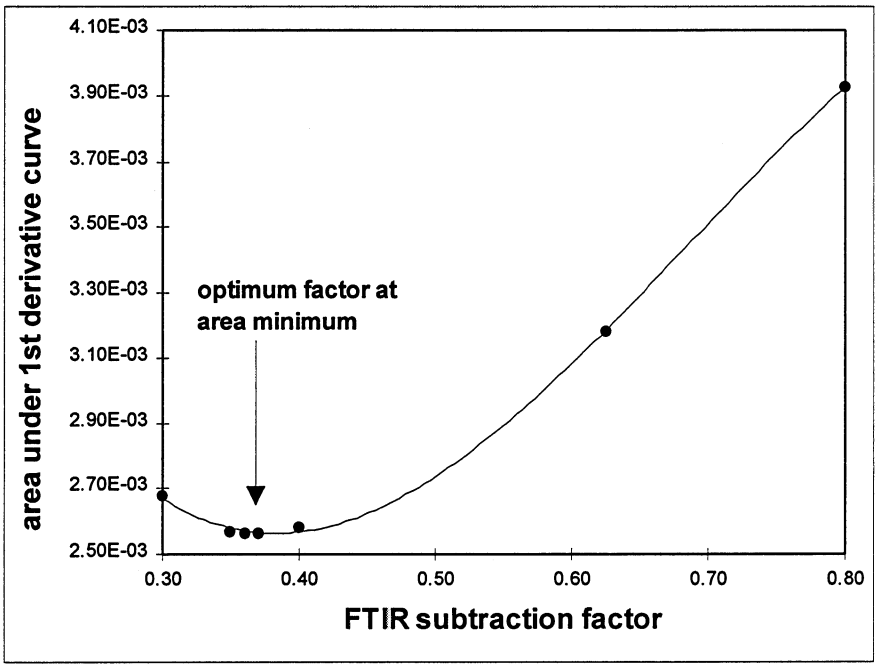

Figure C 6. Selection of optimum FTIR subtraction factor.

It has always been understood that differences in lignin structure from sample to sample may exist. However, the basic premise of the subtraction algorithm is that it is a secondary analysis based on a calibration curve. The differences between lignin structure have been assumed to be kappa related and therefore should allow our analysis to provide us with spectral "FTIR kappa numbers" at the individual fiber level. However, variations of an unknown origin have existed in early spectral determinations of kappa number using this technique. Figure C 4 and Figure C 5 both depict differences between a perfect and an imperfect subtraction standard,

along with an illustration of the results these standards produce. The question remains, "can we assume that imperfect subtraction standards will provide reliable calibration curves?"

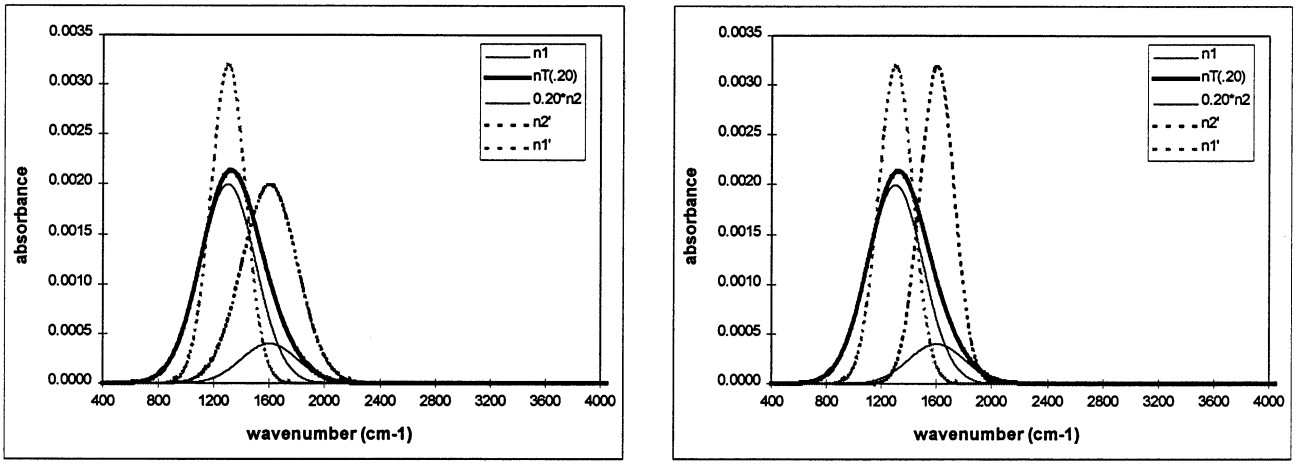

A. **B.**

Figure C 7. A.) standard n2 subtraction peak (n2') and B.) sharp n2 subtraction peak (n2').

Our model allows us to approach an answer to this question in simpler terms through development of calibration curves using two different n2 standards in conjuction with an imperfect n1 standard. Figure C 7 describes the two scenarios, where Figure C 7a depicts the standard n2 spectra using a σ of 200 cm^{-1}, whereas Figure C 7b depicts the imperfect "sharp" n2 subtraction spectra using a σ of 125 cm^{-1}. The internal cellulose subtraction spectra also uses the sharp distribution with a σ of 125 cm^{-1} highlight the relative importance of the internal standard number array.

Calibration curves were produced from 5-20% of the standard lignin spectra combined with the standard cellulose spectra. The overall lignin contribution (n2) then becomes 0.05/1.05 to 0.20/1.20, or 4.8-16.7% lignin.

Figure C 8 shows the response of the overall spectra to the subtraction routine. There are differences in the slopes, where steeper, more useful calibration curves came from the standard n2 subtraction spectra with a σ of 200 cm^{-1}, which happens to be equal to the σ of the lignin in the overall spectra. However, the sharper n2 subtraction standard did produce a useful, though less accurate, calibration curve. It appears that dissimilarities between the simulated lignin "types", based on the σ of the distribution, created this decrease in the dilineation between lignin (n2) and cellulose (n1) in the subtraction.

Lignin Component	Factor lignin standard	Factor lignin sharp	Factor cellulose sharp	Ratio lig/cell standard lignin	Ratio lig/cell sharp lig.
0.167	0.260	0.200	0.365	0.712	0.548
0.130	0.213	0.175	0.365	0.584	0.479
0.091	0.165	0.150	0.365	0.452	0.411
0.048	0.110	0.125	0.365	0.301	0.342

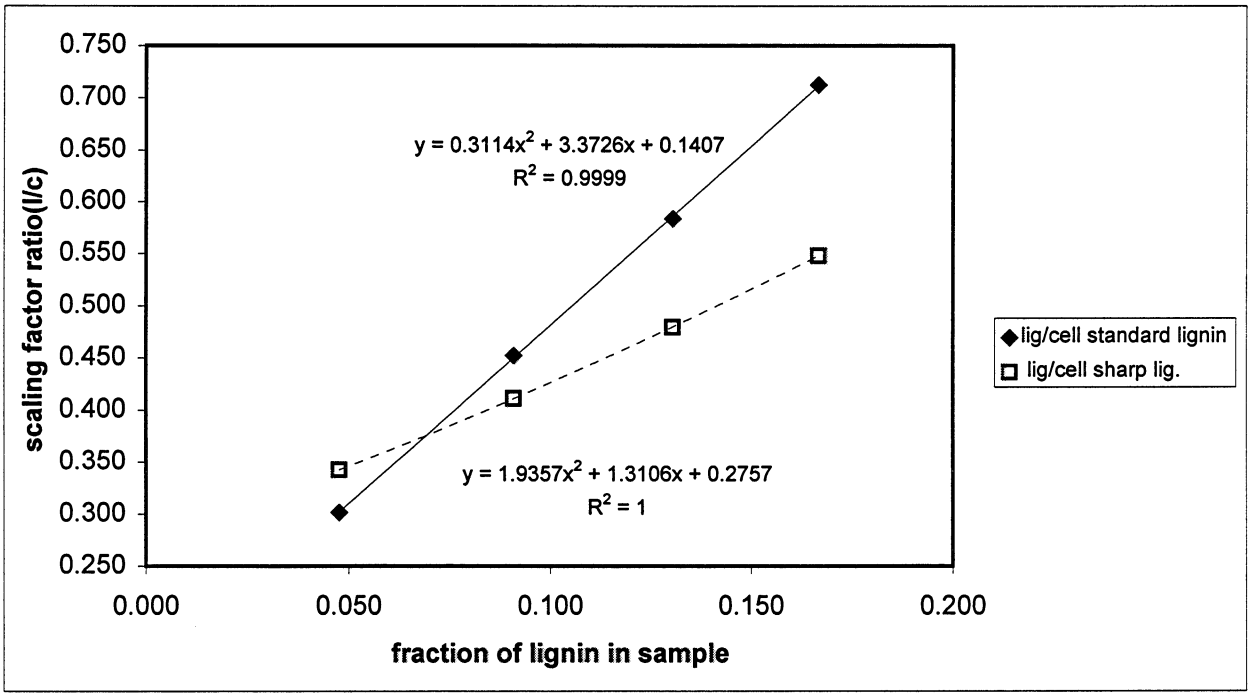

Figure C 8. Comparison of calibration curves obtained from differing peak shapes.

The two plots in Figure C 8 show the calibration curve relationships between the standard lignin subtrahend (n2) and the sharp lignin subtrahend (n2'). When the subtrahend peak was sharpened, the slope of the calibration curve decreased. This suggests that as the similarities between the component and subtrahend decrease, so does the slope of the calibration curve and the accuracy of this secondary analysis technique. These differences may be due to differences in IR technique, specular distortion, baseline drift, over-absorbance, and even subtle changes in instrument calibration. In addition, poor experimental technique can also result in physical inconsistencies such as sample moisture content variations and atmospheric background corrections.

Liquid-cell Model 2^3 Factorial Analysis

The four component liquid-cell model system was chosen to verify the viability of the subtraction algorithm, along with an analysis of how the system works with various functional group types. Three simple chemicals were chosen and mixed in a carbon tetrachloride (D) background to dilineate specific functional group types: (A) toluene, (B) tetrachloroethylene, and (C) acetophenone.

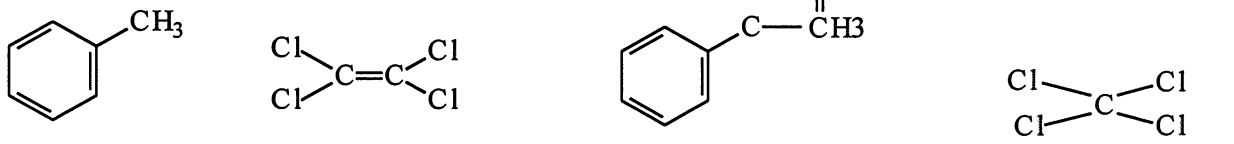

A.) Toluene B.) Tetrachloroethylene C.) Acetophenone D.) Carbon Tetrachloride

Figure C 9. Chemical structures used in liquid-cell model analysis.

Carbon tetrachloride is used particularly for its relatively absorption free character. Figure 44 illustrates the spectra for each of these components. Table C 1 provides a 2^3 factorial analysis of variance for subtraction of these components from a complex mixture.

Yates' algorithm was used to analyze the data in Table C 1, where an analysis of variance was used to calculate effects, sum of squares, mean squares, and the resulting F-values. Yates algorithm compares the effect of changing component concentrations from a low concentration to a high concentration. Also, it has the ability to determine interaction between components. The "file" column contains notation of lower case letters a, b, and c refer to component concentrations. Each cell under "file" refers to a mixture that contains all four components. However, the presence of lower case letters implies that the noted component is at its high level of concentration, whereas the others are at their low level of concentration. The notation (1) refers to all components at a low level of concentration.

The top set of rows from left to top right first contain A,B, and C columns with subtraction factors for each component from the select mixtures. The second set of A, B, and C columns contain "%std" values that indicate the volumetric percent composition of components A, B, and C. The third set of A, B, and C columns contain "%FTIR" values that indicate the percent composition of each component as determined by the subtraction algorithm. The column on the far top right contains the sums of squares for the differences between volumetrically determined concentrations (C_e) and FTIR determined concentrations (C_i). The total of the sums of squares for all components is provided as one value for each mixture The differences between the volumetrically determined concentrations and the FTIR determined concentrations are used to provide a measure of the accuracy of the spectral subtraction technique for this system. The second set of rows contains calibration curve data, where individual components were mixed at various concentrations with CCl_4.

Table C 1. 2^3 factorial analysis for liquid-cell model results: (A) toluene, (B) tetrachloroethylene, and (C) acetophenone.

SUBTRACTIONS MADE ON SELECT SPECTRAL RANGES:													
The components are (A)Toluene, (B)Tetrachloroethylene, and (C)Acetophenone													
	A	B	C	A	B	C			A	B	C		
File	(1000-1650)	(850-1825)	(1200-1725)	(% std)	(% std)	(% std)			(%FTIR)	(%FTIR)	(%FTIR)	$[\Sigma(C_e-C_i)^2]^{1/2}$	
(1)(1)	0.0269	0.03919	0.11932	1.89	1.89	1.89			1.90	2.58	1.52	0.79	
a(1)	0.20145	0.03785	0.10031	16.13	1.61	1.61			14.19	2.48	1.23	2.16	
b(1)	0.02535	0.21361	0.11419	1.61	16.13	1.61			1.79	16.00	1.44	0.27	
ab(1)	0.17955	0.19528	0.10513	14.08	14.08	1.41			12.65	14.59	1.31	1.53	
c(1)	0.0419	0.02345	1.1527	1.61	1.61	16.13			2.95	1.37	17.28	1.78	
ac(1)	0.1822	0.02582	1.0704	14.08	1.41	14.08			12.83	1.56	16.02	2.31	
bc(1)	0.0403	0.17311	1.1379	1.41	14.08	14.08			2.84	12.89	17.05	3.51	
abc(1)	0.18017	0.18593	0.86157	12.50	12.50	12.50			12.69	13.87	12.84	1.43	
(1)(2)	0.0269	0.044	0.12084	1.89	1.89	1.89			1.90	2.95	1.55	1.12	
a(2)	0.18238	0.0318	0.10388	16.13	1.61	1.61			12.85	2.02	1.29	3.32	
b(2)	0.02305	0.18202	0.08927	1.61	16.13	1.61			1.63	13.57	1.07	2.62	
ab(2)	0.15893	0.17278	0.09453	14.08	14.08	1.41			11.20	12.86	1.15	3.15	
c(2)	0.03052	0.02191	1.0341	1.61	1.61	16.13			2.15	1.25	15.47	0.93	
ac(2)	0.16989	0.02198	0.88489	14.08	1.41	14.08			11.97	1.26	13.19	2.30	
bc(2)	0.02659	0.15813	0.92635	1.41	14.08	14.08			1.88	11.73	13.83	2.41	
abc(2)	0.15618	0.14087	0.76872	12.50	12.50	12.50			11.00	10.41	11.42	2.79	
Calibrations:					Yates' Algorithm					contrast			
%	A	B	C	Sample	Obs. 1	Obs. 2	Total	1	2	3		Effect	SS=MS
0.99	0.015	0.019	0.095	(1)	0.79	1.12	1.906	7.387	14.953	32.405	Total		
5.66	0.079	0.077	0.370	a	2.16	3.32	5.480	7.566	17.452	5.563	=8A	0.695	1.934
10.71	0.152	0.146	0.732	b	0.27	2.62	2.891	7.318	5.358	2.995	=8B	0.374	0.561
20.00		0.265	1.331	ab	1.53	3.15	4.675	10.134	0.205	-5.395	=8AB	-0.674	1.819
				c	1.78	0.93	2.707	3.574	0.180	2.499	=8C	0.312	0.390
1.331=0.79852*(0.025/0.015);				ac	2.31	2.30	4.611	1.784	2.816	-5.153	=8AC	-0.644	1.660
corrected for different spacer				bc	3.51	2.41	5.917	1.905	-1.790	2.636	=8BC	0.329	0.434
thickness, using Beers Law				abc	1.43	2.79	4.217	-1.700	-3.605	-1.815	=8ABC	-0.227	0.206
				ANOVA									
				Source	d.f.	effect	SS	MS	F	F-crit(0.05,1,8)		F-crit(0.01,1,8)	
				Main						5.32		11.37	
				A	1	0.695	1.934	1.934	**2.601**				
				B	1	0.374	0.561	0.561	**0.754**				
				C	1	0.312	0.390	0.390	**0.525**				
				2-factor									
				AB	1	-0.674	1.819	1.819	**2.446**				
				AC	1	-0.644	1.660	1.660	**2.232**				
				BC	1	0.329	0.434	0.434	**0.584**				
				3-factor									
				ABC	1	-0.227	0.206	0.206	**0.277**				
				block	1		1.482	1.482					
				error	7		5.205	0.744					
				total	15		13.691						

Yates' algorithm and the analysis of variance finally show us that the critical F-ratio at a 0.05 level of significance far exceeds the F-ratios for main and interactive effects. Therefore, the procedure worked well according to this analysis. Interestingly, the system appeared slightly sensitive to changes in the concentration of component A, toluene. There were negative interaction effects whenever the concentration of toluene was at its high level with another component at its high level. The implication is that the value for the sums of squares increased, or accuracy decreased, when components interacted with toluene in the liquid-cell model system.

KBr Pellet Preparation Variations

Past research has shown that variations in sample preparation create variations in spectral results. The following figures illustrate the presence of water, the effect of oven drying, and the effect of grinding cellulose samples in a Wiley mill and Wig-L-Bug™. A Wiley mill is a centrifugal cutting device that repeats cutting until the fibers pass through a screen of specific size. The Wig-L-Bug™ is a device that is used to ball-mill particles into a powder.

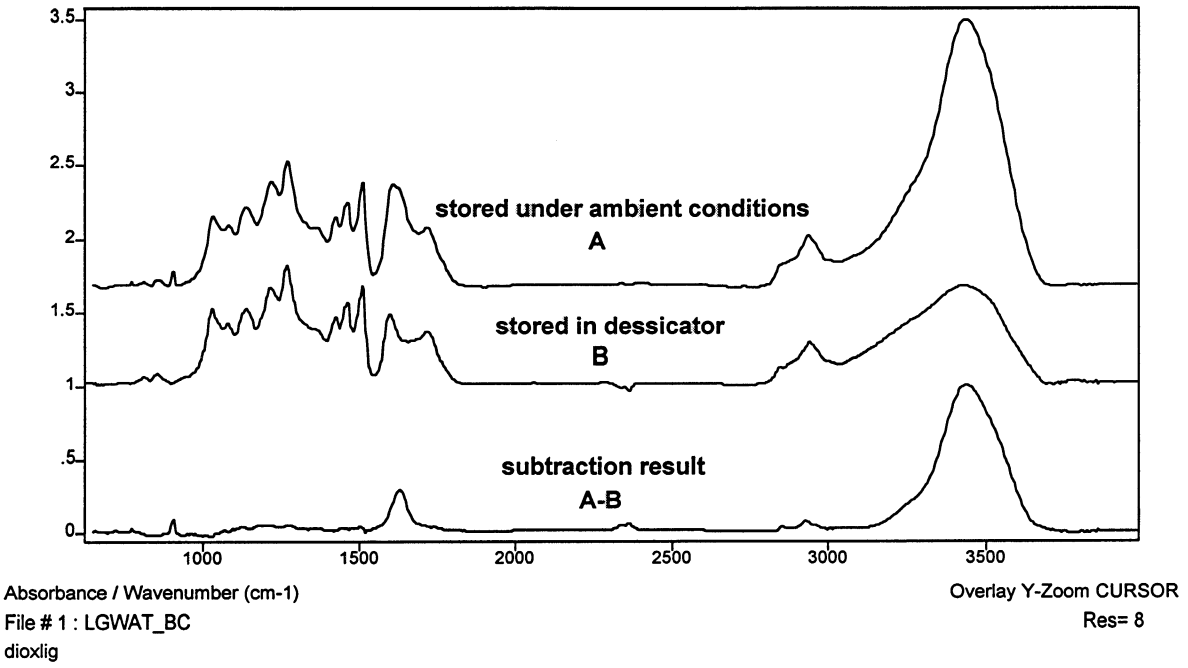

Figure C 10. The presence of water in dioxane lignin.

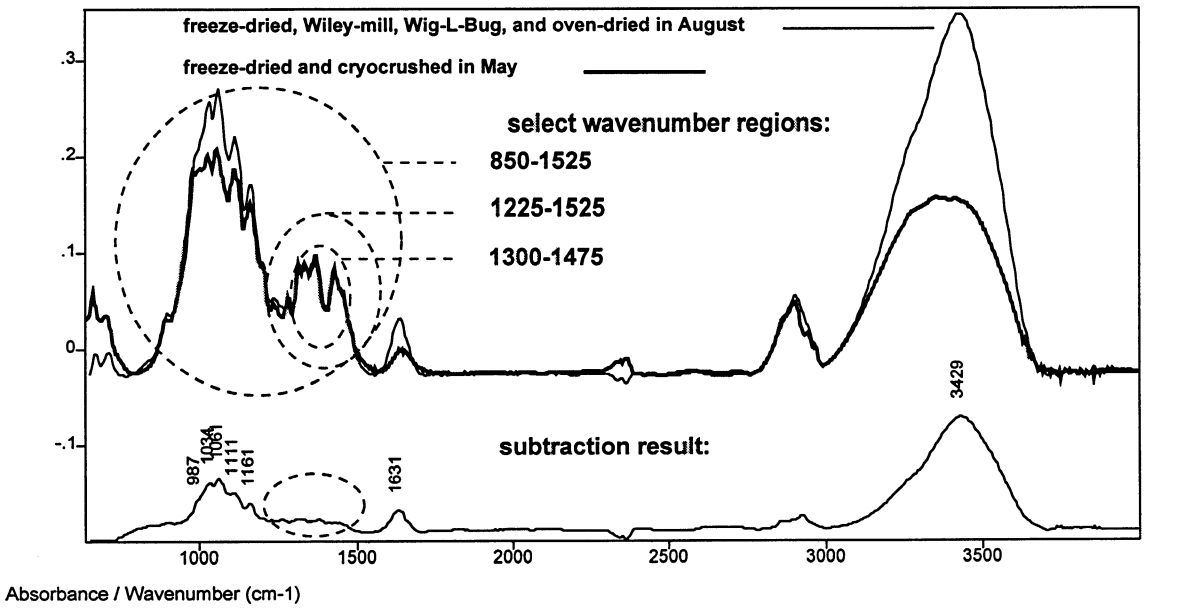

Figure C 11. The presence of water and the effect of oven drying on cotton.

As shown in Figure C 10 and Figure C 11, water is a problem in the 1595 cm^{-1} region regardless of whether or not freeze-dried samples are stored under ambient conditions, in a dessicator, or oven dried immediately prior to analysis. Interestingly, the cellulose sample appears much more sensitive to ambient humidity than to sample preparation. Thus, it is very important to perform subtractions outside of this highly variable region. As a result, the regions of 850-1525 cm^{-1}, 1225-1525 cm^{-1}, and 1300-1475 cm^{-1} were assessed for their subtraction utility with the highly variable infrared spectra.

Finally, and perhaps most importantly, consistent results must exist between samples. Figure C 12 is descriptive of the loss of fine structure that occurs when grinding cellulose samples in the Wiley mill and Wig-L-Bug™ apparatuses.

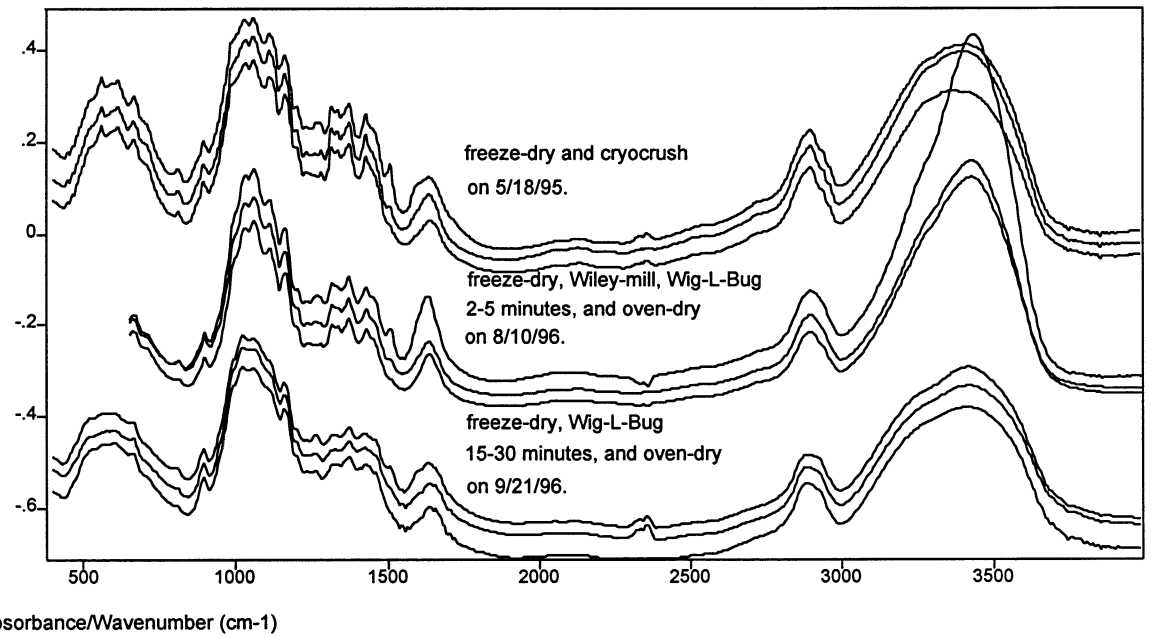

Figure C 12. Various kraft pulp fiber preparation procedures.

The effect of the Wiley mill is indeterminate at this point, however, it is apparent that the Wig-L-Bug creates a pronounced deterioration of fine structure. Therefore, the most reproducible method of acquiring infrared pellet spectra of kraft pulp fibers was through freeze-drying followed by cryocrushing. Cryocrushing may not have been necessary given the fact that most kraft pulp fiber diameters are on the order of 30μm to 50μm. However, cryocrushing did shorten long fibers, making pellet pressing easier. The use of the Wig-L-Bug™ was directed towards producing a more uniform particle size to improve spectral baselines. Unfortunately, the baselines obtained through use of the Wig-L-Bug™ did not appear improved, whereas the loss of spectral information was certainly apparent.

It also becomes important to understand the effect of sample preparation on component spectra. The effect of grinding on the lignin sample is irrelevant, however, the effects of oven-drying and acquiring spectra in the microcompression cell are important to understand.

Likewise, the effect of microcompressing fibers is important to understand prior to attempting subtractions. Figure C 14 describe how a microcompressed fiber, pellet fiber, and pellet lignin sample relate to one another.

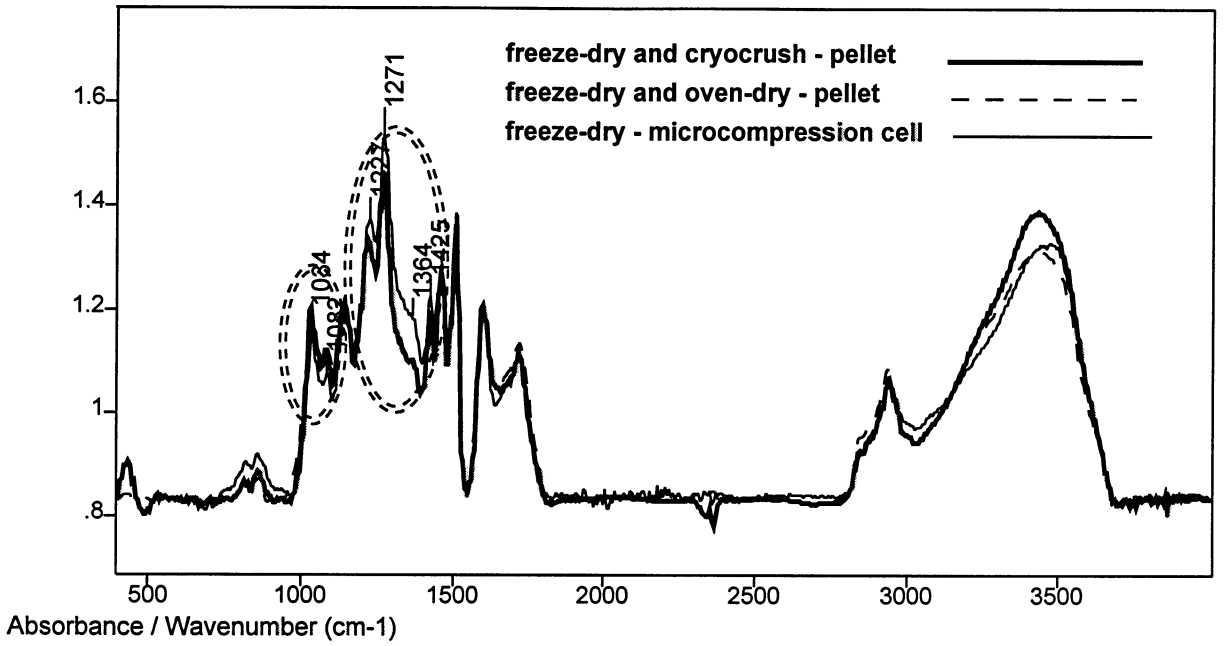

Figure C 13. Effect of oven-drying and microcompressing lignin.

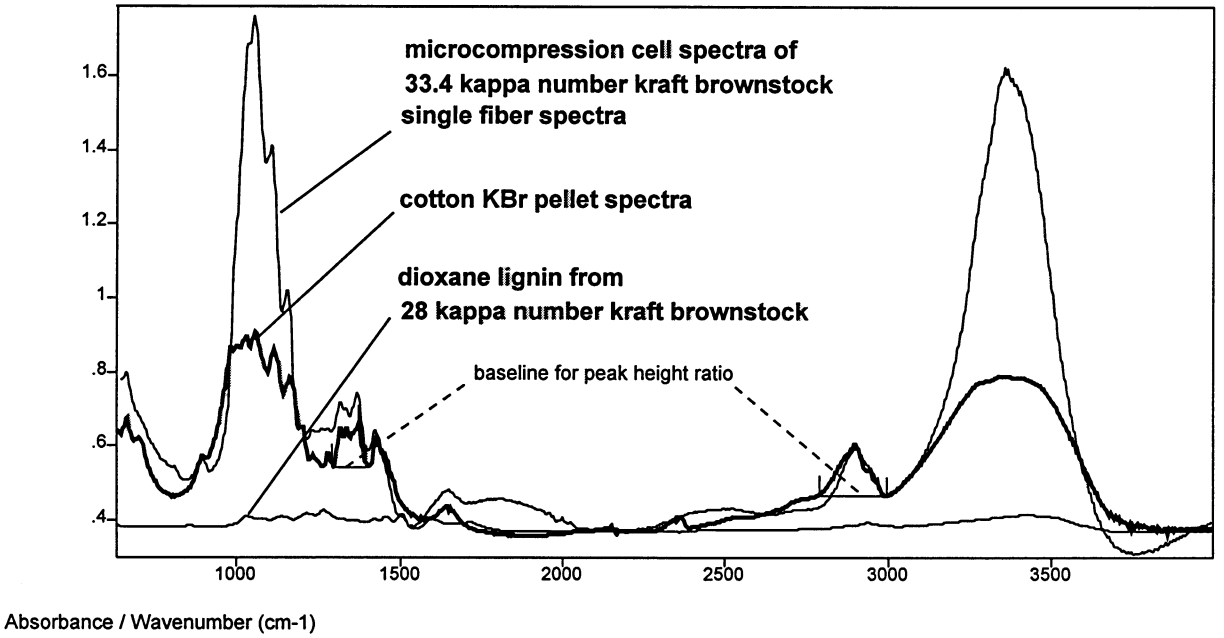

Figure C 14. Comparison of spectra: micrompressed fiber and pellet cellulose relative to pellet lignin.

A dramatic difference exists between microcompressed and pellet fiber spectra. Not only is this an obvious limitation with the secondary analysis, but the magnitude of the lignin spectra present in a 33.4 kappa number pulp is small. In fact, only about 5% lignin is present within a 33.4 kappa number pulp[252]. Differences in band overlap from differences spectral character from the microcompression cell become more of a problem when trying to detect such small component concentrations.

Discussion of Attempted Subtraction Procedures

The FTIR subtraction routine was unsuccessful in correlating pellet calibration curves to individual kraft pulp fiber spectra. Pressure variations in the diamond compression cell created uncontrollable changes in the state of the complex wood fiber matrix. In contrast, it has been shown that pellet spectra can be highly reproducible if sample preparation is carefully controlled. Three different approaches were investigated, and they will now be discussed for future reference.

The first attempt involved direct subtraction of subtrahends from microcompressed fiber spectra within select infrared regions that appeared consistent with pellet spectra. Average kappa numbers and standard deviations in average kappa numbers were inconsistent and out of range. The select spectral regions were chosen based on a high percent similarity between pellet and microcompressed spectra. Percent similarity was based on subtraction of the compressed sample from the pellet sample within the range of interest to produce a "dissimilar" spectra. Next, the microcompression cell spectra was subtracted from the dissimilar spectra to determine the percent of the microcompression cell spectra contained within the dissimilar spectra. Percent

"similarity" is defined as 100*(1-"dissimilar" fraction) within the select spectral regions. The selected infrared ranges were 1300-1475 cm^{-1} for cellulose and 1225-1525 cm^{-1} for lignin.

Table C 2. Percent similarity measurements with associated error.

sample description	select region:	%similarity 1225-1525 (cm-1)	1300-1475 (cm-1)
microcompression cotton and cryocotton pellet			
cotmc1bc and cot12bc			76.48
cotmc2bc and cot12bc			81.96
cotmc3bc and cot12bc			78.25
cotmc4bc and cot12bc			84.94
microcompressed lignin and lignin pellet			
dlgmcbc1 and dlig1_bc		81.79	
dlgmcbc2 and dlig1_bc		82.81	
dlgmcbc3 and dlig1_bc		87.00	
average		**83.87**	**80.41**
stdev.		**2.76**	**3.79**
CV		**0.0329**	**0.0471**

The second approach involved the knowledge that peak intensities can increase as a result of pressure. This is a result of changes in the freedom of molecules to rotate and vibrate when pressure is applied. Unfortunately, these changes in the physical state of the wood component molecules are not reproducible in the diamond compression cell. Perhaps this can be controlled through control of pressure in a modified apparatus; however, the problem had to be addressed differently at this time. Earlier research has shown that cellulose crystallinity can be measured through the ratio of the 2900 cm^{-1} peak to the 1372 cm^{-1} peak. Compression cells have also been shown to increase crystallinity within fiber samples[250]. It was proposed here that compression effects could be indirectly controlled through measurement of changes in relative peak intensities.

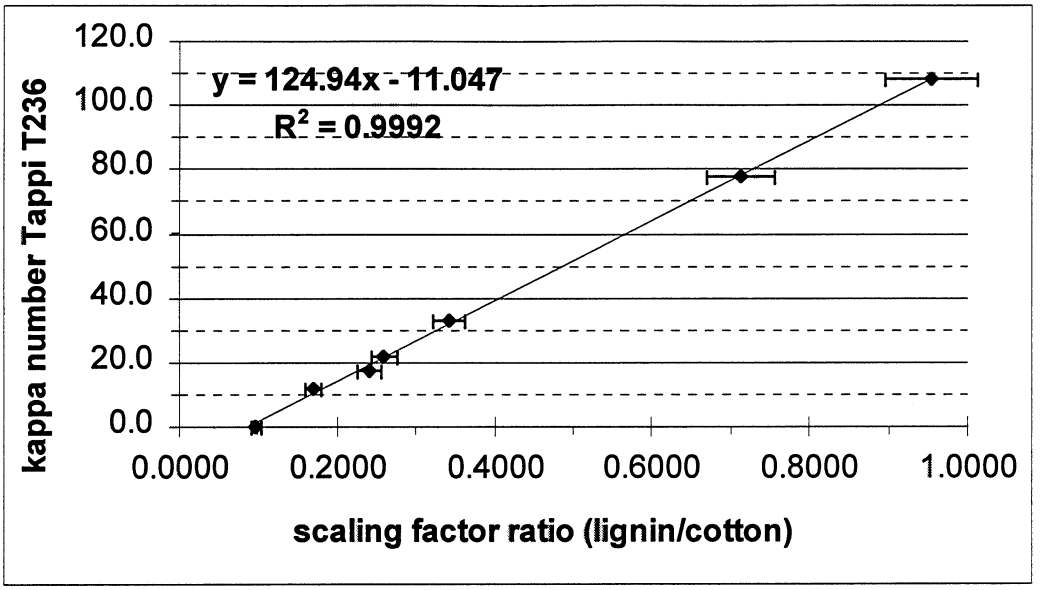

Figure C 15. FTIR calibration curve with error bars for correction factors.

The error bars in the calibration curve relationship were derived from the 6% error inherent in the correction factors chosen for correlation of pellet spectra with microcompression cell spectra. Scaling factor ratios for the microcompression cell spectra were corrected according to the percent similarities between pellet spectra and micrompression cell spectra in Table C 2. In addition, variations in absorption intensity occur with variations in microcompression cell pressure and were estimated using the crystallinity ratio method of O'Connor, since changes in pressure are also known to induce measurable changes in crystallinity[250]. Figure C 16 illustrates baseline corrections and relative peak height ratios for microcompressed cotton and pellet cotton. Conveniently, the 1300-1475 cm^{-1} spectral region coincides with the region used by O'Connor.

Figure C 17 illustrates relative peak height ratios obtained from the pellet calibration set and individual fiber spectra from a 33.4 kappa number brownstock kraft pulp. A consistent decrease in peak height ratio with a decrease in Tappi T236 kappa number exists in the pellet calibration set.

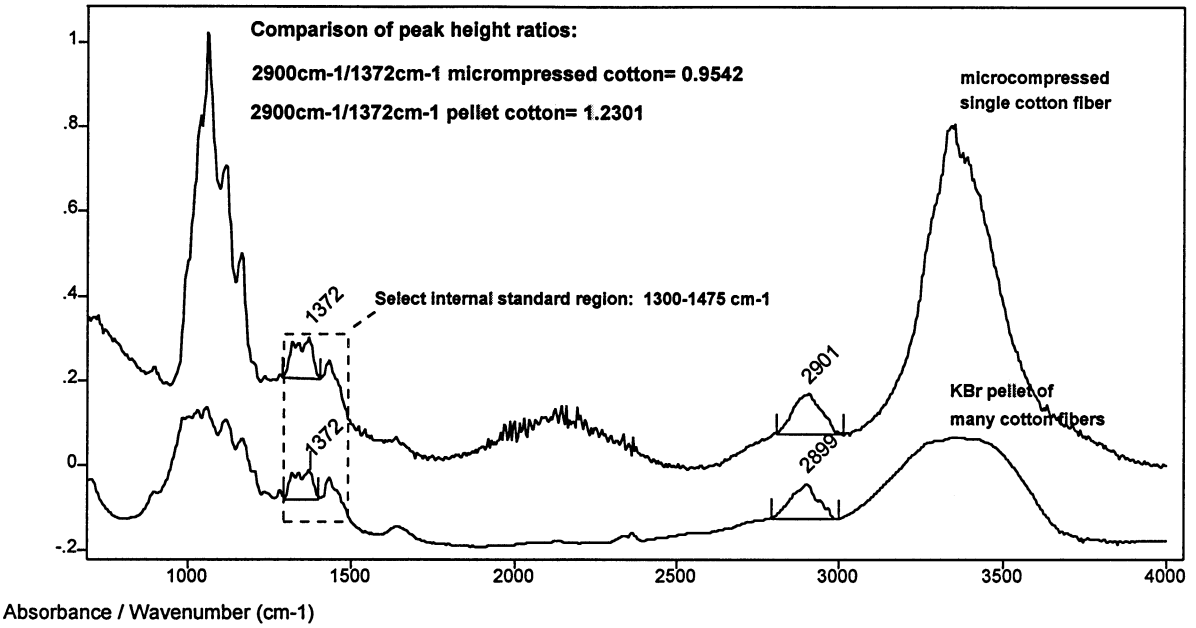

Figure C 16. Peak height ratio technique in relation to select spectral region.

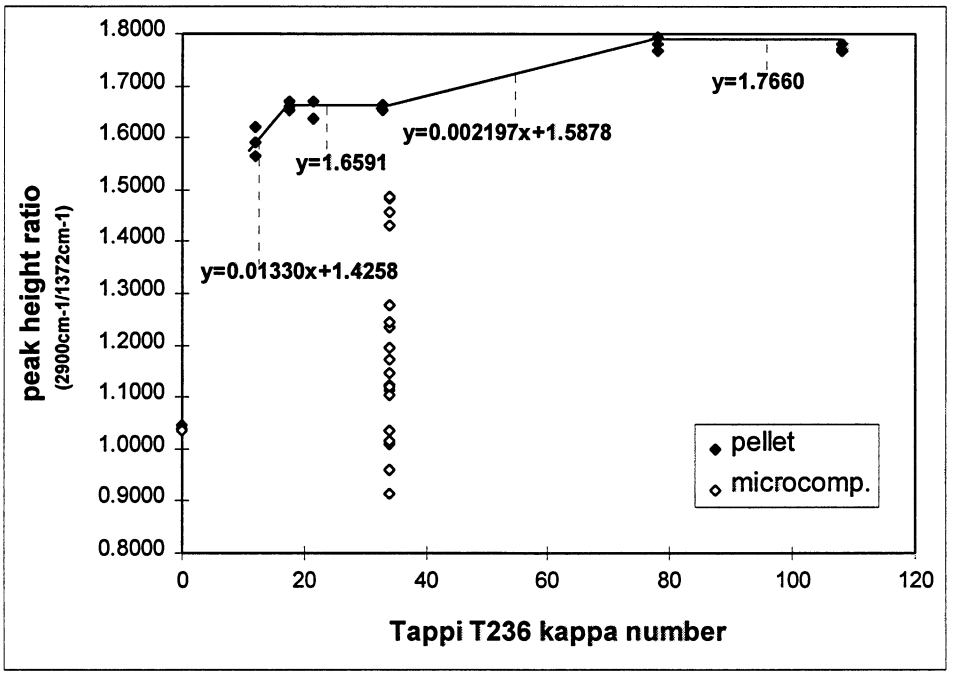

Figure C 17. Variation in FTIR peak height ratios due to pressure.

Figure C 17 is illustrative of large variations in spectral characteristics that can occur within a given pulp sample as a result of microcompression cell pressure variations. A reduction in peak height ratio for the 2900 cm^{-1}/1372cm^{-1} has been shown to correlate well to an increase in percent crystallinity for cotton samples that have undergone alkaline hydrolysis of amorphous regions. In this application, the peak height ratios are used for correction factors in an effort to correlate microcompressed fiber spectra with pellet calibration spectra for secondary analyses of delignification diversity. Pellet spectra peak height ratios are calculated from the linear relationships shown in Figure C 17. The FTIR scaling factor was corrected

as follows:

$$\left(\frac{dlig1\_bc}{\cot 12\_bc}\right)\left(\frac{\%\cot sim.}{\%lig.sim.}\right)\left(\frac{pell.pk.ratio}{mc.pk.ratio}\right) = \text{corrected FTIR scaling factor}$$

where the information from Table C 2 and Figure C 17 were used for the corrections and calculation of the associated 6% error. Table C 3 lists the delignification diversity values calculated using this FTIR spectral analysis procedure.

Table C 3. FTIR kappa number results using percent similarity and pressure corrections.

file	fiber location	chip thickness(cm)	Tappi T236 kappa	FTIR kappa	FTIR stdev
Cook 7m	middle	10.0	33.4	-6.42	19.28
Cook 7e	end	10.0	33.4	41.68	18.38
Cook 9m	middle	2.5	33.9	26.07	14.43
Cook 9e	end	2.5	33.9	31.35	14.67
78 kappa	middle	2.5	78.0	99.96	16.33

Although the relative values of the five data sets appear fairly consistent with expectations, the accuracy of the data is poor. The most questionable value is the negative kappa

number of cook 7m. Aromatic peaks were obviously present in the 1510 cm^{-1} region, however, this was not evident from the spectral subtractions. The standard deviation in average kappa number values were relatively close to expected values. Therefore, the procedure had some merit, but the variability in the individual fiber spectra created too much variability in the subtraction results. The quality of the microcompression cell spectra seems to suffer from specular distortions and should be improved prior to further investigation.

The third approach used the percent similarity technique in an attempt to quantify the 1510 peak. It has been shown multiple times in previous research that this peak correlates well with bulk lignin content. In fact, the 1510 cm^{-1} peak and the 1595 cm^{-1} appear almost exclusive in this regard. Band overlap is probably the reason for this dependence, since band overlap between carbohydrates and lignin predominates outside of these regions. Unfortunately, the 1595 cm^{-1} peak is adjacent to a water band, making this area is subject to much variability. The 1510 cm^{-1} aromatic breathing region remains as the only viable region not subject to a high degree of band overlap from carbohydrates. This final attempt involved use of the subtraction routine to remove the 1510 cm^{-1} "bump" from the 1475-1525 cm^{-1} spectral range. Next, the percent similarity technique was used to determine how much of the original spectra was removed to eliminate the 1510 cm^{-1} peak. This procedure seemed to show some merit, however, the specular distortion from the compression cell technique frequently entered the range of interest and seriously affected results.

LITERATURE CITED

[1] Tikka, P.; Kovasin, K. Displacement vs. Conventional Batch Kraft Pulping: Delignification Patterns and Pulp Strength Delivery. Paperi ja Puu 72(8): 774(1990).

[2] Gustafson, R.R.; Jimenez, G.; McKean, W.T.; Chian, D. The Role of Penetration and Diffusion in Nonuniform Pulping of Softwood Chips. Tappi Journal (8): 163(1989).

[3] Gullichsen, J.; Kolehmainen, H.; Sundqvist, H. On the Nonuniformity of the Kraft Cook. Paperi ja Puu 74(6): 486(1992).

[4] Tikka, P.; MacLeod, J.M.; Kovasin, K. Chemical and Physical Performance of Kraft Cooking: The Impact of Process Alternatives. Tappi Journal (1): 137(1991).

[5] Jimenez, G. McKean, W.T.; Gustafson, R.R. Using a Kraft Pulping Model to Improve Pulp Uniformity. Tappi Journal (7): 173(1990).

[6] Tichy, J.; Procter, A.R. Measurement and Significance of Lignin Content Uniformity in Unbleached Kraft Pulps. Svensk-Papperstidning 84(15): R116(1981).

[7] Atkinson, E.S.; Partridge, H. De V. Effects of Mixing and Degree of Chlorination on Quality and Bleaching Costs. Tappi Journal 49(2): 66A(1966).

[8] Sainiemi, J.; Hiljanen, S. Experiences of Low-Energy Batch Cooking. Tappi Pulping Conference Proceedings: 643(1986).

[9] Meredith, M.D. The Chemistry of Beloit's Displacement Heated Cooking System- RDH. Tappi Pulping Conference Proceedings: 651(1986).

[10] Perala, J.; Hiljanen, S. SuperBatch: Mature and Field Tested Cooking Concept- Practical Considerations and Mill Scale Results of System Performance. Tappi Pulping Conference Proceedings: 1015(1992).

[11] Wizani, W.; Eder, S.; Sinner, M. The Enerbatch: Kraft Pulping Process- Progress in Pulp Uniformity and Extended Delignification. Tappi Pulping Conference Proceedings: 1037(1992).

[12] Abuhasan, M.J.; Sezgi, U.S.; Jameel, H.; Chang, H.; Kirkman, A.G. The Effects of Alkali Charge and White Liquor Sulfidity on Rapid Displacement Heating (RDH) Kraft Pulping. Tappi Pulping Conference Proceedings: 1023(1992).

[13] Mao, B.; Hartler, N. Improved Modified Kraft Cooking: Part I. Pretreatment with a Sodium Sulfide Solution. Paperi ja Puu 74(6): 491(1992).

[14] Mera, F.E.; Chamberlin, J.L. Extended Delignification, An Alternative to Conventional Kraft Pulping. Tappi Journal (1): 132(1988).

[15] Horng, A.J.; Tichy, J.G.; Mackie, D.M. Factors Affecting Pulp Quality from Kamyr Continuous Digesters. Proceedings of the 1985 Spring Conference. CPPA(1985).

[16] Horng, A.J.; Mackie, D.M.; Tichy, J. Factors Affecting Pulp Quality from Continuous Digesters. Tappi Journal (12): 75(1987).

[17] MacLeod, J.M. Is Unbleached Softwood Kraft Pulp Strongest at 30 Kappa Number? 76th Annual Meeting, Technical Section. CPPA: A37(1990).

[18] Tikka, P.; Tahkanen, H.; Kovasin, K. Chip Thickness vs. Kraft Pulping Performance: Experiments by Multiple Hanging Baskets in Batch Digesters. Tappi Journal 76(3): 131(1993).

[19] Becker, E. The Effects of Chip Thickness and Kraft Cooking Conditions on Kraft Pulp Properties. Tappi Pulping Conference Proceedings: 561(1992).

[20] Kleppe, P. Kraft Pulping. Tappi Journal 53(1): 35(1970).

[21] Kleppe, P. The Process of, and Products from Kraft Pulping of Southern Pine. Forest Product Journal 20(5): 50(1970).

[22] MacLeod, J.M.; Cyr, M.; Embley, D.; Savage, P. Where Strength is Lost in Kraft Pulping of Softwoods. Journal of Pulp and Paper Science 13(3): J87(1987).

[23] MacLeod, J.M. The Physical Properties of Kraft Pulp along a Brownstock Line. Tappi Journal (7): 135(1987).

[24] MacLeod, J.M.; Pelletier, L.J. Basket Cases: Kraft Pulps Inside Digesters. Tappi Journal (11): 47(1987).

[25] MacLeod, J.M. The Strength Potential of Unbleached Kraft Pulps. Pulp and Paper Canada 88(9): T330(1987).

[26] MacLeod, J.M.; McPhee, F.J. Basket Cases: Sulfite Pulps Inside Digesters. Tappi Journal (3): 173(1990).

[27] Blume, W.M. Basket cooking in Mill Digesters. Tappi Journal 37(12): 145A(1954).

[28] MacLeod, J.M. New, Improved Kraft Pulp Quality. Paperi ja Puu 72(8): 780(1990).

[29] Tikka, P.; Kovasin, K. Delignification Patterns and Pulp Strength Formation Inside Batch Digesters Operated by Displacement and Conventional Modes. Proceedings of the 1990 Spring Conference. CPPA(1990).

[30] Anderson, D.; Rea, M. Improving Pulp Uniformity with Triple Hanging Baskets. Spring Conference. CPPA(1990).

[31] Hiljanen, S.; Uusitalo, P.; Kovasin, K.; Tuomi, A.; Tikka, P. The Super Batch Cooking Concept Offers New Dimensions in Kraft Cooking- Pulp Quality and Environmental Impact to a

New Level. Proceedings of the 1990 Eu Ce Pa Conference (Pulp Technology Section). Eu Ce Pa Paris: 84(1990).

[32] Cyr, M.E.; Embley, D.F.; MacLeod, J.M. Stronger Kraft Softwood Pulp- Achieved!. Tappi Journal (10): 157(1989).

[33] Knutsson, T.; Stockman, L. The Effect of Mechanical Treatment during the Final Stages of the Cook on the Beating Properties and Strength of Sulphate Pulp. Tappi Journal 41(11): 704(1958).

[34] Annergren, G.E.; Ohrn, O.E.; Rydholm, S.A. Kraft Pulp Quality from Batch and Continuous Cooking. Svensk-Papperstidning 66(4): 110(1963).

[35] MacLeod, J.M.; Kingsland, K.A. Pulp Strength Delivery on a Kraft Linerboard Basestock Production Line. Tappi Journal (2): 121(1990).

[36] MacLeod, J.M. New Improved Kraft Pulp Quality. Proceedings of the 1990 Spring Conference. CPPA(1990).

[37] MacLeod, J.M. Basket Cases: Kraft Pulp Strength Variability Within a Batch Digester. Tappi Journal (10): 185(1990).

[38] MacLeod, J.M. Kraft Pulps from Canadian Wood Species. Pulp and Paper Canada 87(1): T25(1986).

[39] Tikka, P. Conditions to Extend Kraft Cooking Successfully. International Pulping Conference. Tappi Proceedings: 699(1992).

[40] Howard, E.J. Sulphur Reactions in Sulphite Cooking: Part II. Some Physico-Chemical Aspects. Pulp and Paper Magazine of Canada (7): 92(1951).

[41] Elton, E.F. Rate Phenomena in the Neutral Sulfite Delignification of Loblolly Pine. Doctoral Dissertation. IPST, Appleton, WI, 1962.

[42] Leopold, B.; Ahlm, C.E. Chemical Composition and Physical Properties of Wood Fibers. IV. Changes in Chemical Composition of Loblolly Pine Fibers During the Kraft Cook. Tappi Journal 46(2): 102(1963).

[43] Gladstone, W.T.; Barefoot, A.C.; B.J. Zobel. Kraft Pulping of Earlywood and Latewood from Lobolly Pine. Forest Products Journal 20(2): 17(1970).

[44] Labosky, P.; Ifju, G. A Study of Loblolly Pine Growth Increments: Part I. Wood and Tracheid Characteristics. Tappi Journal 55(4): 524(1972).

[45] Labosky, P.; Ifju, G. A Study of Loblolly Pine Growth Increments: Part II. Pulp Yield and Related Properties. Tappi Journal 55(4): 530(1972).

[46] Zobel, B.J.; VanBuijtenen, J.P. Wood Variation: Its Causes and Control. Springer-Verlag Publishers, NY, 1989.

[47] Cole, D. E.; Zobel, B.J.; Roberds, J.H. Slash, Loblolly, and Longleaf Pine in a Mixed Natural Stand; A Comparison of Their Wood Properties, Pulp Yields, and Paper Properties. Tappi Journal 49(4): 161(1966).

[48] Zobel, B.; Thorbjornsen, E.; Henson, F. Geographic, Site and Individual Tree Variation in Wood Properties of Loblolly Pine. Silvae Genetica 9(6): 149(1960).

[49] Zobel, B.J.; McElwee, R.L. Natural Variation in Wood Specific Gravity of Loblolly Pine, and an Analysis of Contributing Factors. Tappi Journal 41(4): 158(1958).

[50] Howard, E.T.; Manwiller, F.G. Anatomical Characteristics of Southern Pine Stemwood. Wood Science 2(2): 77(1969).

[51] Barefoot, A.C.; Hitchings, R.G.; Wilson, E.H.; Kellison, R.C. Related Aspects of the Morphology of Loblolly Pine and Papermaking. Forest Products Laboratory Service: K1(1972).

[52] Koch, P. Utilization of the Southern Pines: Volume I. The Raw Material. U.S. Department of Agriculture Forest Service, 1972.

[53] Paranyi, N.I.; Rabinovitch, W. Determination of Penetration Rate of Liquid Media into Wood Using a Quartz Spiral Balance. Pulp and Paper Magazine of Canada 56(3): 163(1955).

[54] Marton, J. Reactions in Alkaline Pulping, p644. Hergert, H. Infrared Spectra, p267. Sarkanen, K.V., ed.; Ludwig, C.H., ed. in Lignins. Wiley Interscience, NY, 1971.

[55] Paulson, J.C. Unbleached Pulp Uniformity in Prehydrolysis-Kraft pulp from Slash Pine. Svensk-Papperstidning 74(13-14): 397(1971).

[56] Boutelje, J.B.; Johsson, U. Ultraviolet Microscope Photometry of Pulp Fibers. Cellulose Chemistry and Technology 15: 53(1980).

[57] Liu, Y.; Gustafson, R.; Callis, J.; McKean, B. Fluorescence Microphotometry in Determining the Lignin Content of Single Pulp Fibers. ISWPC: T2-1(1997).

[58] Hunt, K.; Hatton, J.V. Tappi Journal 66(10): 103(1983).

[59] Thomson, S.L ; Gustafson, R.R. Effects of Kappa Variability on Pulp Properties. Tappi Pulping Conference Proceedings: 445(1996).

[60] Renard, J.J.; Hanson, D.M. Apparatus and Process for Testing Uniformity of Pulp. U.S. Patent 4,837,446 (June 6, 1989).

[61] Grace, T.M., ed.; Malcolm, E.W., ed.; Kocurek, M.J. Pulp and Paper Manufacture, Volume 5: Alkaline Pulping. Joint Textbook Committee of the Paper Industry, Tappi Press, Atlanta, GA, 1989.

[62] Olm, L.; Tistad, G. Kinetics of the Initial Stage of Kraft Pulping. Svensk-Papperstidning (15): 458(1979).

[63] Whiting, P.; Abbot, J.; Yean, W.Q.; Goring, D.A.I. Topochemical Differences in the Kinetics of Kraft Pulping of Spruce Wood. CPPA Transactions: TR109(December, 1982).

[64] Goring, D.A.I. Some Recent Topics in Wood and Pulping Chemistry. International Symposium on Wood and Pulping Chemistry: 3(1983).

[65] Fogelberg, B.C.; Fugleberg, S. A Study, by the Aid of Radioactive Isotopes, of the Interaction of Different Factors on the Impregnation of Chips. Papper och Tra (3): 97(1965).

[66] Jensen, W.; Fogelberg, B.C.; Johanson, M. Studies on the Possibilities of Using Radioactive Tracers to Follow the Penetration of Cooking Liquors Into Wood. Papper och Tra 42(7): 393(1960).

[67] Tikka, P.; Tahkanen, H.; Kovasin, K. Chip Thickness vs Kraft Pulping Performance: Part I. Experiments by Multiple Hanging Baskets in Batch Digesters. International Pulping Conference. Tappi Proceedings: 555(1992)

[68] Tyler, D.B. Predicting Rejects from Kraft Cooking of Overthick Chips. Svensk-Papperstidning: R180(1982).

[69] Akhtaruzzaman, A.F.M. Influence of Chip Dimensions in Kraft Pulping: Predictive Mathematical Models. Paperi ja Puu 62(10): 607(1980).

[70] Akhtaruzzaman, A.F.M.; Lunabba, P.; Virkola, N.E. Influence of Chip Dimensions and Chip Quality on the Kinetics of Kraft Pulping. Paperi ja Puu 62(3): 133(1980).

[71] Akhtaruzzaman, A.F.M.; Virkola, N.E. Influence of Chip Dimensions in Kraft Pulping: Part I. Mechanism of Movement of Chemicals into Chips. Paperi ja Puu 61(9): 578(1979).

[72] Akhtaruzzaman, A.F.M.; Virkola, N.E. Influence of Chip Dimensions in Kraft Pulping: Part II. Present State and Scope of the Study. Paperi ja Puu 61(10): 629(1979).

[73] Akhtaruzzaman, A.F.M.; Virkola, N.E. Influence of Chip Dimensions in Kraft Pulping: Part III. Effect on Delignification and a Mathematical Model for Predicting the Pulping Parameters. Paperi ja Puu 61(10): 737(1979).

[74] Akhtaruzzaman, A.F.M.; Virkola, N.E. Influence of Chip Dimensions in Kraft Pulping: Part IV. Effect on Screened Pulp Yield and Effective Alkali Consumption; Predictive Mathematical Models. Paperi ja Puu 61(12): 805(1979).

[75] Akhtaruzzaman, A.F.M.; Virkola, N.E. Influence of Chip Dimensions in Kraft Pulping: Part V. Effect on Total Yield and Screening Rejects; Predictive Mathematical Models. Paperi ja Puu 62(1): 15(1980).

[76] Akhtaruzzaman, A.F.M.; Virkola, N.E. Influence of Chip Dimensions in Kraft Pulping: Part VI. Effect on the Viscosity, Fibre Length and Bauer-McNett Classification of Unbleached Pulp; Predictive Mathematical Models. Paperi ja Puu 62(2): 70(1980).

[77] Akhtaruzzaman, A.F.M.; Virkola, N.E. Influence of Chip Dimensions of Kraft Pulping: Part VII. Effect on Strength Properties of Unbleached Pulp; Predictive Mathematical Models. Paperi ja Puu 62(4): 297(1980).

[78] Briere, D.; Therrien, B. Automated Wood Chip Sampler. International Pulping Conference. Tappi Proceedings: 707(1992).

[79] Wood, J.R.; Gosda, G.L. Chip Quality Improvement for Batch Kraft Pulping. International Pulping Conference. Tappi Proceedings: 567(1992).

[80] Twaddle, A.; Watson, W. Shortwood vs Longwood Chipping: What Impact on Chip Distribution?. International Pulping Conference. Tappi Proceedings: 475(1991).

[81] Dubois, M.R.; Watson, W.F.; Wagner, F.G. Sawmill Chip Survey in the Southeastern USA: An Analysis of Processes and Chip Quality. International Pulping Conference. Tappi Proceedings: 481(1991).

[82] Stuart, W.B.; Leary, P.S. Factors Affecting Sawmill Residue Chip Quality. International Pulping Conference. Tappi Proceedings: 485(1991).

[83] Hatton, J.V. Screening Mill Chips for Sizeable Savings. Pulp and Paper Canada 78(3): T57(1977).

[84] Hatton, J.V.; Keays, J.L. Effect of Chip Geometry and Moisture on Yield and Quality of Kraft Pulps from Western Hemlock and Black Spruce. Pulp and Paper Magazine of Canada 74(1): 79(1973).

[85] Smith, D.E.; Javid, S.R. Trends in Chip Thickness Screening. Tappi Journal (9): 185(1990).

[86] Javid, S.R.; Artiano, A. A New Chip Screen for High Efficiency Fines Removal. Spring Conference CPPA Technical Section, Montreal: A239(1989).

[87] Borlew, P.B.; Miller, R.L. Chip Thickness: A Critical Demention in Kraft Pulping. Tappi Journal 53(11): 2107(1970).

[88] Wilder, H.D.; Daleski, E.J. Kraft Pulping Kinetics: Part I. Literature Review and Research Program. Tappi Journal 47(5): 270(1964).

[89] Wilder, H.D.; Daleski, E.J. Delignification Rate Studies: Part II of a Series on Kraft Pulping Kinetics. Tappi Journal 48(5): 293(1965).

[90] Hartler, N.; Onisko, W. The Interdependence of Chip Thickness, Cooking Temperature and Screenings in Kraft Cooking of Pine. Svensk-Papperstidning 65(22): 905(1962).

[91] Sutherland, J.W. Forced Penetration of Liquids into Wood and Its Relation to Structure, Temperature, and Pressure. Pulp and Paper Magazine of Canada 32(2): 163(1932).

[92] Alm, A.; Stockman, L. Chip Impregnation during Sulfite Cooking: Part I. Svensk-Papperstidning 61(1): 10(1958).

[93] Kulkarni, G.R.; Nolan, W.J. The Mechanism of Alkaline Pulping. The Paper Industry (5): 142(1955).

[94] Hartler, N. Peneration and Diffusion Relationship during Sulfate Cooking. Paperi ja Puu 44(7): 365(1962).

[95] Stone, J.E. The Penetrability of Wood. Pulp and Paper Magazine of Canada (6): 139(1956).

[96] Stone, J.E. The Effect of Capillary Cross-Sectional Area of Wood as a Function of pH. Tappi Journal 40(7): 539(1957).

[97] Kleinert, T.N.; Marriccini, L.M.; Dostal, E.J. Alkali Sorption on Wood from Dilute Aqueous Solution. Tappi Journal 43(3): 201(1960).

[98] Talton, J.H.; Cornell, R.H. Diffusion of Sodium Hodroxide in Wood at High pH as Functions of Temperature and Extent of Pulping. Tappi Journal (3): 115(1987).

[99] Woods, N.K. Determination of Penetration Rate of Liquid Media into Wood Using a Quartz Spiral Balance: Part II. Water and a Pre-treated Spruce Chip. Pulp and Paper Magazine of Canada 57(4): 142(1956).

[100] Jensen, W.; Fogelberg, B.C.; Johanson, M. Studies on the Possibilities of Using Radioactive Tracers to Follow the Penetration of Cooking Liquors Into Wood. Papper och Tra 42(7): 393(1960).

[101] Ekman, K.H.; Fogelberg, B.C. Impregnation on Sulphate Cooking Studied by Means of Radioactive Sulfur. Papper och Tra (special 4a): 175(1966).

[102] Ekman, K.; Jarvela, O. Influence of Cooking Conditions in Two-Stage Polysulfide Pulping: Part I. The Impregnation Stage. Tappi Journal 50(2): 75(1967).

[103] Jimenez, G.; Chian, D.; McKean, W.T.; Gustafson, R.R. Experimental and Theoretical Studies to Improve Pulp Uniformity. International Pulping Conference. Tappi Proceedings: 49(1990).

[104] Comstock, G.L. Factors Affecting Permeability and Pit Aspiration in Coniferous Sapwood. Wood Science and Technology 2: 279(1968).

[105] Luner, P. The Effect of Pre-treatments on Diffusion Through Wood. Pulp and Paper Magazine of Canada (Convention Issue): 216(1956).

[106] Bird, R.B.; Stewart, W.E.; Lightfoot, E.N. Transport Phenomena. John Wiley and Sons, 1960.

[107] Gustafson, R.R. The Role of Diffusion During Initial Delignification of Alkaline Pulping. Tappi Journal (4): 145(1988).

[108] Kleinert, T.N. Mechanisms of Alkaline Delignification. I. The Overall Reaction Pattern. Tappi Journal 49(2): 53(1966).

[109] Sjostrom, E. Wood Chemistry. Academic Press, 1981.

[110] Berthold, J.; Salmen, L. Effects of mechanical and chemical treatments on the pore-size distribution in wood pulps examined by inverse size-exclusion chromatography. Journal of Pulp and Paper Science 23(6): J245(1997).

[111] Stamm, A.J. Diffusion and Penetration Mechanism of Liquids Into Wood. Pulp and Paper Magazine of Canada (2): 54(1953).

[112] Macdonald, R.G., ed.; Franklin, J.N., ed. Pulp and Paper Manufacture, Volume 1: The Pulping of Wood. Second Edition. McGraw-Hill Book Company, 1969.

[113] Maas, O. The Problem of Penetration. Pulp and Paper Magazine of Canada 54(8): 98(1953).

[114] Ross, J.H. The Va-Purge Impregnation Pre-treatment: One Solution to the Penetration Problem. Pulp and Paper Magazine of Canada 54(8): 103(1953).

[115] Gullichsen, J.; Sundqvist, H. On the importance of impregnation and chip dimensions on the homogeneity of kraft pulping. Tappi Pulping Conference Proceedings: 227(1995).

[116] McDonough, T.J. In Search of the Ideal Pulp Mill. IPST Technical Paper Series. Number 375, May, 1991.

[117] Gullichsen, J. Process Internal Measures to Reduce Pulp Mill Pollution Load. Water Science Technology 24(3,4): 45(1991).

[118] Courchene, C.E. The Tried, the True, and the New- Getting More Pulp from Chips Modifications to the Kraft Process for Increased Yield. IPST Technical Paper Series Number 698. Submitted to Breaking The Yield Barrier Symposium, Atlanta, GA.(February, 1998).

[119] McDonough, T. Recent Advances in Bleached Chemical Pulp Manufacturing Technology. Part 1: Extended Delignification, Oxygen Delignification, Enzyme Applications, and ECF and TCF bleaching. Tappi Journal 78(3): 55(1995).

[120] Norden, S.; Teder, A. Modified Kraft Processes for Softwood Bleached Grade Pulp. Tappi Journal 62(7): 49(1979).

[121] Johansson, B.; Mjoberg, J.; Sandstrom; Teder, A. Modified Continuous Kraft Pulping- A Way to Decrease Lignin Content and Improve Pulp Quality. STFI-meddelande serie A nr907: 1(June, 1984).

[122] Kaiser, M.; Pitre, R. Beloits (RDH) Displacement Heating at Owens-Illinois, Valdosta, Georgia. Tappi Journal (10): 45(1986)..

[123] Andrews, E.E. RDH Kraft Pulping to Extend Delignification, Decrease Effluent, and Improve Productivity and Pulp Properties. Tappi Journal 72(11): 55(1989).

[124] Andrews, E.K.; Chang, H.M. Bleachability of RDH Kraft Pulps; Emphasis on Low Kappa with Effluent Characterization. International Pulp Bleaching Conference Proceedings: 51(1991).

[125] Mera, F.E. RDH Cooking- Mill Experience. Pacific Paper Expo Technical Conference Program 1: 1-1-0(November, 1990).

[126] Backlund, E.A. Extended Delignification of Softwood Kraft Pulp in a Continuous Digester. Tappi Journal (11): 62(1984).

[127] Kortelainen, V.A. Experiences with Extended Delignification of Hardwood and Softwood Kraft Pulp in a Continuous Digester. Tappi Journal (11): 70(1985).

[128] Whitley, D.L.; Zierdt, J.R.; Lebel, D.J. Mill Experiences with Conversion of a Kamyr Digester to Modified Continuous Cooking. Tappi Journal 73(1): 103(1990).

[129] Walley, C.A. MCC Cooking; Mill Experiences and What's Next. Pacific Paper Expo Technical Conference Program 1: 1-2-0(November, 1990).

[130] Jiang, J.; Greenwood, B; Phillips, JU.R.; Becker, E. Extended Delignification with a Prolonged Mild Countercurrent Cooking Stage. Appita 45(1): 19(1992).

[131] Dillner, B.; Tibbling, P. Isothermal Cooking to Low Kappa Numbers Facilitates TCF Bleaching to Full Brightness. Non-chlorine Bleaching Conference Proceedings: (1993).

[132] Perala, J.; Jiljanen, S. Superbatch™: Mature and Field Tested Cooking Concept--Practical Considerations and Mill Scale Results of System Performance. Tappi Pulping Conference Proceedings: 1015(1992).

[133] Kubelka, V.; Wizani, W.; Neubauer, G., et al. International Non-chlorine Bleaching Conference Proceedings: (1994).

[134] Tikka, P.; Tahkanen, H.; Kovasin, K. Chip Thickness vs. Kraft Pulping Performance, Part 2: Effect of Chip Thickness Screening on Cooking, Oxygen Delignification and Bleaching of Softwood Kraft Batch Pulp. Tappi Pulping Conference Proceedings: 833(1993).

[135] Jimenez, G.; Gustafson, R.R.; McKean, W.T. Modelling Incomplete Penetration of Kraft Pulping Liquor. Journal of Pulp and Paper Science 15(3): J110(1989).

[136] Jansson, L.; Lagergren, S.; Rydholm, S. Studies on the Interfiber Bonds of Wood: Part III. An Investigation on Hot Stock Pressure Refining of NSSC Pulp. Tappi Journal 42(8): 649(1959).

[137] Tikka, P.; Tahkanen, H. Chip Thickness vs. Kraft Pulping Performance, Part 3. Effect of New Optimized Chip Quality on Continuous Cooking, Oxygen Delignification and Bleaching of Softwood Kraft Pulp. Tappi Pulping Conference: 177(1994).

[138] Christensen, T.; Albright, L.F.; Williams, T.J. A Kinetic Model for Kraft Pulping of Wood. International Pulping Conference. Tappi Proceedings: (1983)

[139] Burazin, M. A Dynamic Model of Kraft Anthraquinone Pulping. Ph.D. Thesis. IPST, Atlanta, GA. June, 1986. Tappi Journal 71(3): 165(1988).

[140] Gustafson, R.R.; Ricker, N.L. Use of Simulation in the Optimization of the Kraft Pulping Process. Tappi Journal (11): 115(1982).

[141] Gustafson, R.R.; Sleicher, C.A.; McKean, W.T.; Finlayson, B.A. Theoretical Model of the Kraft Pulping Process. Ind. Eng. Chem. Process Des. Dev. 22: 87(1982).

[142] Smith, D.B.; Edwards, L.; Gustafson, R. Identifying and Prioritizing Variability in Kraft Cooking and Liquor Preparation. Tappi Journal (7): 41(1989).

[143] Kubulnieks, E.; Lundqvist, S.; Pettersson, T. The STFI OPTI-Kappi Analyzer: Applications and Accuracy. Tappi Journal (11): 38(1987).

[144] DeWitt, S.A.; Wang, P.H.; Ulinder, J.D. Oxygen Stage Advanced Control Using On-Line Kappa Sensors. Tappi Pulping Conference Proceedings: 325(1991).

[145] Herngren, T.; Powell, R.P. New Fiber Line Control Concept Minimizes Environmental Concerns. Tappi Pulping Conference Proceedings: 341(1991).

[146] Soderberg, J.; Almaberg, M.; et.al. Operational Experiences from a New Chlorination Control System Based on On-Line Measurements of Kappa Number. Tappi Journal 71(11): 145(1988).

[147] Courchene, C.E.; McDonough, T.J.; Carter, B. Evaluation of Commercially Available Conductivity Sensors in Black Liquor Applications. Measurement Technology Committee. American Forest and Paper Association. Institute of Paper Science and Technology, Atlanta, GA. pp1-39(1993).

[148] Trinh, D.T.; Collins, R.L.; McDonald, J.D. Factors Affecting the Conductivity of Kraft Black Liquor. 76th Annual Meeting. CPPA: A89(1990).

[149] Wells, C.H. Effective Alkali Sensors for Batch Digester Control. Tappi Journal (3): 181(1990).

[150] Juvekar, P.; Genco, J. Alkali Consumption in Kraft Pulping of Softwoods. Tappi Pulping Conference Proceedings: 93(1991).

[151] Milanova, E.; Dorris, G.M. On the Determination of Residual Alkali in Black Liquors. Tappi Pulping Conference Proceedings: 289(1991).

[152] Tikka, P.; Piiroinen, P. Cooking Liquor Analyzer: A New Tool for Controlling a Continuous Digester. Pulp and Paper Canada 88(10): T387(1987).

[153] Marcoccia, B.; Laakso, R.; McClain, G. Lo-solids Pulping: Principles and Applications. Tappi Pulping Conference Proceedings: 915(1995).

[154] Headley, R. Pulp Cooking Developments Focus on Fiber Yield, Lower Chemical Use. Pulp and Paper (10): 49(1996).

[155] Chamblee, W.; Funk, E.; Marcoccia, B.; Prough, J.R.; McClain, G. Lo-level™ Feed System at the Gulf States Paper Mill in Demopolis, Alabama. Tappi Pulping Conference Proceedings: 451(1996).

[156] Rudie, A.; Shakhet, A.; Carter, B.; Greffey, J. A Chlorite Holopulping Method to Evaluate Strength Changes in TMP. IPST Technical Paper Series 570(4): (1995).

[157] Oster, G.; Yamamoto, M. Density Gradient Techniques. Chemical Reviews 63: 257(1963).

[158] Mills, J.M. A Rapid Method of Constructing Linear Density Gradient Columns. Journal of Polymer Science 19(Letters to the Editors): 585(1956).

[159] Tung, L.H.; Taylor, W.C. An Improved Method of Preparing Density Gradient Columns. Journal of Polymer Science 97(21): 144(1956).

[160] Tessler, S.; Woodberry, N.T.; Mark, H. Application of the Density-Gradient Tube in Fiber Research. Journal of Polymer Science 1(5)(Letters to the Editors): 437(1946).

[161] Nickerson, R.F. Hydrolysis and Catalytic Oxidation of Cellulosic Materials: Hydrolysis of Natural, Regenerated, and Substituted Celluloses. Industrial and Engineering Chemistry 33(8): 1022(1941).

[162] Nickerson, R.F. Hydrolysis and Catalytic Oxidation of Cellulosic Materials: Hydrosis of Mercerized Cottons. Industrial and Engineering Chemistry 34(1): 85(1942).

[163] Nickerson, R.F.; Habrle, J.A. Hydrolysis and Catalytic Oxidation of Cellulosic Materials: Determination of Structural Components of Cotton Linters. Industrial and Engineering Chemistry 37(11): 1115(1945).

[164] Conrad, C.C.; Scroggie, A.G. Chemical Characterization of Rayon Yarns and Cellulosic Raw Materials. Industrial and Engineering Chemistry 37(6): 592(1945).

[165] Stamm, A.J. History of two phases of wood physics. History of Wood Science. Paper No.2398 of the Journal Series. North Carolina Agricultural Experiment Station, Raleigh, North Carolina: 186(1966).

[166] Dunlap, F. Density of Wood Substance and Porosity of Wood. Journal of Agricultural Research 11(6): 423(1914).

[167] Wangaard, F. Cell-Wall Density of Wood with Particular Reference to the Southern Pines. Wood Science 1(4): 222(1969).

[168] Hermans, P.H.; Vermaas, D. Density of Cellulose Fibers: Part I. Introduction and Experiments on the Penetration of Liquids into Dry Cellulose; Part II. Density and Refractivity

of Model Filaments; Part III. Density and Refractivity of Natural Fibers and Rayon. Journal of Polymer Science 1(3): 149(1946).

[169] Yiannos, P. The Apparent Cell-wall Density of Wood and Pulp Fibers. Tappi 47(8): 468(1964).

[170] Wilfong, J. Specific Gravity of Wood Substance. Forest Products Journal 16(1): 55(1966).

[171] Davidson, G.F. The Specific Volume of Cotton Cellulose. J. Text. Inst. 18: T175(1927).

[172] Stone, J.E.; Scallan, A.M.; Aberson, G.M.A. The Wall Density of Native Cellulose Fibres. Pulp and Paper Magazine of Canada (5): T263(1966).

[173] Stamm, A.J.; Sanders, H.T. Specific Gravity of the Wood Substance of Loblolly Pine as Affected by Chemical Composition. Tappi Journal 49(9): 397(1966).

[174]Hermans, P.H. Contributions to the Physics of Cellulose Fibers. Elsevier Publishing Co. Amsterdam-Brussels; London-New York, 1946.

[175] Ehrnrooth, E. Change in Pulp Fibre Density with Acid-chlorite Delignification. Journal of Wood Chemistry and Technology 4(1): 91(1984).

[176] Wandelt, P.; Mroz, W. A Rapid Method for Measuring Yield in Semichemical Pulping Processes. Tappi Journal (3): 203(1992).

[177] Air Products, technical service, 7201 Hamilton Blvd., Allentown, PA. 1-800-752-1597.

[178] Gordon, A.; Ford, R. The Chemists Companion. Wiley-Interscience Publishers, NY, 1972.

[179] Vogel, A. Practical Organic Chemistry. 3rd Edition. John Wiley and Sons, NY, 1962.

[180] Davis, M. Vashaw Scientific, Inc. Sales representative, Norcross, GA. (1994).

[181] Techne Incorporated, University Park, 743 Alexander Road, Princeton, NJ 08540-6328. 1-800-225-9243. FAX: 609-987-8177.

[182] Gresham, K. EM Science. 480 S. Democrat Rd., Gibbstown, NJ 08027-1297. Technical sales representative, Atlanta, GA. 770-419-0082, 1-800-222-0342.

[183] Bevington, P.R.; Robinson, D.K. Data Reduction and Error Analysis for the Physical Sciences. 2nd Edition. McGraw-Hill Publishing Co., NY, 1992, p235.

[184] Page, D.H.; El-Hosseiny, F.; Bidmade, M.L.; Binet, R. Birefringence and the Chemical Composition of Wood Pulp Fibers. Applied Polymer Symposium No.28: 923(1976).

[185] Jordan, B.D.; O'Neill, M.A. The Birefringence of Softwood Mechanical Pulp Fines. Journal of Pulp and Paper Science 20(6): J172(1994).

[186] Streitwieser, A. Jr.; Heathcock, C.H. Introduction to Organic Chemistry. Macmillan Publishing Co., 1985, p51.

[187] Preston, R.D. Natural celluloses. Cellulose; Structure, Modification and Hydrolysis. John Wiley and Sons, NY, 1986, p3.

[188] Atalla, R.H.; VanderHart, D.L. Science 223: 283(1984).

[189] VanderHart, D.L.; Atalla, R.H. Macromolecules 17: 1465(1984).

[190] VanderHart, D.L.; Atalla, R.H. The Structure of Cellulose. ACS Symposium Series 340; American Chemical Society, Washington, DC: 88(1987).

[191] Sugiyama, J.; Persson, J.; Chanzy, H. Combined Infrared and Electron Diffraction Study of the Polymorphism of Native Celluloses. Macromolecules 24: 2461(1991).

[192] Sugiyama, J.; Vuong, R.; Chanzy, H. Electron Diffraction Study on the Two Crystalline Phases Occurring in Native Cellulose from an Algal Cell Wall. Macromolecules 24: 4168(1991).

[193] Yoshida, H.; Morch, R.; Kringstad, K. Fractionation of Kraft Lignin by Successive Extraction with Organic Solvents. II. Thermal Properties of Kraft Lignin Fractions. Holzforschung 41(3): 171(1987)

[194] Gierer, J. Chemistry of Delignification. Part I. General Concept and Reactions during Pulping. Wood Science and TDechnology(20): 1(1986).

[195] Virkola, N.E.; Jarvela, O.; Vartiainen, V. Comparison of Various Pulping Methods Utilizing Pine Wood (Pinus silvestris) as Raw Material. Paperi ja Puu (10): 575(1965).

[196] Carno, B.; Norrstrom, H.; Ohlsson, L. The Influence of Cooking Conditions on the Bleachability of Pine Sulphate Pulp. Svensk Papperstidning (4): 127(1975).

[197] Axegard, P.; Norden, S.; Teder, A. Some Principles of Pulp Production for Bleaching. Svensk Papperstidning 81(4): 97(1978).

[198] McDonough, T.J.; Van Drunen, V.J. Pulping to Low Residual Lignin Contents in the Kraft-Anthraquinone and Kraft Processes. Tappi Journal 63(11): 83(1980).

[199] Axegard, P.; Wiken, J.E. Delignification Studies- Factors Affecting the Amount of "Residual Lignin". Svensk Papperstidning: R178(1983).

[200] Gellerstedt, G.; Lindfors, E. Structural Changes in Lignin during Kraft Pulping. Holzforschung 38: 151(1984).

[201] Gellerstedt, G.; Lindfors, E. Structural Changes in Lignin during Kraft Cooking. Part 2. Characterizatiohn by Acidolysis. Svensk-Papperstidning no.9: R61(1984).

[202] Robert, D.; Bardet, M.; Gellerstedt, G.; Lindfors, E.L. Structural Changes in Lignin during Kraft Cooking. Part 3. On the Structure of Dissolved lignins. Journal of Wood Chemistry and Technology 4(3): 239(1984).

[203] Gellerstedt, G.; Lindfors, E. Structural Changes in Lignin during Kraft Cooking. Part 4. Phenolic Hydroxyl Groups in Wood and Kraft Pulps. Svensk Papperstidning no.15: R115(1984).

[204] Gellerstedt, G.; Lindfors, E. On the Formation of Enol Ether Structures in Lignin during Kraft Cooking. Nordic Pulp and Paper Research Journal no.2: 71(1987).

[205] Lai, Y.; Mun, S.; etal. Variation of Phenolic Hydroxyl Contents in Unbleached Kraft Pulps. Holzforschung 49: 319(1995).

[206] Froass, P.; Ragauskas, A. Structural Changes in Lignin during Kraft Pulping and Chlorine Dioxide Bleaching. Ph.D. Dissertation, Institution of Paper Science and Technology, Atlanta, GA(1996).

[207] Kumar, K.R.; Chang, H.; Jameel, H. Effect of Pulping Conditions on the Bleachability of Hardwoods. Tappi Pulping Conference Proceedings: 539(1995)

[208] McDonough, T.J.; Herro, J.L. The Influence of Low-lignin Pulping Conditions on Bleachability. Tappi Journal (9): 117(1982).

[209] McDonough, T.J.; Nelson, D.A.; Cukier, M. Effects of Kraft Pulping Conditions on Oxygen Delignification and Subsequent C_DED Bleaching. Tappi Pulping Conference Proceedings: 345(1983).

[210] Froass, P.; Ragauskas, A.; McDonough, T.; Jiang, J. Relationship Between Residual Lignin Structure and Pulp Bleachability. International Pulp Bleaching Conference Proceedings: (1996).

[211] McDonough, T. Brightness Development in the Final ClO_2 Stages of an ECF Kraft Pulp Bleaching Sequence: Modeling and Effects of Pulping Conditions. Tappi Pulping Conference Proceedings: 201(1996).

[212] Megraw, R.A. Wood Quality Factors in Loblolly Pine. The Influence of Tree Age, Position in Tree, and Cultural Practice on Wood Specific Gravity, Fiber Length, and Fibril Angle. Tappi Press, Atlanta, GA., 1985.

[213] Griffith, P.R.; de Haseth, J.A. Fourier Transform Infrared Spectrometry. Vol. 83. John Wiley and Sons Publishers, NY, 1986.

[214] Streitwieser, A. Jr.; Heathcock, C.H. Introduction to Organic Chemistry. 3rd edition. Macmillan Publishing Co., New York, NY, 1985, p410.

[215] Liang, C.Y.; et al. Infrared Spectra of Crystalline Polysaccharides. VII. Thin Wood Sections. Tappi Journal 43(12): 1017(1960).

[216] Bolker, H.I.; Somerville, N.G. Infrared Spectroscopy of Lignins. Part II: Lignins in Unbleached Pulps. Pulp and Paper Magazine of Canada (4): T187(1963).

[217] Michelle, A.J.; Watson, A.J.; Higgins, H.G. An Infrared Spectroscopic of Delignification of Eucalyptus regnans. Tappi Journal 48(9): 520(1965).

[218] Kolboe, S.; Ellefsen, O. Infrared Investigations of Lignin. A Discussion of Some Recent Results. Tappi Journal 45(2): 163(1962).

[219] Marton, J.; Sparks, H.E. Determination of Lignin in Pulp and Paper Infrared Multiple Internal Reflectance. Tappi Journal 50(7): 363(1967).

[220] Saad, S.M.; Issa, R.M.; Fahmy, M.S. Infrared Spectroscopic Study of Bagasse and Unbleached High-yield Soda Bagasse Pulps. Holzforschung 34: 218(1980).

[221] Schultz, T.P.; etal. Rapid Determination of Lignocellulosics by Diffuse Reflectance Fourier Transform Infrared Spectrometry. Analytical Chemistry 57(14): 2867(December, 1985).

[222] Faix, O. Investigation of Lignin Polymer Models by FTIR Spectroscopy. Holzforschung 40(5): 273(1986).

[223] Berben, S.A.; etal. Estimation of Lignin in Wood Pulp by Diffuse Reflectance Fourier Transform Infrared Spectrometry. Tappi Journal (11): 129(1987).

[224] Schultz, T.P.; Burns, D.A. Rapid Secondary Analysis of Lignocellulose: Comparison of NIR and FTIR. Tappi Journal (5): 209(1990).

[225] Backa, S.; Brolin, A. Determination of Pulp Characteristics by Diffuse Reflectance FTIR. Tappi Journal (5): 218(1991).

[226] Wallbacks, L.; Edlund, U.; et al. Multivariate Characterizations of Pulp using Solid State CNMR, FTIR and NIR. Tappi Journal (10): 201(1991).

[227] Friese, M.A.; Banerjee, S. Lignin Determination by FTIR. Applied Spectroscopy 46(2): 246(1992).

[228] Sarkanen, K.V.; Chang, H.; Ericsson, B. Species Variation in Lignins. I. Infrared Spectra of Guaiacyl and Syringyl Models. Tappi Journal 50(11): 572(1967).

[229] Sarkanen, K.V.; Chang, H.; Allan, G.G. Species Variation in Lignins II. Conifer Lignins. Tappi Journal 50(12): 583(1967).

[230] Sarkanen, K.V.; Chang, H.; Allan, G.G. Species Variation in Lignins. III. Hardwood Lignins. Tappi Journal 50(12): 587(1967).

[231] Marrinan, H.; Mann, J. Infrared Spectra of the Crystalline Modifications of Cellulose. Journal of Polymer Science 21: 301(1956).

[232] Mann, J.; Marrinan, H.J. Crystalline Modifications of Cellulose. Part II. A Study with Plane-polarized Infrared Radiation. Journal of Polymer Science 32: 357(1958).

[233] Mann, J.; Marrinan, H.J. Polarized Infrared Spectra of Cellulose I. Journal of Polymer Science 27(115): 595(1958)

[234] Liang, C.Y.; Marchessault, R.H. Hydrogen Bonds in Native Celluloses. Journal of Polymer Science 35(129): 529(1959).

[235] Liang, C.Y.; Marchessault, R.H. Infrared Spectra of Crystalline Polysaccharides. I. Hydrogen Bonds in Native Celluloses. Journal of Polymer Science 37: 385(1959).

[236] Liang, C.Y.; Marchessault, R.H. Infrared Spectra of Crystalline Polysaccharides. II. Native Celluloses in the Region from 640 to 1700 cm^{-1}. Journal of Polymer Science 39: 269(1959).

[237] Marchessault, R.H.; Liang, C.Y. Infrared Spectra of Crystalline Polysaccharides. III. Mercerized Cellulose 43: 71(1960).

[238] Marchessault, R.H.; Liang, C.Y. The Infrared Spectra of Crystalline Polysaccharides. VIII. Xylans. Journal of Polymer Science 59: 357(1962).

[239] Higgins, H.G.; Stewart, C.M.; Harrington, K.J. Infrared Spectra of Cellulose and Related Polysaccharides. Journal of Polymer Science 51: 59(1961).

[240] O'Connor, R.T. Infrared Absorption Spectroscopy in the Evaluation of Cellulose and Cellulose Derivatives. Tappi Journal 52(4): 566(1969).

[241] Saksena, B.D.; Agarwal, K.C.; Jauhri, G.S. Infrared Spectrum of Cellulose I in Relation to Its Structure. Journal of Polymer Science 62: 347(1962).

[242] Polymer Handbook. 2nd edition. Wiley Interscience, NY, 1975, V87.

[243] Deeds, W.E.; Duckett, K.E. The Laser in Single Fiber Infrared Microspectroscopy. Microtecnic 21(4): 391(1967).

[244] Lang, P.L.; et al. The Identification of Fibers by Infrared and Raman Microspectroscopy. Microchemical Journal 34: 319(1986).

[245] Sweeney, K.M. FTIR Microscopy of Pulp and Paper Samples. Tappi Journal (2): 171(1989).

[246] Mirabella, F.M.; Westphal, S.P. Infrared Microspectroscopy: Analysis of Multilayer Films, Contaminants, and Inclusions. Tappi Journal (7): 143(1991).

[247] Katon, J.E.; Sommer, A.J. IR Microspectroscopy; Routine IR Sampling Methods Extended to the Microscopic Domain. Analytical Chemistry 64(19): 931(1992).

[248] Sommer, A.J.; Katon, J.R. Infrared Microspectroscopy: A High Information Content Microanalytical Technique for the Analysis of Contaminants in the Pulp and Paper Making Industry. Tappi Pulping Conference Proceedings: 543(1993).

[249] Humecki, H. Practical Guide to Infrared Microspectroscopy. Practical Spectroscopy Series Volume 19. Marcell Dekker, Inc., NY, 1995.

[250] Tungol, M.; etal. Forensic Examination of Synthetic Textile Fibers by Microscopic Infrared Spectrometry. Practical Guide to Infrared Microspectroscopy. Volume 19. Marcell Dekker, Inc., NY, 1995, p245.

[251] Bouchard, J.; Douek, M. Structural and Concentration Effects on the Diffuse Reflectance FTIR Spectra of Cellulose, Lignin and Pulp. Jounal of Wood Chemistry and Technology 13(4): 481(1993).

[252] Tasman, J.E; Berzins, V. The Permanganate Consumption of Pulp Materials. III. The Relationship of the Kappa Number to the Lignin Content of Pulp Materials. Tappi Journal 40(9): 699(1957).

[253] Walpole, R.; Myers, R. Probability and Statistics for Engineers and Scientists. 5th edition. Macmillan Publishing Co., NY, 1993, p344.